A wavelet-fuzzy based algorithm for condition monitoring and fault detection of a voltage source inverter.

Mamat-Ibrahim, Mohd Rosailan bin

DEPARTMENT OF ELECTRICAL AND ELECTRONIC ENGINEERING

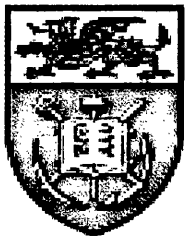

UNIVERSITY OF WALES SWANSEA

A WAVELET – FUZZY BASED ALGORITHM FOR CONDITION MONITORING AND FAULT DETECTION OF A VOLTAGE SOURCE INVERTER

BY

MOHD ROZAILAN BIN MAMAT @ IBRAHIM

Thesis submitted to the University of Wales in candidature for the degree of

Doctor of Philosophy

JULY, 2003

DECLARATION

This work has not been accepted in substance for any degree and is not being concurrently submitted in candidature for any degree.

Signed ..... (candidate)
Date.....21/07/03.....

STATEMENT 1

This thesis is the result of my own investigations, except where otherwise stated. Other sources are acknowledged by footnotes giving explicit references. A bibliography is appended.

Signed ..... (candidate)
Date.....21/07/03.....

STATEMENT 2

I hereby give consent for my thesis, if accepted, to be available for photocopying and for inter-library loan, and for the title and summary to be made available to outside organisations.

Signed ..... (candidate)
Date.....21/07/03.....

CONTENTS

CHAPTER 5 PROPOSED FAULT DIAGNOSIS ALGORITHM

CHAPTER 6 EXPERIMENTAL RESULTS AND DISCUSSION

ACKNOWLEDGEMENT

First of all, my gratefulness to the Almighty God for his love, protection and care for all these years.

Special thanks and respect to Dr. M.S.Khanniche, my Director of Studies for his help and supervision throughout my time at Swansea University, which helped me tremendously in concluding this research.

I would also like to thank my parents and family especially my loving wife, Dzulhaida for her patience, support and sacrifices all this time. Also to my three adoring sons Amir Asyraf, Amir Shazwan and Amir Danial, whose love and attention has been an inspiration and kept me going.

My gratitude also goes to University Malaya and Malaysian Government for sponsoring my PhD study.

SUMMARY

The popularity of the variable-speed induction machine as a drive mechanism has increased rapidly. This has led to the voltage source inverter induction machine being used to drive numerous applications such as electric vehicles and trains. Unfortunately, the condition monitoring and fault detection of these types of drives is an area, which has been left largely untouched by the research community. This is due to the high harmonic contents of the machine supply making the rigorous mathematical analysis of the drive complex.

Fortunately, the interesting development in signal processing theory, especially wavelet transform, has sparked a new interest in condition monitoring of voltage source inverter induction machine. The wavelet transform have two important features, which, are important for the condition monitoring and fault detection purpose; time localization ability and multi-resolution analysis. Furthermore, the wavelet can be combined with artificial intelligent system to provide an acceptable system with high accuracy and reliability.

The work herein presented is a contribution to voltage source inverter induction machine condition monitoring and fault detection using the combination of wavelet transform and fuzzy logic. The research was concentrated on some typical fault events of voltage source inverter that allow reduced operating conditions of the drive system without triggering the short circuit protection.

NOMENCLATURE

A/D	:	analogue to digital converter
ac	:	alternating current
AI	:	artificial intelligent
CPC	:	cubic phase coupling
CSI	:	current source inverter
CWT	:	continuous wavelet transform
D4	:	daubenchies 4 wavelet
dc	:	direct current
DFT	:	discrete fourier transform
DSC	:	direct self control
DSP	:	digital signal processor
DWT	:	discrete wavelet transform
emf	:	electromotive force
FLC	:	fuzzy logic control
FT	:	fourier transform
GA	:	genetic algorithm
GTO	:	gate-turn-off thyristor
HOS	:	higher order spectra
HSI	:	high speed input
HSO	:	high speed output
HP	:	horse power
IDWT	:	inverse discrete wavelet transform
IGBT	:	insulated gate bipolar transistor
IM	:	induction motor
M	:	medium fuzzy set for sliding surfaces
mmf	:	magnetomotive force
NB	:	negative big fuzzy set
NM	:	negative medium fuzzy set
NN	:	neural network
NS	:	negative small fuzzy set
PB	:	positive big fuzzy set
PM	:	positive medium fuzzy set
PS	:	positive small fuzzy set
PSD	:	power spectral density
PWM	:	pulse width modulation
rms	:	root mean square value
SPWM	:	sinusoidal pulse width modulation
v/f	:	voltage frequency
VSI	:	voltage source inverter
WT	:	wavelet transform

C	:	dc link capacitor
T	:	time period
T_i	:	power diodes, i = 1, 2, 3, 4, 5, 6
V_{dc}	:	dc link Voltage
V_{rms}	:	rms value of inverter output voltage
ω	:	angular frequency
t	:	time variable
V_{AN}, V_{BN}, V_{CN}	:	phase voltages
V_{AB}, V_{BC}, V_{CA}	:	line voltages
V_{AO}, V_{BO}, V_{CO}	:	PWM pole voltages
VM	:	VSI condition
Li	:	load disturbance, i= A, B, C
T_{ofi}	:	switching power devices open-circuit fault, i= 1,2,3,4,5 6
T_{ifa}	:	switching power devices intermittent misfiring fault, a = 1,2,3,4,5,6
f_c	:	carrier frequency
f_m	:	modulating frequency
f_r	:	frequency ratio
M_a	:	modulation index
T_c	:	carrier period
t_1, t_2	:	time instants
t_k, t_{k+1}	:	time samples
δ_p	:	pulse width
δ_k^p	:	sampled pulse width
$m(t)$	:	modulating signal
δ_k^-, δ_k^+	:	switching instants
ω_s	:	synchronous speed in electrical rad/sec
ω_r	:	rotor speed in electrical rad/sec
ω_{slip}	:	slip frequency in electrical rad/sec
R_s	:	per-phase resistance of the stator winding
L_{ls}	:	per-phase leakage reactance of the stator winding
L_s	:	per-phase stator self inductance
R_r	:	per-phase resistance of the rotor winding
L_{lr}	:	per-phase leakage reactance of the rotor winding
L_r	:	per-phase rotor self inductance
L_m	:	per-phase mutual (magnetising) inductance
I_r	:	rotor current in Amps
I_s	:	stator current in Amps
I_A, I_B, I_C	:	Phase stator currents in Amps
I_{in}	:	input current
I_{Si}	:	switch currents in Amps
SF_i	:	switching function
S	:	slip speed
P_{in}	:	total input power to the equivalent circuit of the IM in Watt
P_c	:	power representing iron loss in Watt
P_s	:	power representing stator copper loss in Watt

T_L : load torque in N.m
T_d : detection period in sec
T_s : sampling period in sec
θ_r : rotor angle in radians
θ_s : stator angle in radians
a : spatial operator
f_s : general stator variable
t_l : load torque
P : number of pole pair
ρ : derivative operator (d/dt)
J : moment of inertia
B : damping constant
$\overline{f_s^f}$: stator variable space vector in the synchronous reference frame
$\overline{f_r^f}$: rotor variable space vector in the synchronous reference frame
A, B : fuzzy sets
U, V, W : universe of discourse
μ : degree of membership
x, y, z : elements in universe of discourse
R_f : fuzzy relation
x_o : crisp input value to the fuzzy controller
y_o : crisp output value from the fuzzy controller
μ_{agg} : aggregate degree of membership
e_o : speed error
Δe_o : speed error change
k : sampling interval
i_{sq}^* : torque current command
Δi_{sq}^* : torque current command change
u : control signal
x_1, x_2 : system states
v/f : Volts / Hertz scalar control
E_g : air-gap voltage
ω_{ref} : reference speed in mechanical rad/sec
ω_{sl}^* : slip frequency command in rad/sec
ω_s^* : stator frequency command in rad/sec
ω_{fr} : rotational frequency in rad/sec
τ_r : rotor time constant
N : constant representing the length of sequence of data
m : constant representing the length of successive sub-sequences of data
ω_c : cut-off frequency in Hz
ω_{samp} : sampling frequency in Hz
$\psi(x)$: wavelet

$\varnothing$	:	scaling function
s	:	wavelet scale parameter
$\tilde{h}$	:	low pass filter
$\tilde{g}$	:	high pass filter
C	:	signal coefficient
$\tilde{a}$	:	wavelet approximation coefficients
$\tilde{b}$	:	wavelet detail coefficients
c_k	:	filter coefficient
M	:	wavelet vanishing moment
p	:	high-pass filter vanishing moment
$T(n)$	:	sampled data

LIST OF FIGURES

LIST OF TABLES

CHAPTER 1

INTRODUCTION

1.1 General Introduction

With the development of power electronics, microprocessor and digital signal processor (DSP), induction motors are predominantly fed from pulse width modulation (PWM) inverters for variable-speed operation. PWM inverter fed motors are usually more reliable than those supplied directly on-line. For example, the problem of broken rotor bars, mainly due to excessive starting torque, is practically avoided by the technique of soft starting with an inverter [1,2].

However, a previous study of three-phase voltage-fed inverter demonstrated that they can also develop various faults which is preventing their wide spread application [3-6]. These faults can lead to motor failure if left undetected. As we all aware, motor problems can cause crises that are expensive and quite annoying, in particular, if the problem could be prevented [7-10].

To solve this problem, the condition monitoring and fault detector of voltage source inverter (VSI) is necessary. The condition monitoring, fault detection and diagnosis system allow preventive and condition-based maintenance to be arranged for the system during scheduled downtime. This will prevent an extended period of downtime caused by extensive machine failures, which will improve the overall availability and performance, while reducing maintenance costs.

Condition monitoring means the continuous assessment of the performance and health of the system throughout its useful operating life. Diagnosis, though, is a special case of the more general problem of condition data interpretation, as it sets out to determine the source of any abnormality in the data, based on a given set of possible cause and effect symptoms. The aim of diagnosis is: based on a minimum amount of input data, using the

minimum and simplest analysis, to determine and isolate as fast as possible, the cause of any inadequate performance or any actual equipment failure.

An effective condition monitoring system will necessarily consist of the following criteria:

1. the system should be non-invasive
2. the measuring of selected parameters which can be analysed to give an early indication of damage or wear
3. easy extension to a wider range of monitoring requirements should be possible
4. recommended actions based upon the analysis
5. remote operation should be possible

In the early days, monitoring tasks were performed by the people who actually operated the system. They could assess the system condition based on their own personal experience. Later, when the system became more complex, measurement systems were introduced to measure and analyse the key parameters, and to provide an objective judgement of the system condition.

It is important to stress here the difference between *protection* and *condition monitoring*. Protection is basically designed to act only once a fault has occurred, and will normally result in some executive action, such as activating a main circuit breaker to switch off the power if an excessive current is detected. Monitoring should be designed to pre-empt such occurrences and give an early indication of the onset of possible malfunctions [7].

1.2 Condition Monitoring

The ultimate objective of any condition monitoring and fault diagnosis process is to recognise the development of faults at early stage, so as to assist maintenance personnel and, where necessary, to activate alarms. The overall requirement is to act in a convenient and quick manner so as to control the cause of a fault.

To determine the cause of any problem, two forms of condition monitoring of a system are normally used:

Off-line monitoring. With this method, system parameters, such as current, voltage or vibration [11-13], are measured, recorded and analysed in the field or in a laboratory. Advanced signal processing techniques are usually required for in-depth fault diagnosis. The effectiveness of off-line fault diagnosis depends mainly on the quality of the data obtained, the suitability of the data-analysis equipment and the technique used to derive the information from the data. Off-line monitoring is commonly used on many complex systems where continuous measurement is expensive or where data measurements must be made at many different locations in the system or plant.

On-line monitoring. With this method, directly measurable parameters, such as current, voltage, temperature and speed are measured continuously. These parameters, together with derived, non-measurable quantities (in the form of state variables or parameter estimation), are compared continuously to permitted levels, or suitably processed to determine trends. Typically, this method requires rapid processing and hence, complex signal processing and fault diagnosis techniques should be avoided.

On-line monitoring is particularly important in safety-critical applications where the system is mainly to survive most minor faults. Normally, an artificial intelligent (AI) technique is integrated into on-line condition monitoring and fault diagnosis system [14,15]. Such technique required "minimum configuration intelligence" since no detailed analysis of the fault mechanism is necessary, nor is any modelling of the system required. A modern condition monitoring and fault diagnosis system may also be augmented by a system that advises the operator on action to be taken when a certain fault occurs.

1.3 Fault Signatures

A *fault* is a physical defect in a system element or component. It can cause changes in the element's behaviour and possibly, in related element's, which can result in a failure of a whole system. These changes could manifest themselves in different ways, such as overheating [16], over speed, excessive vibration or deterioration in the relationship between the input/output parameters of the element or system. Often, more than one type of change will occur in a single defective element.

These observable changes in a faulty element's behaviour can be considered as *fault signatures*. The signature will depend on the element itself, its input and/or output, and the type of defection.

Normally, changes in the element behaviour can be well observed from the signal patterns, obtained from the sensors. The inherent nature of many sensors is that their output is an electrical signal, with a characteristic pattern of voltage or current and, with 'information' held in signal magnitude, frequency or phase. Advance signal processing techniques such as fast fourier transform (FFT) [17], higher order spectra [18-20], Park's vector analysis [21] and wavelet transform [22,23] are required to extract embedded information that indicates deviation from normal operating conditions. For that reason, some signal processing techniques will be reviewed in Chapter 2.

1.4 Research Objective

A number of common practical faults of voltage source inverter (VSI), are identified [3,4,24], the drive system can operate for a considerable period of time, but with degraded performance. This operating mode is, of course, accompanied by disturbed output voltage waveforms and will overstress other switching devices. Also, VSI faults generate load disturbances related to the presence of a pulsating electromagnetic torque and a substantial dc component in the stator current, which will saturate the machine and induce an oscillating air gap torque at the fundamental frequency. These situations can lead to catastrophic breakdown of the motor if left undetected. Continuous monitoring for such condition is of great importance.

The objectives of the present work are to study, investigate and design the real-time, non-invasive condition monitoring and fault diagnosis algorithm of three-phase pulse width modulation (PWM), VSI for closed-loop, fuzzy logic, voltage/frequency (v/f) speed control strategy of an induction motor drive. The research concentrated on some typical true fault events of VSI that allow reduced operating conditions of the drive without involving the short circuits protection. The proposed algorithm should be robust and simple, which is important for the implementation of on-line monitoring system. For this

reason, the combination of wavelet transform technique and fuzzy logic system is proposed.

For the development of such algorithms, it is advantageous to test their effectiveness and validity through computer modelling and simulation. Indeed, this represents a very important step to the initial design of an efficient algorithm for the condition monitoring and fault diagnosis system. In the present work, computer simulations have been carried out with the simulation package MATLAB and SIMULINK [25,26]. Then, the reliability and accuracy of the proposed algorithm are verified using the real experimental data.

1.5 Overview Of The Thesis

Chapter 2 provides an overview of the condition monitoring fault diagnosis system. Their related works and the theory of monitoring process and signal analysis techniques are included.

Chapter 3 describes the voltage source inverter (VSI) and the pulse width modulation (PWM) techniques. The operation principles for single-phase and three-phase are presented. This is followed by the discussion of VSI faults.

Chapter 4 outlines the modelling and simulation process of three-phase inverter and induction motor drive. The system is simulated in MATLAB/SIMULINK environment.

Chapter 5 describes the proposed fault diagnosis algorithm for three-phase PWM VSI induction motor drive using the combination of wavelet transform and fuzzy logic system. The development of the proposed scheme is thoroughly discussed.

Chapter 6 demonstrates an application of the proposed algorithm. The experimental set-up is presented in detail. This is followed by illustrating the performance of a proposed detection system. Comparison studies between the acquired experimental results with the simulation results, are also presented.

Chapter 7 draws together the main conclusion of the thesis and outlines some possible future directions.

1.6 Publications

As a result, 6 papers have been published.

a) Refereed Journal Publications

i) Khanniche, M.S., and Mamat-Ibrahim., M.R., "Fault detection and diagnosis of 3-phase inverter system", International Journal of Reveu Des Energies Renouvelables, 2001.

b) Refereed Conference Publications

i) Khanniche, M.S., and Mamat-Ibrahim., M.R., "Condition monitoring of PWM voltage source inverters", IEEE International Conference on Electrical and Electronics Technology (TENCON), 2000, Malaysia.

ii) Khanniche, M.S., and Mamat-Ibrahim., M.R., "Advanced DSP based fault detection of PWM voltage source inverters", International University Power Engineering Conference (UPEC), 2000, Ireland.

iii) Khanniche, M.S., and Mamat-Ibrahim., M.R., "Fault detection of 3-phase voltage source inverter using wavelet transform", IEEE International Symposium on Diagnostics for Electrical Machines, Power Electronics and Drives, 2001, Italy.

iv) Khanniche, M.S., and Mamat-Ibrahim., M.R., "Fault detection and diagnosis of 3-phase voltage source inverter", International University Power Engineering Conference (UPEC), 2001, United Kingdom.

v) Khanniche, M.S., and Mamat-Ibrahim., M.R., "Fault detection of voltage source inverter using combination of wavelet transform and fuzzy logic system", IEEE International Symposium on Diagnostics for Electrical Machines, Power Electronics and Drives, 2003, USA (accepted for publication).

CHAPTER 2

CONDITION MONITORING AND FAULT DIAGNOSIS

2.1 Introduction

The increase of productivity requirements and better performance specifications lead to more demanding operating conditions of many engineering systems. Such condition will increase the possibility of the system failure, which are characterised by critical and unpredictable changes in the system dynamics. In general, the feedback control algorithm, which is designed to control small perturbation that may arise under normal operating condition, cannot accommodate abnormal behaviour due to the component faults [27]. The system may collapse completely.

Most of the power electronic devices normally operate in an environment requiring rapid speed variation, frequent stop / starting and constant overloading. The circuits are subjected to constant abuse of over-current surges and voltage overswings. Although protection devices such as snubber circuits are commonly used, switching devices are physically small and thermally fragile. Even a small electrical disturbance can cause thermal rating to be exceeded resulting in rapid destruction [16].

Generally, the malfunctioning of power electronics system may due to multiple and complex causes. This fact is due to the high integration and interaction of multiple heterogeneous components. External causes such as swell/dips at the input of an inverter or short-circuit of the output load are low dynamic failures and can often be stopped before the destruction of the device. On the other hand, internal causes such as semiconductor breakdown or faulty control signals provide high dynamic failures and it may be very difficult to limit the failure and save all the components. For example, a leg short-circuit in a 2-level IGBT inverter must be less than 10 μs to save the power devices [154].

In many cases, occasional failures may be tolerated, but, in the case of expensive, high power systems, multi-converter integrated automation systems and safety critical systems, advanced indication of unusual performance, which may lead to sudden system failure is mandatory.

Therefore, the knowledge and information about the fault behaviour of power electronic circuits is important to improve system design, protection and fault tolerant control.

2.2 Overview of Related Work

Condition monitoring of the power electronics circuit, especially VSI has received considerable attention in recent years. The literature concerns mostly with the classification and the analysis of true fault operation of single components of power electronic circuits. In the following, some selected, related works published recently, are described.

An early study was made by Gentile [28], who in 1993, analysed inverter-fed induction motor faults based on the space vector theory. Two types of modulation technique are discussed: six step modulation and sinusoidal PWM. The inverter faults like the open of a phase, the failure to turn-on of the transistor and the delay in a branch command are detected using current spectrum and dc component in the phase currents. The authors also discussed the remedial strategies to reduce the damage level of the electrical drive.

Renfew [29] in 1993, have investigated the technique to detect the 3-phase inverter faults by using the simplest criteria available in input and output waveform. The value of dc component in current and voltage was used as main indicators to detect the faults. Then the knowledge-based system was implemented to analyse the results. In this paper, three different types of converter were considered: single-phase converter, three-phase converter and cycloconverter. The results showed that the chosen criteria could be used effectively to detect the faults, which can lead to a reduction of performance in the motor operation.

Also in 1993, Craig [30] presented a fault detection procedure for single-phase bridge converter, based on device firing signals, phase current direction and fly wheeling currents. In the published paper, it was shown that the system is able to continuously monitor the condition of a single-phase bridge, identify the faulty device and its mode of failure.

A difference approach was reported by Wiechmann [31] in which they described a real-time converter operation surveillance. Fault detection is based on a real-time signal error produced by comparison between real time simulated and acquired data. The error is then compared with characteristic anomalous signal patterns to produce a diagnosis.

Aris [32] in 1994, reported the use of digital signal processing and a knowledge based approach to detect and analyse all possible faults in the 3-phase inverter circuit. The dc level of phase currents and the amplitude of phase voltages are used as an input to the fuzzy logic. The implementation of fuzzy logic technique was successfully demonstrated by interfacing it with the power electronic design tool package run on SUN workstation.

Debaprasad [3], also in 1994, have investigated the various fault modes of a 3-phase voltage-fed PWM inverter system for induction motor. The important fault modes are clearly identified. The predicted faults performances are then substantiated by simulation study. The result has been used to determine stresses in power circuit components and to evaluate satisfactory post–fault steady-state operating region.

Smith [4] in 1997, have developed a real time condition monitoring method to detect the intermittent loss of firing pulses of an individual switching device in 3-phase PWM inverter induction motor drives. The method is based on the time-domain response analysis of the induction motor current space vector and is claimed to be adaptive to changes in the operating point during variable-speed operation.

Blaabjerg [33] also in 1997, proposed a new topology for low cost, fully fault protected 3-phase PWM-voltage source inverter with true phase current information. The phase current is reconstructed from a dc link current measurement and the output is protected by a special arrangement in the dc link. This paper also proposed a new method to ensure a reliable and correct phase current reconstruction. The acquisition technique has added a

controlled dc link sampling, which gives a noiseless sampling and a correct average value of the phase current.

Retiere in [34] demonstrated a VSI fault detection scheme based on space vector technique. This technique utilised voltage and flux vectors, in order to detect the inverter leg short circuit and single gate-turn-off thyristor (GTO) short circuit. He showed that the space vector offers a great potential to detect the consequences of GTO faults with respect to initial condition, the machine parameters and the control strategy. Such faults can cause severe electrical and mechanical damage. A 5 kW induction motor had been used to validate his approach.

In 1998, Mendes [35] described a Park's vector approach on detecting and diagnosing the 3-phase inverter fault in variable speed ac drives. The phase currents are used as an input to the Park's vector system. Power switch faults either an open-circuit or short-circuit are characterised by distinctive patterns of the Park's vector, where angular orientation is associated with the faulty power switch. The location of the faulty device can be obtained using an auxiliary sectogram. The prototype model was built to prove the practicality of this technique.

Filipetti [24] in 2000, suggested that it is possible to use spectrum and instantaneous value of supply currents and voltages for detecting VSI faults in open-loop drive systems. He showed that the significant changes are clearly visible to distinguish between the healthy and faulty condition. Also, he suggested that for closed-loop drives system, more sophisticated procedures and techniques should be adopted in order to assess VSI condition. Advance artificial intelligent (AI) techniques such as genetic algorithm (GA) are highly recommended because they are simple, powerful, general purpose, derivative free, stochastic global optimisation method (search algorithm) inspired by the laws of natural selection and genetics.

2.3 Monitoring Process

Condition monitoring process covers a range of activities starting from data collection to user display. The activities involved can be divided into a number of easily identifiable

functional stages, which are often referred as the elements of a condition monitoring process. In general, condition monitoring and fault detection process can be divided into three main stages: Pre-processing, signal processing and user interface [36,37]. Figure 2-1 below shows the general operation of the condition monitoring and fault diagnosis process.

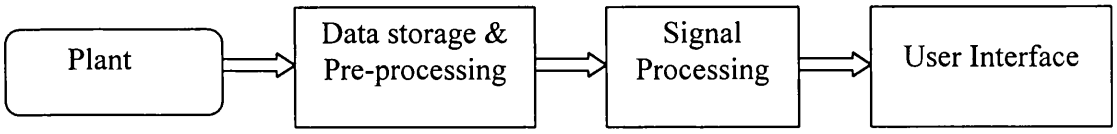

Figure 2-1: General operation of condition monitoring and fault diagnosis.

2.3.1 Pre-processing

Condition monitoring systems depend on sensors for obtaining the information signals. These sensors might measure voltage, currents, vibration, temperature, speed etc. In the case of three-phase induction motor drive system, stator currents and voltages are normally preferred because they allow for the realization of non-invasive diagnostic systems and the sensors required are usually present in the drive.

The pre-processing stage converts the sampled signal to a suitable format for the processing stage. At this stage, sensor failure should be detected. The reliability of the sensors can be increased by monitoring the sensors themselves. Sensor fault detection methods can be divided into direct and model based. The direct method is based on an evaluation of the actual sensor signals while model based methods use information about the monitored system to create an 'analytic' sensor redundancy. Model based methods can identify less prominent sensor faults than the direct method.

2.3.2 Signal Processing

In the processing stage, the condition and type of fault of the system is determined. This can be implemented using several methods. The three basic methods, which are normally used for fault diagnosis of drive, are:

1. Signal processing using model based on first principles
2. Signal processing using feature extraction and pattern recognition
3. Signal processing using knowledge base.

The methods mentioned above use different amounts of process knowledge, as illustrated in Figure 2-2, [36]. The amount of available process knowledge limits the applicable methods. The choice of a method, however, is determined by a required performance and may not require all available process knowledge. It is known that each method has it's own advantages and disadvantages. In the following, they are introduced respectively.

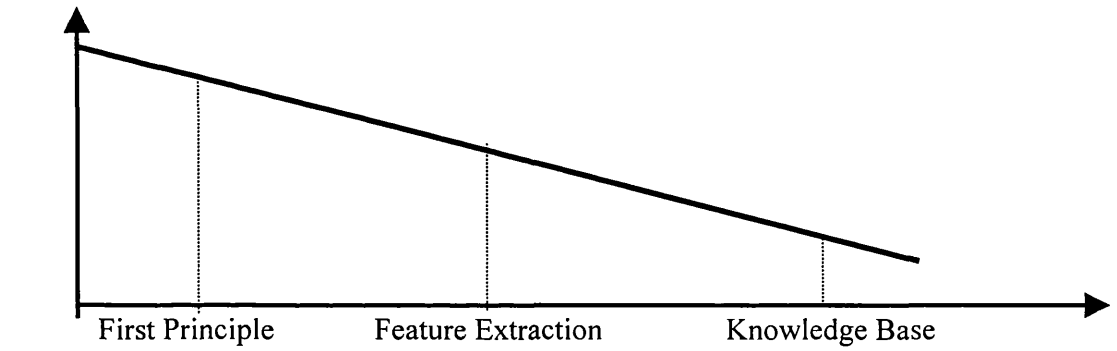

Figure 2-2: Required process knowledge.

2.3.2.1 First Principle Method

The first principle method, known as model based method, uses a mathematical model for generating a description of the behaviour of the system, both for healthy and faulty conditions. Different approaches and techniques for condition monitoring using mathematical models were developed in the last 20 years [38-40]. It include parameter estimation [41-44] and state estimation [45-47].

The parameter estimation technique used the undesired changes of physical parameters to detect and diagnose faults directly. Because of the obvious physical meaning of parameters, this technique is of great advantage to fault diagnosis. One main advantage of

parameter estimation is a drive system can be modelled accurately by balancing the equations [44]. According to the magnitude of parameter change, the degree of seriousness of the fault can be estimated. However, it may be difficult to get the unique physical parameter according to the mapping relationship between the physical parameter and model parameter [48].

On the other hand, the state estimation method makes use of predicted outputs to generate a residual series. Faults can be detected by analysing the information available in the residual series. When the state estimation technique is used, the influence of large modelling error cannot be ignored.

The advantages of first principle method are:

1. Only a limited amount of measured data is needed.
2. Much insight into the behaviour of the system is gained and this information can be used for other applications.
3. The method is well suited for newly design system.

The disadvantages are:

1. The model is only an approximation of the real system.
2. Through process knowledge is needed for development of the model.
3. Only a limited subset of faults can be modelled.

2.3.2.2 Feature Extraction and Pattern Recognition Method

Feature extraction and pattern recognition method, typically using statistical analysis are widely used to solve various fault diagnosis problems [49]. These methods are based on the classification and recognition of signal waveform. The classification is done by matching (part of) the signal with a set of reference signals [50,51]. The sensor signal will be classified a member of the class that corresponds with the best matching reference signals.

The isolation of part of the signal that is unique for the classes results in a better control of the classification problem. The influence of fluctuations in the signal that are caused by

instabilities and noise will be reduced to a minimum. The process of isolating these parts of the signal is called the feature extraction process, while the matching process is known as pattern recognition [36].

This method is suitable to monitor the system for which an accurate model is not available. But, some mathematical descriptions or a look-up table are required for each feature that corresponds with a fault, over a wide range of operating condition.

Several faults can be detected independently using the same signal if there is no correlation between the patterns of the features for the different faults. Further, this method can be extended with new functions for the detection of new faults without changing the existing condition monitoring and fault diagnosis system.

The advantages of the feature extraction and pattern recognition method are:

1. The method is suitable for the system when a mathematical model is not available.
2. Little process knowledge is required.
3. The detection algorithms are only triggered by predefined patterns of the sensor signals. This reduces the noise influence.

The disadvantages are:

1. Detailed knowledge of the behaviour of the signal is needed to determine which parts of the signals are relevant.
2. Measurement data of faults are required.
3. High performance computing techniques might be needed.

2.3.2.3 Knowledge Based Method

Method based on knowledge, also known as an artificial intelligent (AI) include expert system [52,53], neural network (NN) [54-57], fuzzy logic (FL) [32,58-60], fuzzy-neural [61,62] and genetic algorithm (GA). In knowledge based systems, several quantities can be utilised as an input function such as currents, voltages, vibration and magnetic field. Also, fault detection and evaluation can be accomplished without an expert [63]. The

essence of an expert system is the ability to manage knowledge based production rules that model the physical system [64].

The neural networks are general non-linear function approximators. This function is achieved by using an appropriate network built up from artificial neurons, which are connected by appropriate weights. However, the exact architecture of a NN is not known in advance, which usually obtained after a trial and error method. NN are able to learn expert knowledge by being trained using representative sets of data. At the beginning of a NN's training session, the NN will not be accurate. An error quantity is measured and used to adjust the neural network's internal parameter in order to produce more accurate output decisions. This process is repeated until a suitable error is achieved. Once the network is sufficiently trained and parameters have been saved, the NN's contain all the necessary knowledge to perform their tasks [65-68,90].

Fuzzy logic systems are expert, rule-based systems, but they can also be considered to be general non-linear function approximator. In contrast to NN, FL give a clear physical description of how the function approximation is performed [69-71]. The details on FL are given in the Appendix A.

Fuzzy-NN technique is basically NNs with fuzzy features [72]. Neural networks are used to tune membership functions of fuzzy systems that are employed as decision-making systems. Although FL can encode expert knowledge directly using rules with linguistic labels, it usually takes a lot of time to design and tune the membership function, which quantitavely define these linguistic labels. Neural network learning techniques can automate this process and substantially reduce development time and cost while improving system performance.

The genetic algorithm can solve the problem that do not have a precisely defined solving method, or if they do, when following the exact solving method would take far too much time. GA works by creating many random solutions to the problem at hand. Being random, these starting solutions are not very good: schedules overlap and itineraries do not traverse every necessary location. This population of many solutions will then be subjected to an imitation of the evolution of species. All of these solutions are coded as a series of zeroes and ones. The evolution like process consists in considering these 0s and

1s as genetic chromosomes that, like their real life, biological equivalents, will be made to mate by hybridisation, also throwing in the occasional spontaneous mutation. The offspring generated will include some solutions that are better than the original, purely random ones. The best offspring are added to the population while inferior ones are eliminated. By repeating this process among the better elements, repeated improvements will occur in the population, survive and generate their own offspring. Further reading about GA is recommended in [73-76].

The advantages of knowledge based method are:

1. Very fast. This is useful for real-time systems.
2. Little process knowledge is needed.
3. Robust, especially regarding noise.

The disadvantages are as follow:

1. An extensive set of measured data is required for all classes of conditions, including faults.
2. Training period especially neural network is time consuming.

2.3.3 User Interface

Once the pre-processing and processing stages have been done, the result should be presented to the user/operator. The use of screens can improve the presentation of information significantly. The regular process variables and the condition monitoring diagnosis should be displayed. Furthermore, the best maintenance advice also should be given.

The design of the user interface should be ergonomic and user friendly. For condition monitoring systems, it is useful to distinguish between two types of display: survey display and specific display [36]. During normal operation, the survey display presents the status of the system. The specific display will be used during faulty condition.

2.4 Signal Analysis Technique

A variety of other signal processing techniques are available for analysing different types of signals. In what follows, techniques that can be associated to the current signature analysis will be briefly discussed.

2.4.1 Fourier Transform (FT)

The Fourier transform, in essence, decomposes or separates a waveform or function into sinusoidal of different frequency which sum to the original waveform. It identifies and distinguishes the different frequency sinusoids and their respective amplitudes. In many situations, FT-based stator current signature analysis was found the best medium for signature analysis [54 - 59].

Mathematically, Fourier transform can be expressed as

$$F(j\omega) = \int_{-\infty}^{\infty} f(t)\, e^{-j\omega t}\, dt \tag{2.1}$$

Essentially, $f(t)$ is the time-domain signal, which is composed of a sum of sinusoidal waves. $f(t)$ is multiplied by series of rotating phasors $e^{-j\omega t}$, where $\omega = 2\pi f$ and $j=\sqrt{-1}$. $F(j\omega)$ is a complex variable and is known as the Fourier transform of $f(t)$. We can then expand the Fourier transform into its complex form,

$$F(j\omega) = \mathrm{Re}(j\omega) + j\,\mathrm{Im}(j\omega) = \left| F(j\omega) \right| e^{j\varnothing(\omega)} \tag{2.2}$$

$$\left|F(j\omega)\right| = \left[\mathrm{Re}^2(j\omega) + \mathrm{Im}^2(j\omega)\right]^{1/2} \tag{2.3}$$

where $\left|F(j\omega)\right|$ is the amplitude density, or the amplitude spectral density, and $\varnothing(\omega)$ is the phase angle. The Fourier transform can be viewed differently according to the type of signal being handled, and it is particularly useful to consider continuous periodic, non-

periodic signals and discrete signals. These cases will be discussed in the following section.

2.4.1.1 Fourier Series Analysis

Continuous periodic function, such as an analog current or voltage signal, may be represented by a Fourier series consisting of the sum of sine waves whose frequencies are all multiples of the fundamental frequency. The amplitudes of the sine waves are known as the Fourier coefficients. An additional constant term, equal to the mean value of the waveform during the period τ, is included as an effective dc value. The function is expressed mathematically as

$$f(t) = a_o + \sum_{n=1}^{\infty} a_n \sin n\omega t + \sum_{n=1}^{\infty} b_n \cos n\omega t \tag{2.4}$$

$$f(t) = \sum_{n=1}^{\infty} C_n \sin (n\omega t + \theta_n) \tag{2.5}$$

where

$$C_n = \left[a_n^{\,2} + b_n^{\,2} \right]^{1/2}$$

$$\theta_n = \tan^{-1} \frac{a_n}{b_n}$$

$$a_n = \frac{2}{\tau} \int_{-\tau/2}^{\tau/2} f(t) \cos n\omega t \; dt$$

$$b_n = \frac{2}{\tau} \int_{-\tau/2}^{\tau/2} f(t) \sin n\omega t \; dt$$

$$a_o = \frac{1}{\tau} \int_{-\tau/2}^{\tau/2} f(t) \; dt$$

A continuous periodic time function can be therefore represented as a discrete series of frequencies in the frequency domain. Thus, a continuous signal can be represented

(approximately) to a required accuracy by a finite, often small, set of numbers representing frequency, amplitudes and phase shifts. This compaction of data usually allows trends to be easily recognised.

In practical terms, Fourier analysis usually determines the C_n coefficients by two possible methods. This is done, firstly, by passing the time-domain signal through a number of filters tuned to different frequencies, and then measuring the power transmitted at each frequency by an appropriate detector.

Secondly, the Fourier transform can be directly calculated by transforming the continuous signal into a discrete signal, via a sampling process, and then using the Discrete Fourier Transform to calculate the coefficients. It can be easily processed using digital techniques.

2.4.1.2 Discrete Fourier Transform (DFT)

In practice, the Fourier components of the signal are obtained by digital computation rather than by analogue processing. The analogue signals have to be sampled at regular intervals and the sampled values then, converted into digital form. This is normally achieved by using a sample-and-hold circuit, followed by an analogue to digital (A/D) converter. Provided that the number of samples recorded per second is adequate, the waveform will be fully represented. The theoretically necessary sampling rate is called the *Nyquist rate frequency*, and this is given by $2f_{max}$, where f_{max} is the frequency of the highest frequency sinusoidal component in the original signal of significant amplitude.

Under these considerations, the equivalent equation to that given in equation (2.1) becomes,

$$F(j\omega)=\frac{1}{N}\sum_{n=1}^{N-1} f(nT)\, e^{-jkn\omega T}\ , k = 0,1,2,3,.....,N-1 \qquad (2.6)$$

and the corresponding inverse transform is,

$$f(t) = \sum_{k=1}^{N-1} F(j\omega)\, e^{j2\pi nk/N} \qquad (2.7)$$

where k represents the harmonic number of the transformed component.

In practice, a large number of multiplication and addition operations are required when calculating the discrete Fourier transform (DFT). Each term on the right hand side of the equation (2.6) needs to be calculated and this involves the multiplication of an exponential term (which is always a complex number) by another term, which is either real or complex. Then, the entire product must be added together. Therefore, to calculate N sampled numbers will require N^2 mathematical operations. An algorithm, which can reduce the number of calculations, is the so-called fast Fourier transform (FFT) [17, 77,78]. This algorithm permits an adequate representation in the frequency domain for all forms of time-domain signals.

The main limitation of Fourier analysis is that it is difficult to recognise periodicity in complicated signals, such as in some vibration signals (example, from gear box), which appear as a repetitive harmonic amongst a series of harmonics in the spectral space. Secondly, if at some point in the signal *f(t),* there is a local oscillation (possibly representing a particularly interesting feature), this will contribute to the calculation of the Fourier transform, but its location on the time axis will be lost. There is no way of knowing whether the value of $F(\omega)$, at a particular frequency, is derived from frequencies present throughout the life of signal *f(t)*, or just during one, or a few, selected periods. These drawbacks to the Fourier transform have led to the development of other signal processing techniques.

2.4.2 Higher Order Spectra (HOS)

Higher order spectra is a relatively new tool for signal processing. Several key papers in HOS were published in the 1960's [79-81], but most of these papers took a statistical and theoretical viewpoint of the subject. It was not until the 1970's [82,83],

that researchers started to apply HOS technique to real signal processing problems. That interest has recently been extended to the area of condition monitoring [83-89].

HOS measures are extensions of second-order measures (such as the power spectrum) to higher orders, such as at 3rdand 4th order. The 3rd order polyspectrum is the easiest to compute, and hence the most popular, and is called the *bispectrum*. The 4th order polyspectrum is called the *trispectrum*.

Given a discrete time signal $x(n)$, the DFT of $x(n)$ is defined as

$$X(f) = \sum_{n=-\infty}^{\infty} x(n)\, e^{-2j\pi n} \tag{2.8}$$

The well known second-order measure, the power spectral density (PSD) $P(f)$ of $x(n)$ can be defined in terms of $X(f)$ as

$$P(f) = E[\, X(f)\, X^{*}(f)\,] \tag{2.9}$$

where E[] is the statistical expectation, or average, and $X^{*}(f)$ is the complex conjugate of $X(f)$. The PSD is a linear transform and is a function of the frequency index f. Extending these definations to third and fourth-order measures, gives rise to the bispectrum $B(f_1, f_2)$ and trispectrum $T(f_1, f_2, f_3)$, defined as

$$B(f_1, f_2) = E[\, X(f_1)\, X(f_2)\, X^{*}(f_1 + f_2)] \tag{2.10}$$

$$T(f_1, f_2, f_3) = E[\, X(f_1)\, X(f_2) X(f_3)\, X^{*}(f_1 + f_2 + f_3)] \tag{2.11}$$

From equations (2.10) and (2.11), it may be seen that, unlike the PSD, the bispectrum and trispectrum are functions of more than one frequency index. Further, it may also be seen that they are complex quantities, which contain both magnitude and phase information about the original time series.

The bispectrum detects the phenomenon known as *quadrant phase coupling* (QPC). QPC occurs among the three frequencies f_1, f_2 and $f_1 + f_2$, when the phases of the three frequency components sum to zero, i.e, $\varnothing_{f1} + \varnothing_{f2} = \varnothing_{f1+f2}$. QPC is indicated by a peak in the bispectrum at the *bifrequency* $B(f_1, f_2)$ and when the associated biphase $\Phi(f_1, f_2)$ tends to zero.

Similarly, the trispectrum detects the presence of *cubic phase coupling* (CPC). CPC occurs among the four frequencies f_1, f_2, f_3 and $f_1 + f_2 + f_3$, when the phases of the four frequency components sum to zero, i.e, $\varnothing_{f1} + \varnothing_{f2} + \varnothing_{f3} = \varnothing_{f1+f2+f3}$. CPC is indicated by a peak at the *trifrequency* $B(f_1, f_2)$ and by the associated triphase $\Phi(f_1, f_2, f_3)$ approaching zero.

The bispectrum and trispectum have been proved in [88,89] as the optimum tools for detecting phase coupling when the induction motor drive is considered to be a simple system.

2.4.3 Introduction To Wavelet Transform (WT)

Wavelets are functions that satisfy certain mathematical requirements and are used in representing data or other functions. This idea is not new. Approximation using superposition of functions has existed since the early 1800's, when Joseph Fourier discovered that he could superpose sines and cosines to represent other functions. However, in wavelet analysis, the *scale* that is used to look at data plays a special role. Wavelet algorithms process data at different *scales* or *resolutions.* If a signal is look at a large "window", one would notice gross feature. Similarly, if a signal is look at a small window, the small features will be noticed. The result in wavelet analysis is to see both the forest *and* the trees, so to speak. This feature makes wavelets interesting and useful.

The wavelet analysis procedure is to adopt a wavelet prototype function, called a *mother wavelet.* Temporal analysis is performed with a contracted, high-frequency version of the prototype wavelet, while frequency analysis is performed with a dilated, low-frequency version of the same wavelet. Because the original signal or function can be represented in terms of a wavelet expansion (using coefficients in a linear combination of the wavelet

functions), data operations can be performed using just the corresponding wavelet coefficients. The best wavelets are adapted to the data, or truncate the coefficients below a threshold, the data is sparsely represented. This sparse coding makes wavelets an excellent tool in the field of data compression. The detailed discussion about WT will be given in Chapter 5.

2.4.4 Park's Vector

A two dimensional representation can be used for describing three-phase VSI phenomena, a suitable one being based on the current Park's vector [21,35]. As a function of mains phase variables (i_a, i_b, i_c), the current Park's vector components (i_d, i_q) are;

$$i_d = \sqrt{\frac{2}{3}}\, i_a - \frac{1}{\sqrt{6}}\, i_b - \frac{1}{\sqrt{6}}\, i_c \tag{2.12}$$

$$i_q = \frac{1}{\sqrt{2}}\, i_b - \frac{1}{\sqrt{2}}\, i_c \tag{2.13}$$

Under ideal conditions, three-phase current lead to a Park's vector with the following components

$$i_d = \frac{\sqrt{6}}{2}\, i_M \sin \omega_s t \tag{2.14}$$

$$iq = \frac{\sqrt{6}}{2}\, i_M \sin(\omega_s t - \frac{\pi}{2}) \tag{2.15}$$

where iM is the maximum value of supply current and ωs is the supply frequency. Its representation is a circular pattern centred at the origin of the coordinate, as illustrated by Figure 2-3 [35]. The identification of fault (in this case, power switches open-circuit fault) can be obtained by determining the sector of the fault-finding sectogram, as shown in Figure 2-4.

2.5 Summary

In this Chapter, the overview of the condition monitoring and fault detection has been presented. The condition monitoring process covers a range of activities starting from data collection to user display. In general, it can be divided into three main stages: Pre-processing, signal processing and user interface. The following are the main points made in this Chapter.

1. Electrical drive faults, are normally preceded by a deterioration of the electrical characteristic of the drive. If this deterioration can be detected by measurement, then an observation of this degradation will be a valuable means of monitoring when catastrophic breakdown occurs.

2. To achieve a high degree of accuracy in detection and fault identification, a suitable signal processing technique must be applied. A variety of signal processing techniques are available such as Fourier transform, higher order spectra, wavelet transform and park's vector.

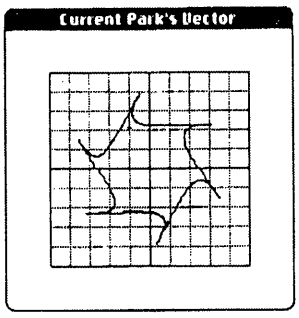

Figure 2-3: Park's vector pattern for healthy voltage source inverter.

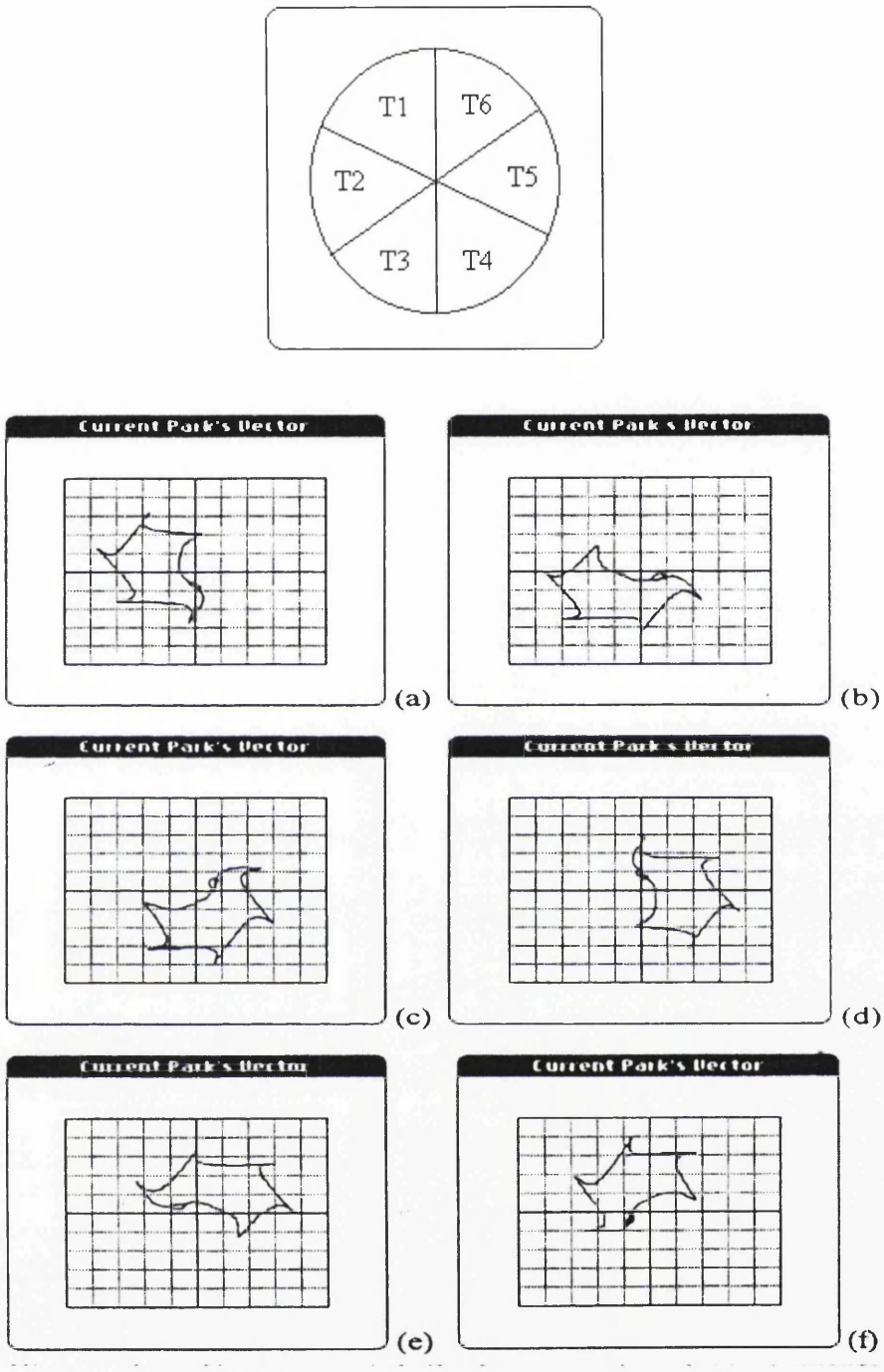

Figure 2-4: Transistor base drive open-circuit fault finding sectogram (a) T1, (b) T2, (c) T3, (d) T4, (e) T5 and (f) T6

CHAPTER 3

VOLTAGE SOURCE INVERTER AND PWM SWITCHING TECHNIQUES

3.1 Introduction

The function of the inverter circuit is to generate an ac output close to sinusoidal shape with controllable magnitude and frequency. A variable output voltage can be obtained by varying the gain of the inverter whereas the switching frequency is determined by the rate at which the semiconductor devices are switched on and off. This can be accomplished by pulse-width-modulation (PWM) within the inverter circuitry [92-97, 108].

The inverter circuits can be classified as either voltage source inverter (VSI) or current source inverter (CSI). In the case of VSI, the inverter is supplied by a constant or low impedance dc voltage source such as a battery or a rectifier and independent of the load current drawn. On the other hand, the current-source inverter (CSI) is supplied with a controlled current from a dc source with high impedance [98-104]. In the present work, only the VSI is considered throughout the thesis. The VSI can be single-phase or three-phase, depending on the application as depicted in Figures 3-1 and 3-2 respectively.

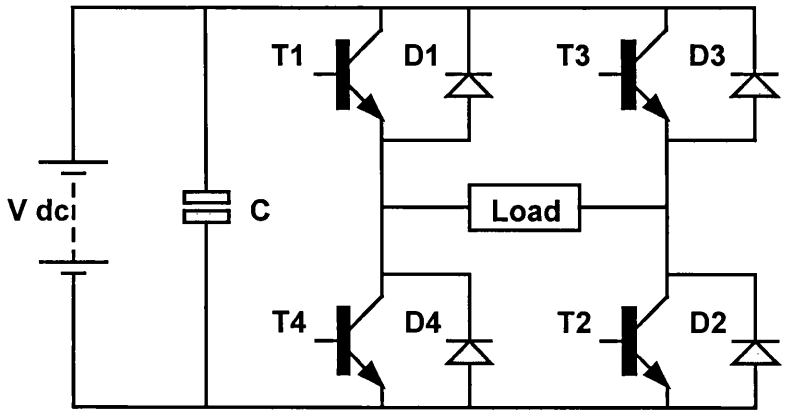

Figure 3-1: Single-phase bridge inverter.

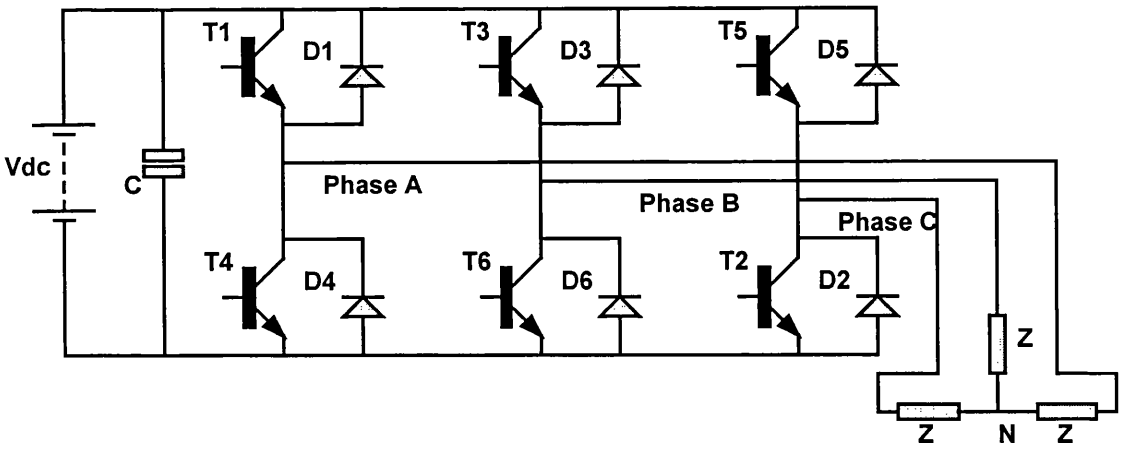

Figure 3-2: Three-phase bridge inverter.

3.2 Single Phase Bridge VSI Inverter

The basic circuit of single-phase bridge VSI inverter is shown in Figure 3-1. It consists of four power switching devices acting as choppers. The feedback diodes are connected across the devices to provide a return path for the current in the case of an inductive load. The shunt capacitor C is used to filter out the ac ripple and provides a stiff dc source to the inverter.

When transistors *T1* and *T2* are turned on and *T3* and *T4* are turned off at the same instant of time, the input dc voltage V_s appears across the load. If transistors *T3* and *T4* are switched on and *T1* and *T2* are off, the voltage across the load is reversed and becomes $-V_s$. If the aforementioned sequence of switching is kept the same for alternate 180-degree intervals, an alternate output voltage would appear across the load. The gating signals of the four transistors and the output voltage are shown in Figure 3-3. The rms value of the output voltage is given by

$$V_{rms} = \sqrt{\frac{1}{T}\int_0^T (V_{dc})^2 d(\omega t)} = V_{dc} \tag{3.1}$$

For a purely resistive load, the load current has an identical square shape to the output voltage. As a result, the feedback diodes are unnecessary because load current reverses immediately when the output voltage changes polarity.

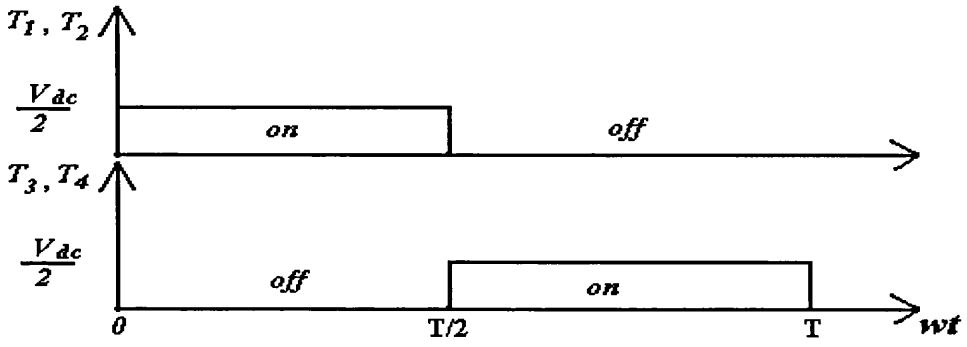

(a)

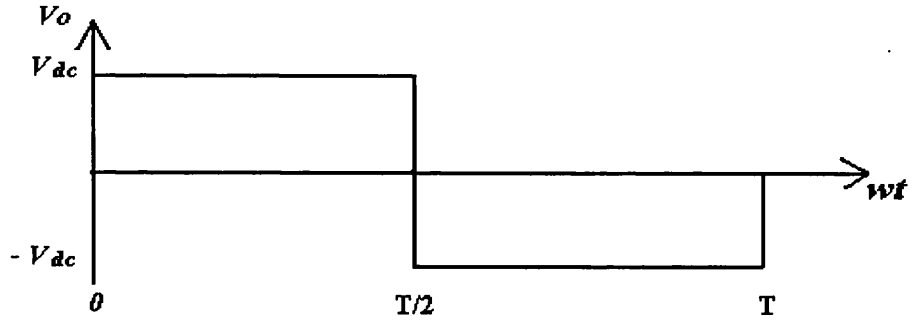

(b)

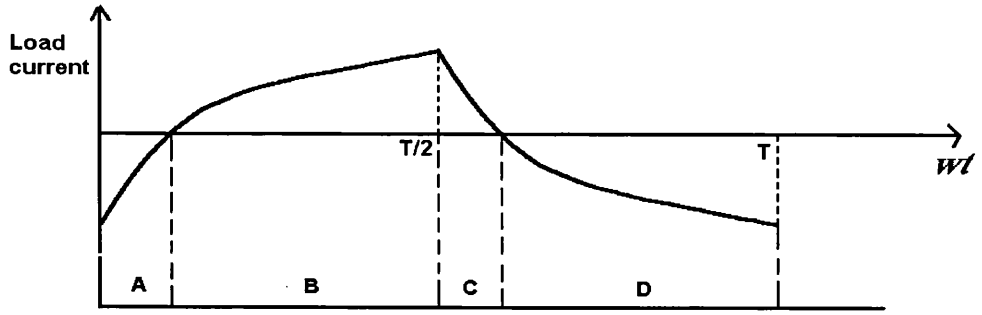

(c)

Figure 3-3: Voltage and current waveforms for a single phase bridge inverter with inductive load; (a) gate signals; (b) load voltage; (c) load current, A= D1, D2, B= T1, T2, C= D3, D4, D= T3, T4

However, if the inverter supplies an inductive load, there will be a phase shift between the load current and the load voltage. Figure 3-3 (c) shows the load current waveform in the case of an inductive load. For an interval when the load voltage changes polarity, the load power becomes negative as the voltage and current have opposite signs. This signifies a reverse power flow from the load to the dc supply through the inverter feedback diodes.

3.3 Three Phase Bridge VSI Inverter

The three-phase bridge inverter has been widely used in high power applications such as variable speed ac motor drives and uninterruptible ac power supplies. Figure 3-2 shows the basic circuit of the three-phase bridge inverter supplied by a dc link from a voltage source and connected to a three-phase balanced ac load. A symmetrical three-phase output is generated by keeping a phase displacement of 120° between the switching sequences in the three arms of the bridge inverter. Two types of operation can be applied to the transistors: 180° conduction or 120° conduction. Throughout the thesis, only the 180° conduction is used.

This mode of operation implies each transistor is to be turned on and off for an interval of 180°. This signifies that each output terminal of the inverter is connected alternately for the same interval to the positive and negative terminals of the dc supply. Three transistors remain on at any instant of time to provide the positive and negative rails for the current. For example, if *T1* is switched on, terminal *A* (phase A) is connected to the positive terminal of the dc input terminal, while if *T4* is switched on, terminal *A* is connected to the negative terminal of the dc input terminal. There are six modes of operation in one cycle and the duration of each mode is 60°. Hence the term *three phase six-step VSI inverter.*

The gating signals for the transistors in the sequence of *T1, T2, T3, T4, T5* and *T6* are shifted from each other by 60° as shown in Figure 3-4. If this type of inverter is used to feed a balanced star connected load, the phase voltage waveform has six steps per ac cycle and is termed a six-step wave. The equivalent circuits for the six steps and the calculation of the phase voltage waveforms are presented in Appendix B. Resulted phase

and line-to-line voltage waveforms in the case of three phase balanced resistive load are depicted in Figure 3-5. However, these waveforms are not load dependent and they are valid for any balanced three-phase linear load or ac motors.

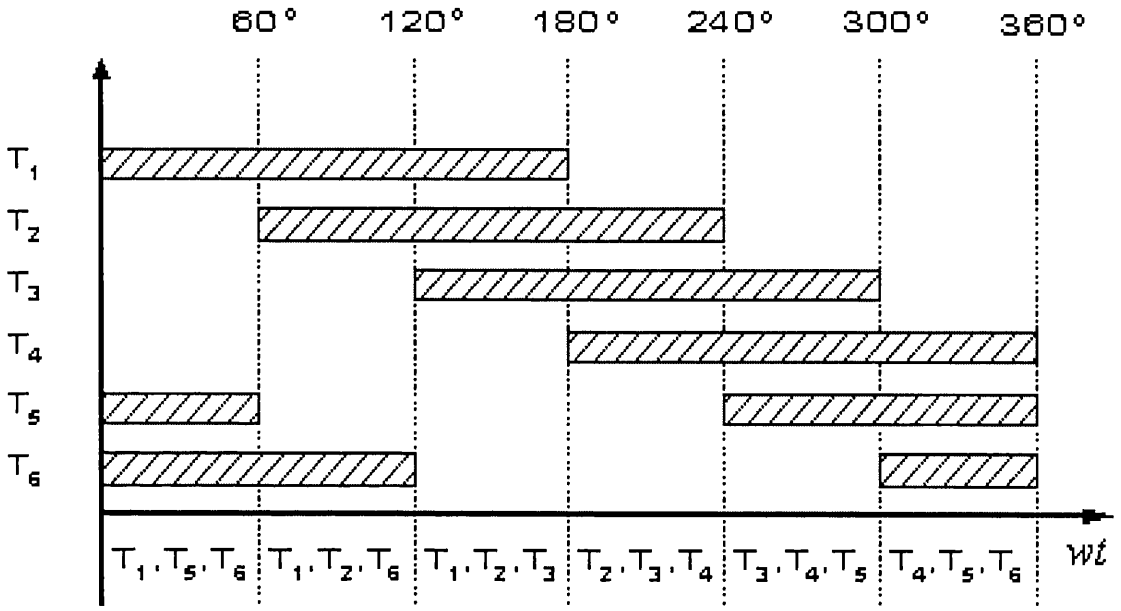

Figure 3-4: Gating signals for 180° operation.

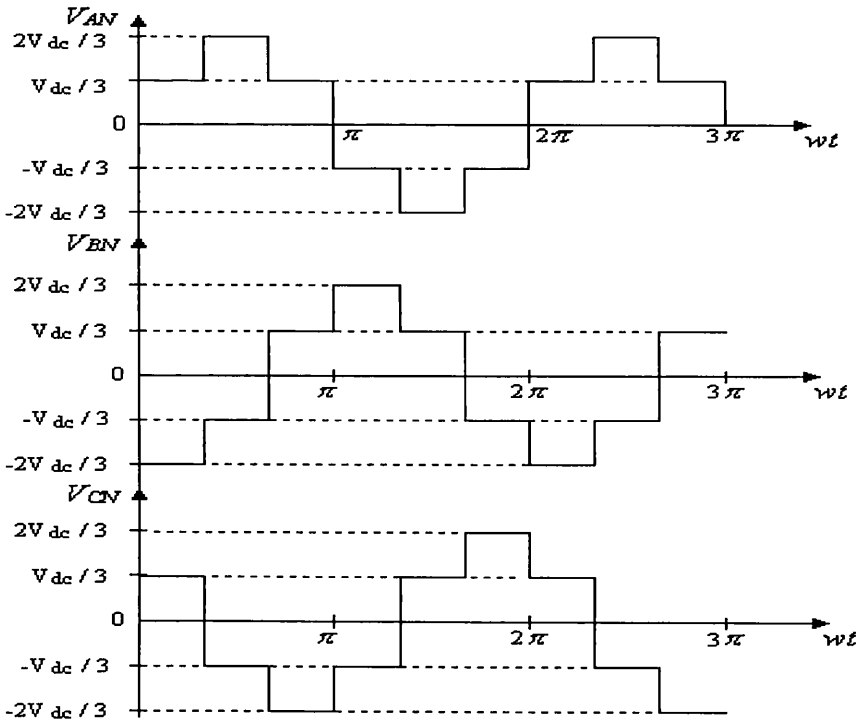

(a)

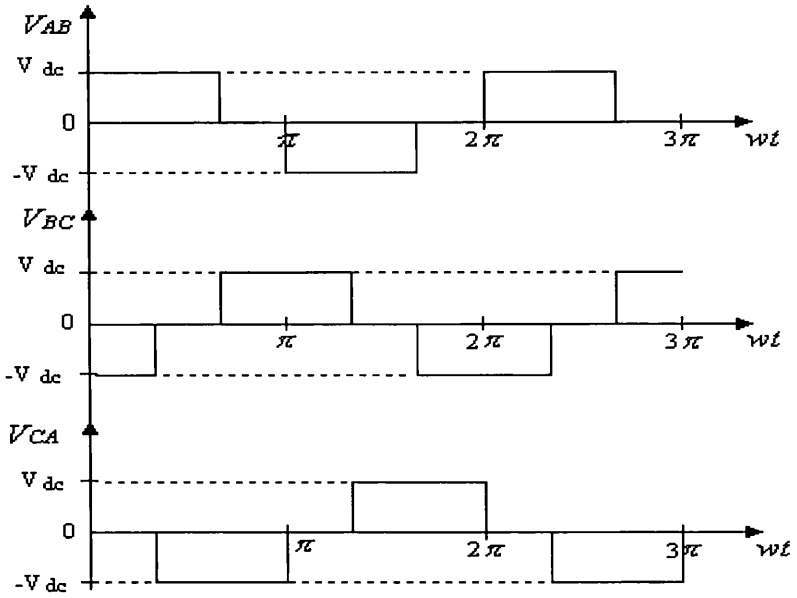

(b)

Figure 3-5: Voltage waveforms for six-step VSI with 180 ° operation; (a) phase voltages; (b) line-to-line voltages.

3.4 PWM Switching Techniques

As previously mentioned in section 3.1, the semiconductor devices are switched on and off in order to control the output of the inverter. However, the switching action of the inverter normally results in non-sinusoidal ac waveforms. In other words, the output waveform would suffer from the presence of low order harmonics. As a result, the generated power due to the harmonic contents in the waveforms is dissipated as heat and increases the motor (load) temperature, and consequently reduces efficiency.

PWM technique is then identified as a technique that can overcome the mentioned problem. The PWM signals are pulse trains with variable pulse widths. The frequency of a PWM signal must be much higher than that of the modulating signal, the fundamental frequency, such that the energy delivered to the motor and its load depends mostly on the modulating signal [105]. In general, the PWM technique controls amplitude and frequency of the output ac waveforms and at the same time minimises the harmonics content. Several PWM techniques have been developed in the past. The most popular

PWM techniques applied in ac drives are sinusoidal PWM (SPWM), space vector PWM (SVPWM) and current-impressed or hysteresis PWM (HPWM). Only the SPWM is considered throughout the thesis.

3.4.1 Sinusoidal PWM (SPWM)

SPWM refers to the generation of PWM outputs with a sine wave as the modulating signal. In this technique, the modulating signal is compared directly with a high frequency carrier triangular wave and the intersection points define the switching instants of the pulses, as shown in Figure 3-6. The amplitude of the carrier signal is fixed, while the amplitude of the modulating signal is variable. The carrier signal frequency determines the number of pulses per ac cycle and this gives the switching frequency.

As for the harmonic contents in the output voltage waveform, the PWM pushes the harmonics into a higher frequency range around the carrier frequency f_c. In other words, the predominant harmonics would occur as side bands of the carrier frequency f_c and its multiples [98,100,106,107].

As stated before, this type of sampling is only appropriate for analogue implementation and therefore it is not possible to define the pulse widths using direct analytical expression. That is because the switching instants are defined by the instantaneous intersection of the carrier wave and the modulating wave. As illustrated in Figure 3-6, the modulating wave is varying while the sampling process is taken place. This means that the pulse width is proportional to the height of the modulating wave at the instant when switching occurs (t_1 and t_2) [92,94]. Hence, the centers of the resulted pulses are not uniformly spaced. However, according to [94] the pulse width can be defined using a transcendental equation of the form,

$$\delta_p = \frac{T_C}{2}\left[1+\frac{M_a}{2}\{\sin(\omega t_1)+\sin(\omega t_2)\}\right] \tag{3.2}$$

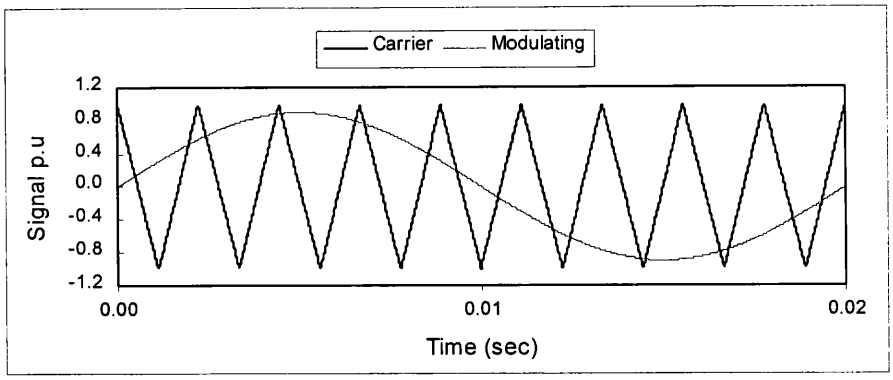

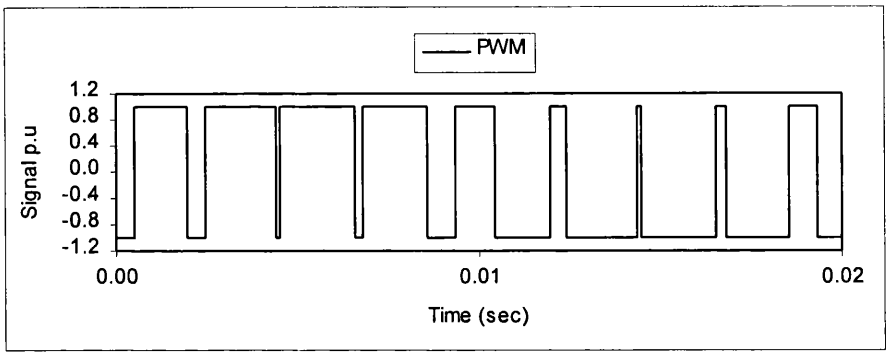

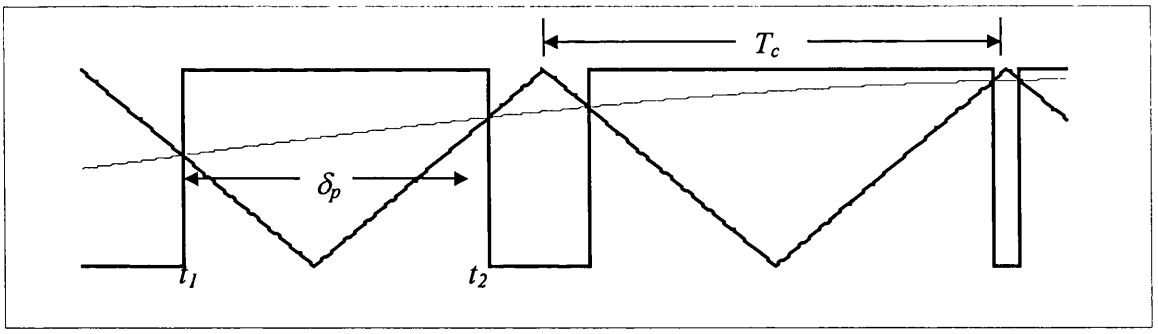

Figure 3-6: 2-level Natural sampling generation

where T_c is the carrier period and M_a is the modulation index. It is also shown in [94] that the switching instants of the pulses are defined via a non-linear equation. Consequently, these equations can be simply solved using numerical techniques such as Newton-Raphson. It should be noted that the PWM waveforms shown in Figure 3-6 swings between two voltage levels +1 and –1, and therefore it is usually referred to as *2-level* PWM waveform [92,94,100]. On the other hand, it is possible to produce a *3-level* PWM waveform by switching between +1, 0 and –1 as shown in Figure 3-7.

The pulse width can be defined using a transcendental equation of the form,

$$\delta_p = \frac{T_C}{2} Ma\{\sin(\omega t_1) + \sin(\omega t_2)\} \tag{3.3}$$

A wide variety of SPWM techniques can be derived from the foregoing 2-level and 3-level natural sampling generation in order to improve the overall system performance and the generated input and output harmonics content. Some of these techniques will be discussed in the following sections.

3.4.2 Modified SPWM

It is clear as shown in Figures 3-6 and 3-7, that the peak output voltage of the SPWM inverter depends on the modulation ratio. Higher output voltage can be obtained by increasing modulation ratio towards 1. However, the inverter output deteriorates when modulation ratio approaches 1. This is because the widths of the pulses that are near the peak of the sine wave do not vary significantly with the variation of modulation ratio, which is due to the characteristics of a sine wave.

SPWM can be modified so that the carrier signal is applied during the first and last 60° intervals per half cycle of the output ac waveform, while the 60° to 120° intervals are kept unmodulated, as shown in Figure 3-8, below. This modified SPWM increases the magnitude of fundamental components compared to the SPWM technique and reduces the number of switching of power devices. However, it generates a low order harmonic component in the output waveform due to the unmodulated interval between 60° and 120° (also between 240° and 300°) [97,99]. Also the hardware implementation is rather complex.

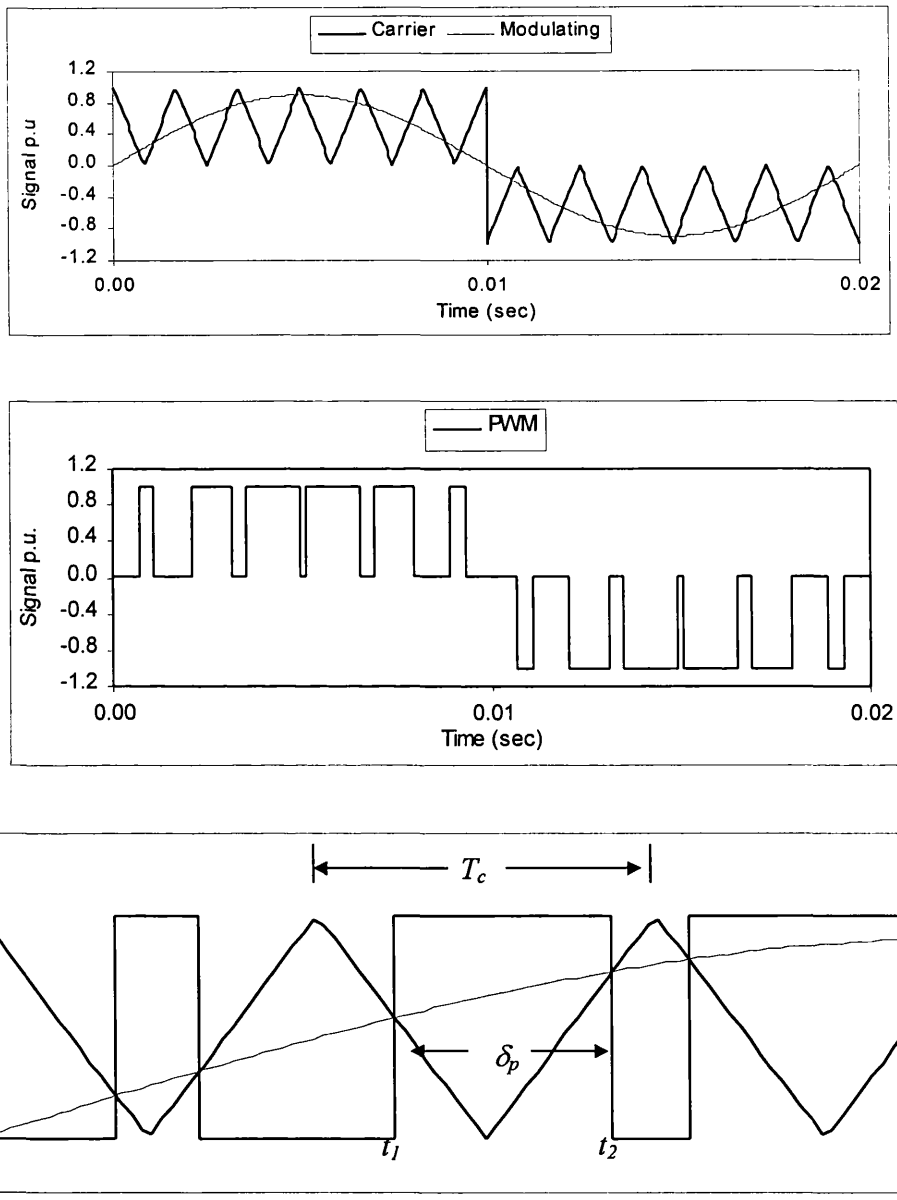

Figure 3-7: 3-level Natural sampling generation

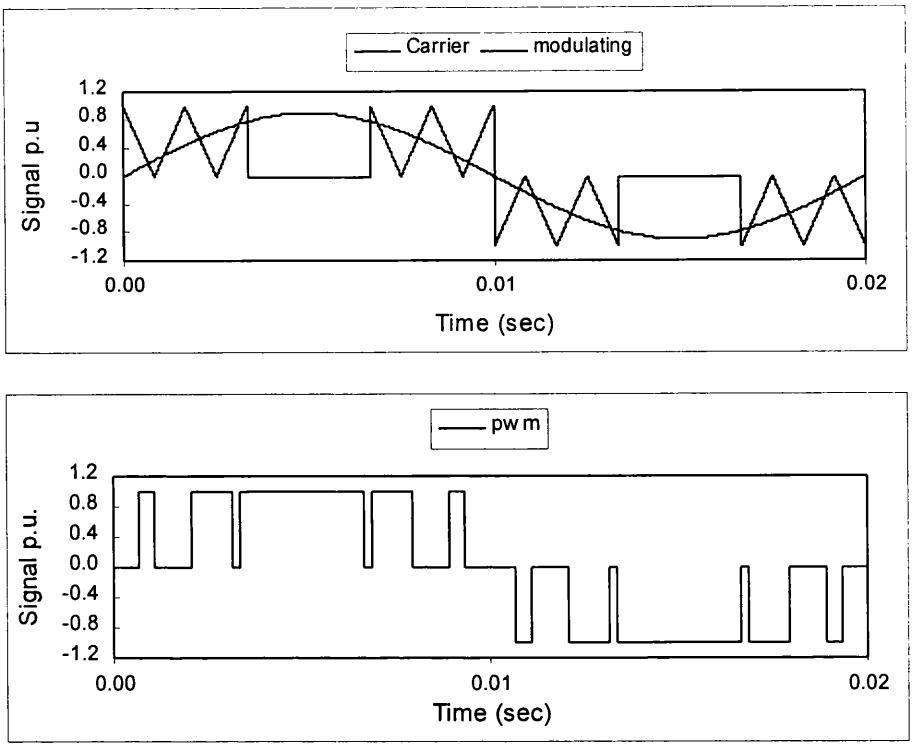

Figure 3-8: Modified SPWM generation.

3.4.3 Third-Harmonic Injection SPWM

This is an improved technique derived from the SPWM through the injection of approximately 17% third harmonic component to the original sine modulating wave. This results in a nearly flat-topped modulating wave that increases the fundamental output voltage by approximately 20%, while maintaining a low harmonic distortion [95,97]. Moreover, it has been shown that the hardware implementation of this technique is quite simple [97]. Furthermore, it should be noted that the addition of the third harmonic to the original modulating signal doesn't affect the quality of the output voltage because the output of the three phase inverter doesn't contain triplen harmonics [97,99]. The modulating wave would be of the form,

$$m(t) = M[\sin(\omega t) + 0.17\sin(3\omega t)] \tag{3.4}$$

The modulating wave with third harmonic injection is shown in Figure 3-9.

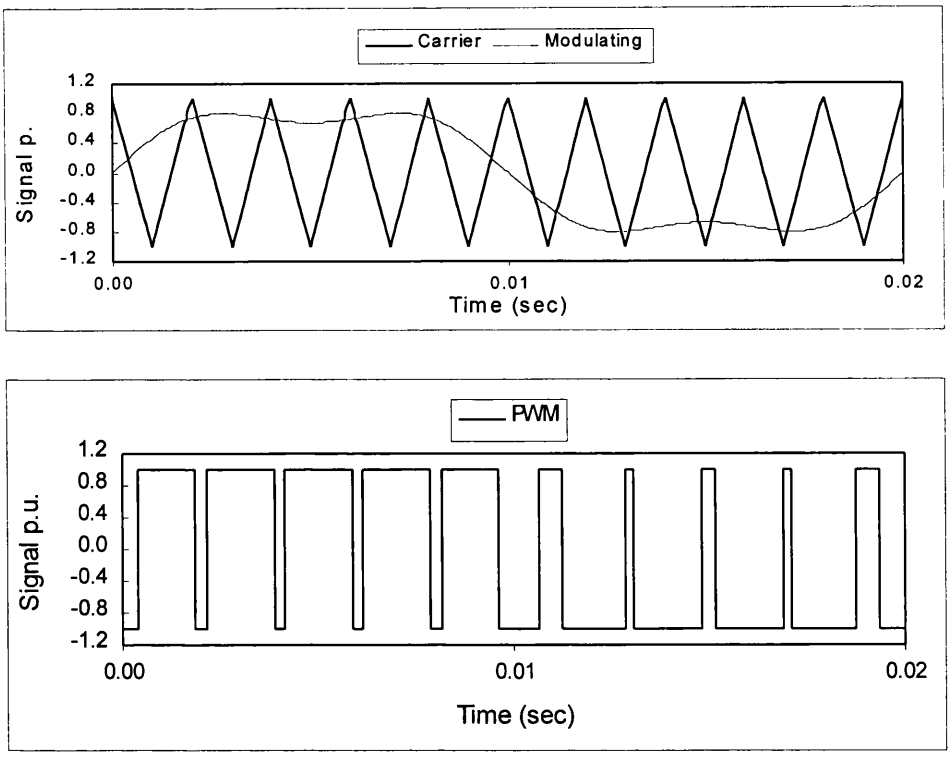

Figure 3-9: 2-level 3rd harmonic injection natural sampling SPWM generation.

3.5 VSI Faults

A voltage source inverter induction motor drive system, as shown in Figure 3-10, can develop various types of faults that can be classified as follows:

- Input supply single line to ground (F1)
- Rectifier diode short-circuit fault (F2)
- Earth fault on dc bus (F3)
- DC link capacitor short-circuit fault (F4)
- Inverter transistor base drive open-circuit fault (F5)
- Inverter transistor short-circuit fault (F6)
- Inverter transistor intermittent misfiring fault
- Line to line short-circuit fault at machine terminal
- Single phasing fault at machine terminal (F7)

Faults may also occur inside the machine itself. The common machine fault is the winding insulation failure, which is due to excessive voltage or current stress, is practically avoided if an inverter power supply is used. This is because the line voltage surges are absorbed at the converter input, and converter over-current protection limits the machine current [3,6].

In this section, only inverter faults, which reduce the operating condition of the motor without involving a drive protection system, will be discussed. They are inverter base drive open-circuit fault, inverter transistor intermittent misfiring fault and single phasing fault at machine terminal.

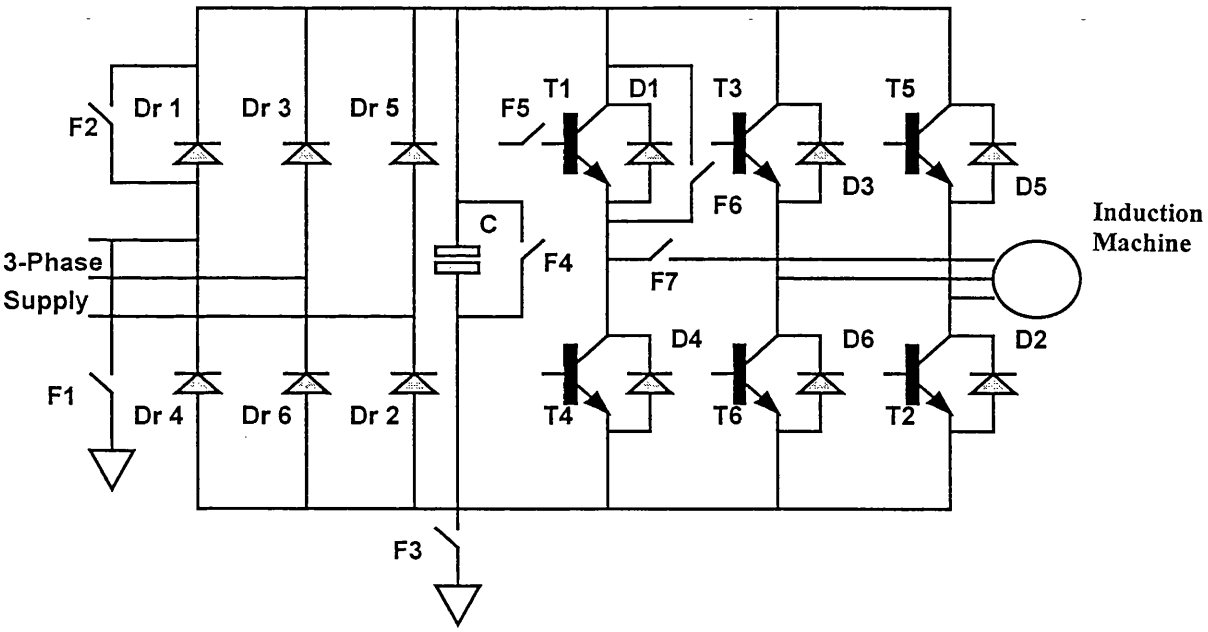

Figure 3-10: A PWM VSI system indicating the possible failures mode.

3.5.1 Inverter Transistor Base Drive Open-Circuit Fault

To operate power transistors such as MOSFETs or IGBTs, an appropriate gate voltage must be applied in order to drive transistors into the saturation mode for low on-state voltage. Malfunctioning of gate drive circuits can lead to the transistor base drive open-circuit fault.

Since the transistor *T1* has now an open-circuit fault (F5), the phase *A* of the induction machine is connected to the positive dc rail through the diode *D1*. The machine phase *A* voltage is then determined by the polarity of current and the switching pattern of transistor *T4*. The phase voltage (V_A) will be clamped to the negative rail if stator current phase *A*, (i_A) is positive. On the other hand, the phase voltage V_A will be clamped to the negative rail when transistor *T4* is switch on, and then to the positive rail when transistor *T4* is off and *D1* is on, if i_A is negative.

The dc offset current in phase *A* will be equally divided between the phase *B* and phase *C* and worsen the current stress of the switching devices in phases *B* and *C*.

If the inverter system is connected to the induction motor, the maximum average torque capability of the drive is substantially reduced because the dc offset will produce a braking torque. Also, interaction between the dc offset component of the stator flux and the fundamental frequency rotor current will cause a fundamental frequency pulsating torque that can be particularly harmful at low operating frequency and low shaft inertia.

3.5.1.1 Circuit Analysis

The circuit considered in this analysis is 180° conduction mode. For this analysis, *T1* is off all the time (*T1* base drive open-circuit fault). These modes of faulty operation are given below in Table 3.1.

If this inverter is used to feed a balanced star connected load, as shown in Figure 3-2, the phase voltage waveform has six steps per ac cycle. The equivalent circuits for the six modes of operation in a full cycle are shown in Figure 3-11. The computation of the phase and line voltages for a single mode of operation can be defined as follows:
During mode 1 for $0° \leq \omega t < 60°$, the phase voltages are:

$$V_{AN} = 0 \tag{3.5}$$

$$V_{BN} = -\frac{V_{dc}}{2} \tag{3.6}$$

$$V_{CN} = \frac{V_{dc}}{2} \tag{3.7}$$

while the line voltages are,

$$V_{AB} = V_{AN} - V_{BN} = 0 - \left(-\frac{V_{dc}}{2}\right) = \frac{V_{dc}}{2} \tag{3.8}$$

$$V_{BC} = V_{BN} - V_{CN} = -\frac{V_{dc}}{2} - \frac{V_{dc}}{2} = -V_{dc} \tag{3.9}$$

$$V_{CA} = V_{CN} - V_{AN} = \frac{V_{dc}}{2} - 0 = \frac{V_{dc}}{2} \tag{3.10}$$

If the same procedures applied to the remaining modes of operations, Table 3.2 is constructed, in which the six step phase and line voltages are given. The phase and line-to-line voltage waveforms in case of inverter transistor base drive open-circuit faults are shown in Figure 3-12. It can be clearly seen from the phase and line voltages that there will be a dc offset and harmonics present. The voltages are unbalanced and non-sinusoidal.

Table 3.1: Switching patterns of three phase bridge inverter using 180° mode of operation for T1 base drive open-circuit fault.

IGBTs Intervals	T_1	T_2	T_3	T_4	T_5	T_6
0° - 60°	off	off	off	off	on	on
60° - 120°	off	on	off	off	off	on
120° - 180°	off	on	on	off	off	off
180° - 240°	off	on	on	on	off	off
240° - 300°	off	off	on	on	on	off
300° - 360°	off	off	off	on	on	on

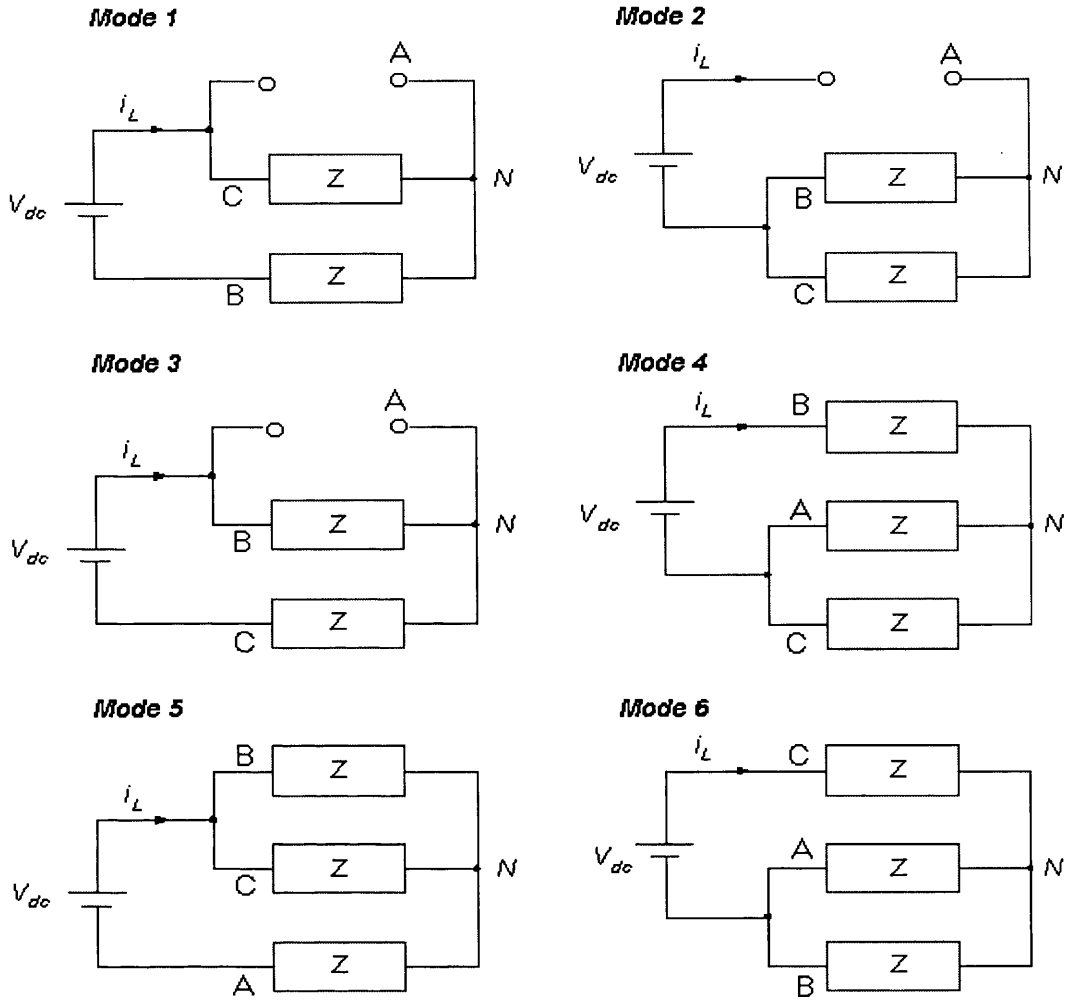

Figure 3-11: Equivalent circuits when T1 base drive open-circuit fault.

Table 3.2: Six-step phase and line voltages for a balanced wye-connected load.

	Mode 1	*Mode 2*	*Mode 3*	*Mode 4*	*Mode 5*	*Mode 6*
V_{AN}	*0*	*0*	*0*	*-1/3 V_{dc}*	*-2/3 V_{dc}*	*-1/3 V_{dc}*
V_{BN}	*-1/2 V_{dc}*	*0*	*1/2 V_{dc}*	*2/3 V_{dc}*	*1/3 V_{dc}*	*-1/3 V_{dc}*
V_{CN}	*1/2 V_{dc}*	*0*	*-1/2 V_{dc}*	*-1/3 V_{dc}*	*1/3 V_{dc}*	*2/3 V_{dc}*
V_{AB}	*1/2 V_{dc}*	*0*	*-1/2 V_{dc}*	*- V_{dc}*	*- V_{dc}*	0
V_{BC}	*- V_{dc}*	0	*V_{dc}*	*V_{dc}*	0	*- V_{dc}*
V_{CA}	*1/2 V_{dc}*	*0*	*-1/2 V_{dc}*	0	*V_{dc}*	*V_{dc}*

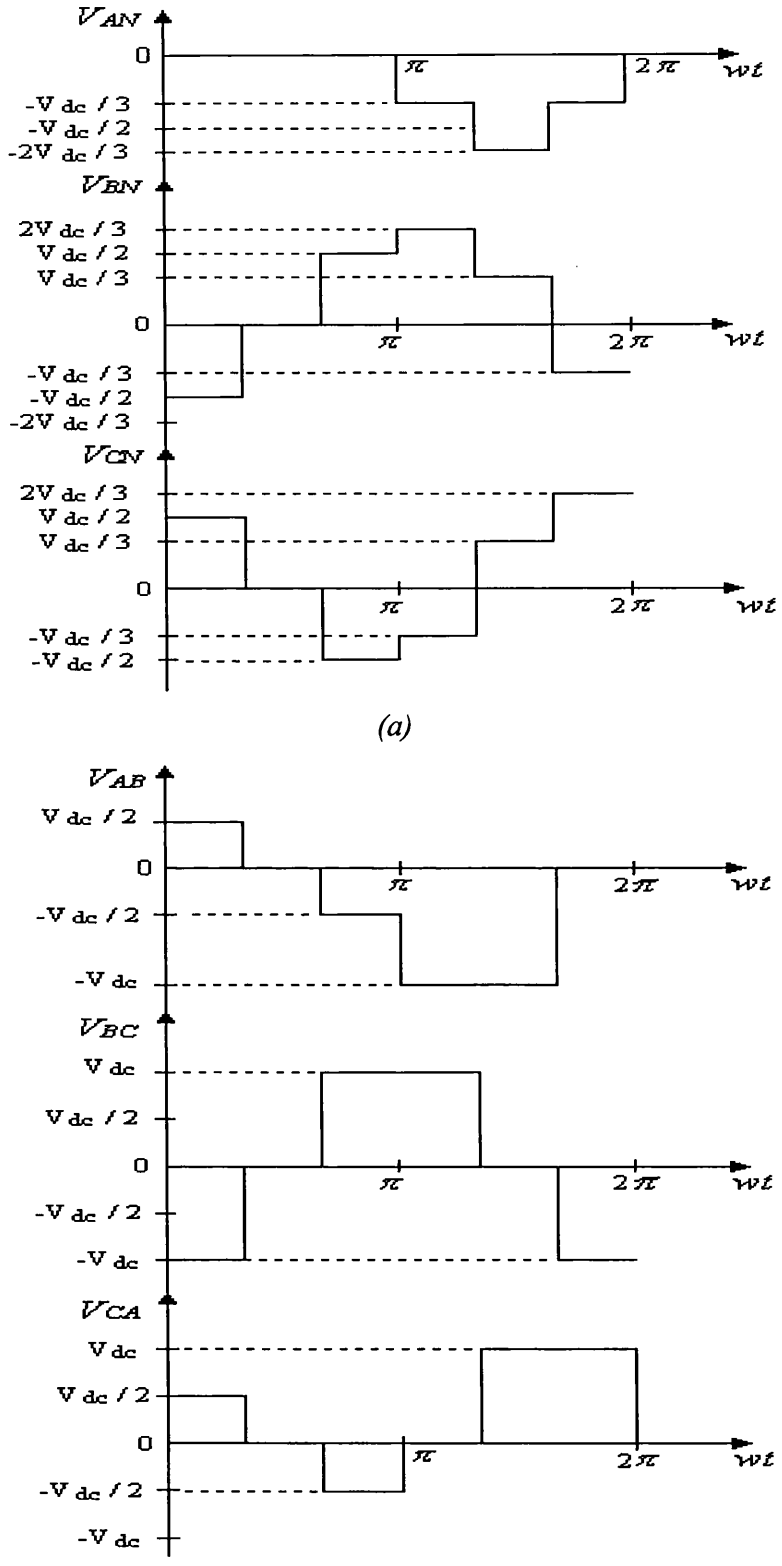

(a)

(b)

Figure 3-12: Voltage waveforms of six-step VSI with 180 ° operation for inverter transistor T1 base drive open-circuit fault;(a) phase voltage; (b) line-to-line voltages.

3.5.2 Intermittent Misfiring

Intermittent misfiring in the inverter is one of the possible faults. The misfiring can be caused by a number of conditions such as a base drive open-circuit fault due to control circuit element deterioration or degraded caused by EMI. Misfiring of one switching device will cause part of the output voltage waveform (positive or negative) to be lost. Therefore, the stator current waveshape will also change following the short duration voltage disturbance.

Denoting the normal three-phase output voltage of the inverter as $V_{ABC}(t)$, a misfiring disturbance can be modeled using an incremental output voltage $\Delta V_{ABC}(t)$, which lasts for a pulsewidth. Depending on the location of the faulty device, vector $\Delta V_{ABC}(t)$ is in one of the A, $-A$, B, $-B$, C and $-C$ directions where A, B and C coincide with the three-phase winding axes. For example, a misfiring fault of switching device $T1$ (during the positive half cycle of phase A) will produce a voltage disturbance in the $-A$ direction, because a positive voltage pulse is lost in the corresponding phase. Therefore, $\Delta V_{ABC}(t)$ can be expressed as a pulse function with known amplitude and duration

$$\Delta V_{ABC}(t) = V_{dc}\, e_{ABC}.\, u(t - t_o)\, [1 - u(t - t_o - \Delta t)] \qquad (3.11)$$

where V_{dc} is the dc-link voltage, e_{ABC} is a unity vector representing the direction of the voltage disturbance in the stator coordinates, $u(t)$ is the unit step function, t_o and Δt indicates the starting instant and duration of the lost voltage pulse [4].

The duration of the fault is dependent on the frequency of the PWM carrier and the reference output voltage. The later switching pattern is not changed by the disturbance. The other two phases of the inverter may be disturbed simultaneously. This fault will over stress other switching devices and degrade the output voltage waveform. The fault occurring at the peak of the output voltage has a more significant effect than that when the reference voltage is crossing zero.

3.5.3 Single Phasing

The condition in which the three-phase motor operates with one of its stator phase open-circuited (F7) is referred to as single phasing, as shown in figure 3-10. In practice, single phasing of three-phase motor can often be the result of one of the supply fuses being blown, commonly by a shoot through fault occurring due to missing blanking pulses in the base drive inverter circuit [6]. Also, a transistor might fail due to current stress or voltage stress. The failure due to current stress occurs when the device is carrying load current whereas the voltage failure occurs when device is switching off the load current or blocking forward voltage.

Following the fault, the three-phase motor can operate in single-phase mode with reduced load torque only if the fault is detected and isolated while the motor is still in motion. The three-phase motor operated in single-phase mode with one phase open-circuit can supply only 33% of rated three-phase motor torque without exceeding machine current rating. Since single-phase motor do not produce starting torque, the special remedial strategies need to be implemented in order to start the motor from the zero speed [6, 91].

3.6 Summary

In this Chapter, the types of voltage source inverters (VSI) for single-phase and three-phase were introduced. Then followed by SPWM techniques. The remainder of the chapter then focussed on various VSI faults. The following are the main points made in this Chapter.

1. An inverter circuit can be classified as either voltage-source or current-source. In the case of the voltage source inverter (VSI), the inverter is supplied by a constant or low-impedance dc voltage source such as a battery or a rectifier. On the other hand, the current source inverter (CSI) is supplied with a controlled current from a dc source with high impedance.

2. There are several typed SPWM techniques to improve the source utilisation and reduce the harmonic contents in the generated current and voltage waveforms.

These techniques can be derived from 2-level or 3-level natural sampling modulation.

3. A voltage source inverter can develop various types of faults. In this research, only the inverter faults, which reduce the operating condition of the motor without triggering the drive protection system is discussed. They are inverter base drive open-circuit fault, inverter transistor intermittent misfiring fault and single phasing fault. These types of faults have a high potential to cause the catastrophic breakdown.

CHAPTER 4

MODELING AND SIMULATION OF INVERTER SYSTEM

4.1 Introduction

In power electronic systems, the simulation is mainly performed to analyse and design the circuit configuration and the applied control strategy. With the help of several powerful computer simulation tools, which are currently available on the market such as MATLAB/SIMULINK and Pspice, the analysis and design process can be very effective. The power electronic circuits can be schematically expressed by using actual power semiconductor device models and passive elements. Furthermore, particularly in MATLAB/SIMULINK, the circuits also can be modelled by using state equations [109-115] and the switching function concept [116-118].

This chapter describes the simulation model for the 3-phase VSI. The model was based on the switching function concept and implemented using the functional block of MATLAB/SIMULINK package. Using the switching functional concept, the power conversion circuits can be modelled according to their function, rather than circuit topologies. Therefore, a simplification of the power conversion circuit can be achieved [118].

4.2 General Theory of Switching Function

The converters/inverters can be modelled as a black box with the input and output ports; dc, ac and control, as shown in Figure 4-1. The dc and ac ports can be inputs or outputs depending on the mode of operation. The control port consists only of inputs. In order to describe the task to be performed by the circuit, the transfer function needs to be obtained, also the transfer function is required to compute a dependent variable in terms of its

respective independent circuit variable. Therefore, the general transfer function can be defined as

$$\text{Transfer Function} = \frac{\text{Dependent Variable}}{\text{Independent Variable}} \tag{4.1}$$

With the applied control strategy, each transfer function consists of the various particular switching functions. Using the switching function theory, the detailed relationship between the input and output variables can be obtained. Therefore, the proper switching function is important in order to describe the role of the static power converters.

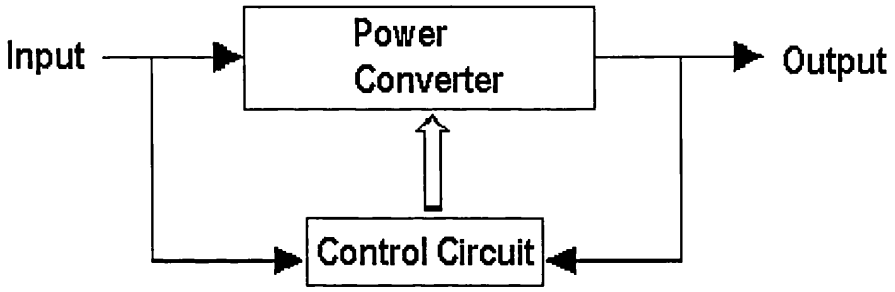

Figure 4-1: Block diagram for the general static power conversion.

4.3 Switching Function for 3-Phase VSI

Figure 4-2 shows the circuit configuration and variables for the VSI circuit. Based on the transfer function theory, input current (I_{in}) and output voltage (V_{AB}, V_{BCc}, V_{CA}) are the dependent variables. While the input voltage (V_{dc}) and output currents (I_A, I_B, I_C) are the independent variables. Therefore, the relationship between the input and output variables can be defined as

$$[V_{AB},\ V_{BC},\ V_{CA}] = TF.\ V_{dc} \tag{4.2}$$

$$I_{in} = TF\left[I_A,\ I_B,\ I_C\right] \tag{4.3}$$

where TF is the transfer function of VSI circuit.

In order to define the switching functions, a control technique to be applied to the system should be selected. In this project, the SPWM technique is used as a control strategy. Two switching functions (SF_1, SF_2) are obtained from SPWM, as shown in Figure 4-3. The switching function SF_1 expresses the output voltage V_{AO}, V_{BO} and V_{CO}. The SF_1 is used to calculate the inverter line-to-line voltages (V_{AB}, V_{BC}, V_{CA}) and the phase voltages (V_{AN}, V_{BN}, V_{CN}). On the other hand, the switching function SF_2 designates the voltage across the switch. It can be used to derive the load currents (I_A, I_B, I_C) as a ratio of voltages and respective impedances.

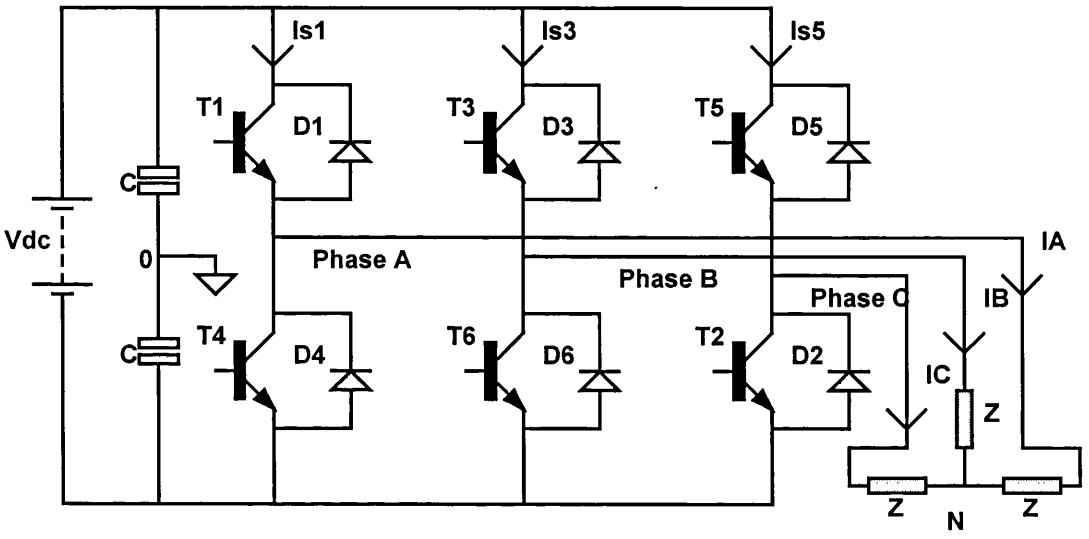

Figure 4-2: Circuit configuration of VSI

Generally, the transfer function consists of the several switching functions as

$$TF = [SF_1, SF_2, ...] \tag{4.4}$$

Based on the above-mentioned theoretical explanation, SF_1 and SF_2 can be expressed as

$$SF_1 = \sum_{n=1}^{\infty} A_n \sin(n\omega t) \tag{4.5}$$

$$SF_2 = B_o + \sum_{n=1}^{\infty} B_n \sin(n\omega t) \tag{4.6}$$

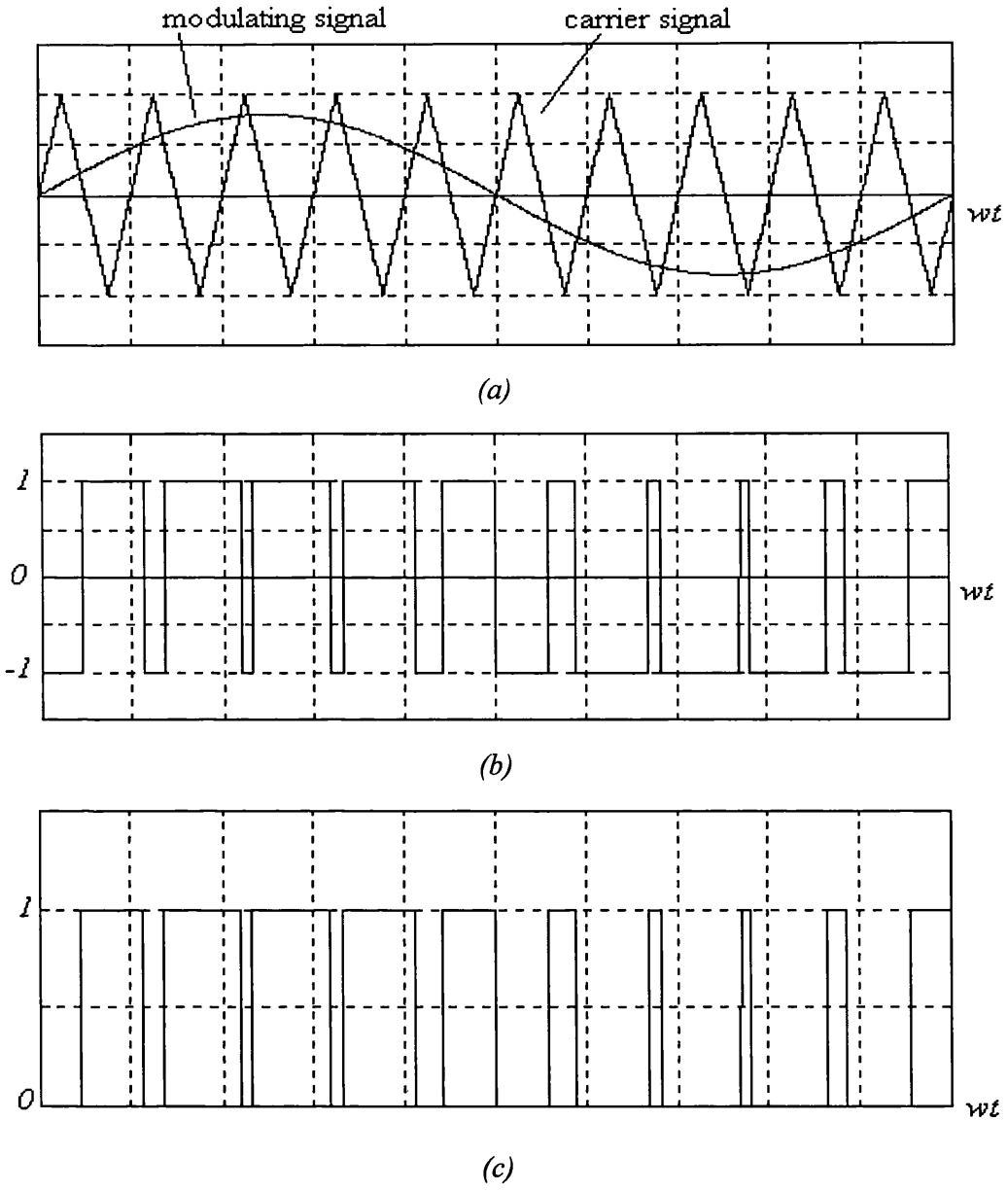

Figure 4-3: SPWM control strategy and switching function. (a) Modulation and carrier signals, (b) Switching function SF_1, (c) Switching function SF_2

For a three-phase VSI system, each phase has two switching functions such as SF_{1_A}, SF_{1_B}, SF_{1_C}, SF_{2_A}, SF_{2_B} and SF_{2_C}. Then, by using the switching function SF_{1_ABC}, the equations for V_{AO}, V_{BO} and V_{CO} can be obtained as

$$V_{AO} = \frac{V_{dc}}{2} SF_{1\_A}$$

$$= \frac{V_{dc}}{2} . \sum_{n=1}^{\infty} A_n \sin(n\omega t) \tag{4.7}$$

$$V_{BO} = \frac{V_{dc}}{2} SF_{1\_B}$$

$$= \frac{V_{dc}}{2} . \sum_{n=1}^{\infty} A_n \sin(n\omega t - 120°) \tag{4.8}$$

$$V_{CO} = \frac{V_{dc}}{2} SF_{1\_C}$$

$$= \frac{V_{dc}}{2} . \sum_{n=1}^{\infty} A_n \sin(n\omega t + 120°) \tag{4.9}$$

Therefore, the inverter line-to line voltage equations can be derived as

$$V_{AB} = V_{AO} - V_{BO} = \frac{\sqrt{3}}{2} V_{dc} \sum_{n=1}^{\infty} A_n \sin n(\omega t + 30°) \tag{4.10}$$

$$V_{BC} = V_{BO} - V_{CO} = \frac{\sqrt{3}}{2} V_{dc} \sum_{n=1}^{\infty} A_n \sin n(\omega t - 90°) \tag{4.11}$$

$$V_{CA} = V_{CO} - V_{AO} = \frac{\sqrt{3}}{2} V_{dc} \sum_{n=1}^{\infty} A_n \sin n(\omega t + 150°) \tag{4.12}$$

From the VSI circuit diagram in Figure 4-2 (balance operating system), V_{NO} is calculated as

$$V_{NO} = \frac{1}{3} (V_{AO} + V_{BO} + V_{CO}) \tag{4.13}$$

Using equations (4.7), (4.8), (4.9) and (4.13), the phase voltages can be written as

$$V_{AN} = (V_{AO} - V_{NO})$$

$$= \frac{2}{3} V_{AO} - \frac{1}{3}(V_{BO} + V_{CO}) \tag{4.14}$$

$$V_{BN} = (V_{BO} - V_{NO})$$

$$= \frac{2}{3} V_{BO} - \frac{1}{3}(V_{AO} + V_{CO}) \tag{4.15}$$

$$V_{CN} = (V_{CO} - V_{NO})$$

$$= \frac{2}{3} V_{CO} - \frac{1}{3}(V_{AO} + V_{BO}) \tag{4.16}$$

Assume the loads connected to the 3-phase VSI are *R-L* loads and balanced. Then, the load currents can be derived as a ratio of the phase voltages and respective impedances as

$$I_A = \frac{V_{AN}}{R + j\omega L} \tag{4.17}$$

$$I_B = \frac{V_{BN}}{R + j\omega L} \tag{4.18}$$

$$I_C = \frac{V_{CN}}{R + j\omega L} \tag{4.19}$$

The switch currents (I_{s1}, I_{s3}, I_{s5}) are calculated by the product of the load currents with their switching function $SF_{2\_A,B,C}$.

$$I_{S1} = I_A \, (SF_{2\_A}) \tag{4.20}$$

$$I_{S3} = I_B \, (SF_{2\_B}) \tag{4.21}$$

$$I_{S5} = I_C \, (SF_{2\_C}) \tag{4.22}$$

4.4 Implementation of Functional Model

Figure 4-4 shows the functional model for 3-phase VSI. The model consists of 6 main blocks: 3Phase_Ref_Signal, PWM, VSI_ Switching_ Function, Inverter_ Circuit, Load_ Currents and Switching_ Currents. A detail blocks description is given below.

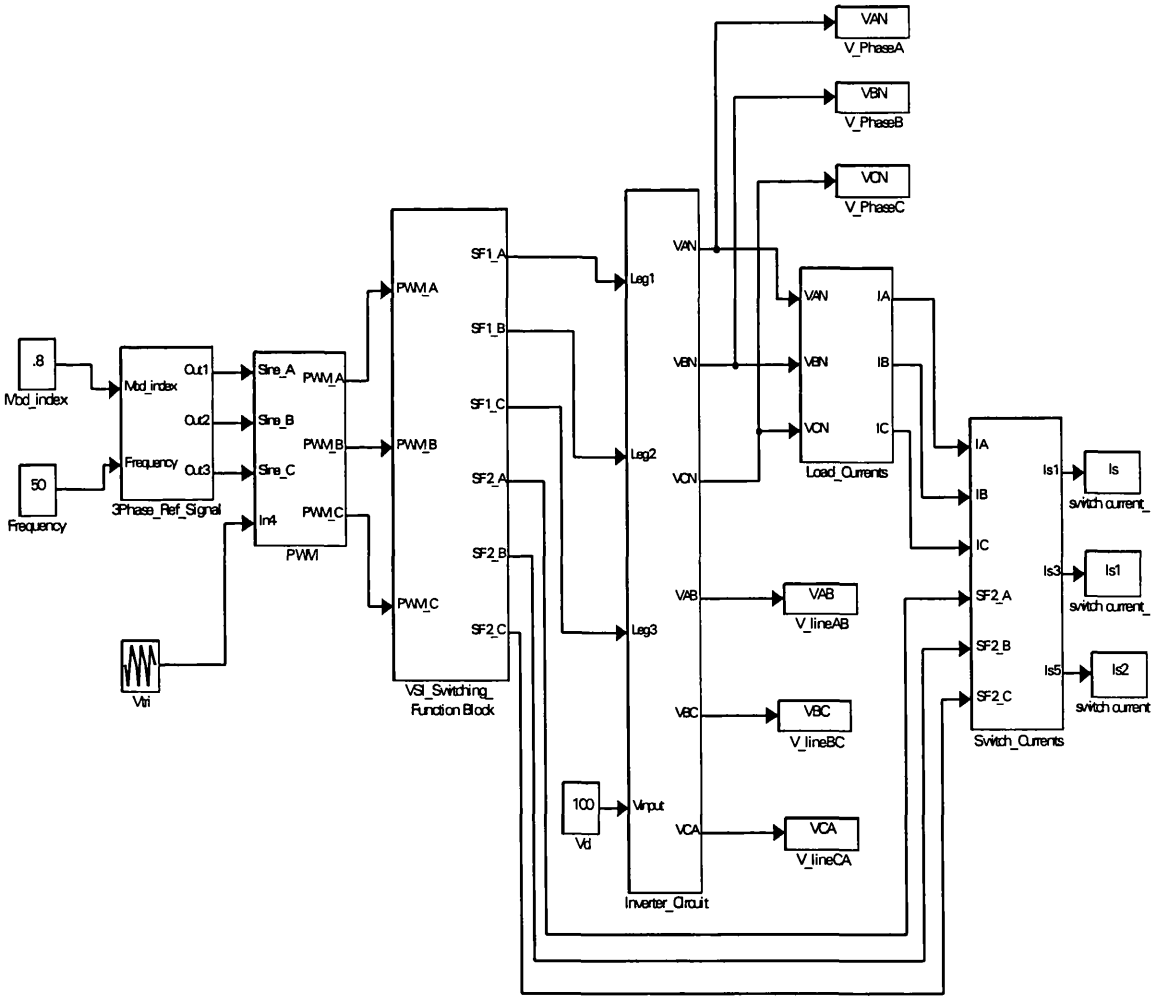

Figure 4-4: Block diagram of simulation model for 3-phase VSI using switching function concept.

3Phase_Ref_Signal block: This functional block produces a 3-phase sinusoidal control signal, as shown in Figure 4-5. The frequency and amplitude of the signal is determined by Mod_index and Frequency blocks.

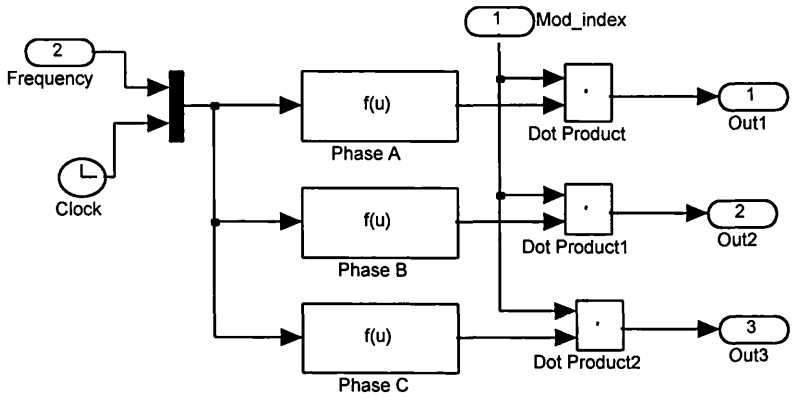

Figure 4-5: The unmask of 3Phase_Ref_Signal block.

PWM block: This functional block generates a PWM signal by comparing a modulation signal and carrier signal, as shown in Figure 4-6. The MATLAB program used to compare the signals is given in Appendix C(i).

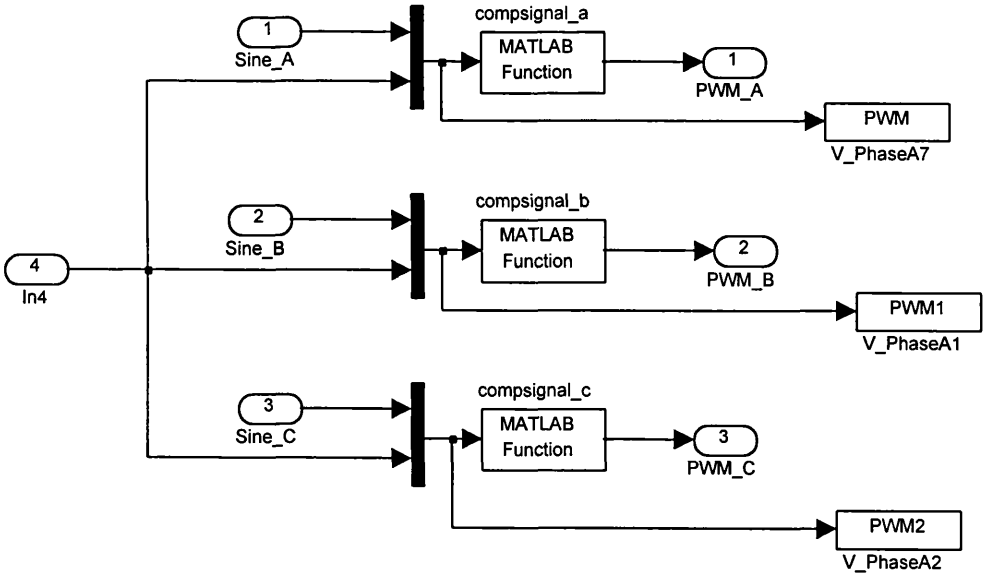

Figure 4-6: The unmask of PWM block.

VSI_Switching_Function block: This functional block implements the switching function concept of VSI. The block accepts three PWM signals and generates two switching function for phase A, phase B and phase C, as shown in Figure 4-7. The MATLAB program used in this block is given in Appendix C(ii).

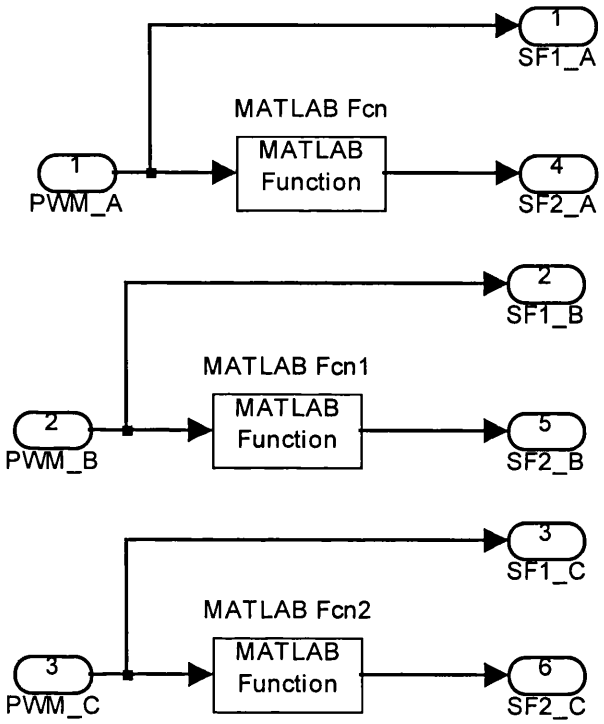

Figure 4-7: The unmask of VSI_Switching_Function block.

Inverter_Circuit block: This functional block performs the 3-phase inverter operation circuit. The dc input is supplied by the vd block (in this project, 80V). The block outputs are: line to line voltages (V_{AB}, V_{BC}, V_{CA}) and phase voltages (V_{AN}, V_{BN}, V_{CN}). The Inverter_Circuit block details are shown in Figure 4-8.

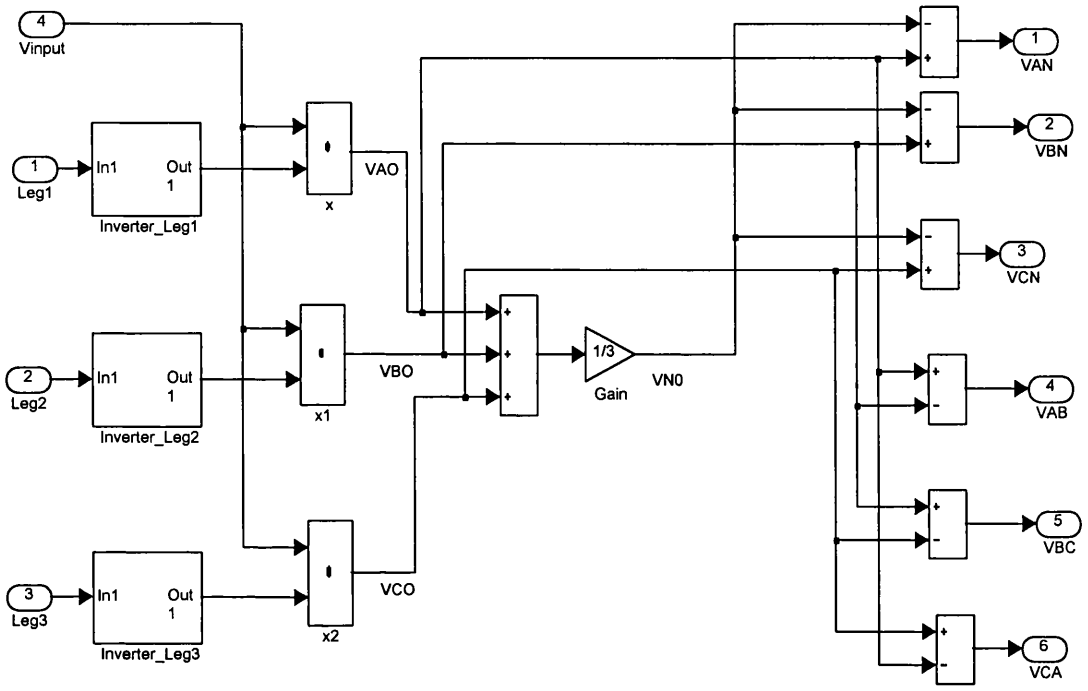

Figure 4-8: The unmask of Inverter_ Circuit block.

Load_Currents block: This block generates the load currents output by implementing the equations (4.17), (4.18) and (4.19), as shown in Figure 4-9. The inputs to the block are phase voltages. The *R-L* loads are assumed to be balanced.

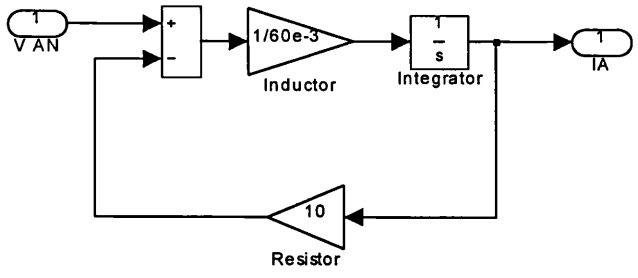

Figure 4-9: The unmask of phase A Load _ Currents block.

Switch_Currents block: This functional block produces the switch current output by multiplying load currents and switching function SF_2. The block diagram is shown in Figure 4-10 below.

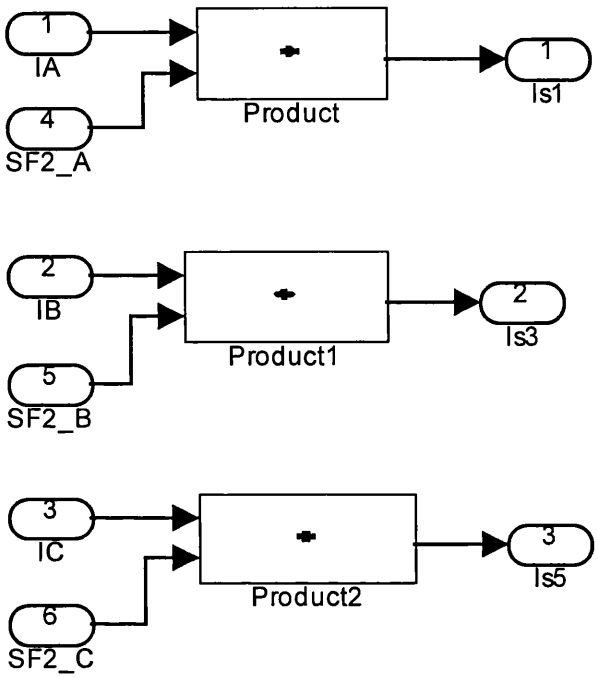

Figure 4-10: The unmask of Switch_ Current block.

4.5 The Simulation Results of 3-Phase VSI

The simulation parameters are as follows: dc link input voltage, V_{dc} = 100V, resistor load , R = 10Ω, inductor load, L =60 mH, carrier signal frequency f_c = 7kHz, modulation signal frequency, f_m = 50Hz. In order to verify the developed model, the system was tested with three different modulation index values, M_a = 0.8, 0.6 and 0.4.

The switching function signals SF_1 and SF_2 for the SPWM control strategy, voltage waveforms and current load waveforms for M_a = 0.8, 0.6 and 0.4 are shown in Figures 4-

11, 4-12 and 4-13, respectively. It can be seen that the load currents are sinusoidal and their amplitude is proportional to M_a.

Figures 4-14 to 4-19 show the simulation results of transistor *T1*, *T2*, *T3*, *T4*, *T5* and *T6* open circuit fault, respectively. The modulation index value is $M_a = 0.4$. As can be clearly seen, this type of fault introduced the dc offset to the currents. Since the system is symmetrical and balanced, a larger dc offset magnitude is observed in faulty phase, and this magnitude is equally divided between the other two phases with opposite polarity.

Due to the dc offset, the stress on the healthy transistor becomes excessive because it now carries the entire phase current. Also, the upper leg and the lower leg of other transistor carries unequal current stress. Such conditions may lead to catastrophic breakdown to the inverter system.

Figures 4-20 to 4-22 show the simulation results of transistor *T1, T2* and *T3* intermittent misfiring fault for 0.01s. The modulation index value is $M_a = 0.4$. It can be seen that the load currents distorted for a while before they returned back to their normal condition.

Figures 4-23 to 4-25 show the simulation results of phase A, phase B and phase C single phasing fault. The modulation index value is $M_a = 0.4$. Inspection of the load currents indicates that no dc offset introduced, but the magnitude of the other two phases are decreased about 14% compared to normal 3-phase condition. This agreed with the equations (4.13), (4.17), (4.18) and (4.19).

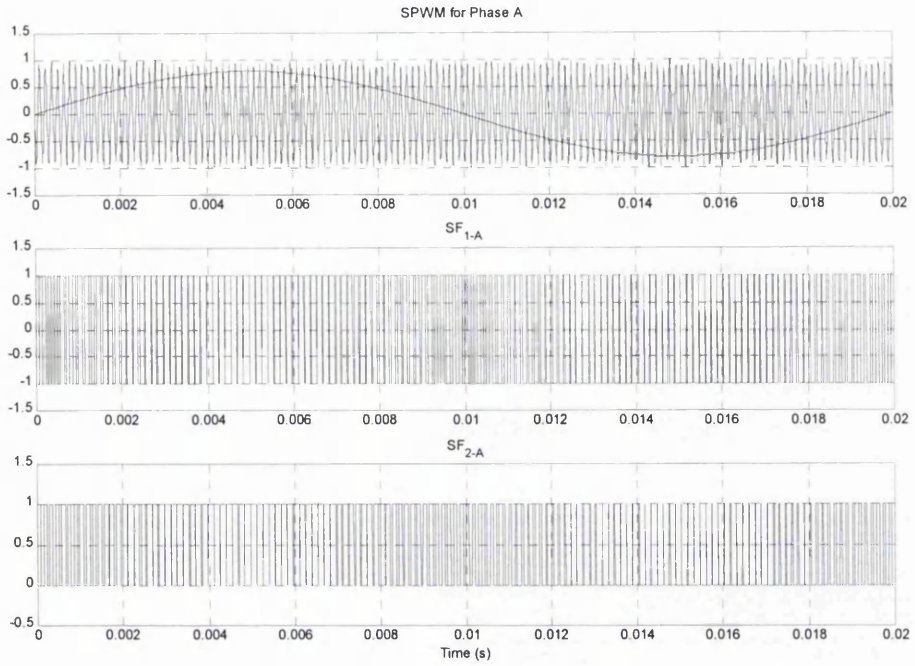
SPWM for Phase A
SF1-A
SF2-A
Time (s)

(a)

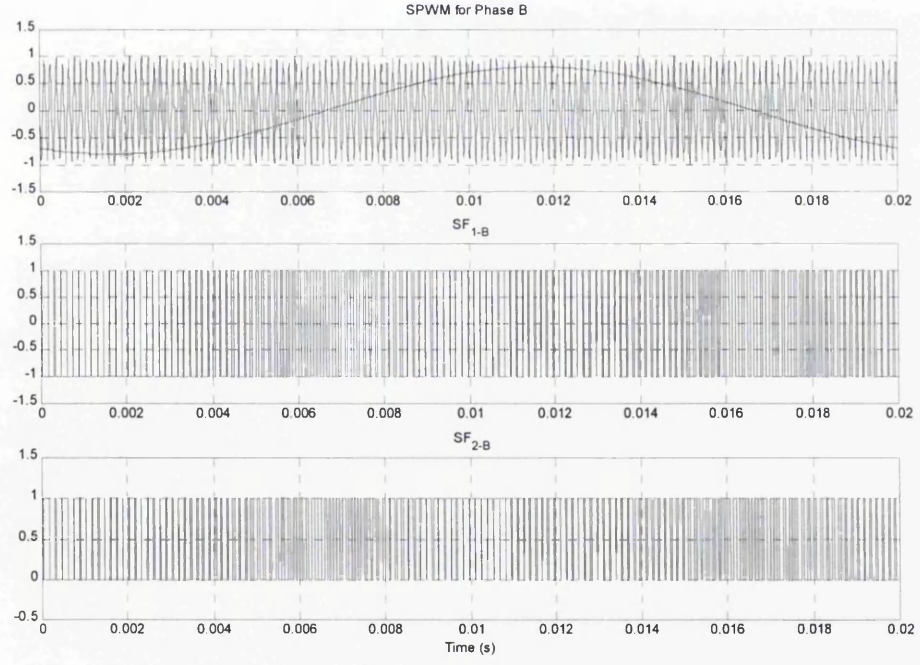
SPWM for Phase B
SF1-B
SF2-B
Time (s)

(b)

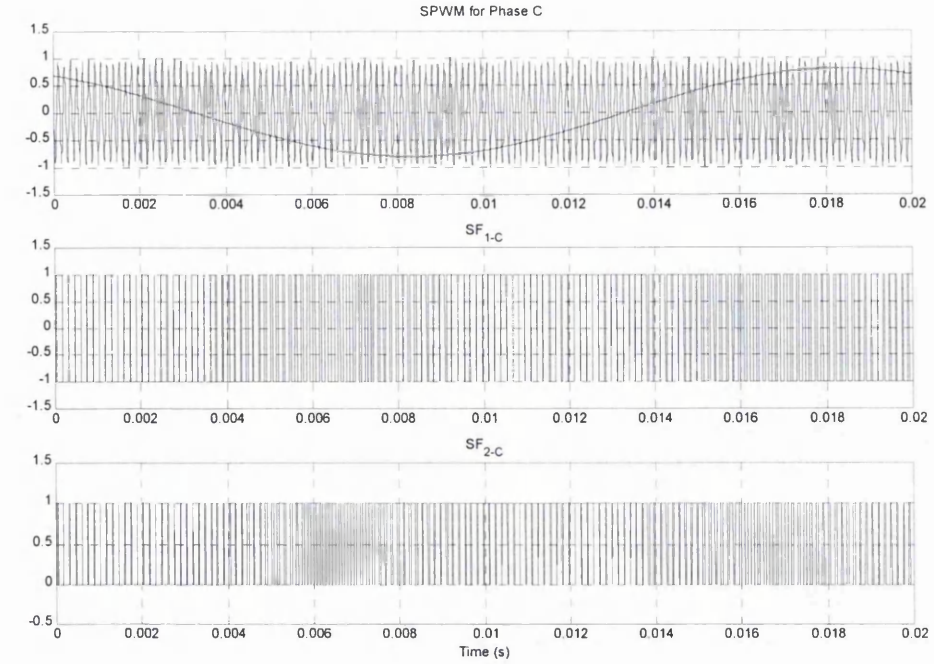

(c)

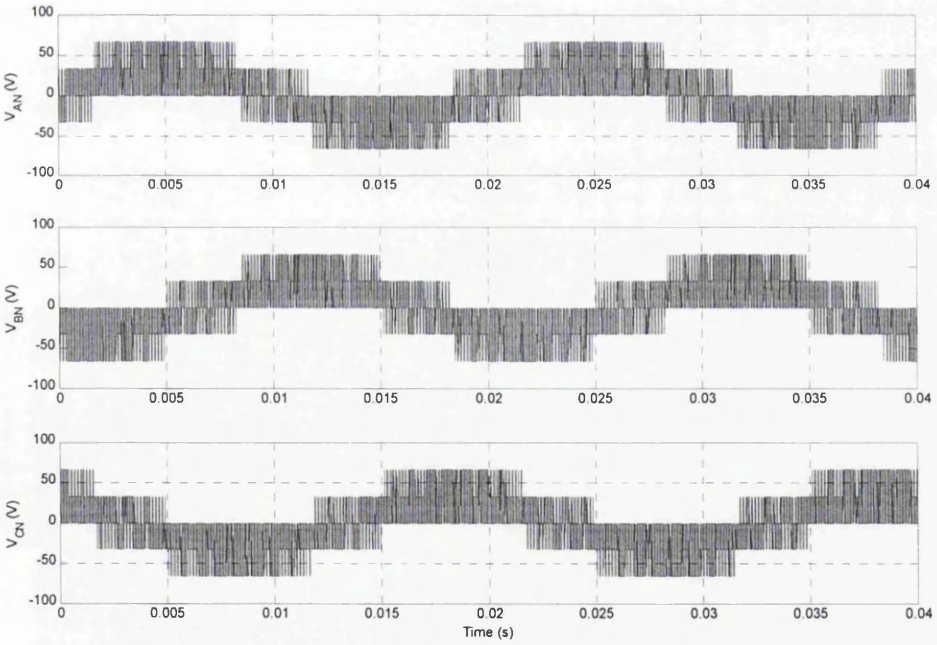

(d)

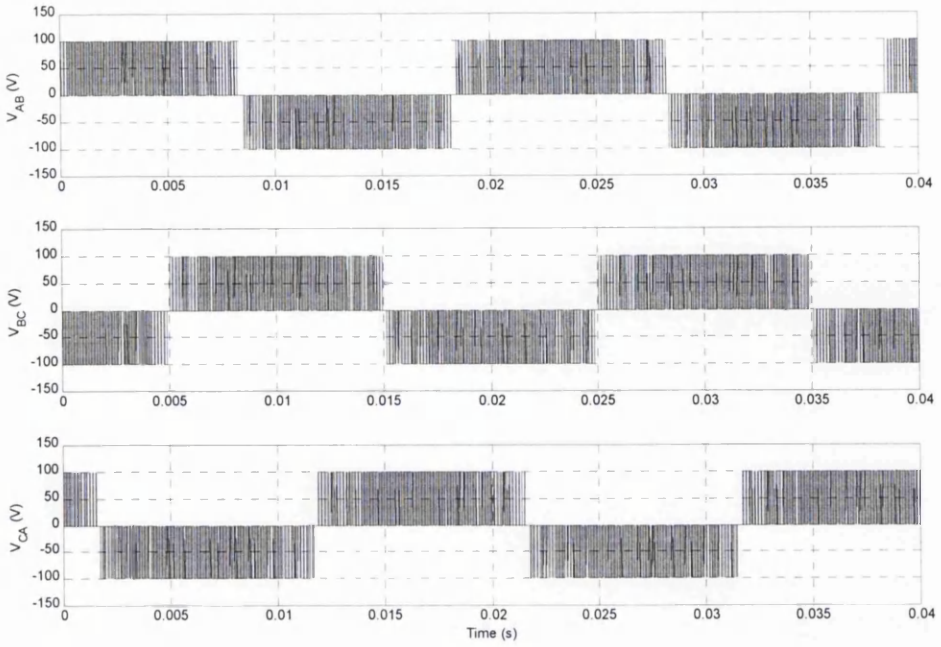

(e)

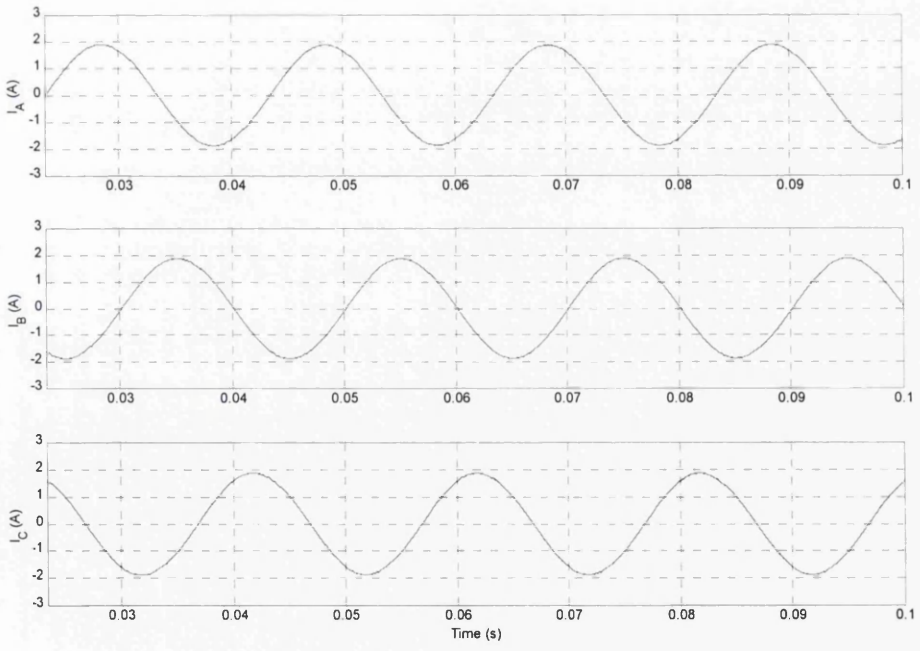

(f)

Figure 4-11: Switching functions, voltage and current waveforms of VSI with the SPWM control for M_a = 0.8. (a) Phase A switching function SF_1 and SF_2 (b) Phase B switching function SF_1 and SF_2 (c) Phase C switching function SF_1 and SF_2 (d) Phase voltages (e) Line to line voltages (f) Load currents.

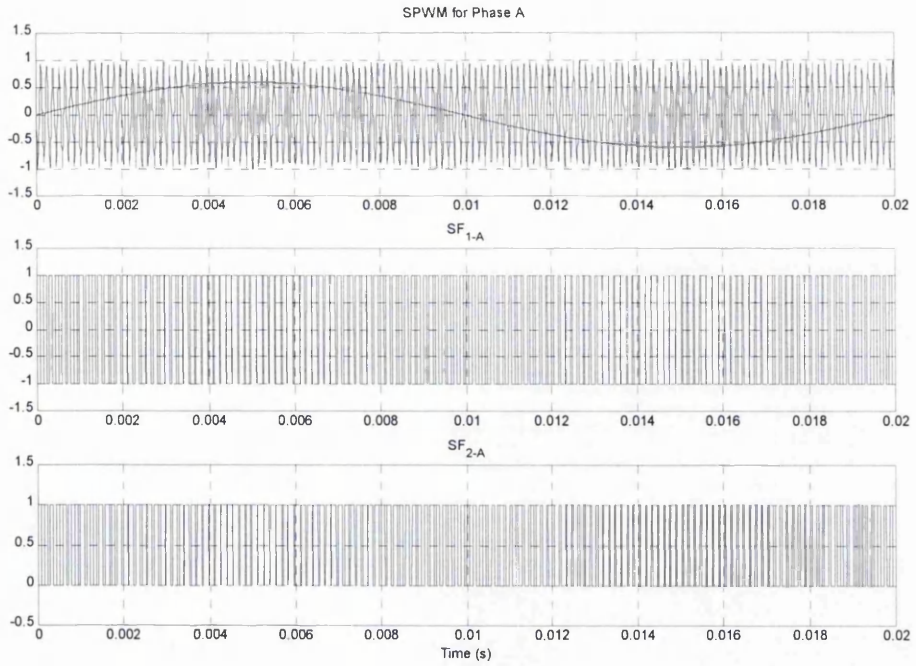
SPWM for Phase A
SF1-A
SF2-A
Time (s)

(a)

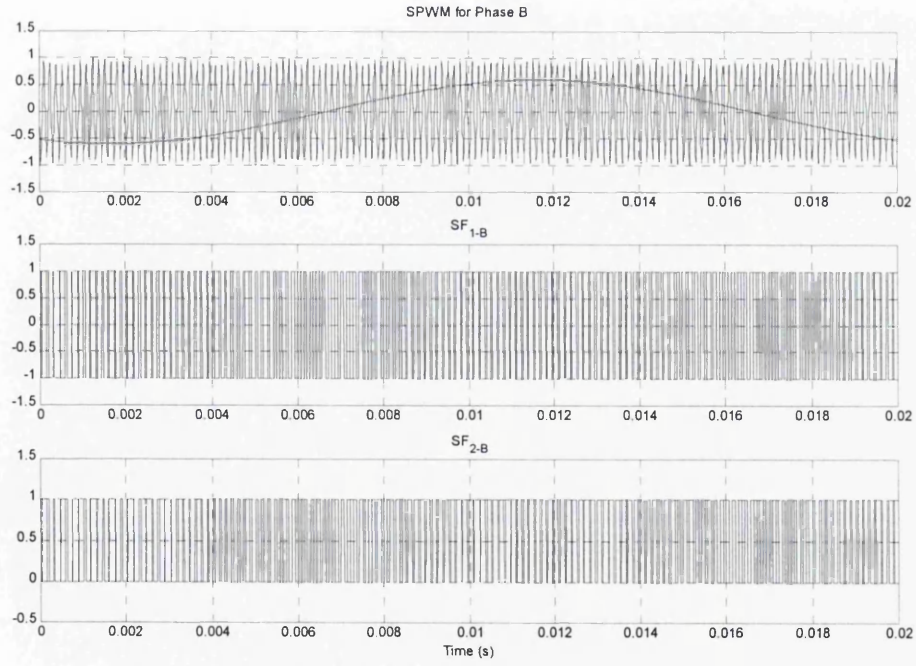
SPWM for Phase B
SF1-B
SF2-B
Time (s)

(b)

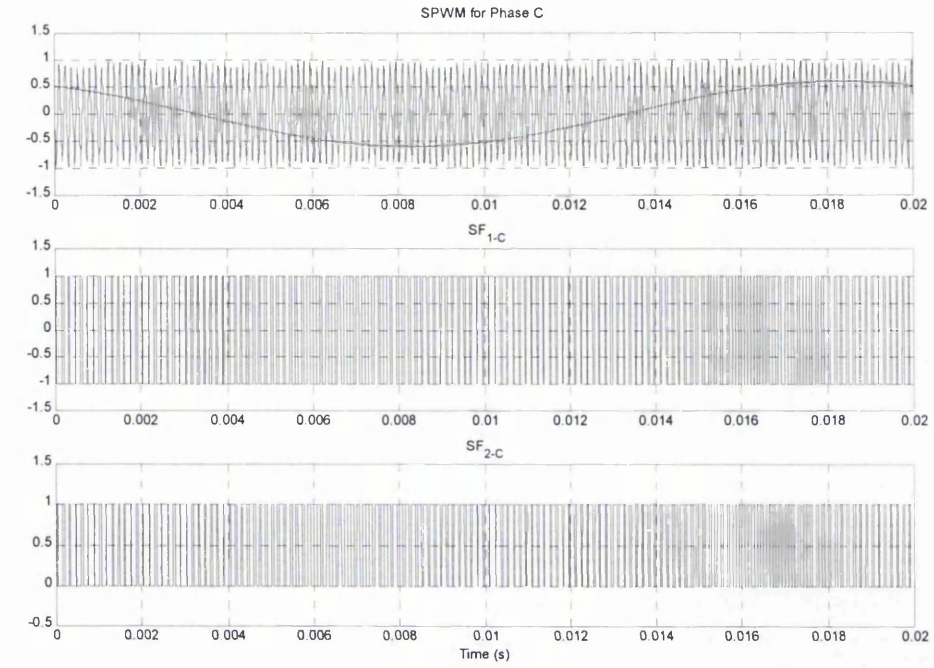

(c)

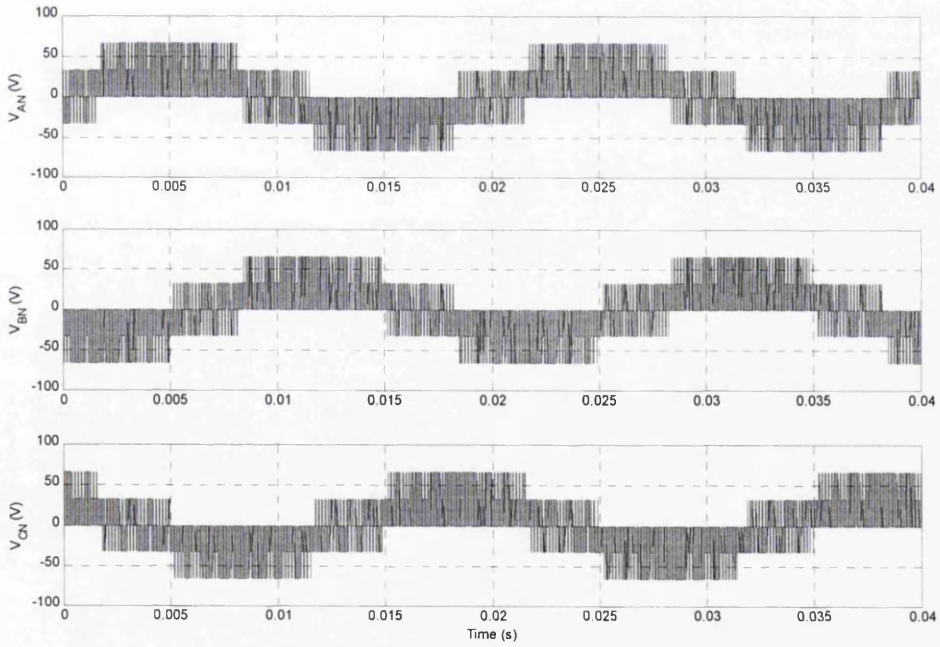

(d)

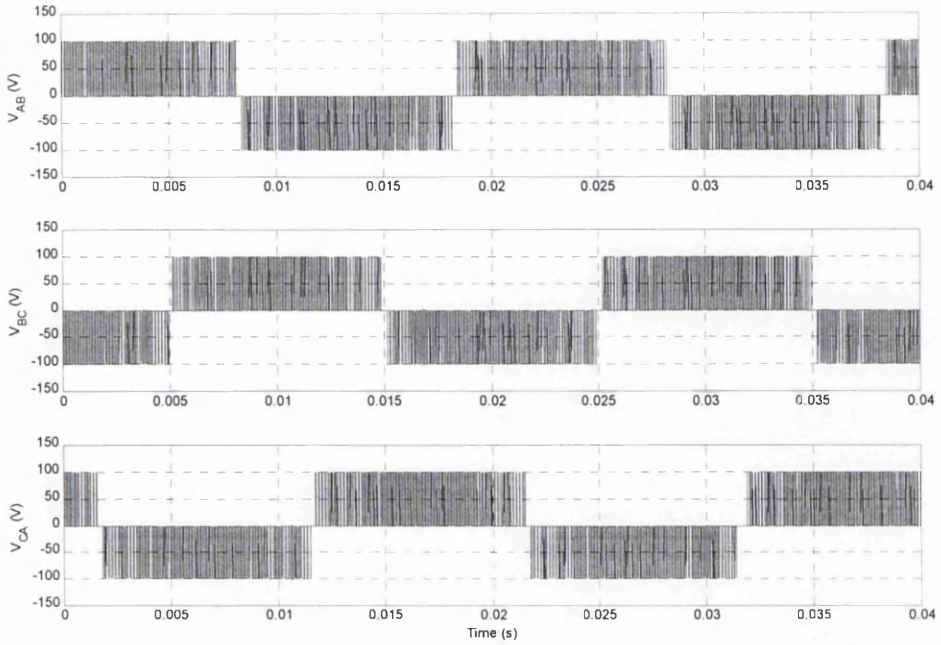

(e)

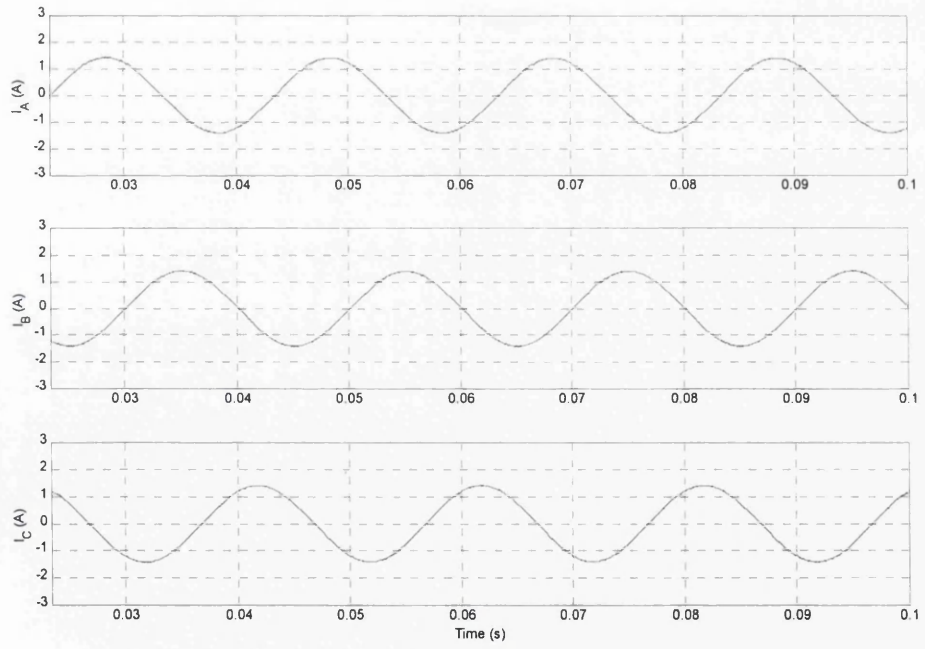

(f)

Figure 4-12: Switching functions, voltage and current waveforms of VSI with the SPWM control for M_a = 0.6. (a) Phase A switching function SF_1 and SF_2 (b) Phase B switching function SF_1 and SF_2 (c) Phase C switching function SF_1 and SF_2 (d) Phase voltages (e) Line to line voltages (f) Load currents.

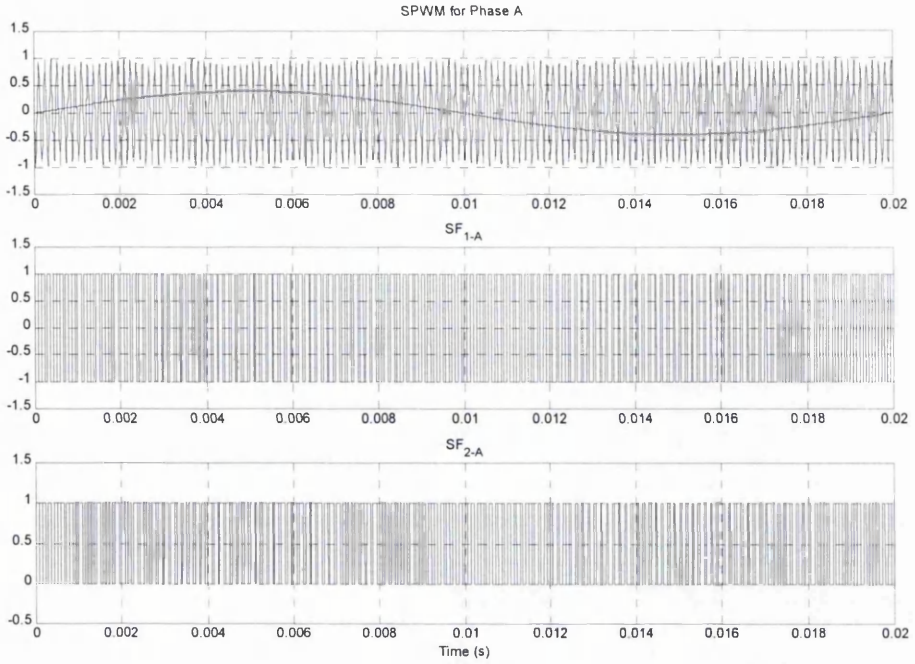
SPWM for Phase A
SF1-A
SF2-A
Time (s)

(a)

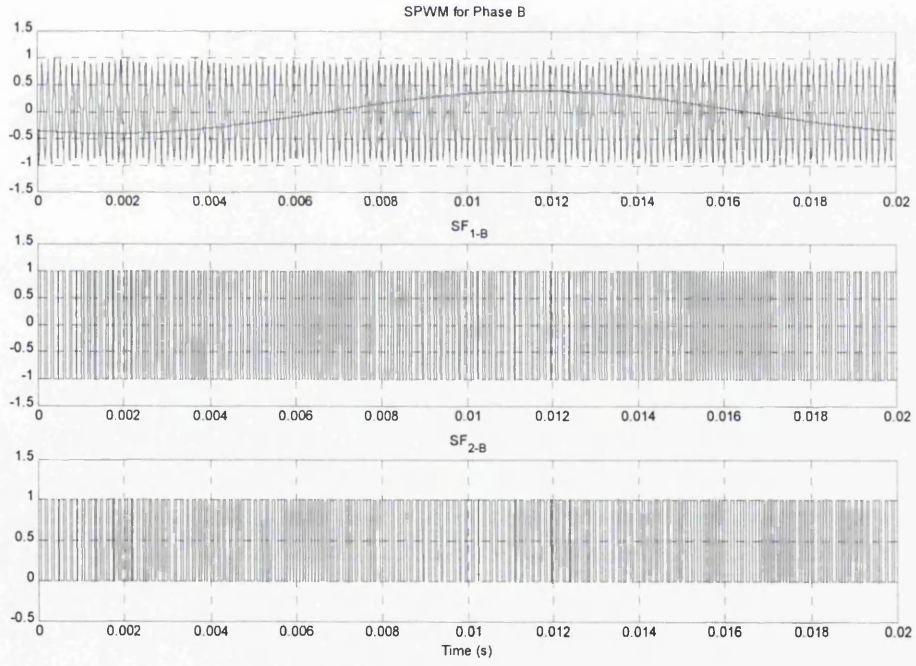
SPWM for Phase B
SF1-B
SF2-B
Time (s)

(b)

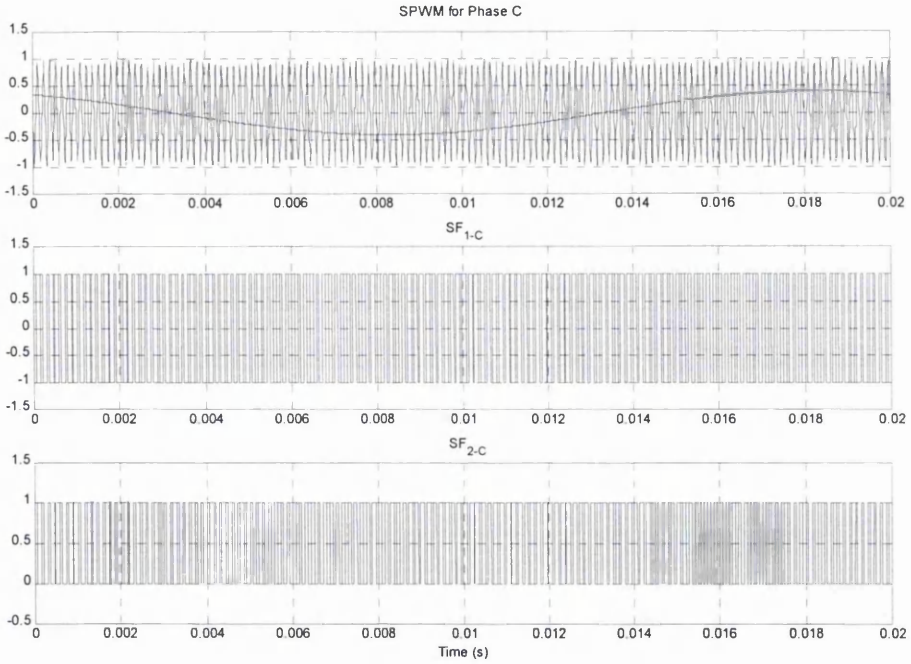

(c)

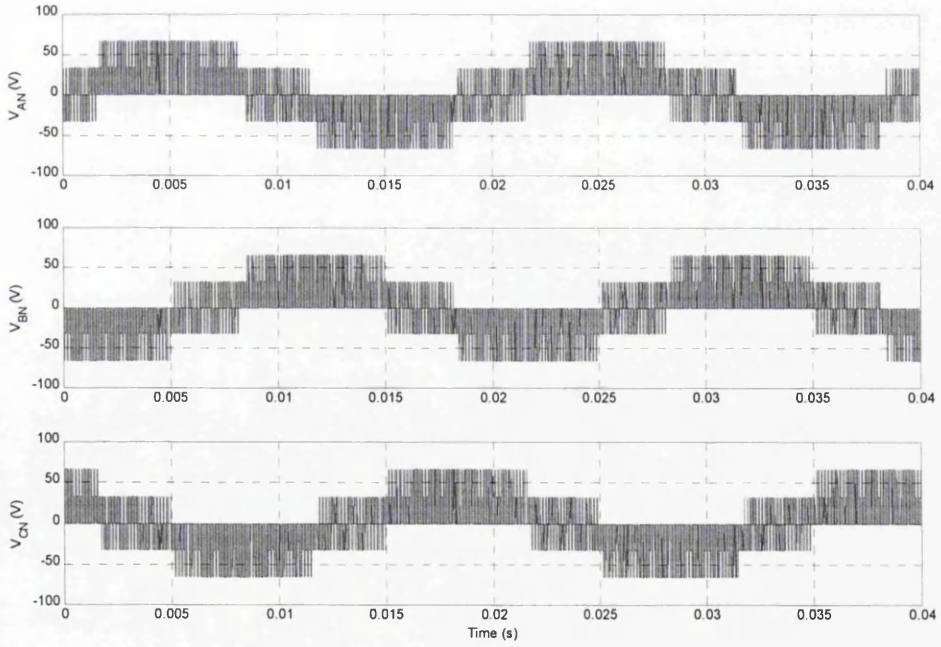

(d)

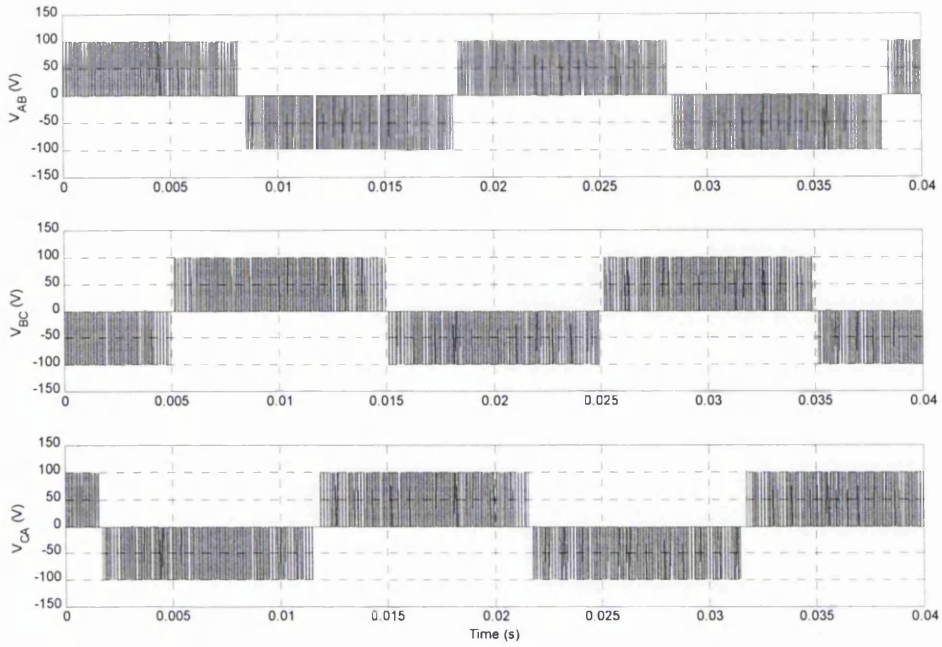

(e)

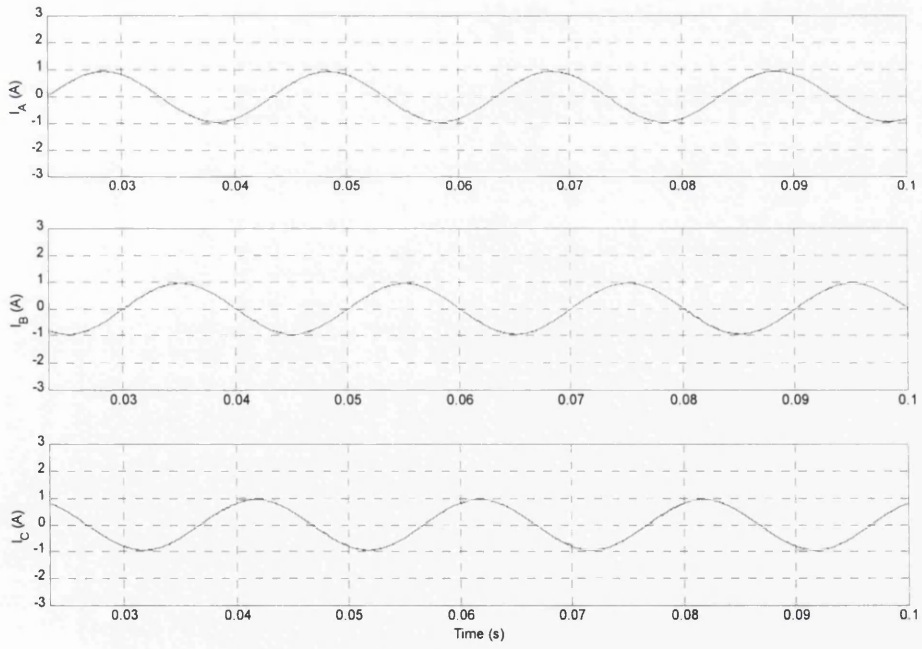

(f)

Figure 4-13: Switching functions, voltage and current waveforms of VSI with the SPWM control for M_a = 0.4. (a) Phase A switching function SF_1 and SF_2 (b) Phase B switching function SF_1 and SF_2 (c) Phase C switching function SF_1 and SF_2 (d) Phase voltages, (e) Line to line voltages (f) Load currents.

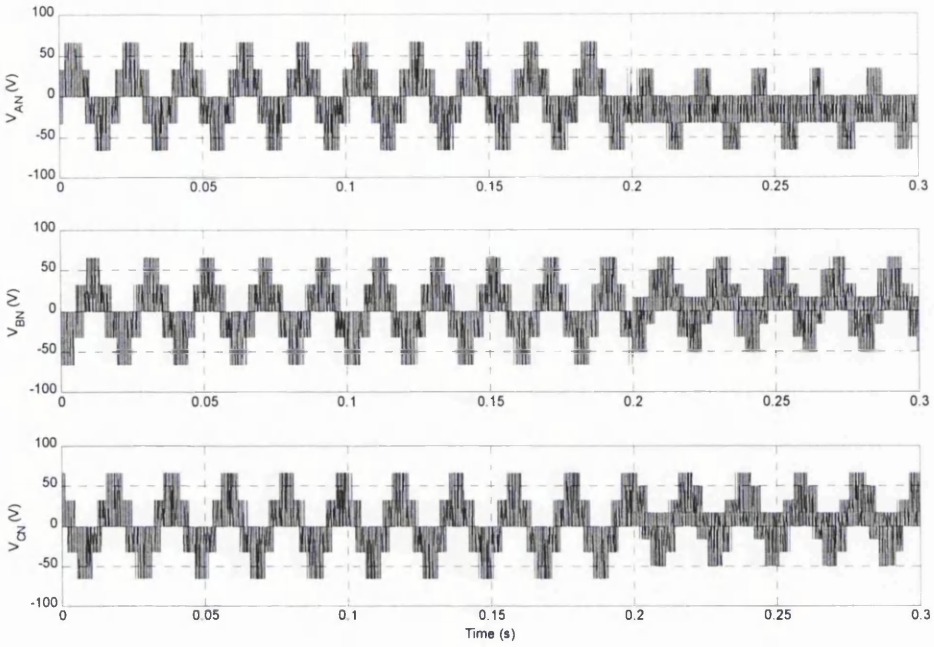

(a)

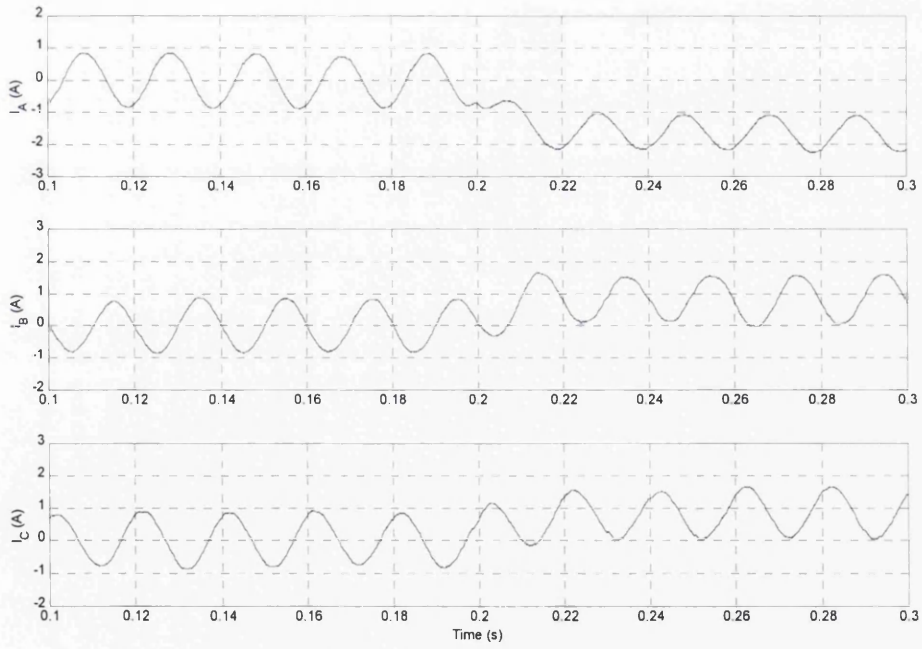

(b)

Figure 4-14: Simulation results of VSI with transistor T1 open-circuit fault at t=0.2s. (a) Phase voltages (b) Load currents

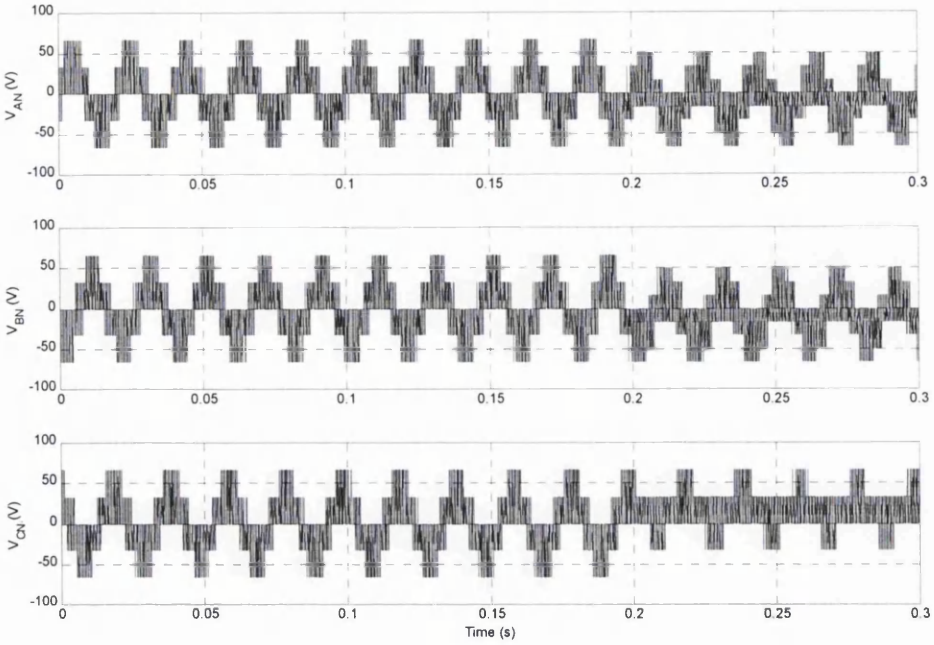

(a)

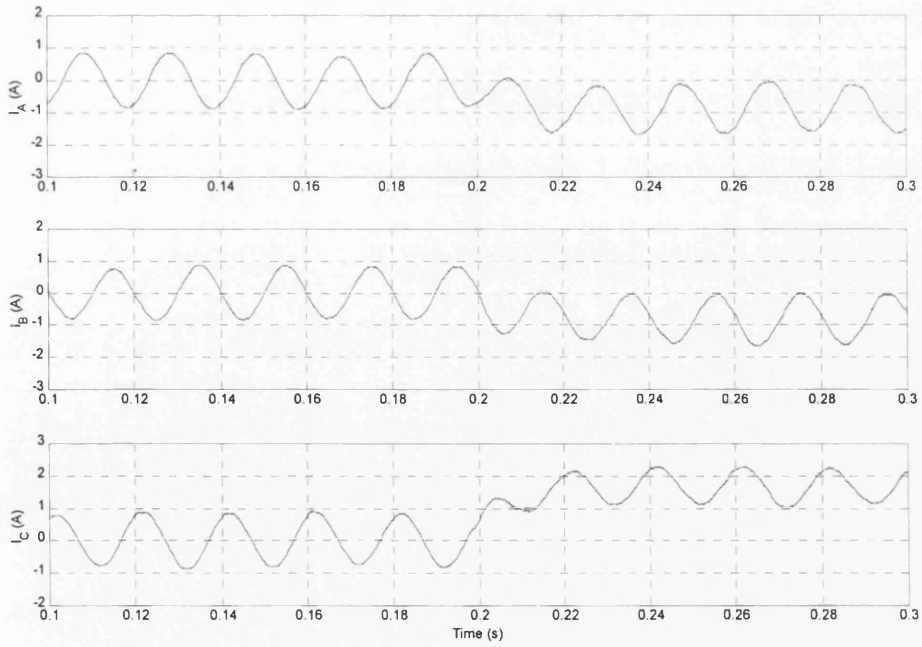

(b)

Figure 4-15: Simulation results of VSI with transistor T2 open-circuit fault at t=0.2s. (a) Phase voltages (b) Load currents

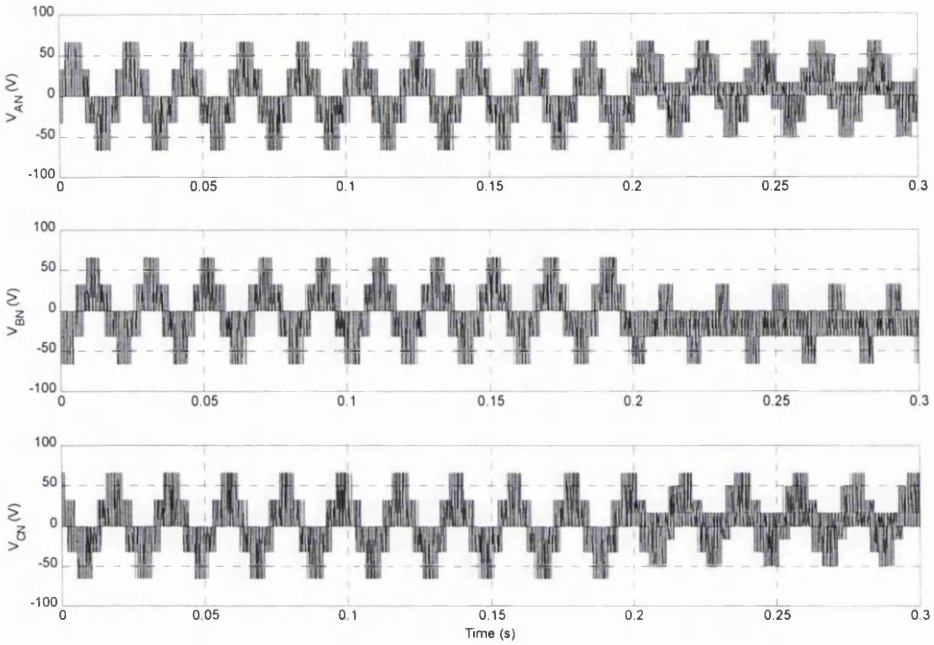

(a)

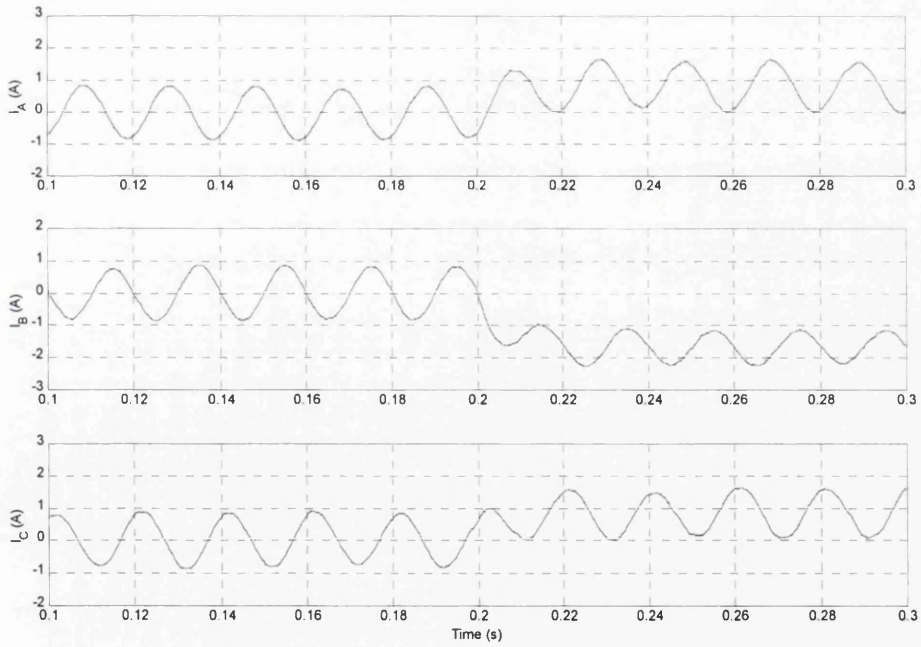

(b)

Figure 4-16: Simulation results of VSI with transistor T3 open-circuit fault at t=0.2s. (a) Phase voltages (b) Load currents

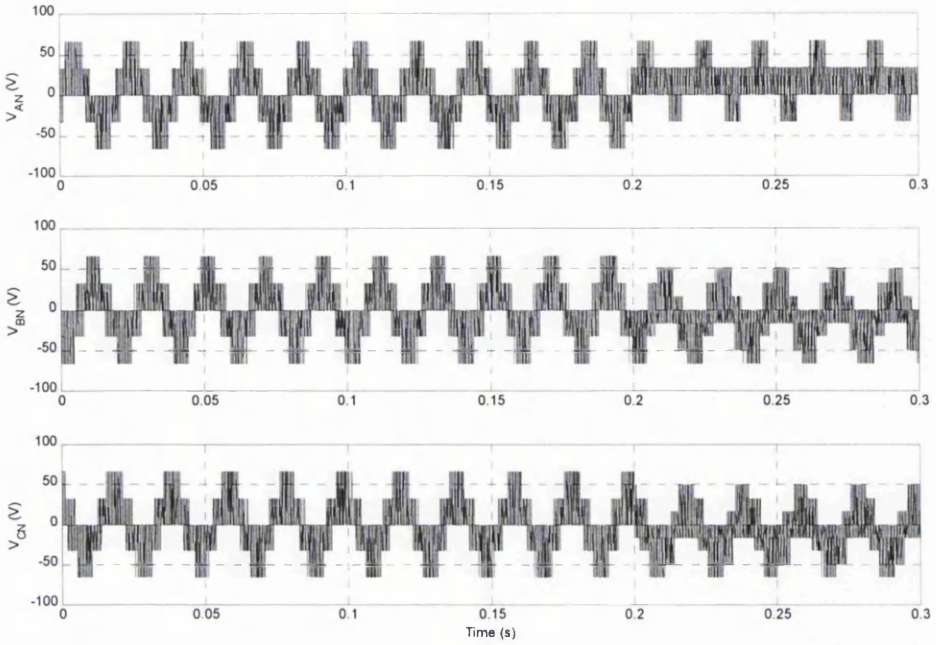

(a)

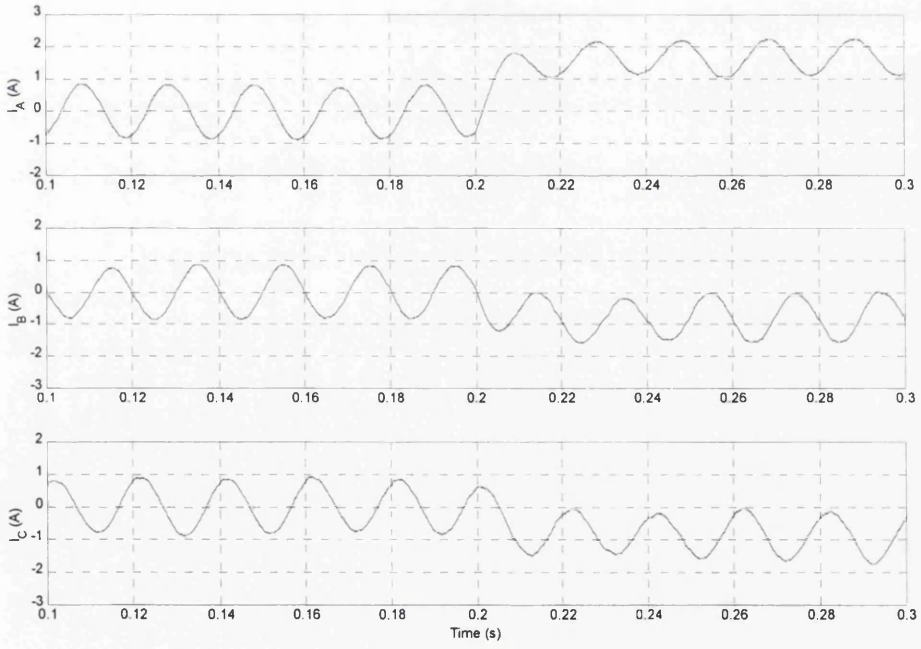

(b)

Figure 4-17: Simulation results of VSI with transistor T4 open-circuit fault at t=0.2s. (a) Phase voltages (b) Load currents

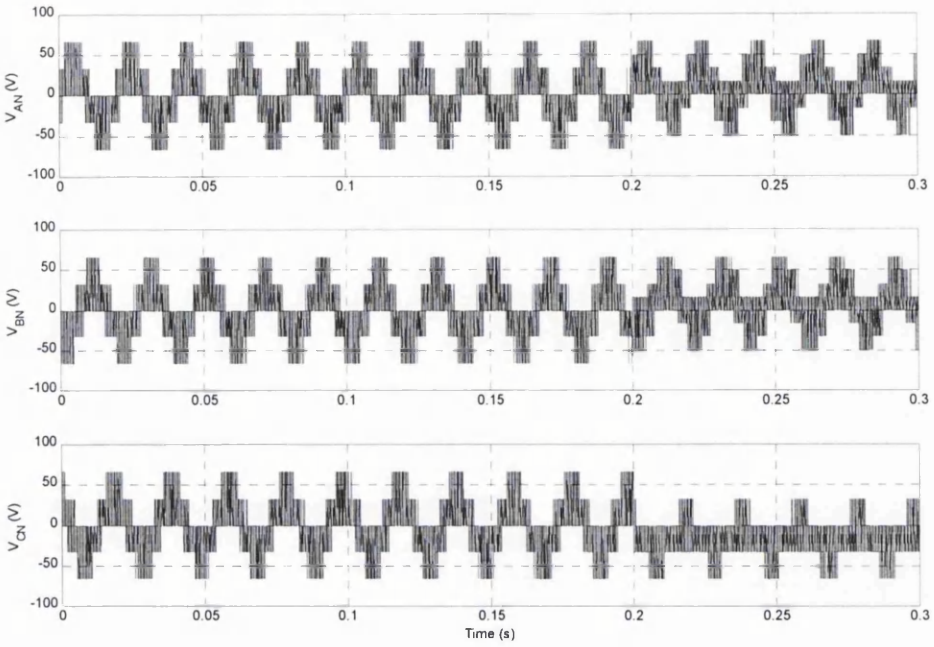

(a)

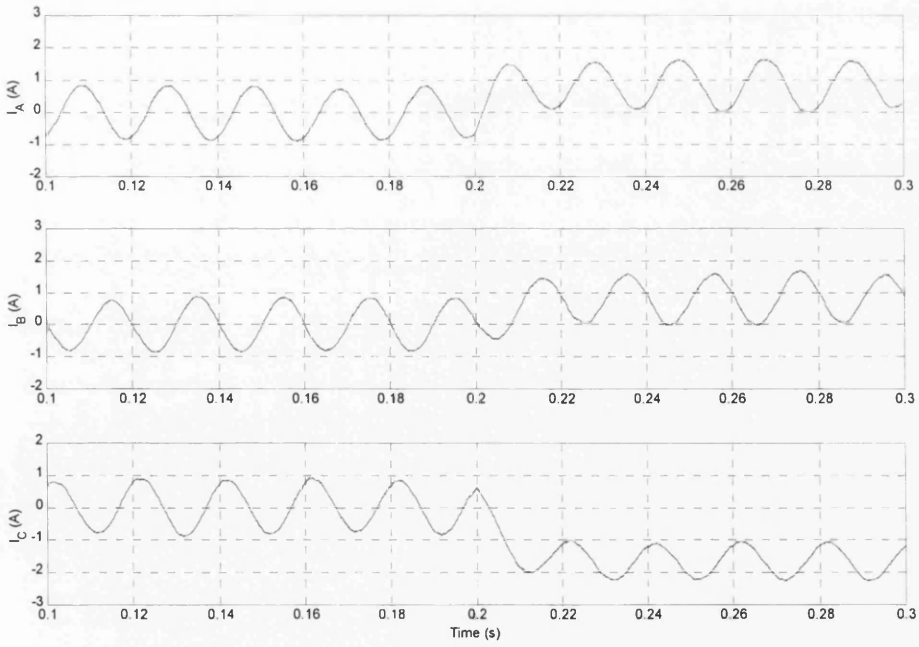

(b)

Figure 4-18: Simulation results of VSI with transistor T5 open-circuit fault at t=0.2s. (a) Phase voltages (b) Load currents

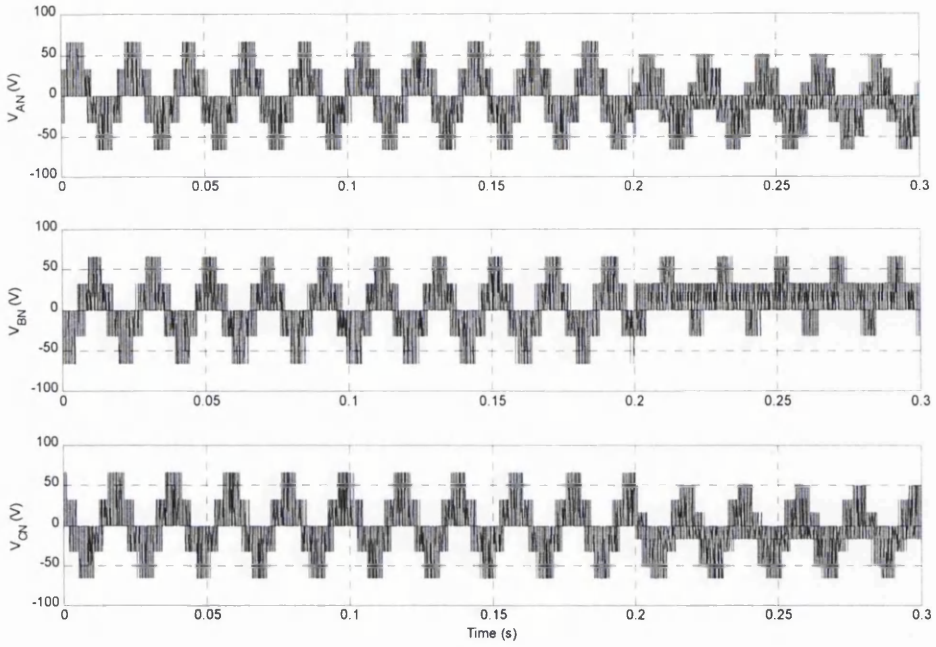

(a)

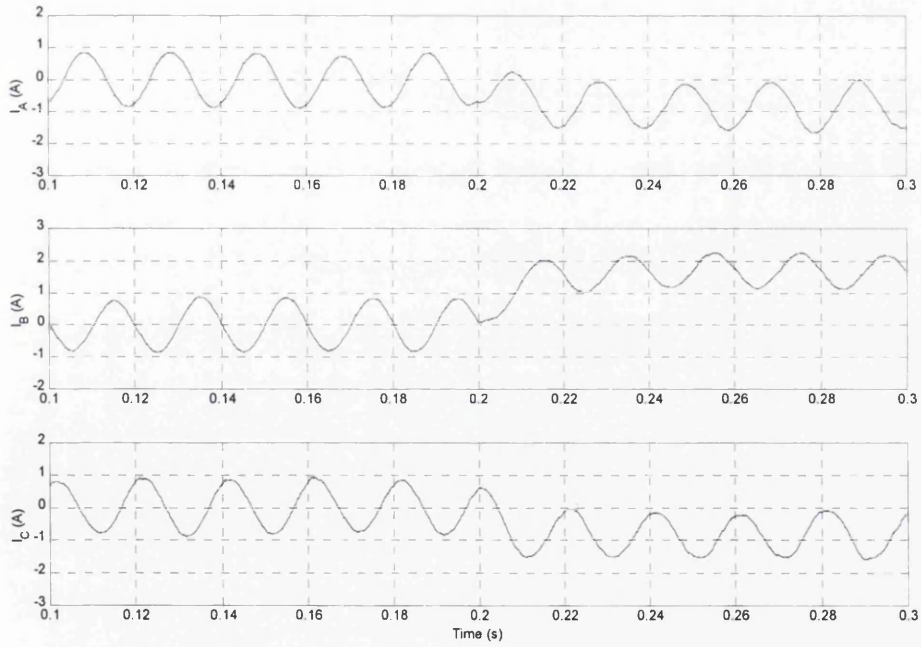

(b)

Figure 4-19: Simulation results of VSI with transistor T6 open-circuit fault at t=0.2s. (a) Phase voltages (b) Load currents

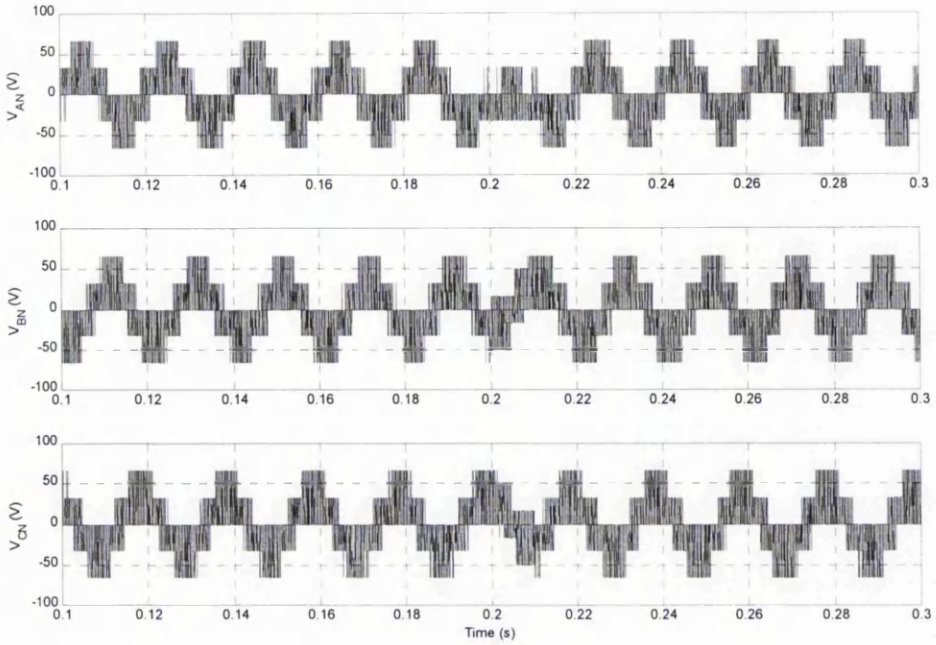

(a)

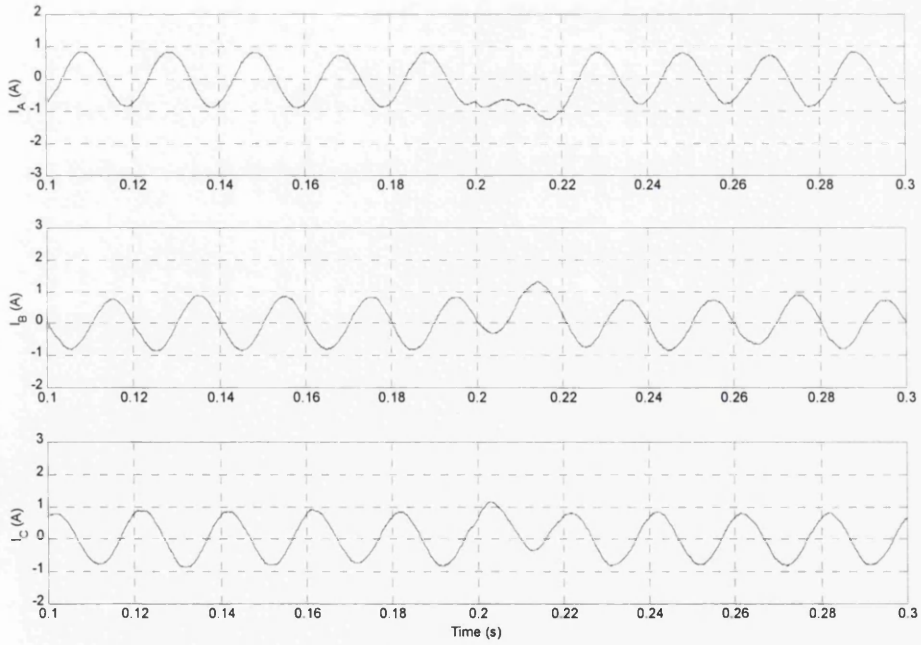

(b)

Figure 4-20: Simulation results of VSI with transistor T1 intermittent misfiring fault at t=0.2s for 0.01s. (a) Phase voltages (b) Load currents

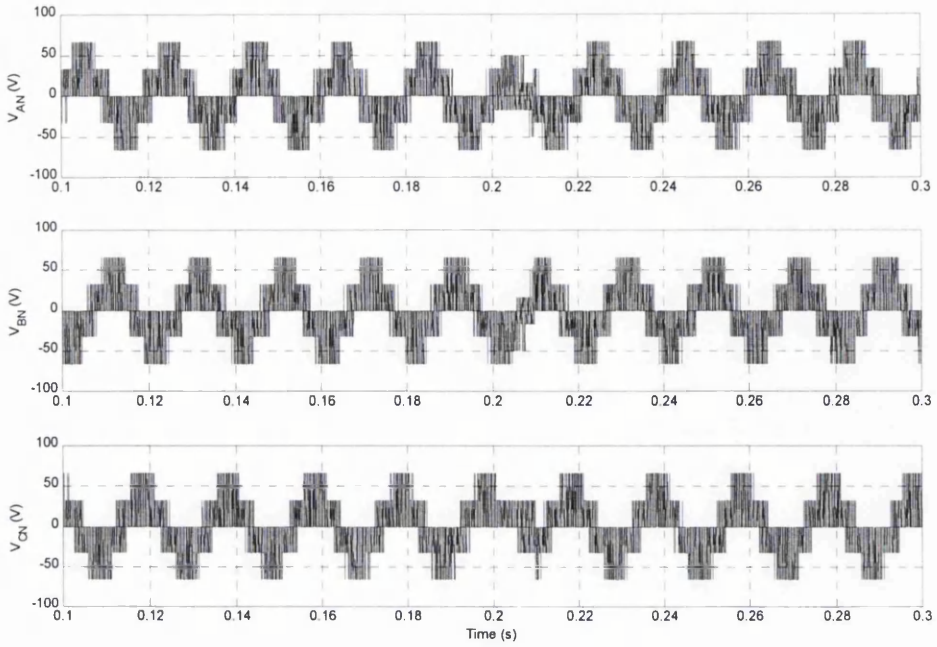

(a)

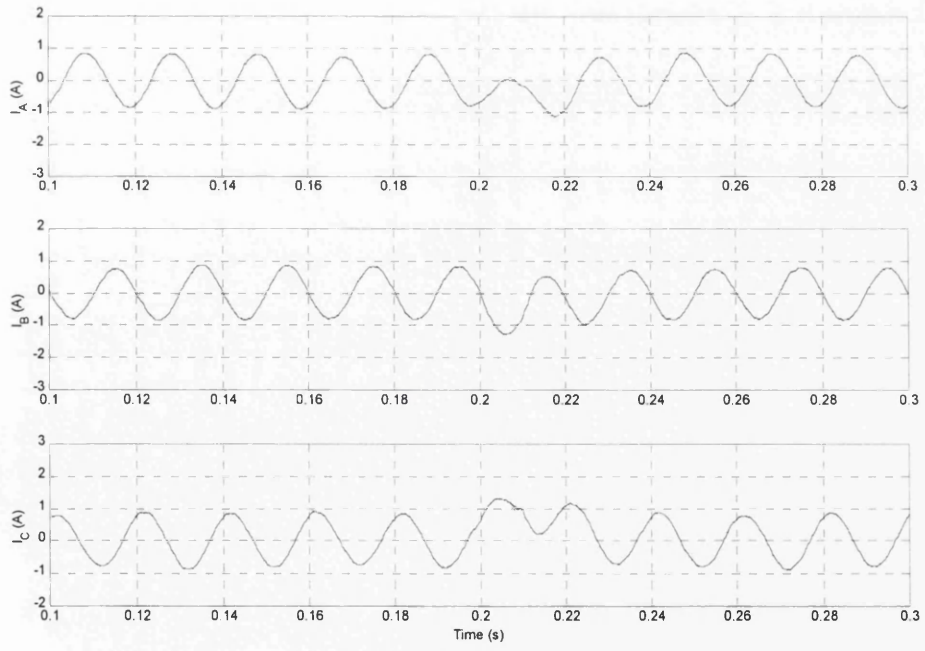

(b)

Figure 4-21: Simulation results of VSI with transistor T2 intermittent misfiring fault at t=0.2s for 0.01s. (a) Phase voltages (b) Load currents

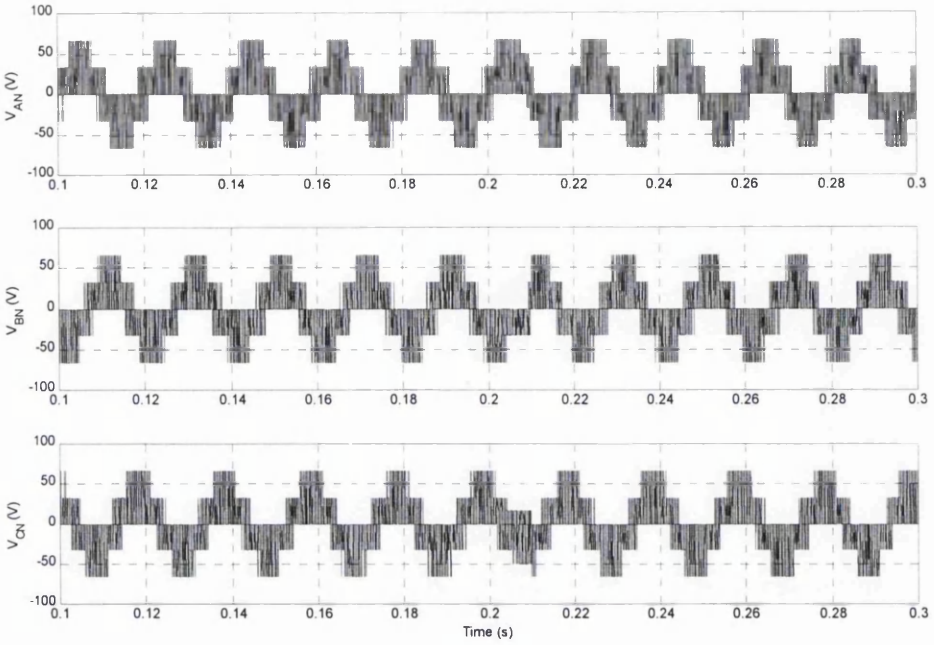

(a)

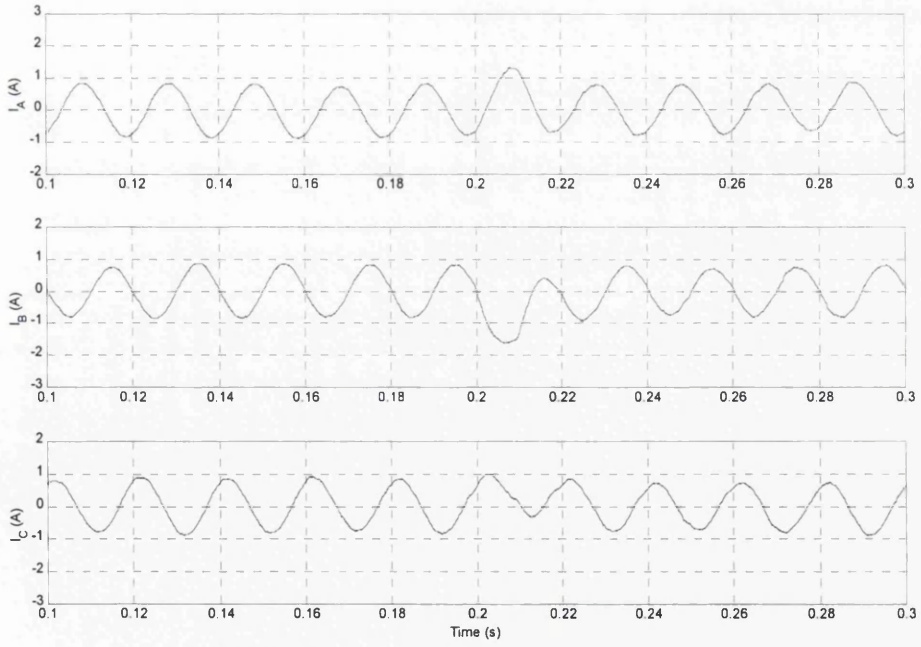

(b)

Figure 4-22: Simulation results of VSI with transistor T3 intermittent misfiring fault at t=0.2s for 0.01s. (a) Phase voltages (b) Load currents

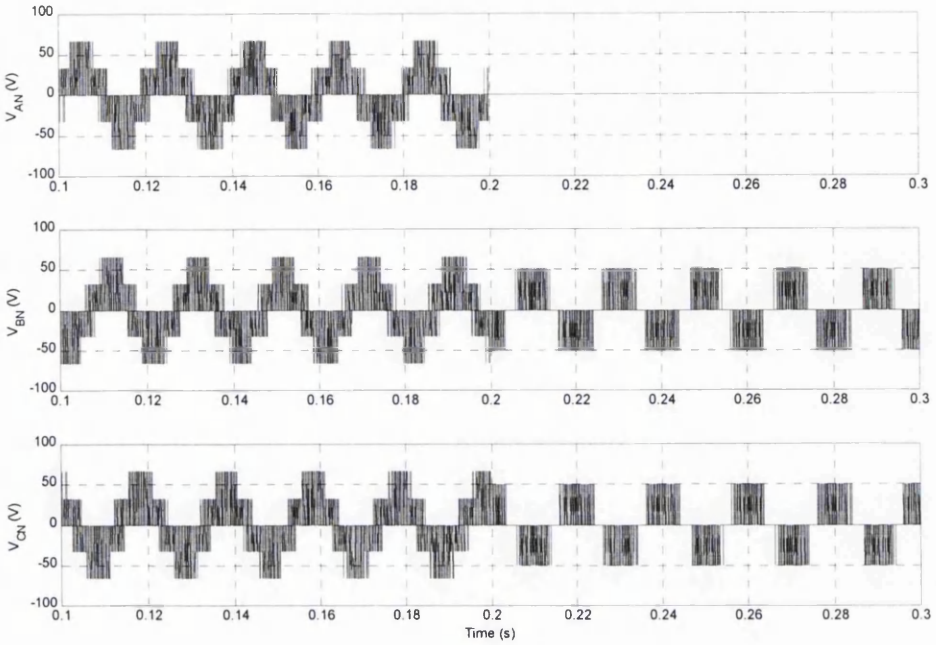

(a)

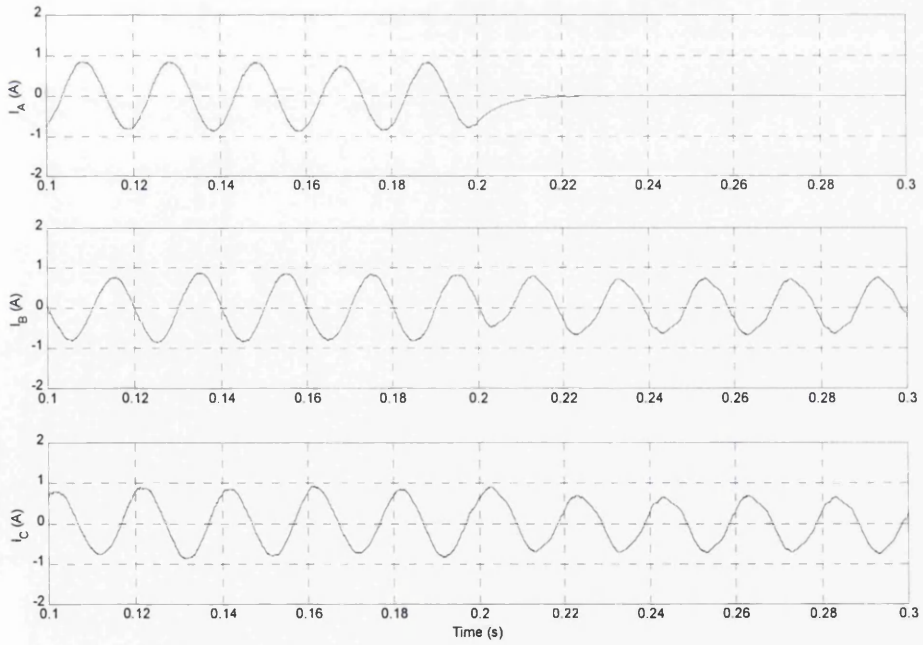

(b)

Figure 4-23: Simulation results of VSI with phase A single phasing fault at t=0.2s. (a) Phase voltages (b) Load currents

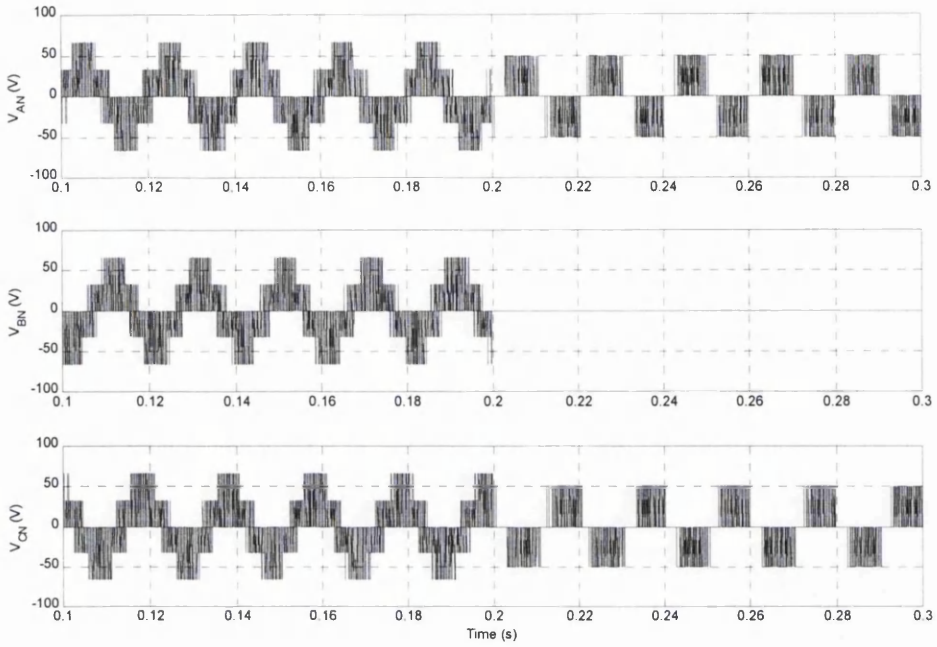

(a)

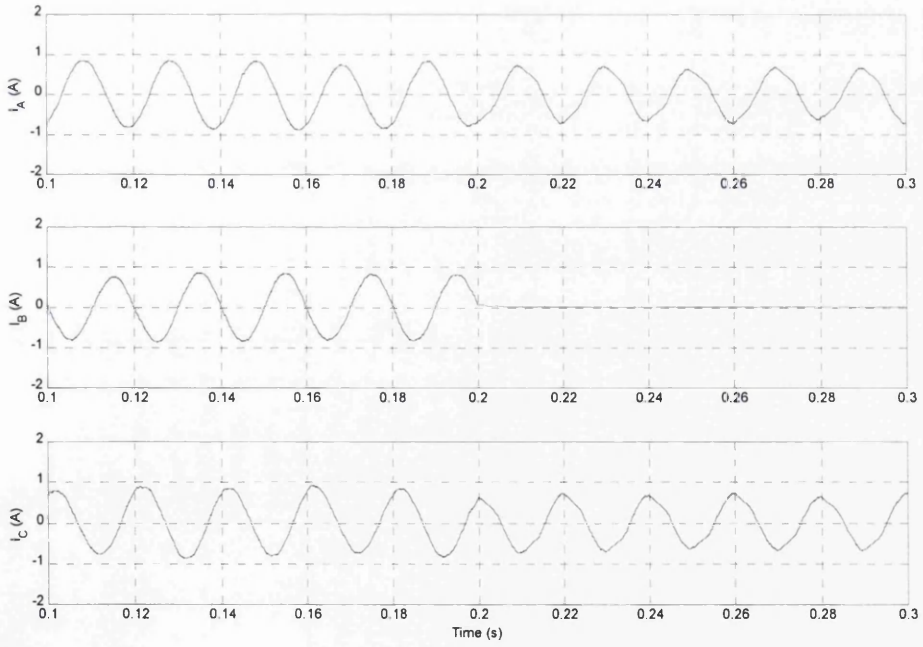

(b)

Figure 4-24: Simulation results of VSI with phase B single phasing fault at t=0.2s. (a) Phase voltages (b) Load currents

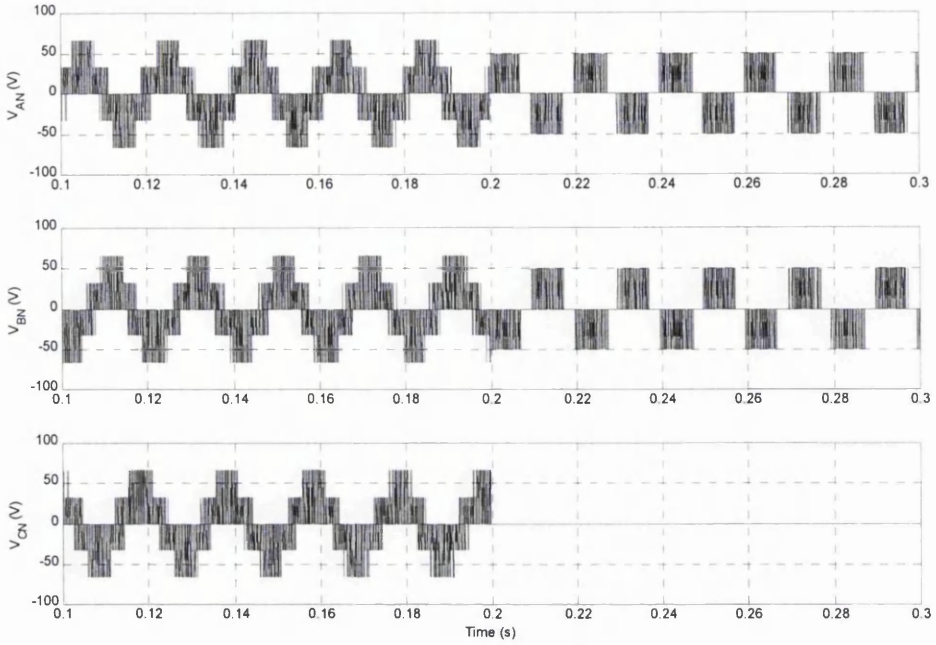

(a)

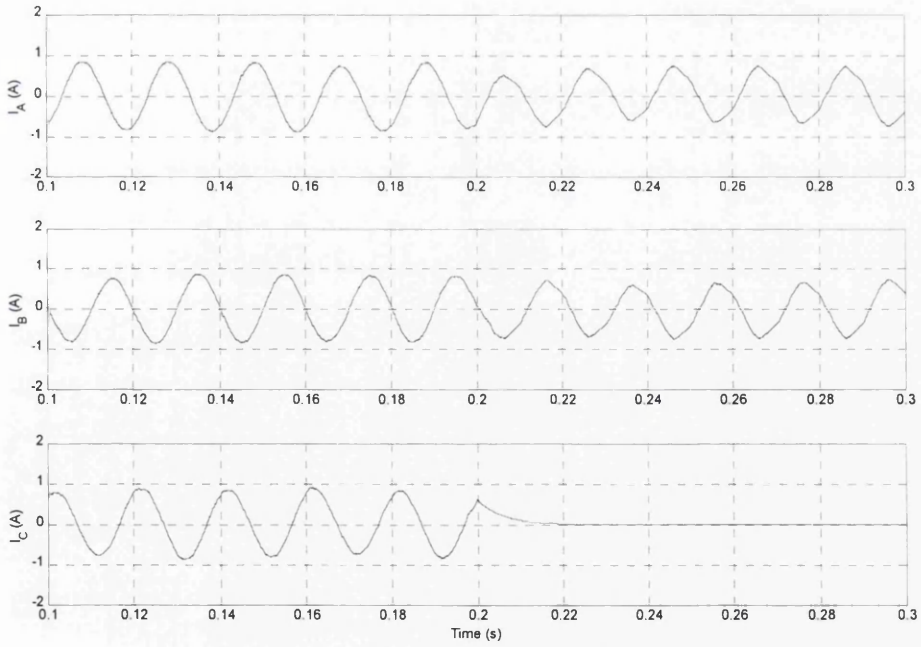

(b)

Figure 4-25: Simulation results of VSI with phase C single phasing fault at t=0.2s. (a) Phase voltages (b) Load currents

4.6 The Simulation of 3-Phase Induction Motor Drive

In this section, the 3-phase PWM VSI is connected to the induction motor drive. The induction motor is simulated using the dynamical equations that are formulated in the synchronous reference frame, as discussed in [108]. The rated parameters of the simulated induction motor were determined experimentally and are given in table 4.1.

Figure 4-26 shows the functional model for the system. The model consists of 4 main blocks: Inverter block, Fuzzy Controller block, Gate driver block and Induction motor block.

Table 4.1 : The rated parameters for induction motor

	Stator	Rotor	Magnetising Parameter
3hp, 410V, 50Hz 4 poles, 1415rpm Friction constant = 0.0028N.m/rad/sec Drive inertia = 0.055kg.m^2	$R_s = 1.88\Omega$ $L_{ls} = 0.0125$H $L_s = 0.1649$H	$R_r = 2.72\Omega$ $L_{lr} = 0.0125$H $L_r = 0.1649$H	$L_m = 0.1545$H

The Fuzzy Controller block has two inputs and one output. The inputs are the reference speed and the actual rotor speed. Inside the block, the speed error (the error between the rotor speed and the reference speed) and its rate of change is calculated using the following equations

$$e_0(k) = \omega_r^*(k) - \omega_r(k) \tag{4.23}$$

$$\Delta e_0(k) = e_0(k) - e_0(k-1) \tag{4.24}$$

where $\omega_r^*(k)$ is the speed command in kth sampling interval, $\omega_r(k)$ is the rotor speed response in the kth sampling interval, $e_o(k)$ is the speed error in the kth sampling interval, and $\Delta e_o(k)$ is the speed error change in the kth sampling interval. On the other hand, the output of the FLC is the current command change Δi_{sq}^*, which is integrated at regular kth sampling intervals and yields the following current command

$$i_{sq}^*(k) = i_{sq}^*(k-1) + G_0 \Delta i_{sq}^*(k) \tag{4.25}$$

where the integral gain G_0 can be varied to tune the output of the fuzzy controller for a desired performance. The detailed description of Fuzzy Controller block is given in [108].

The Gate Driver block has two inputs (Δi_{sq}^{*} and actual rotor speed) and four outputs (a synchronous speed ω_s, phase A voltage controller signal (A sig), phase B voltage controller signal (B sig) and phase C voltage controller signal (C sig)). The phase voltage signals are fed to a 3Phase_Inverter to produce the stator voltages. On the hand, the ω_s, is feed to the Induction Motor block.

The Induction Motor block has six inputs and one output. The inputs are phase A stator voltage (V_{sa}), phase B stator voltage (V_{sb}), phase C stator voltage (V_{sc}), ω_s, Load value and disturbance. The output is the actual rotor speed.

Figure 4-27 shows the rotor speed response and the stator currents during starting operation for open-loop induction motor drive. Throughout the simulation, the motor is running at the rated parameters and torque. The speed is set to 1000rpm. Observations of the results show that the rotor takes 0.8s to reach 1000rpm. The starting current reaches the maximum five times the steady state value.

Figure 4-28 shows the rotor speed response and stator currents during the soft starting closed-loop FLC operation. Inspection of the results show that the rotor speed reaches its reference speed from stand still at t= 0.5s with no overshoot. As the motor accelerates and the speed builds up, the starting current reaches the maximum four times the steady state value. These results show that the FLC increased the speeding time for the rotor to reach the reference speed by 37.8% compared to open-loop drive. Also the soft-starting algorithm employed in the closed-loop drive reduced the starting current by 20%.

The third simulation is to examine the transient characteristics of the speed drive system during step changes in load torque, as shown in figure 4-29. The motor was initially operated at 1000rpm at no load when a rated load was applied to the rotor shaft. The FLC restore the rotor speed to the reference speed within 0.6s with a maximum speed variation of 60rpm.

4.7 Summary

In this Chapter, the computer simulation of VSI carried out in MATLAB/SIMULINK has been presented. The model was based on the switching function concept. This was followed by the derivation of the motor in d-q synchronous rotation reference frame and the simulation results. The following are the main points made in this Chapter.

1. By using the switching function concept, simplification of the power conversion circuit can be achieved. The design parameters such as voltage and current ratings of the power device and the load current can be easily calculated.

2. The per-phase equivalent circuit of the induction motor is sufficient to highlight the essential features of the motor performance under steady state operation. An alternative model, termed the dynamic model, is used to represent the dynamics of the induction motor and describe its real performance under both transient and steady state conditions, which are based on the selection of desired reference frames. The most common reference frames are the stationary frame, the rotor frame, and the synchronous frame. The model equations expressed in the synchronous frame are the most commonly used model for transient and steady state analysis

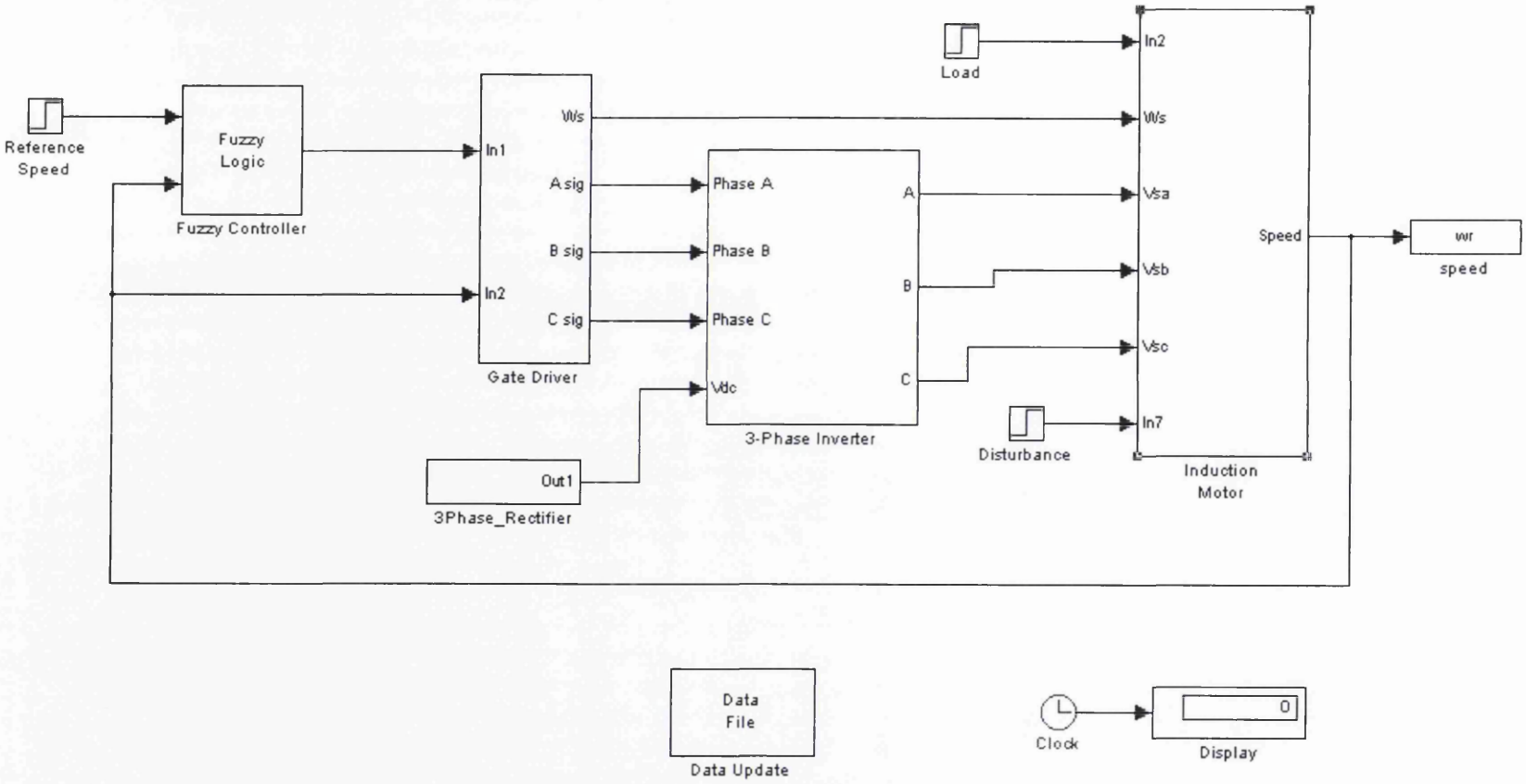

Figure 4-26: Block diagram of simulation model for 3-phase VSI induction motor drive with fuzzy controller.

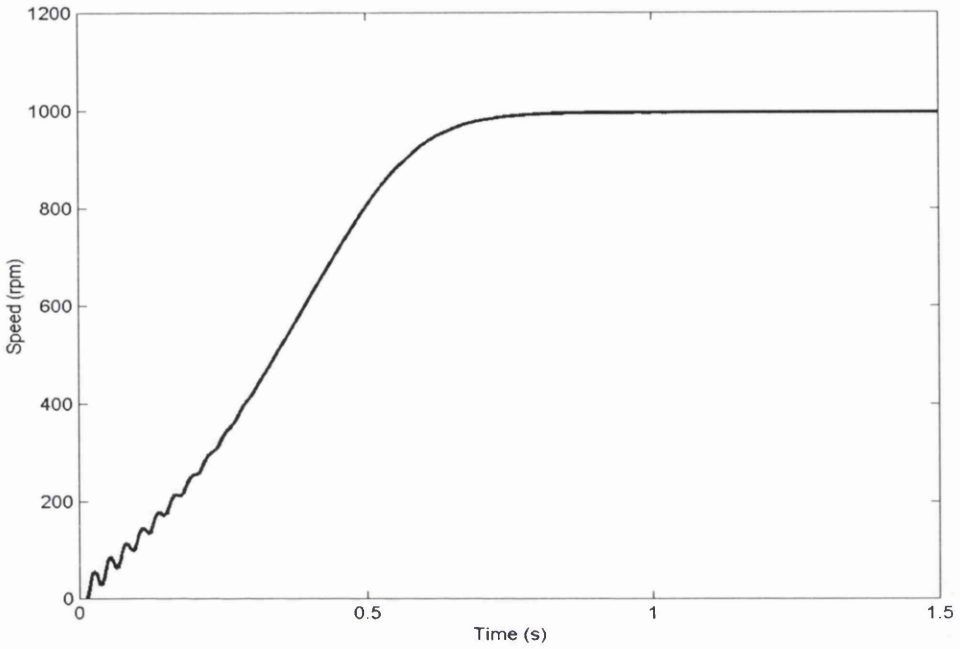

(a)

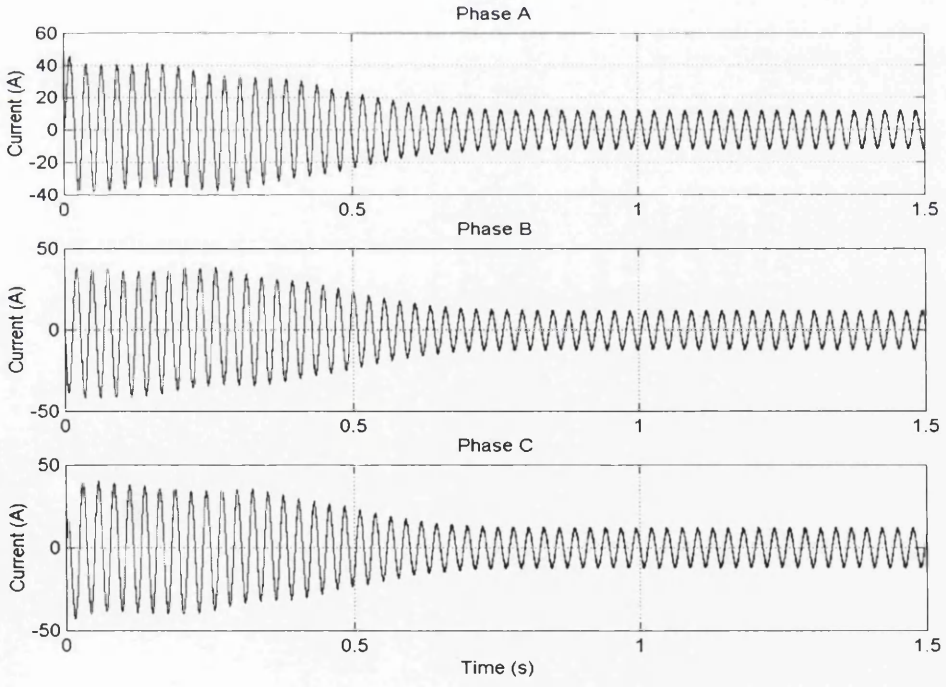

(b)

Figure 4-27: Simulation results of open-loop induction motor drive at rated parameters. (a) Rotor speed response (b) The stator currents.

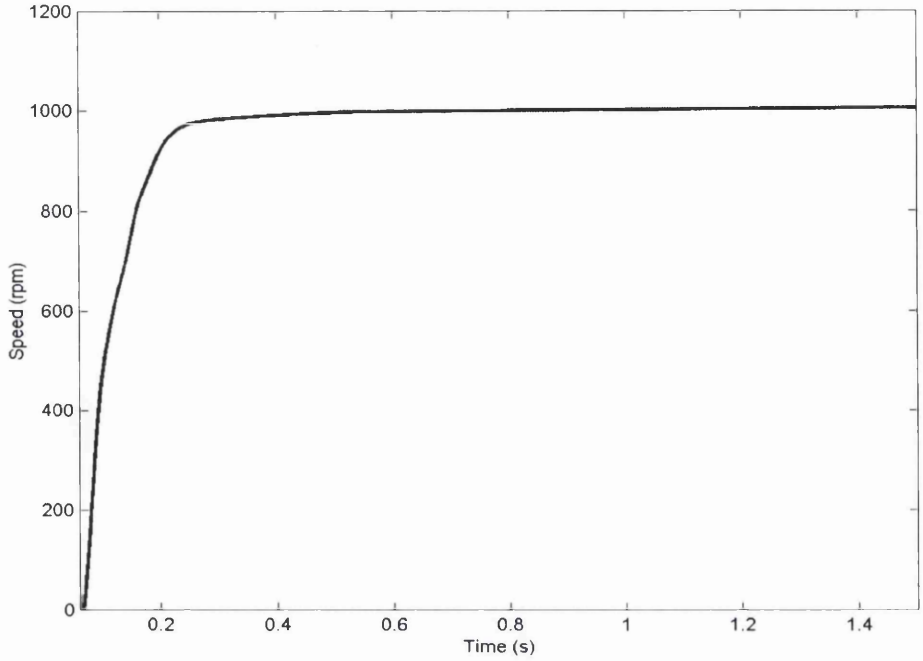

(a)

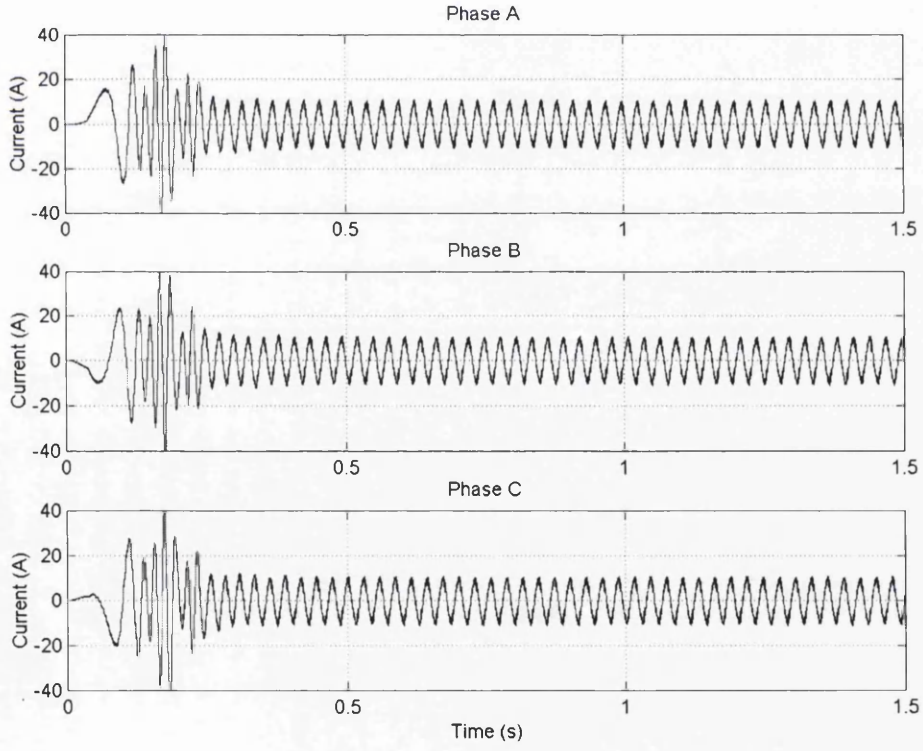

(b)

Figure 4-28: Simulation results of closed-loop FLC induction motor drive at rated parameters. (a) Rotor speed response (b) The stator currents.

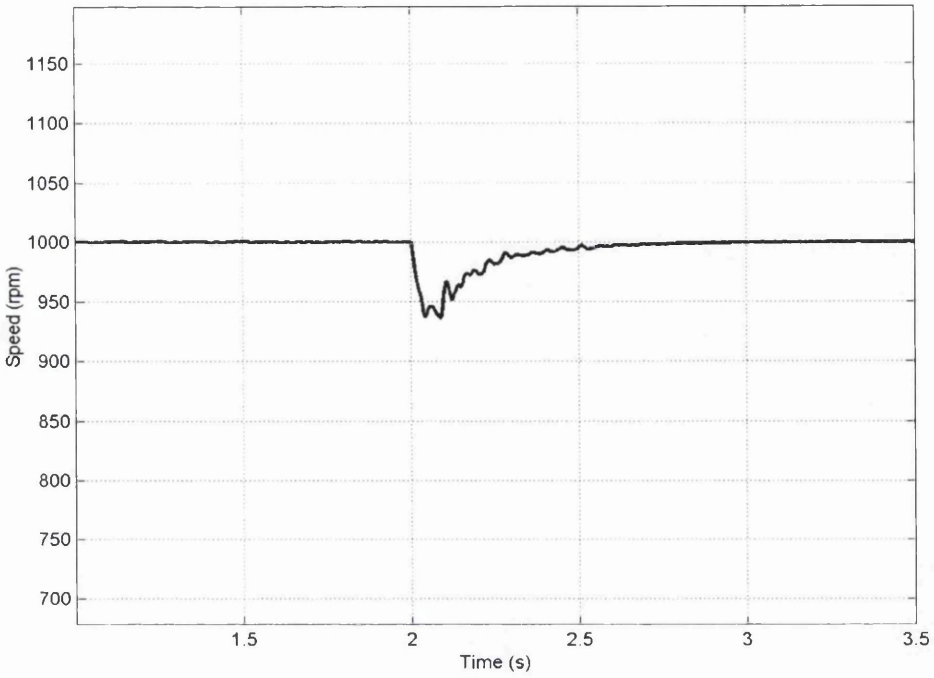

(a)

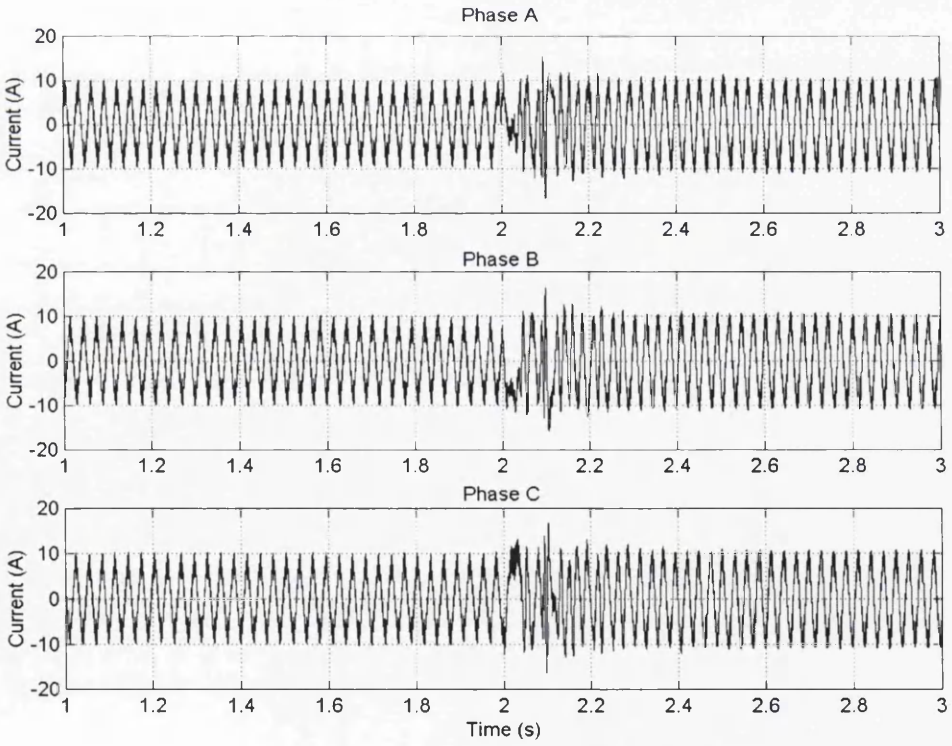

(b)

Figure 4-29: Simulation results of closed-loop FLC induction motor drive during step change in load torque. (a) Rotor speed response (b) The stator currents.

CHAPTER 5

PROPOSED FAULT DIAGNOSIS ALGORITHM

5.1 Introduction

Real time condition monitoring systems of modern electrical drives, even though quite expensive, allows the operator to obtain a full and effective identification of system working conditions. This can improve the reliability of industrial processes and reduce costs due to forced outages of drives. In fact, by early detection and correct identification of faults, an electrical drive can work even if a failure is going to occur. It is just necessary to keep fault development under control and to schedule maintenance stop. Therefore, costs due to drive service can be reduced and repair work becomes easier due to fault identification

In this chapter, a description of the proposed fault diagnosis algorithm for 3-phase pulse width modulation (PWM) voltage source inverter (VSI) for closed-loop, fuzzy logic v/f speed control strategy of an induction motor drive is given. A combination of wavelet transform (WT) and fuzzy logic (FL) is chosen to detect and identify the faults. This method offers good detection efficiency and reliability

5.2 System Design

Figure 5-1 below shows the flowchart of the fault detection scheme proposed. The process can be divided into three main stages: detection, feature extraction and fault identifier. The development of the proposed scheme is based on wavelet transform and fuzzy logic, which is thoroughly discussed in the following subsection.

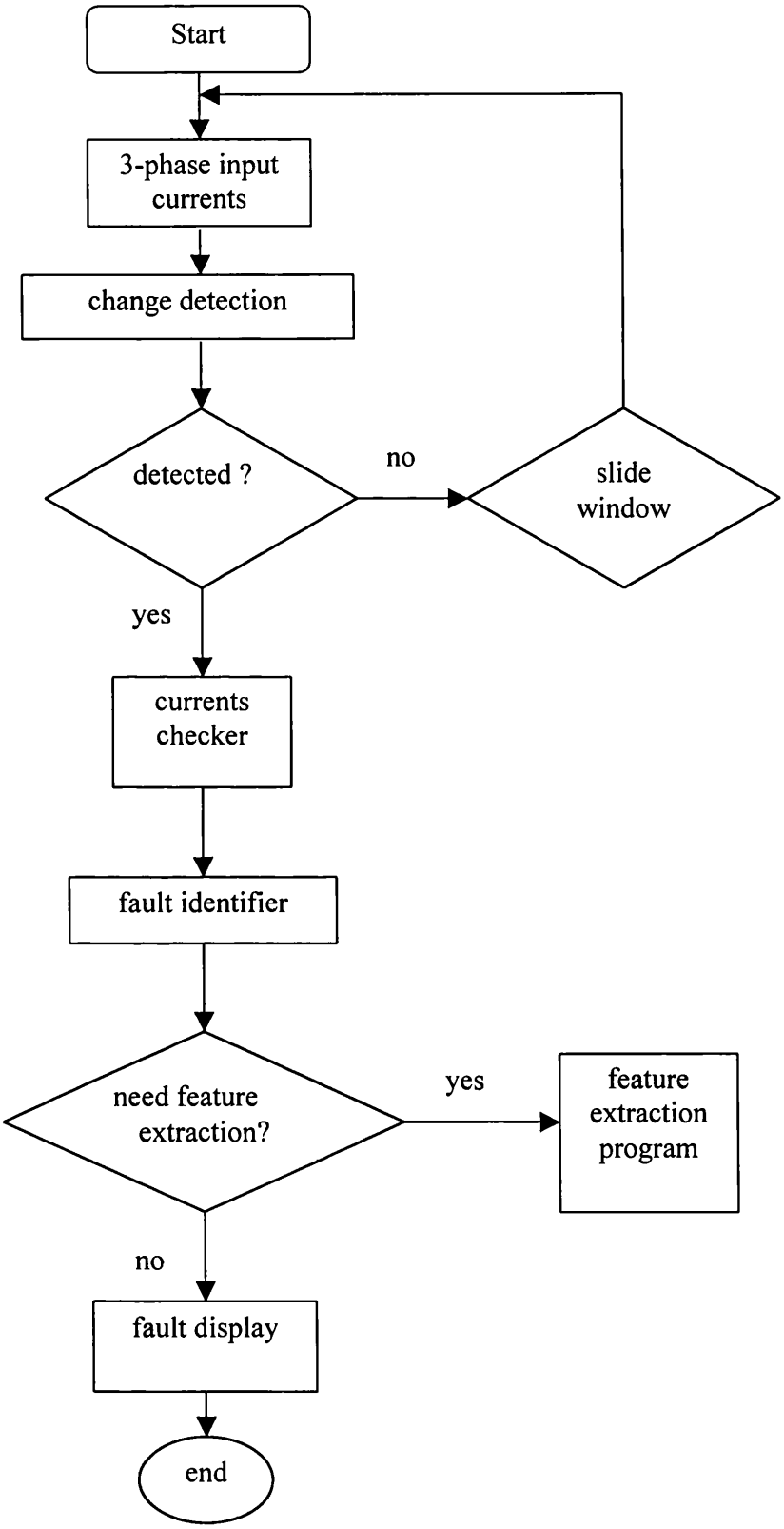

Figure 5-1(a): Flowchart of fault detection process

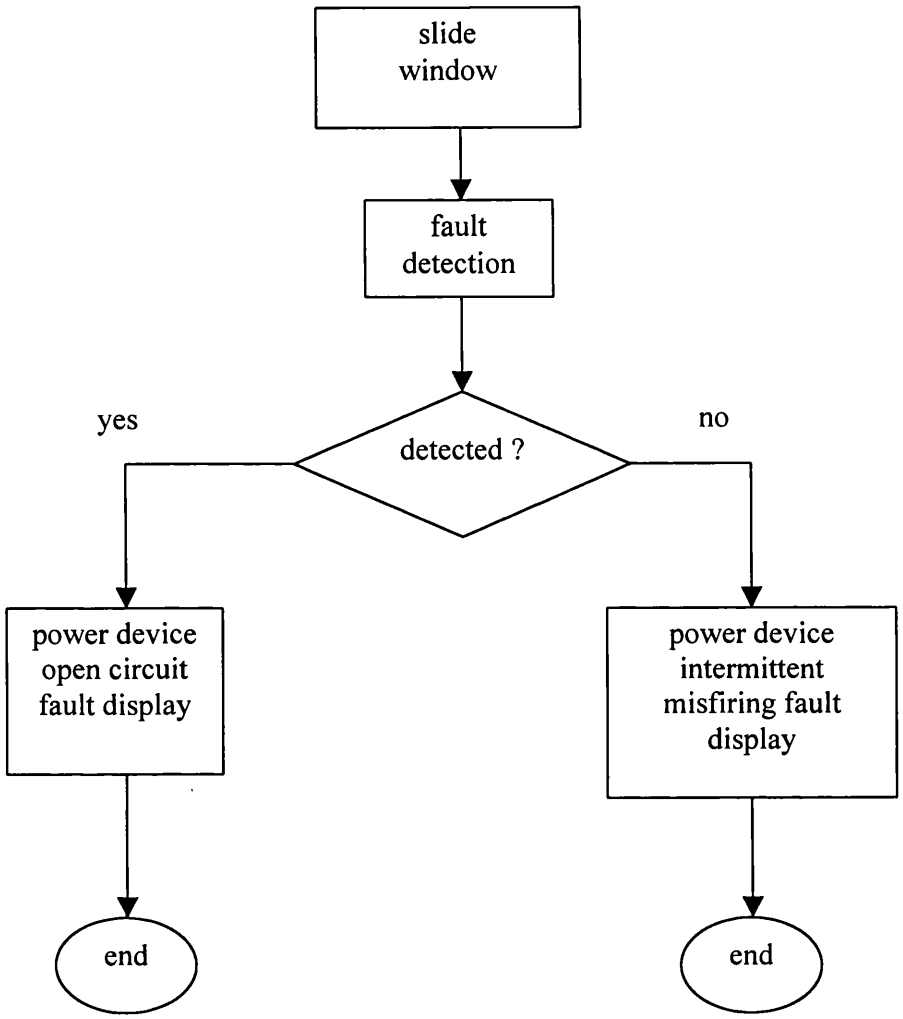

Figure 5-1(b): Flowchart of feature extraction program

5.2.1 Change Detection of Stator Currents

A change in stator current waveform is defined as the instant at which a sudden increase, decrease, transient or irregularity are observed in the current. Thus, the application of the wavelet analysis is well suited. The wavelet transform provides a good means of studying how the frequency content changes with time and consequently, is able to detect and localise short-duration malfunctions. A detailed discussion about wavelet transform is given in the next section.

In this project, a discrete wavelet transform (DWT) is used to detect the change with the aid of a 'sliding data window'. The window slide across the current waveforms by a time step of 1 cycle while capturing 4 cycles of the waveform at each time step. At each time step, the data in the window is fed to the DWT algorithm to compute the corresponding DWT coefficients. A change is considered to have occurred in the stator current waveforms if any wavelet coefficient spike exceeds or falls below a given band. On detecting the current waveform change, the sliding data window aligns itself to the point when the change was detected. Then, the dc offset in the currents is computed before feeding them to the fuzzy logic system algorithm.

The DWT program used in this thesis project is written in MATLAB M-file [25], which is given in Appendix D.

5.2.1.1 Wavelet Transform

In 1982, Morlet et al [119, 120] introduced octave decompositions for seismic data. Two years later, the link between Morlet's work and the theory of wavelets was placed on a firm footing by Grossman and Morlet [121]. Wavelet functions are localised in time and frequency. The wavelet functions are created from a single characteristic shape, known as the wavelet mother function, by dilating and shifting the window as shown in Figure 5-2. Dilation involves stretching and compressing the mother wavelet in time.

The wavelet can be expanded to a coarse scale to analyse low frequency, long duration features in the signal. Correspondingly, the wavelet can be shrunk to a fine scale to analyse high frequency, short duration features. It is this ability to change the scale of observation to study different-scale features in the signal that has become a hallmark of wavelet analysis.

The wavelet transform of the signal is generated by finding a linear combination of the wavelet functions to represent the signal. The weights of this linear combination are termed the wavelet coefficients. The reconstruction of the signal from these wavelet coefficients arises from much older theory known as CalderÓns reproducing identity [121]. The existence of a reconstruction formula reassures the preservation of information

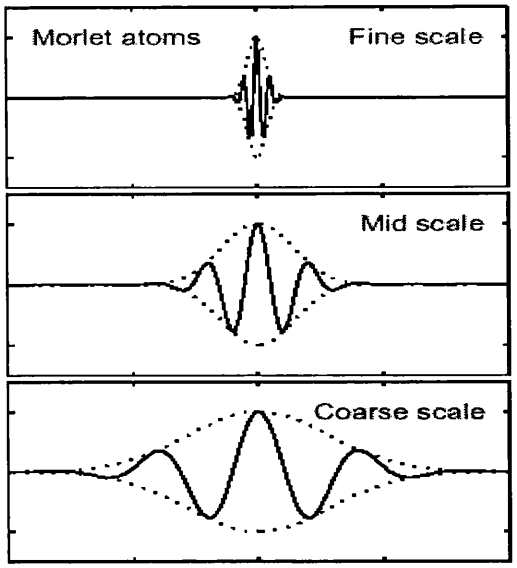

Figure 5-2: Time frequency atom used in wavelet transform, where the wavelet atoms change the width of window function.

in the transform (except for a constant dc offset).

An important development in wavelet theory was the construction of smooth orthogonal wavelets with finite support by Daubenchies in 1988 [122]. Because the wavelet functions are orthogonal, a fast transform known as the discrete wavelet transform (DWT) can be used and the reconstruction of the signal from its wavelet coefficient is straightforward and stable. Finite support means that the wavelet functions are only non-zero over a finite duration, which is important if the wavelet transform is to represent local features in the signal. Interestingly, the simplest member of Daubechies family of wavelets was found by Haar in 1909 (but possesses no smoothness).

Shortly after the discovery of orthogonal wavelets, biorthogonal wavelets were introduced [123] in which the reconstruction wavelets are biorthogonal to the analysis wavelets. This has led to more freedom in the design of wavelet functions. Since then, several other wavelet-like families have been developed including wavelet packet [124] and local trigonometric bases [125].

A major feature of wavelet is their smoothness which leads to their use in representing locally smooth signals. The representation of smooth functions in the wavelet domain is often sparse as the signal can be accurately reproduced using only a small number of wavelets. A technique called thresholding, in which insignificant wavelet coefficients are set to zero, leads to effective applications in compression and noise-removal. In addition, because wavelets are localised in time, wavelet techniques are particularly suited to the signals containing transient features as shown in figure 5-3, which are difficult to study with conventional methods. Fault detection has become one of the most successful applications of wavelet analysis [126-132].

In general, the non-orthogonal wavelet transform, commonly known as the continuous wavelet transform (CWT), is mostly used for data analysis where the redundancy of information aids in both qualitative and quantitative interpretation. In contrast, the DWT is used in applications where the efficiency and compression properties of the transform are important. The range of applications that have been proposed over the past ten years is enormous. It seems that wavelets have found a use in almost every branch of science and engineering. Some useful overviews and tutorials of wavelet applications in a range of fields can be found in [133-138]. Due to rapid pace of development, many recent applications and software can be found on the World-Wide Web (WWW). A good place to start is the wavelet digest at http://www.wavelet.org/.

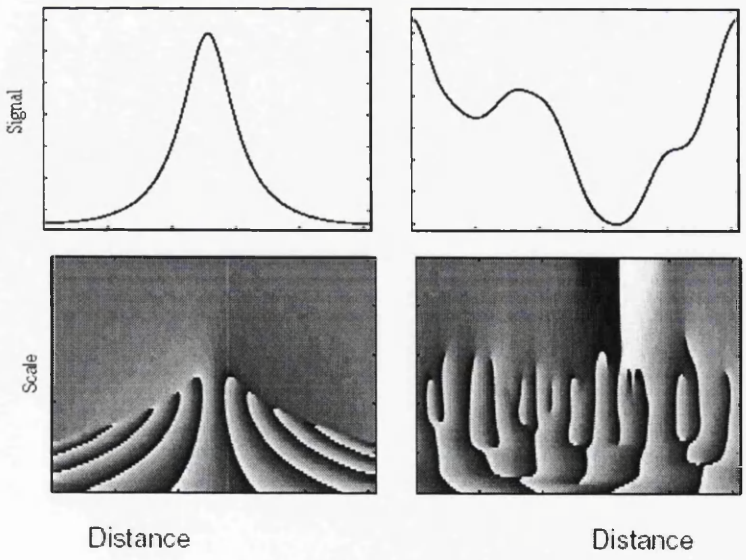

Figure 5-3: Wavelet phase coefficient

5.2.1.2 The Continuous Wavelet Transform

The continuous wavelet transform (CWT) is a time-frequency decomposition, which links a time (or space) domain function to its time-scale wavelet domain representation. The concept of scale is broadly related to frequency. Small scales relate to short duration, high frequency features and correspondingly, large scale relate to long duration, low frequency features. The CWT is defined as

$$C(x,s) = T(x)\ \psi^*\left(\frac{x}{s}\right) \tag{5.1}$$

where $T(x)$ is the measured signal, $\psi(x)$ is the analysing wavelet, x is a location, s is the scale parameter and $C(x,s)$ is the two-parameter array of wavelet coefficients. The asterisk superscript * denotes complex conjugation.

The CWT in equation (5.1) is calculated by convolving the wavelet function with the signal over a range of carefully chosen scales. Using the convolution theorem, we can simplify the CWT in the frequency domain.

$$\hat{C}(w,s) = \hat{T}(\omega)\hat{\psi}^*(s\omega) \tag{5.2}$$

where $\hat{C}, \hat{T}$ and $\hat{\psi}$ are the Fourier transforms of C, T and ψ respectively. Note that here we define $\psi^*\left(\frac{x}{s}\right)$ and $\hat{\psi}^*(s\omega)$ as a Fourier transform pair for simplicity [158].

The frequency domain representation in equation (5.2) highlights the link between the CWT and filter-bank transforms. In fact, the CWT originated from the design of an octave-band decomposition by Morlet et.al in 1982 [119,120]. Morlet applied a series of band-pass filters, each centered about a power-of-two multiple of some base frequency, in order to study the time-frequency content of seismic signals. In addition, Morlet required the impulse response of each of these band-pass filters to have a constant number of oscillations.

The result was essentially the CWT given in equations (5.1) and (5.2) with each wavelet ψ interpreted as a band-pass filter. Morlet choose a Gaussian-modulated complex exponential as the characteristic filter function because of its optimal localisation in both time and frequency. The coefficient C therefore provided a measure of the local frequency content of the signal in a series of octave bands.

The importance of this method of filter-bank construction was described two years later by Grossman and Morlet [121] who found that the filters chosen by Morlet met the conditions of CalderÓn's identity. CalderÓn's identity allows us to reconstruct the original signal T in terms of the filter function and the coefficient C. The key difference between the CWT and earlier filter-bank transforms is that the CWT filters are all generated from a single characteristic function by dilations and shifts.

5.2.1.3 The Discrete Wavelet Transform

The CWT described in the previous sections is an over determined transform. This redundancy of information is very useful for analysing the space-frequency content of signals. However, the cost of this extra information is an increased computational time for the transform. The discrete wavelet transform (DWT) uses an orthogonal or biorthogonal basis to represent the signal. Thus, in applications requiring good computational efficiency the DWT may be preferable to the CWT.

The discrete wavelet transform DWT can be simply thought of filter banks. A filter bank is defined as a set of filters, which are applied to a signal together with changes in sampling rates. The simplest case is the two-channel filter bank, which consist of a low-pass filter and a high-pass filter, represented by the coefficients $\tilde{h}$ and $\tilde{g}$ respectively. The DWT applies these filters to the data vector keeping only every second data point in the filtered response. The subsampling operation is termed downsampling. The DWT can be represented in matrix form by the composite matrix Y where

$$Y = \begin{bmatrix} \tilde{L} \\ \tilde{B} \end{bmatrix} \tag{5.3}$$

and

$$\widetilde{L} = \frac{1}{\sqrt{2}} \begin{bmatrix} \ddots & & & & & & & & \\ \cdots & \widetilde{h}_{M-1} & \widetilde{h}_{M-2} & \widetilde{h}_{M-3} & \cdots\cdots\cdots & \widetilde{h}_2 & \widetilde{h}_1 & \widetilde{h}_0 & \cdots \\ & & \widetilde{h}_{M-1} & \widetilde{h}_{M-2} & \widetilde{h}_{M-3} & \cdots\cdots & \widetilde{h}_2 & \widetilde{h}_1 & \widetilde{h}_0 & \cdots \\ & & & & & \ddots & & & \end{bmatrix} \tag{5.4}$$

$$\widetilde{B} = \frac{1}{\sqrt{2}} \begin{bmatrix} \ddots & & & & & & & & \\ \cdots & \widetilde{g}_{M-1} & \widetilde{g}_{M-2} & \widetilde{g}_{M-3} & \cdots\cdots\cdots & \widetilde{g}_2 & \widetilde{g}_1 & \widetilde{g}_0 & \cdots \\ & & \widetilde{g}_{M-1} & \widetilde{g}_{M-2} & \widetilde{g}_{M-3} & \cdots\cdots & \widetilde{g}_2 & \widetilde{g}_1 & \widetilde{g}_0 & \cdots \\ & & & & & \ddots & & & \end{bmatrix} \tag{5.5}$$

where M is a wavelet vanishing moment.

The filter coefficients $\widetilde{h}$ and $\widetilde{g}$ are normalised by a factor of $\left(1/\sqrt{2}\right)$ to preserve the energy of the filtered output following the downsampling. The downsampling is achieved in matrix form by removing every second row of the standard filtering matrix, resulting in the double column shift between the start of each row of filters in Y. The DWT matrix Y now has a block-banded structure and still possesses the sparsity required for fast multiplication. The DWT is performed by applying Y to a signal $T = T(n)$ to obtain a transformed vector containing the downsampled low-pass output $\widetilde{a}$ and high-pass output $\widetilde{b}$.

$$YT = \begin{bmatrix} \widetilde{L} \\ \widetilde{B} \end{bmatrix} \mathrm{T} = \begin{bmatrix} \widetilde{a} \\ \widetilde{b} \end{bmatrix} \tag{5.6}$$

The low-pass coefficients $\widetilde{a}$ are known as the approximation coefficients. Correspondingly, the high-pass coefficients $\widetilde{b}$ are known as the detail coefficients.

The inverse discrete wavelet transform (IDWT) is performed by applying the inverse matrix Y^{-1} to the transform coefficients. The matrix Y^{-1} is a filtering matrix composed of low-pass and high-pass coefficients, h and g, known as the synthesis filters.

$$T = Y^{-1}\begin{bmatrix}\widetilde{a}\\ \widetilde{b}\end{bmatrix} = \begin{bmatrix}L' & B'\end{bmatrix}\begin{bmatrix}\widetilde{a}\\ \widetilde{b}\end{bmatrix} \tag{5.7}$$

The submatrices L and B are constructed from h and g just as in equations (5.4) and (5.5).

5.2.1.4 Daubechies Wavelet

When the DWT scheme is applied to the signal, the correct choice of wavelet to be used is very important. It depends on the required analysis. For space-frequency analysis, we need a wavelet that is optimally localised in terms of both spatial width and frequency bandwidth. For smooth signals, we generally want a wavelet that is itself smooth and therefore has a good frequency localisation. In contrast, signals that contain discontinuities are better analysed using wavelets with good spatial localisation to accurately map rapid changes in the signal.

The Daubechies wavelet transform is named after its inventor [122]. The Daubechies wavelet is a continuous and compactly supported wavelet. The compact support of the wavelet allows the wavelet transformation to efficiently represent functions or signals, which have localized features. Many real world signals have these features, and decompositions such as the Fourier transform are not well suited to represent such signals. The efficiency of the representation is important in signal detection applications.

In this approach, Daubechies used the scaling function to compute the wavelet ψ. The scaling function and wavelet are defined by [157]:

$$\phi(x) = \sum_{k=0} c_k \sqrt{2}\, \phi(2x - k) \tag{5.8}$$

$$\psi(x) = \sum_{k=0} (-1)^k c_{1-k} \sqrt{2}\, \phi(2x - k) \tag{5.9}$$

The Daubechies 4 (D4) wavelet, which has four vanishing moments is proposed in this thesis to detect the transient of the signal. The selection is decided after a series of tests were made with the real experimental data. The D4 was found to offer a better sensitivity and clear spike in detecting the faults compared with the other Daubechies families. Chang et.al [128] demonstrated that the Daubechies wavelet is the best wavelet to detect the transient and irregularity of the signal. In fact, D4 is only the most compact of sequence of a wavelet sets [22].

5.2.1.5 Wavelet Filter Coefficients for D4

A particular set of wavelets is specified by a particular set of numbers, called wavelet filter coefficients. The simplest and most localized member of Daubechies wavelet is called D4, has only four coefficients c_0, c_1, c_2 and c_3.

Consider the following transformation matrix acting on a column vector of data to its right:

$$\begin{bmatrix} c_0 & c_1 & c_2 & c_3 & & & & & & & & \\ c_3 & -c_2 & c_1 & -c_0 & & & & & & & & \\ & & c_0 & c_1 & c_2 & c_3 & & & & & & \\ & & c_3 & -c_2 & c_1 & -c_0 & & & & & & \\ \vdots & \vdots & & & & & \ddots & & & & & \\ & & & & & & & c_0 & c_1 & c_2 & c_3 & \\ & & & & & & & c_3 & -c_2 & c_1 & -c_0 & \\ c_2 & c_3 & & & & & & & & c_0 & c_1 & \\ c_1 & -c_0 & & & & & & & & c_3 & -c_2 & \end{bmatrix} \tag{5.10}$$

Blanks entries signify zeroes. The first row of matrix generates one component of the data convolved with the filter coefficients c_0, c_1, c_2 and c_3. Likewise the third, fifth and the other odd rows. Meanwhile, the even rows perform a different convolution with coefficients c_3, $-c_2$, c_1 and $-c_0$. The action of the matrix, overall, is thus to perform two related convolutions, then to decimate each of them by half (throw away half the values), and interleave the remaining halves.

The filter c_0, c_1, c_2 and c_3 is called low-pass filter, and the filter c_3, $-c_2$, c_1 and $-c_0$ is called high-pass filter. These two filters are called *quadrature mirror filters* [138]. In fact, the c's are chosen so as to make high-pass filter yields, insofar as possible, a zero response to a sufficiently smooth data vector. This is done by requiring the sequence c_3, $-c_2$, c_1 and $-c_0$ to have a certain number of vanishing moments. When this is the case for p moments, a set of wavelets is said to satisfy an approximation condition of order p. This results in the output of low-pass filter, decimated by half, accurately representing the data's approximate information. The high-pass filter output is referred to as the data's detail information.

For such a characterisation to be useful, it must be possible to reconstruct the original data vector of length N from its $N/2$ approximation components and its $N/2$ detail components. That is effected by requiring the matrix in equation (5.10) to be orthogonal, so that its inverse is just the transposed matrix.

$$\begin{bmatrix}
c_0 & c_3 & & & \cdots & & & & & c_2 & c_1 \\
c_1 & -c_2 & & & \cdots & & & & & c_3 & -c_0 \\
c_2 & c_1 & c_0 & c_3 & & & & & & & \\
c_3 & -c_0 & c_1 & -c_2 & & & & & & & \\
 & & & & \ddots & & & & & & \\
 & & & & & c_2 & c_1 & c_0 & c_3 & & \\
 & & & & & c_3 & -c_0 & c_1 & -c_2 & & \\
 & & & & & & & c_2 & c_1 & c_0 & c_3 \\
 & & & & & & & c_3 & -c_0 & c_1 & -c_2
\end{bmatrix} \tag{5.11}$$

The matrix in equation (5.10) is inverse to matrix in equation (5.11) if and only if these two equations hold,

$$c_0^2 + c_1^2 + c_2^2 + c_3^2 = 1 \tag{5.12}$$

$$c_0\, c_2 + c_1\, c_3 = 0 \tag{5.13}$$

If additionally the approximation of order p = 2, then two additional relations are required,

$$c_3 - c_2 + c_1 - c_0 = 0 \tag{5.14}$$

$$0c_3 - 1c_2 + 2c_1 - 3c_0 = 0 \tag{5.15}$$

Equations (5.12), (5.13), (5.14), and (5.15) first recognized and solved by Daubechies. The solution is

$$c_o = \frac{1+\sqrt{3}}{4\sqrt{2}} \tag{5.16}$$

$$c_1 = \frac{3+\sqrt{3}}{4\sqrt{2}} \tag{5.17}$$

$$c_2 = \frac{3-\sqrt{3}}{4\sqrt{2}} \tag{5.18}$$

$$c_3 = \frac{1-\sqrt{3}}{4\sqrt{2}} \tag{5.19}$$

5.2.1.6 The Implementation of DWT

In this project, the DWT is implemented using multiresolution signal decomposition algorithm. The stator current signal *T(n)* (sampled at 2 kHz, and 400 samples per window) is passed through a series of a high pass filters to analyse the high frequency and a series of low pass filter to analyse the low frequency.

At the first level, the signal is passed through the high pass and low pass filters, followed by sub-sampling by 2. The output of the high pass filter has 200 samples (half the time

resolution) and the frequency range of 1 kHz to 2 kHz (double the frequency resolution). These 200 samples constitute the first level of DWT coefficients, $\tilde{b}_1$. The output of the low pass filter, DWT coefficient $\tilde{a}_1$, also has 200 samples, but it spans the other half of the frequency band, frequencies from 0 to 1 kHz.

At the second level, $\tilde{a}_1$ is passed through the high pass and low pass filters, and followed by sub-sampling by 2. The output of the high pass filter, $\tilde{b}_2$ has 100 samples points (half the time resolution of the first level) and the frequency range of 500 Hz to 1 kHz (twice the frequency resolution of the first level). Meanwhile, the output of the low pass filter, DWT coefficient $\tilde{a}_2$, also has 100 samples, but it spans the other half of the frequency band, frequencies from 0 to 500 Hz. The process continues until it reached the level $j = 3$.

The information about the system disturbance or fault is obtained from the detail coefficients $\tilde{b}_3$. These coefficients are non-zero when disturbance exists. The DWT process is illustrated in Figure 5-4.

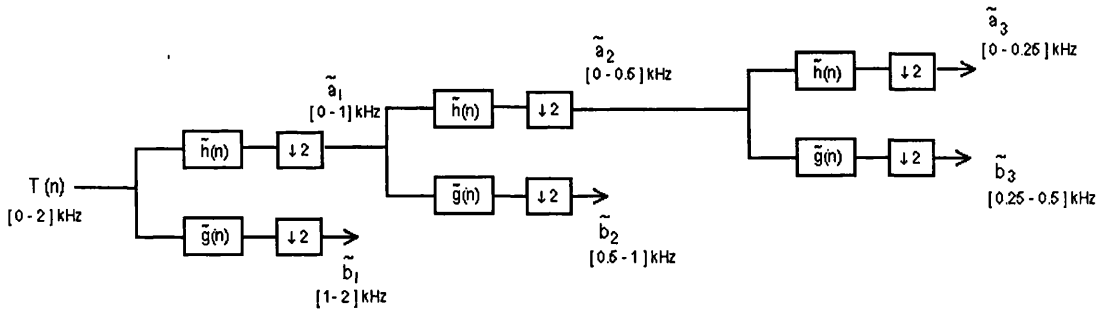

Figure 5-4: Multiresolution signal decomposition

5.2.1.7 Recent Development of Fault Detection Using Wavelet Transform

With no doubt, the potential of wavelet transform in fault detection applications is great. As a result, it has recently attracted a significant attention in the condition monitoring and fault detection research community worldwide.

Chao-Ming Chen and Keneth A. Laparo [126] in 1998, proposed an algorithm based on discrete wavelet transform to detect electrical faults in vector-controlled induction motor system. The algorithm computes a 'fault index' in stator currents to determine the stator winding faults. The simulated results have showed that the fault signature can be clearly observed.

In 1999, Arturi et.al [127] presented a dynamic analysis of electromechanical converters by means of wavelet transform. The analysis proposed in this paper is realised by connecting a four-quadrant converter to an induction machine. Under this technique, a specific behaviour which occurred during the transient conditions is used as a tool to define the optimal working conditions of the system and the suitable control strategies.

Wavelet transform has been also used to detect the remote short-circuit in dc railway system, as proposed by Chang et.al [128], in 2000. The remote short-circuit current is determined mainly by the steel rail impedance, which is time varying due to the skin effect. The results showed that the wavelet transform, through the displays of its coefficients is successfully able to discriminate the remote short-circuit current from the train starting current. The detailed experimental results are given by Chang et.al [130], in 2001. In the latter paper, the wavelet analysis is combined with a neural network to produce a complete and efficient remote short-circuit detection system.

The combination of wavelet transform and neural network was proposed by Borras et.al [129], in 2001 as a new tool for diagnosis of power system disturbances. This system will automatically detect, compact and classify the disturbances. The simulated results showed that this combination technique offered great potential for electrical power system diagnosis, especially in the area of power quality problem.

Zhongming and Bin [131] presented the same technique to detect rotor bar breakage of 3-phase induction motors. New features of rotor bar faults are obtained by wavelet packet decomposition of the stator current. These features are of multiple frequency resolutions and obviously differentiate the healthy and faulty conditions. The features with different frequency resolutions are used together with the speed slip as the input sets of a 4-layer perceptron network. The laboratory result showed that the proposed technique is able to detect the faulty rotor bar with high accuracy.

Recently, Peng and Andrew [132], in 2002 proposed an algorithm to classify wheel bearing faults of train in wayside conditions using a combination of optimal wavelet features and neural network. By using the tree structure strategy, the authors reported that the missing rate of condemnable bearing is reduced to less than 1 %. The algorithm is proved fast and robust in wayside condition. To support these claims, the experimental results are supplied by the authors.

5.2.2 Fault Identifier

The fault identifier process by fuzzy logic system leads to the determination of particular faults, occurring in the system. This process takes place after a system checked the status of stator currents. The currents need to be checked to ensure that all three-phase currents are connected to the system. Otherwise, the fuzzy system will prompt a single phasing fault.

On detecting faults, the system will calculate the value of dc offset in the currents. The value and polarity of the dc offset is then fed to the fuzzy logic system to determine the faults. Fuzzy logic algorithms adopted in the proposed fault identifier are systematically designed according to intuition and experiences about the 3-phase VSI behaviour. The advantage of using fuzzy logic is that it is easy to apply heuristics knowledge and 'rule-of-thumb' experience. In this project, the level of dc offset of all three stator currents are considered as the variables to the fuzzy system.

5.2.2.1 The Proposed Fault Identifier Using Fuzzy Logic System

To identify the faults is not always a straightforward case, particularly when in practice, the signal always contains noise and disturbance. For instance, a slight load unbalance during normal operation may introduce a low level dc offset on one of the phase currents. Measurement and sensor errors may also give misleading information. To exclude such cases from faulty operation category, fuzzy rules should be carefully designed.

A. Fuzzy System Input-Output Variables

In this thesis, the stator current dc offset of phase A (I_{Adc}), phase B (I_{Bdc}) and phase C (I_{Cdc}) are considered as the input variables to the fuzzy system. The VSI condition VM is chosen as the output variable. All the fuzzy system input and output variables are defined using fuzzy set theory as below.

$$I_{Adc} = \{ \mu_{IAdc}(i_{Adcj}) / i_{Adcj} \in I_{Adc} \} \quad (5.20)$$

$$I_{Bdc} = \{ \mu_{IBdc}(i_{Bdcj}) / i_{Bdcj} \in I_{Bdc} \} \quad (5.21)$$

$$I_{Cdc} = \{ \mu_{ICdc}(i_{Cdcj}) / i_{Cdcj} \in I_{Cdc} \} \quad (5.22)$$

$$VM = \{ \mu_{VM}(vm_j) / vm_j \in VM \} \quad (5.23)$$

where i_{Adcj}, i_{Bdcj}, i_{Cdcj} and vm_j are the elements of the discrete universe of discourse I_{Adc}, I_{Bdc}, I_{Cdc} and VM, respectively. Also, $\mu I_{Adc}(i_{Adcj})$, $\mu I_{Bdc}(i_{Bdcj})$, $\mu I_{Cdc}(i_{Cdcj})$,and $\mu VM(vm_j)$ are, respectively, the corresponding membership functions.

B. Construction Of The Fuzzy And Membership Functions

Fuzzy rules and membership functions are constructed by observing the input data set. For the measurements related to the stator currents dc offset, more insight into the data is required. Therefore, membership functions will be generated for negative dc offset (-DC), zero dc offset (Z) and positive dc offset (+DC).

For the measurement related to VSI condition, it is necessary to know if the VSI is in good condition (G), load disturbance (L_A, L_B, L_C), switching device intermittent misfiring fault (T_{1if}, T_{2if}, T_{3if}, T_{4if}, T_{5if}, T_{6if}), or power device base open-circuit fault (T_{1of}, T_{2of}, T_{3of}, T_{4of}, T_{5of}, T_{6of}). The optimised membership functions for this project are shown in Figure 5-5.

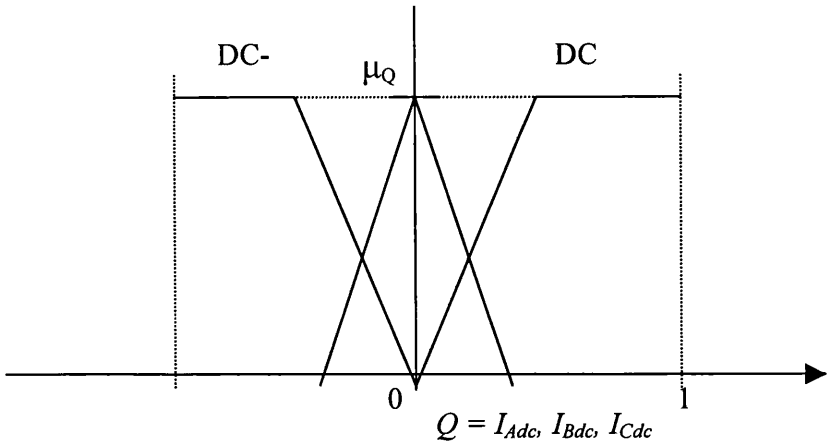

Figure 5-5: Fuzzy membership function for stator currents DC offset.

5.2.3 Feature Extraction

The feature extraction process is introduced to enhance the difference between the transistor base drive open-circuit fault and an intermittent misfiring of inverter switching devices. The process takes place only after a fault has been detected by FLS in the stator current waveforms. On detecting and identifying the fault, the system will wait for 4 cycles before checking the fault for the second time. The transistor base drive open-circuit fault is considered to have happened if the dc offset still exists in the stator currents.

However, if the dc offset is found to be zero or near zero in the later event, the intermittent is considered to have happened. In case of intermittent misfiring, as described by K.S. Smith et.al [4] the currents normally take a few cycles to settle back to normal operating condition, depending on drive controller type.

Once the form of the initial membership functions has been determined, fuzzy *If-Then* rules can be derived. The rules for this proposed VSI fault diagnosis and feature extraction algorithm are shown in Table 5.1 and Table 5.2 respectively. For instance, from the tables:

The first *If-Then* rule statements are,

If I_{ADC} = Z and I_{BDC} = Z and I_{CDC} = Z,

Then VM = G

The second *If-Then* rule statements are,

If I_{ADC} = -DC or +DC, and I_{BDC} = Z and I_{CDC} = Z

Then $VM = L_A$

The fifth *If-Then* rule statements are,

If I_{ADC} = -DC and I_{BDC} = +DC and I_{CDC} = +DC,

Then $VM = T_{1if}$ or T_{1of}

The system will wait for 4 cycles before checking the dc offset for the second time.

If I_{ADC} = -DC and I_{BDC} = +DC and I_{CDC} = +DC,

Then $VM = T_{1of}$

Or

If I_{ADC} = Z and I_{BDC} = Z and I_{CDC} = Z,

Then $VM = T_{1if}$

5.3 Summary

In this Chapter, a detailed description of the proposed fault diagnosis algorithm for 3-phase pulse width modulation (PWM) voltage source inverter VSI) for closed-loop, fuzzy logic voltage frequency (v/f) speed control strategy of induction motor has been presented. The algorithm proposed was based on the combination of wavelet transform and fuzzy logic. The following are the main points made in this Chapter.

1. The wavelet transform is generated by finding a linear combination of wavelet functions to represent the signal. The weight of this linear combination is called the wavelet coefficients. The wavelet is localised in time, which is important to study the transient signal.

2. The fault identifier algorithm by the fuzzy logic system leads to the determination of particular faults in VSI. Fuzzy logic adopted in this project is systematically designed according to intuition and experiences. The advantage

of using fuzzy logic is that it is easy to apply heuristics knowledge and rule-of-thumb experience.

Table 5.1:Fuzzy If – Then rules

Rule no.	If				Then																
		- DC	Z	+ DC	VSI status	G	L_A	L_B	L_C	T_{1if}	T_{2if}	T_{3if}	T_{4if}	T_{5if}	T_{6if}	T_{1of}	T_{2of}	T_{3of}	T_{4of}	T_{5of}	T_{6of}
1	I_{ADC}		√																		
	I_{BDC}		√		VM	√															
	I_{CDC}		√																		
2	I_{ADC}	√		√																	
	I_{BDC}		√		VM		√														
	I_{CDC}		√																		
3	I_{ADC}		√																		
	I_{BDC}	√		√	VM			√													
	I_{CDC}		√																		
4	I_{ADC}		√																		
	I_{BDC}		√		VM																
	I_{CDC}	√		√					√												
5	I_{ADC}	√								√						√					
	I_{BDC}			√	VM																
	I_{CDC}			√																	

Table 5.1:Fuzzy If – Then rules (continued)

Rule no.	If				Then																
		- DC	Z	+ DC	VSI status	G	L_A	L_B	L_C	T_{1if}	T_{2if}	T_{3if}	T_{4if}	T_{5if}	T_{6if}	T_{1of}	T_{2of}	T_{3of}	T_{4of}	T_{5of}	T_{6of}
6	I_{ADC}			√																	
	I_{BDC}	√			VM							√						√			
	I_{CDC}			√																	
7	I_{ADC}			√																	
	I_{BDC}			√	VM									√						√	
	I_{CDC}	√																			
8	I_{ADC}			√																	
	I_{BDC}	√			VM								√						√		
	I_{CDC}	√																			
9	I_{ADC}	√																			
	I_{BDC}			√	VM										√						√
	I_{CDC}	√																			
10	I_{ADC}	√																			
	I_{BDC}	√			VM						√						√				
	I_{CDC}			√																	

Table 5.2: Fuzzy If – Then rules for feature extraction

Rule no.	If				Then							
		- DC	Z	+ DC	VSI status	T_{if}	T_{1of}	T_{2of}	T_{3of}	T_{4of}	T_{5of}	T_{6of}
1	I_{ADC}		√									
	I_{BDC}		√		VM	√						
	I_{CDC}		√									
2	I_{ADC}	√										
	I_{BDC}			√	VM		√					
	I_{CDC}			√								
3	I_{ADC}			√								
	I_{BDC}	√			VM				√			
	I_{CDC}			√								
4	I_{ADC}			√								
	I_{BDC}			√	VM						√	
	I_{CDC}	√										
5	I_{ADC}			√								
	I_{BDC}	√			VM					√		
	I_{CDC}	√										
6	I_{ADC}	√										
	I_{BDC}			√	VM							√
	I_{CDC}	√										
7	I_{ADC}	√										
	I_{BDC}	√			VM			√				
	I_{CDC}			√								

CHAPTER 6

EXPERIMENTAL RESULTS AND DISCUSSION

6.1 Introduction

In this chapter, a general description of the experimental set-up of the induction motor drive system is given. The implementation of fuzzy logic controller (FLC) algorithms is utilised on the single chip, Intel 80C196KC 16-bit embedded microcontroller, a low cost derivative of the MCS-96 architecture.

This is followed by practical results of the proposed condition monitoring and fault detection system. Comparison studies between the practical results and simulation results are included.

6.2 Experimental Set-up of The Induction Motor Drive System

The experimental set-up of the complete induction motor drive system used in this thesis project is shown in Figure 6-1 and Figure 6-2. The drive system is comprised of five primary sections. The first section is the full-wave uncontrolled diode bridge, which converts the three-phase ac voltage to a rectified dc voltage.

The second section is the dc-link, which embraces an energy storing capacitor (6600μF with rated voltage of 350V). The capacitor is connected across the dc-link terminals to provide a smooth and constant dc supply.

The third section of the system is the PWM inverter bridge and the gate driver circuits. The dc input voltage is converted to a symmetrical ac output voltage of desired magnitude and frequency. The power devices used in the inverter bridge are the insulated gate bipolar transistors (IGBTs). The IRGPH40F IGBTs used in this project are rated at a maximum voltage of 1200V, peak current of 58A and a continuous current of 29A.

The ultra fast recovery diodes are connected across the IGBTs to allow freewheeling in the circuit. The reciprocal circuit is added to the inverter circuit so that the switching signal of any power devices on the same arm is complemented. A dead time is introduced to the complementary signals to prevent short-circuiting the dc-link. The TLP 759 opto-coupler is used to isolate the microcontroller board circuit from the driver circuit. In addition, protection circuits against over current, over voltage and short circuit are included.

In order to develop near-sinusoidal current waveforms with minimum low-order harmonics content, the sinusoidal pulse width modulation (SPWM) with a switching frequency of 3.5kHz is used. It should be noted that, higher switching frequencies could reduce torque pulsation, which is normally notable at low speed operation. Hence, the motor acoustic noise is minimised. However, the switching losses become excessive because of the increase in the switching frequency. Also, this can heave the temperature of the power devices and thus shorten their lives.

The fourth section is the microcontroller circuit. In this project, the Intel EV80C196KC single evaluation board is used. The board comprises a single chip 80C196KC microcontroller, two 16-bit and one 8-bit memory banks, a UART for host communication and digital I/O facilities. The microcontrollers main tasks are summarised below:

a) Calculation of motor speed by counting the encoder pulses through the HSI interrupts service routine.
b) Digital filtering for speed measurements and estimation of motor acceleration
c) Closed –loop speed regulation using fuzzy logic control
d) Calculation of the SPWM switching instants
e) Generation of the SPWM pulses through the HSO interrupt service routine.

Detailed descriptions of the microcontroller and the implementation of closed loop fuzzy logic speed controller are given in [108,156].

The fifth section of the drive system is the 3-phase ac induction motor, dc shunt generator and speed sensor. The induction motor used is a star-connected with the following specifications:
2.2 W, 4 poles, 410V, 50Hz, 1415r/min, 5A and rated torque of 15.1N.m.

A variable resistor bank, which is used to produce the load torque, is connected to the output terminals of the dc generator. The generator is mechanically coupled to the shaft of the induction motor. The rated values of the generator are as follows:
110V, 1.5kW, 1440r/min and 13.6A.

In this project, the speed of the motor is sensed via an optical shaft encoder, which is mounted on the induction motor shaft. The encoder used is capable of generating 1024 pulse per one rotor revolution. The M/T speed estimation method is implemented in the system. The M/T method offered high resolution and high accuracy in a short detection time [155]. The principle of this method is given in [156].

6.3 Experimental Results

In this section, the assessment of the proposed condition monitoring and fault detection algorithm for three-phase PWM, VSI for closed-loop, fuzzy logic, v/f speed control strategy of an induction motor drive is considered. A series of normal and faulty condition tests have been conducted rigorously in order to bring out the effectiveness of the proposed technique.

Throughout this test, the induction motor is running constantly at a speed of 1000rpm and lightly loaded. The dc-link of the inverter is set to a value of 100V dc. Then the inverter faults condition is suddenly applied to the system. The phase currents which, are sampled at 2kHz, are examined as a function of failure modes and their wavelet transform are shown, in order to detect the inverter failures and to study the effectiveness of the proposed algorithm. The occurrence of a fault is detected by a sharp rise or drop in the magnitude of the D4 wavelet coefficient.

If the fault is detected, the fuzzy logic system will be activated to determine the type of fault. The fault is then determined by checking the value and the polarity of the dc offset in the phase currents.

6.3.1 Inverter Transistor Base Drive Open-Circuit Fault

Figures 6-3 to 6-14 shows the phase currents and wavelet coefficient D4 when the transistor *T1*, *T2*, *T3*, *T4*, *T5* and *T6* is open-circuit fault, respectively. It should be noted that this fault introduced the dc offset to the phase currents, as can be clearly seen. A larger dc offset magnitude is detected in faulty phase, as compared to the other phases. Also, the polarity of dc offset in the faulty phase is opposite with the other phases.

There is no doubt that the DWT is able to capture the significant irregular data pattern such as sharp "jumps" in current waveforms, as clearly observable in Figures 6-4, 6-6, 6-8, 6-10, 6-12 and 6-14. Immediately after the fault occurrence, a sharp spike appears in the detail coefficient signal indicating the occurrence of the fault. As mentioned before, the wavelet is localised in time. This feature is important to determine the exact instant when the fault has occurred. Here is a noteworthy example of an advantage of DWT analysis.

In addition, Figures 6-15 to 6-20 demonstrate simulation results obtained for the aforementioned faults. The same operating conditions applied in the experimental tests are considered here for the simulation. The inspection of these figures indicates the experimental results agree with those of the simulation results. But in the simulation results, the transient response that is created by the controller for maintaining the speed when the fault has occurred is clearly visible. This is because the sampling time used in simulation is 10kHz compared 2kHz used for experimental works.

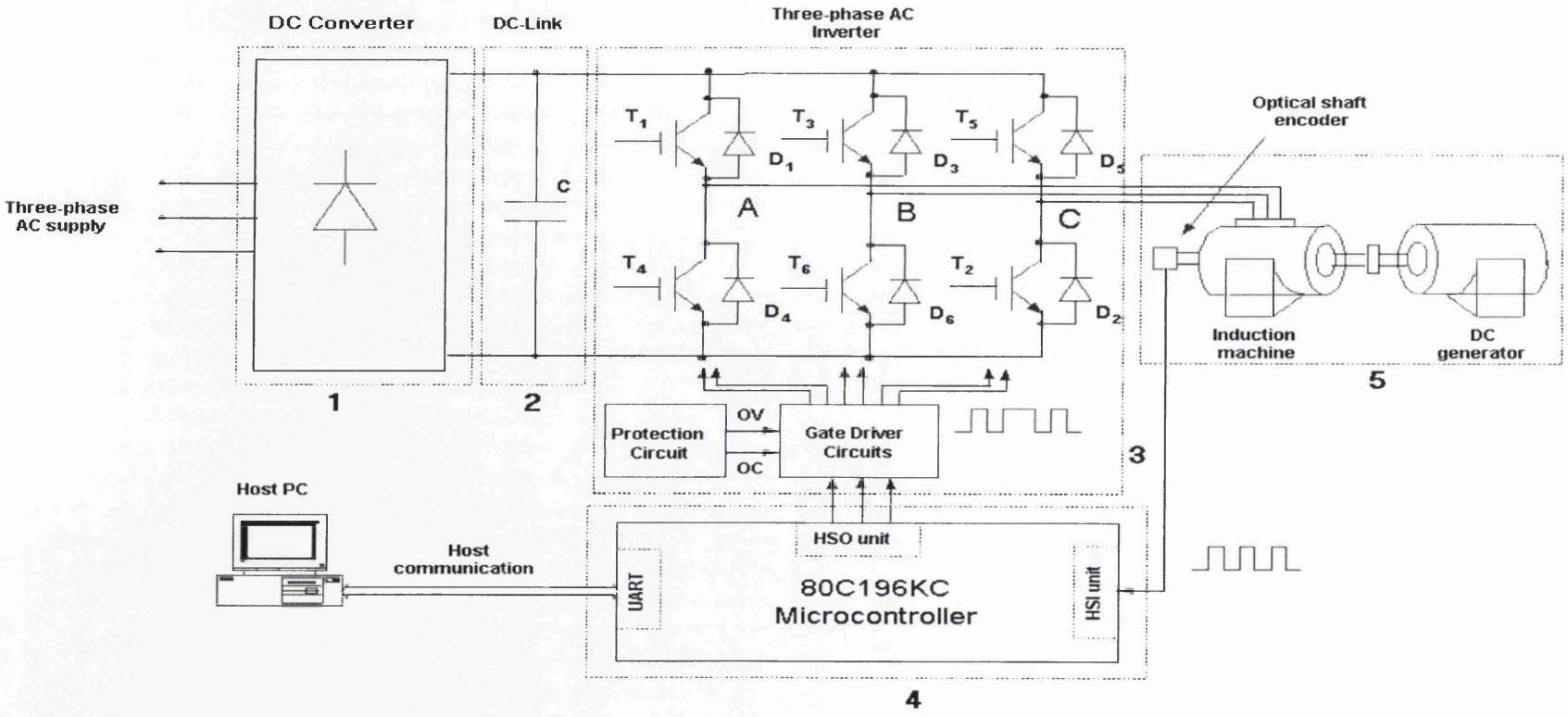

Figure 6-1 Schematic diagrams of the hardware set-up for induction motor drive system

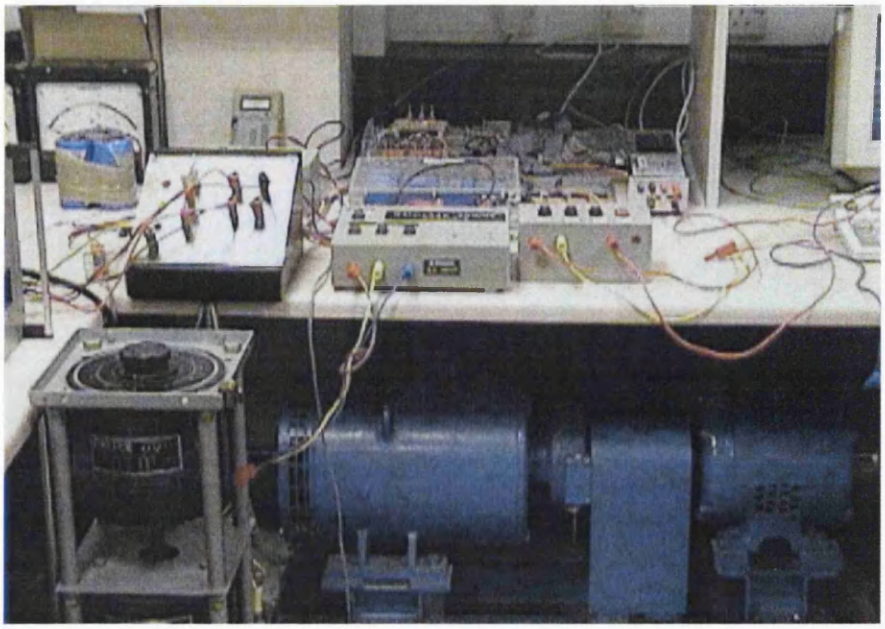

(a)

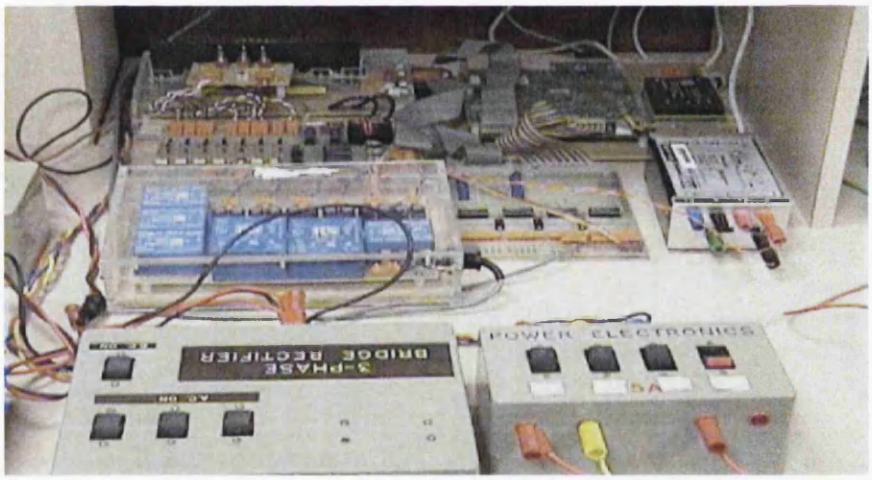

(b)

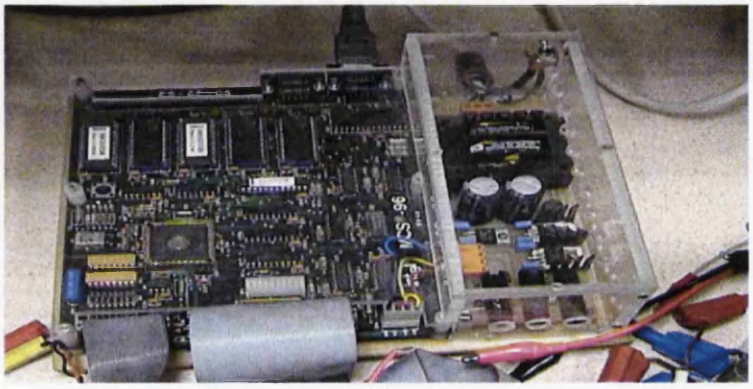

(c)

Figure 6-2: Photos of experimental set-up for induction motor drive. (a) The complete system, (b) Power electronic circuits, and (c) Microprocessor board.

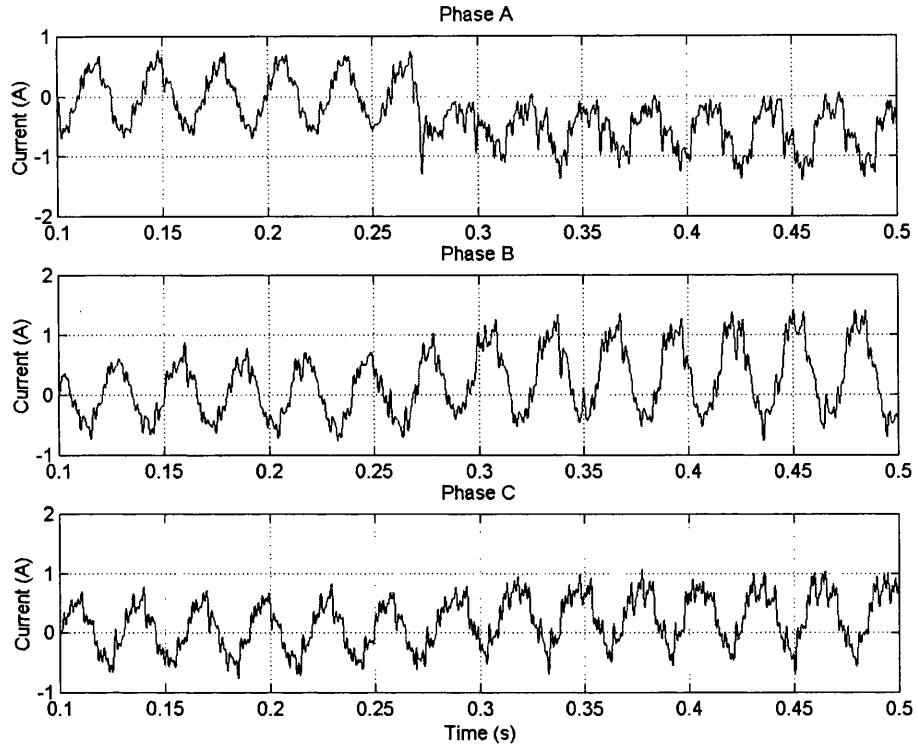

Figure 6-3: The experimental current waveforms for inverter transistor T1 open-circuit fault.

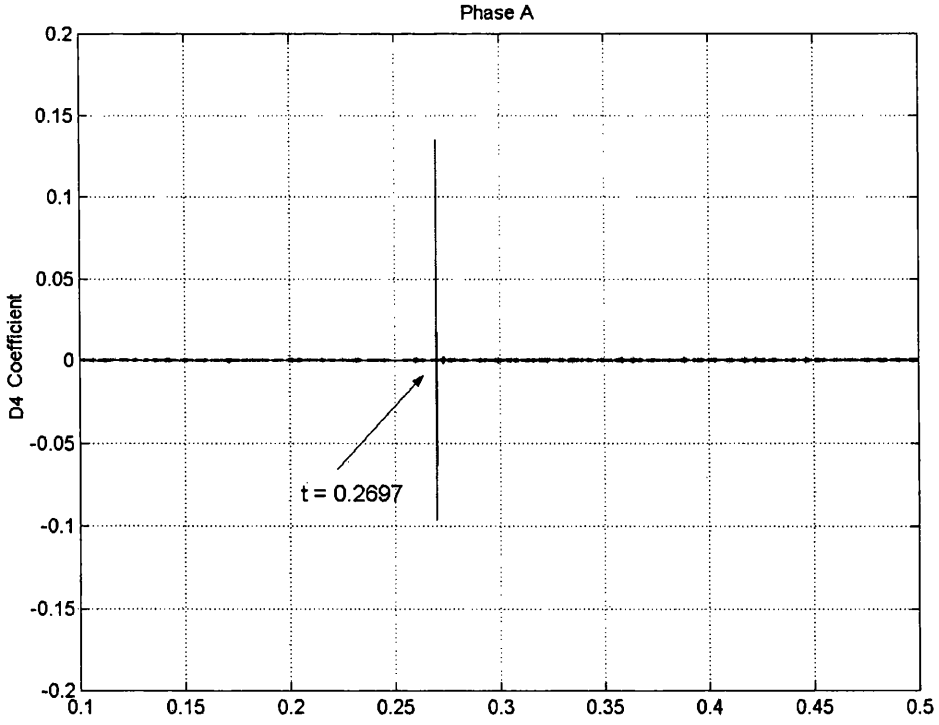

Figure 6-4: The D4 coefficient of phase A for inverter transistor T1 open-circuit fault.

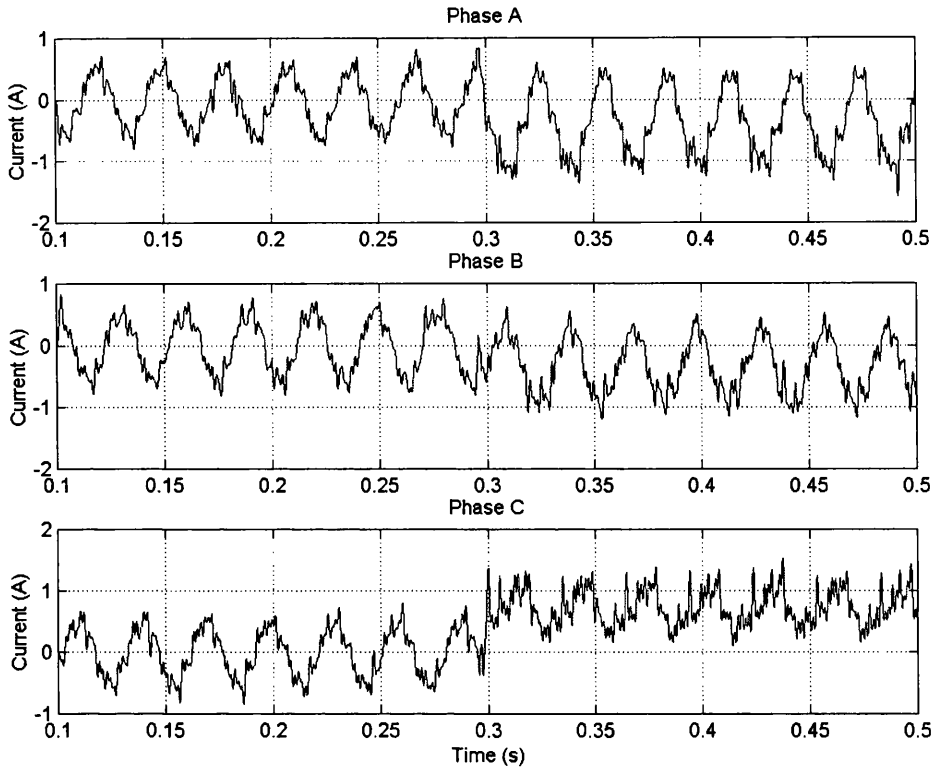

Figure 6-5: The experimental current waveforms for inverter transistor T2 open-circuit fault.

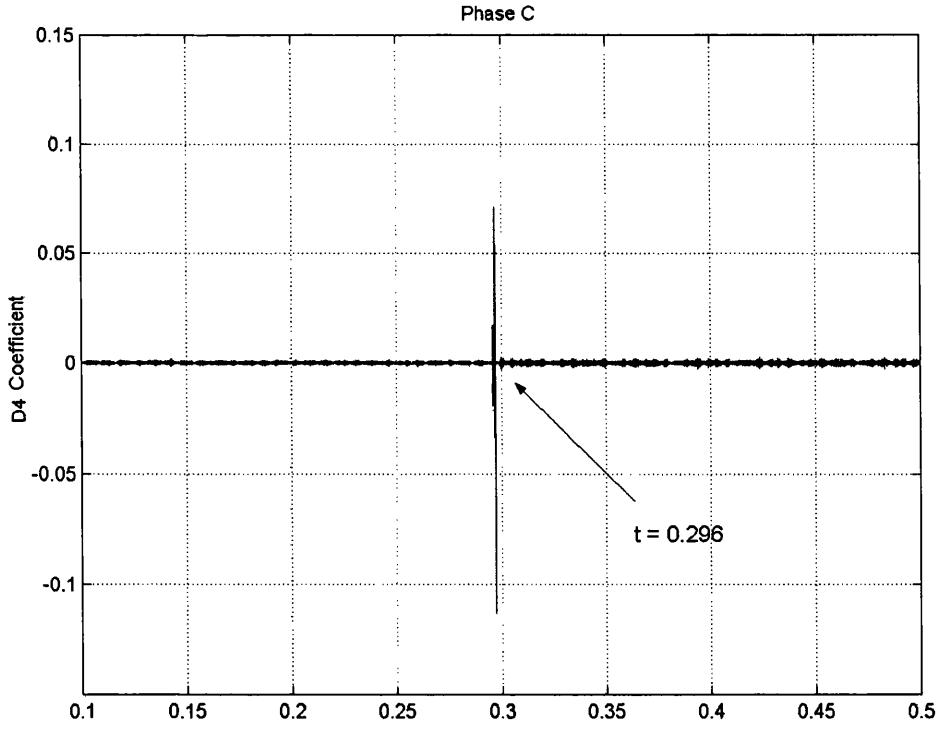

Figure 6-6: The D4 coefficient of phase C for inverter transistor T2 open-circuit fault.

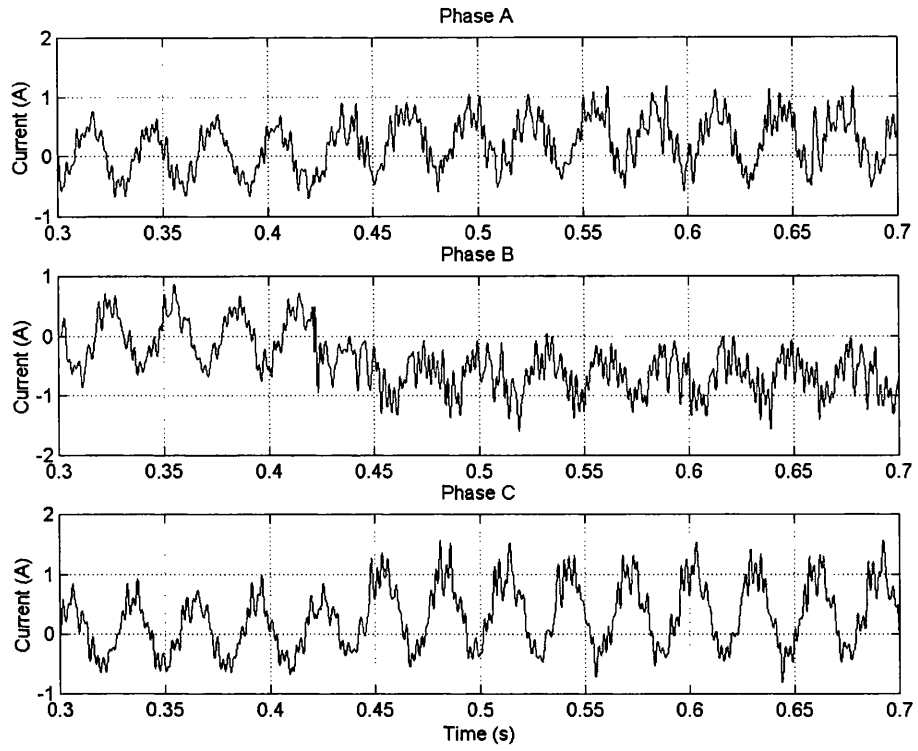

Figure 6-7: The experimental current waveforms for inverter transistor T3 open-circuit fault.

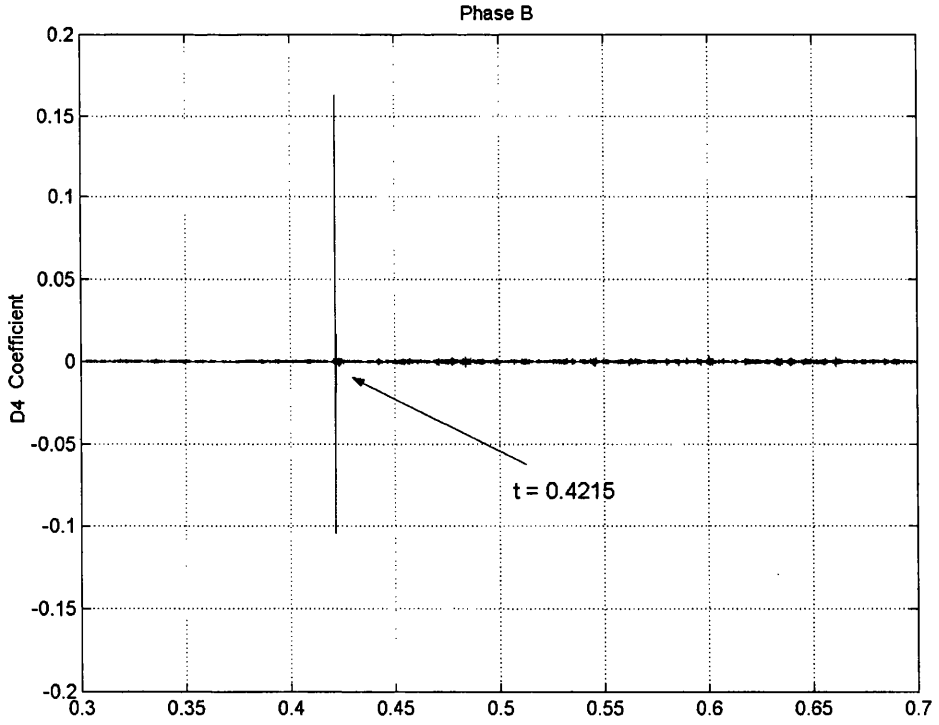

Figure 6-8: The D4 coefficient of phase B for inverter transistor T3 open-circuit fault.

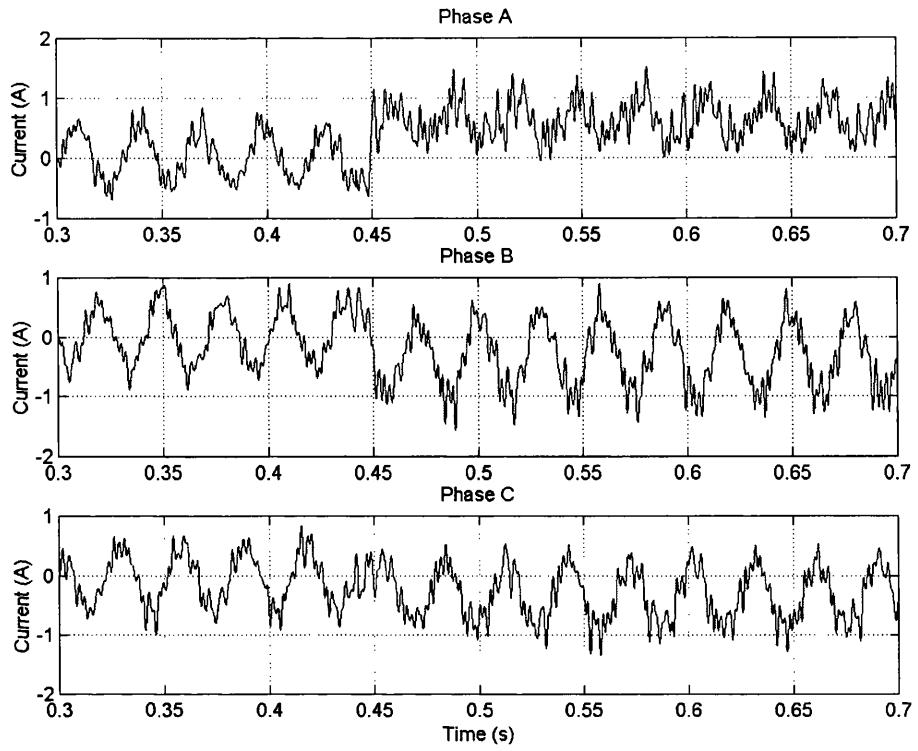

Figure 6-9: The experimental current waveforms for inverter transistor T4 open-circuit fault.

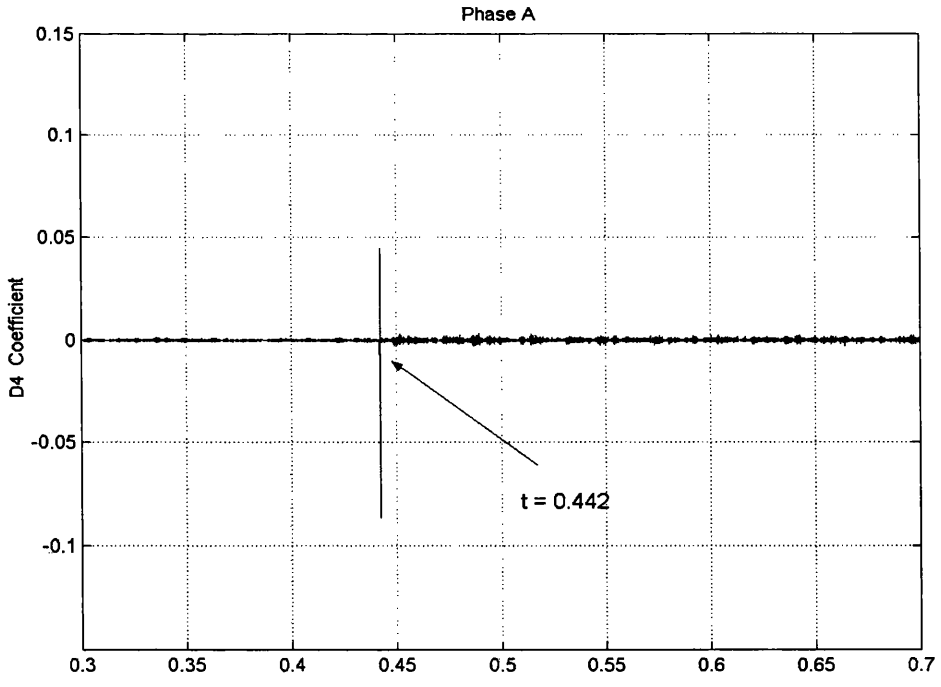

Figure 6-10: The D4 coefficient of phase A for inverter transistor T4 open-circuit fault.

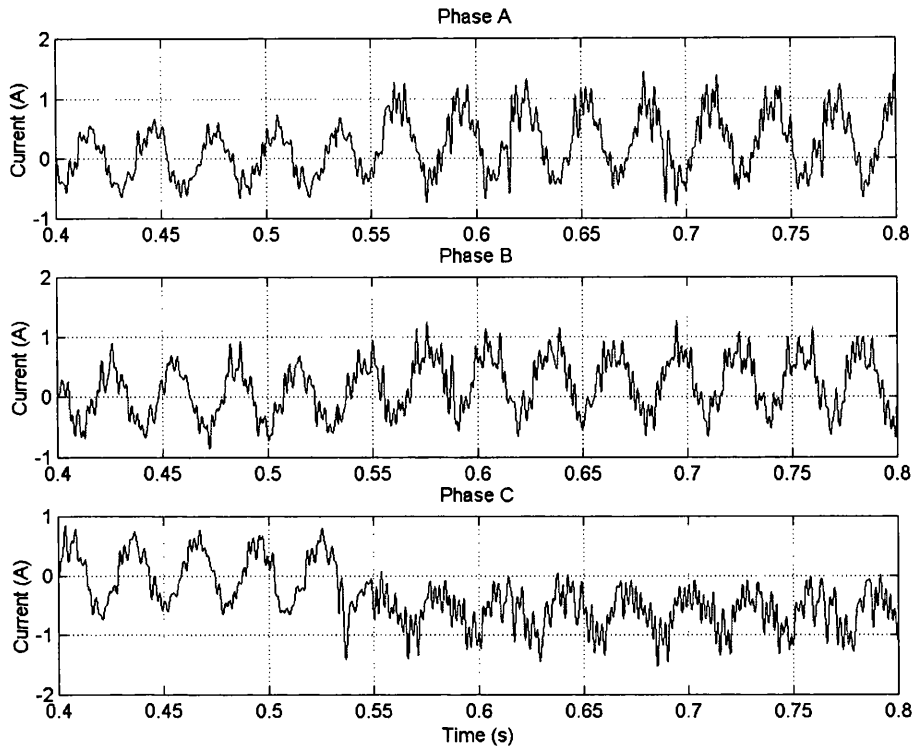

Figure 6-11: The experimental current waveforms for inverter transistor T5 open-circuit fault.

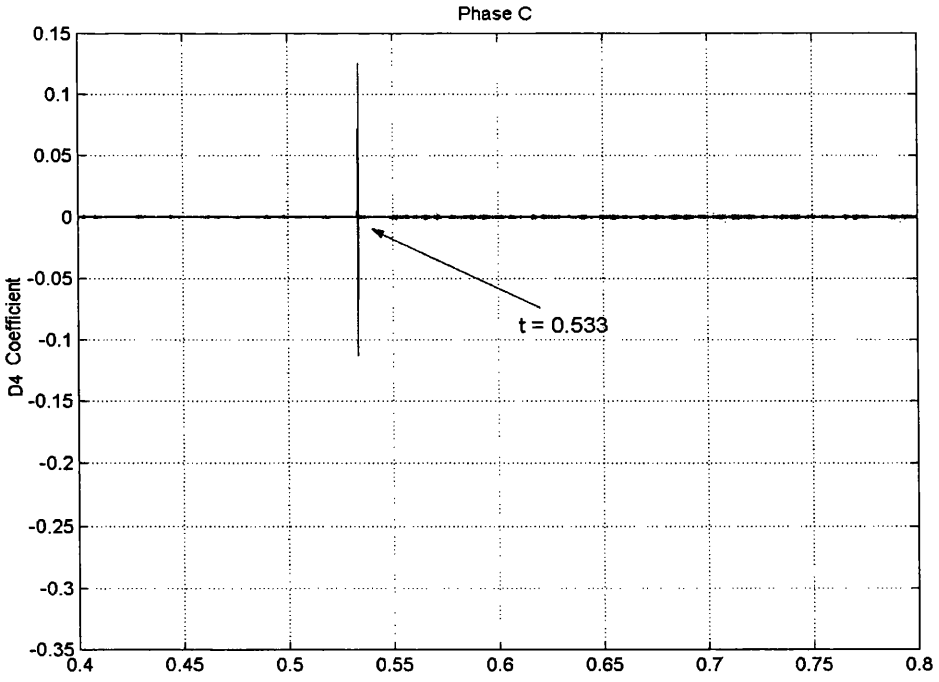

Figure 6-12: The D4 coefficient of phase C for inverter transistor T5 open-circuit fault.

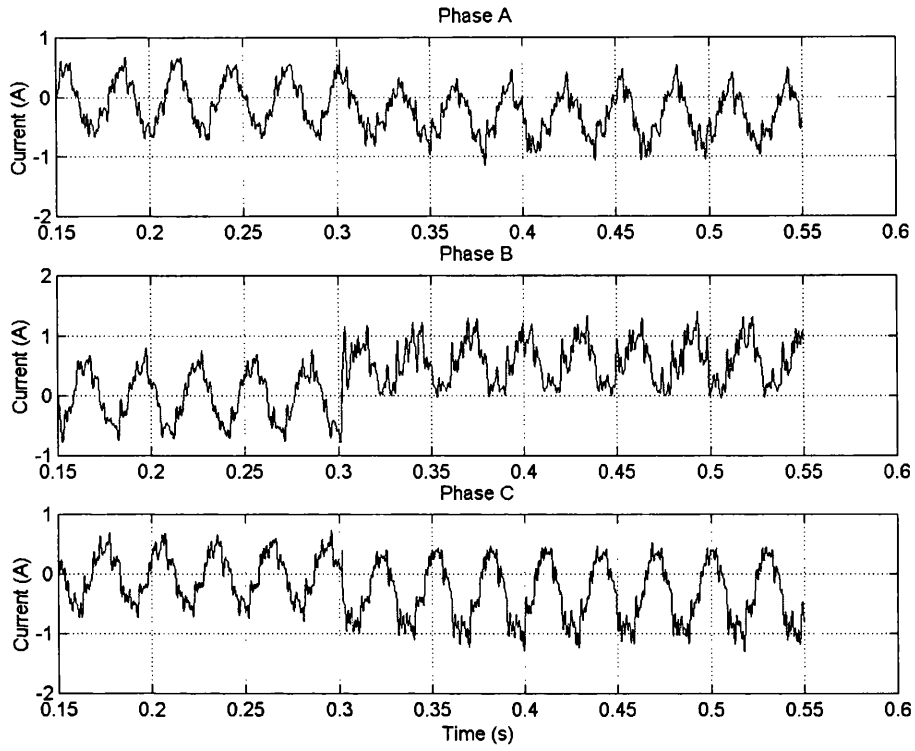

Figure 6-13: The experimental current waveforms for inverter transistor T6 open-circuit fault.

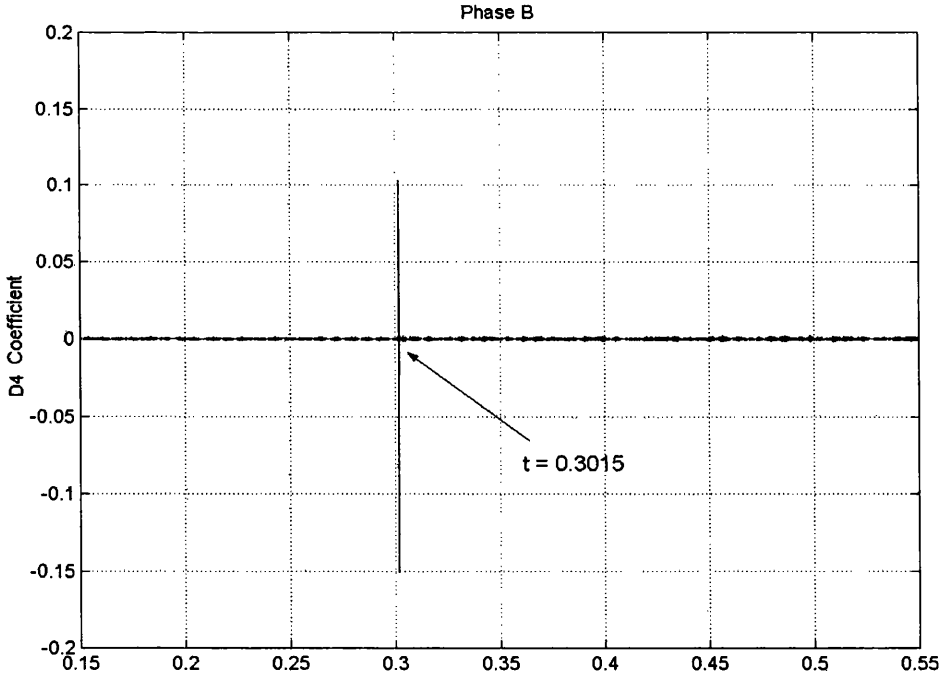

Figure 6-14: The D4 coefficient of phase B for inverter transistor T6 open-circuit fault.

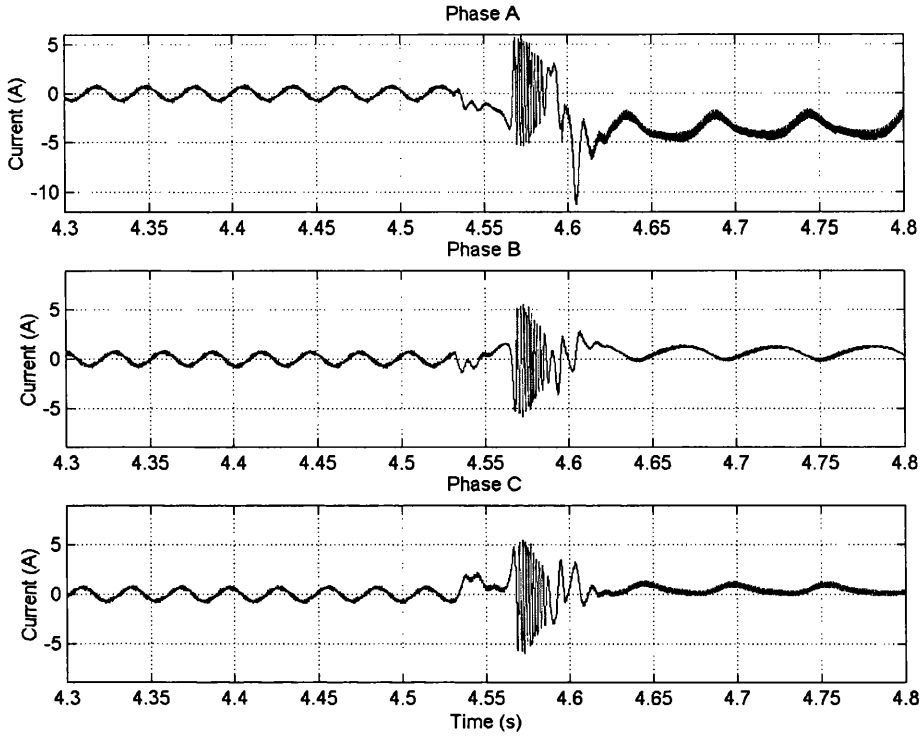

Figure 6-15: The simulated current waveforms for inverter transistor T1 open-circuit fault.

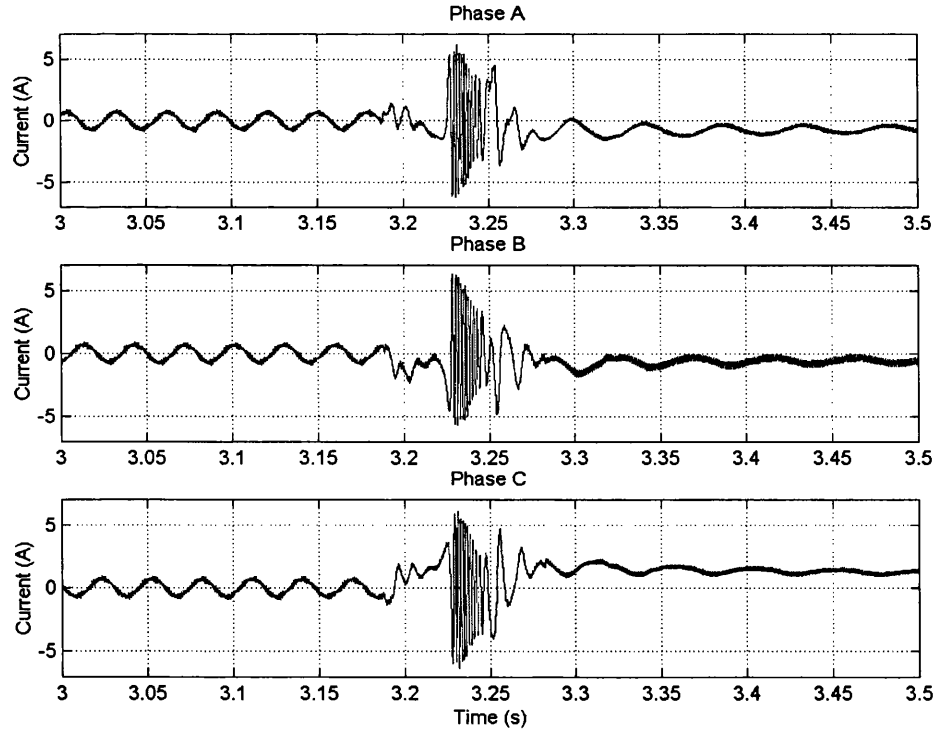

Figure 6-16: The simulated current waveforms for inverter transistor T2 open-circuit fault.

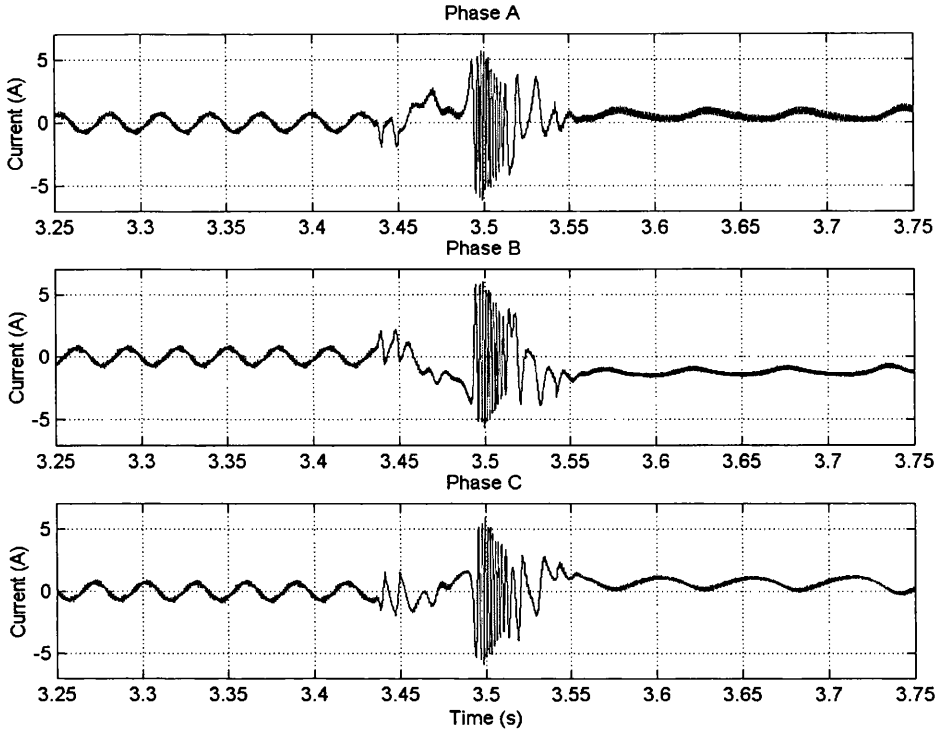

Figure 6-17: The simulated current waveforms for inverter transistor T3 open-circuit fault.

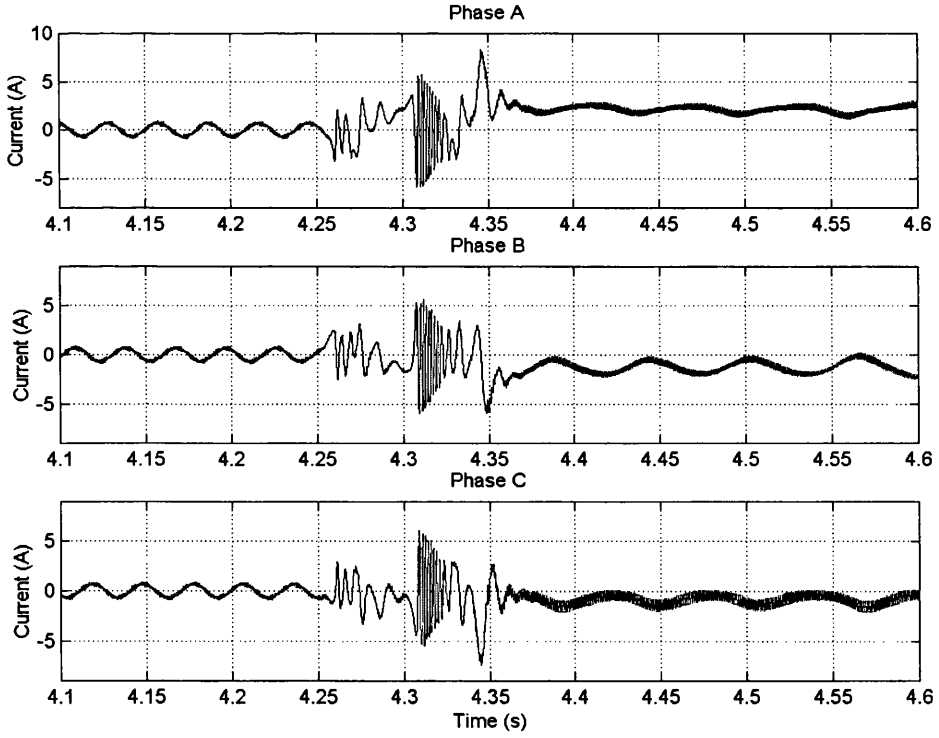

Figure 6-18: The simulated current waveforms for inverter transistor T4 open-circuit fault.

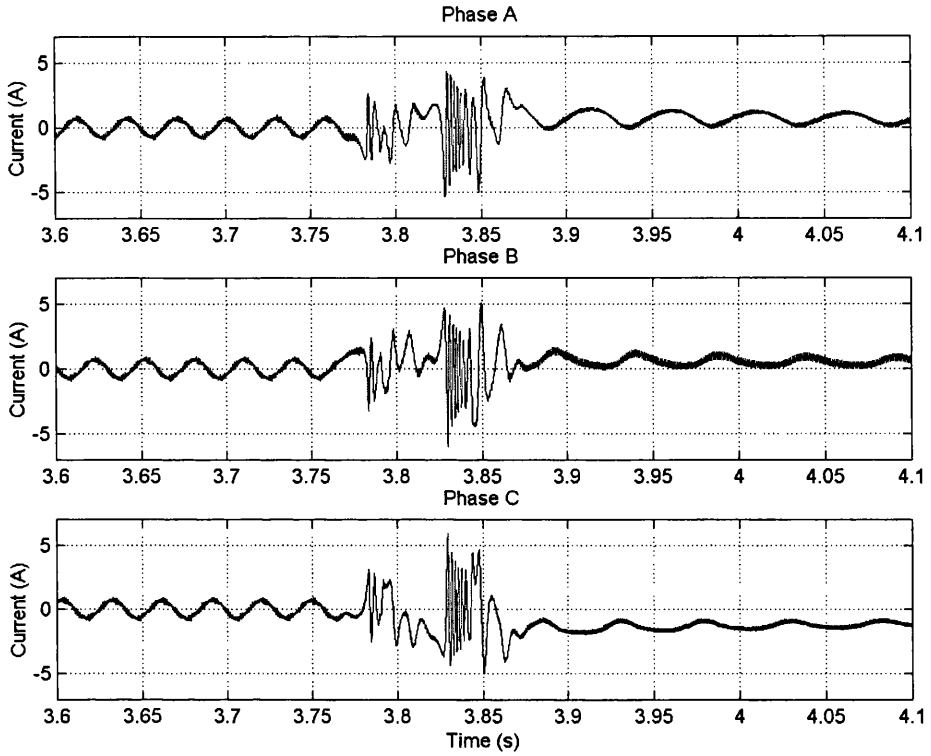

Figure 6-19: The simulated current waveforms for inverter transistor T5 open-circuit fault.

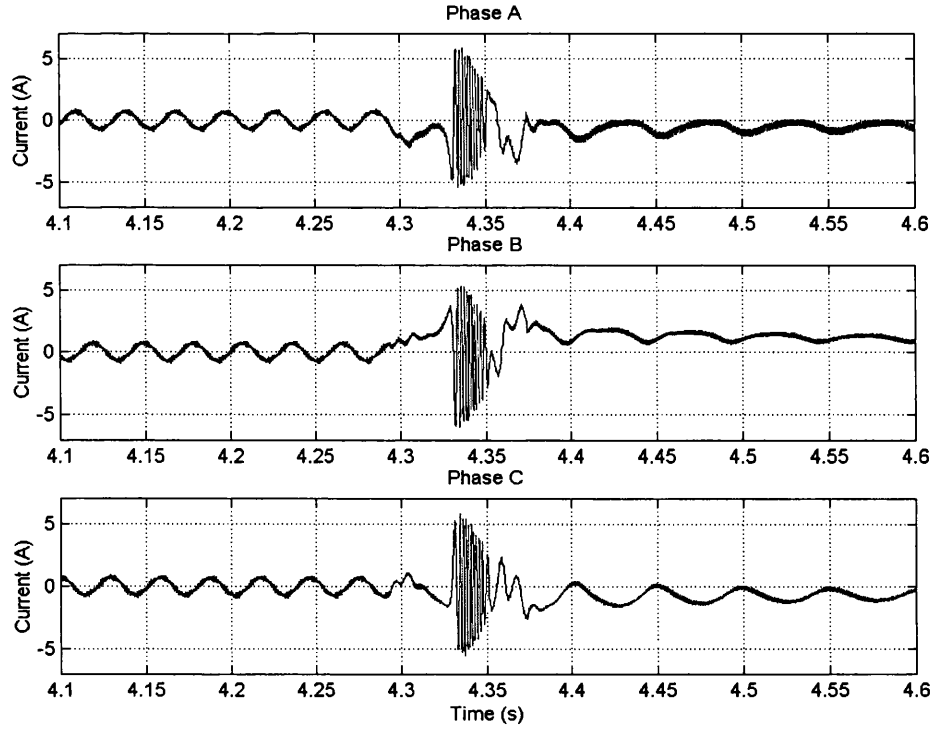

Figure 6-20: The simulated current waveforms for inverter transistor T6 open-circuit fault.

6.3.2 Inverter Transistor Intermittent Misfiring Fault

In this test, the transistor intermittent fault is introduced in the inverter circuit by suppression of firing pulse to the transistor for a short period of time. Figure 6-21, 6-23 and 6-25 shows the phase currents when the intermittent fault of *T1*, *T2* and *T3* occurred, respectively.

It can be seen that the system is able to recover from the disturbance and the phase current distortion decays in few output cycles under the effect of the fuzzy logic controller. These results agree with the experiment results mentioned in [4].

The DWT coefficient successfully detects the intermittent misfiring fault, as shown in Figure 6-22, 6-24 and 6-26. The sharp spikes appeared when the fault started and vanished. In addition, by observing the D4 coefficient, the instant when the fault started and vanished can be obtained. This information is very useful for the machine operator. If the intermittent misfiring faults happen so frequently, the system might need to be stopped to avoid catastrophic breakdown caused by the high current transient.

Figures 6-27 to 6-29 show the simulated results of the inverter transistor intermittent misfiring fault. These results agree with the experimental results.

6.3.3 Single Phasing Fault

Throughout this test, the single phasing fault condition is introduced by switching off one of the induction motor phases. Figure 6-30, 6-32 and 6-34 show the experimental phase current responses when the single phasing fault occurred in the circuit. Inspection of the current waveforms indicates that the current magnitudes of the other two phases are increased significantly. No dc offset was introduced with this fault.

Under this type of fault, as mentioned in Chapter 3, the three-phase motor will continue to operate but as a single-phase motor. This motor will be unable to restart with a single-phase supply, unless a rotating magnetic field somehow produced at standstill [6].

The D4 wavelet coefficient for the phase currents is shown in Figure 6-31, 6-33 and 6-35. It may be clearly seen that the coefficient surging has occurred, in response to the faulty current condition. As a result, the single phasing fault can be easily detected by the wavelet coefficient.

Figures 6-36 to 6-38 show the simulated results of the single phasing fault condition. As shown, there is a fair agreement between the simulated and experimental results.

6.3.4 Dc Offset

Once the fault is detected by the DWT, the system will start to calculate the currents dc offset. Then, the dc offset value and the polarity will be fed to the fuzzy logic system to determine the type of fault, as previously described in section 5.2.2.1. Table 6.1 below show the value and the polarity of dc offset for experimental base drive open-circuit faults and intermittent misfiring faults. The 1st reading is taken just after the fault is detected, for the duration of 4 cycles while the 2nd reading is taken 4 cycles after the 1st reading, also for the duration of 4 cycles. The table shows that the proposed fault identifier algorithm agrees with the experimental results. In this thesis project, if the dc offset magnitude is less than 0.1, it will be considered as a healthy condition.

Example 1:

1st reading:

I_{ADC} = -0.399 and I_{BDC}= 0.2644 and I_{CDC} = 0.1776

Then wait for 4 cycles

2nd reading:

I_{ADC} = -0.6057 and I_{BDC} = 0.4029 and I_{CDC} = 0.2776

Result: T1 base drive open-circuit fault.

Example 2:

1st reading:

I_{ADC} = -0.5197 and I_{BDC}= 0.3271 and I_{CDC} = 0.0866

Then wait for 4 cycles

2nd reading:

I_{ADC} = 0.0452 and I_{BDC} = 0.0189 and I_{CDC} = -0.0879

Result: T1 intermittent misfiring fault.

6.4 Summary

In this Chapter, a description of the experimental set-up for the proposed fault diagnosis algorithm for 3-phase pulse width modulation (PWM) voltage source inverter (VSI) for closed-loop, fuzzy logic voltage frequency (v/f) speed control strategy of an induction motor has been presented. Illustration of the stator current waveforms when the VSI is subjected to different types of fault follows this. The wavelet transform of stator currents were obtained, which demonstrated the validity of the designed condition monitoring and fault detector algorithm. Comparison studies between the acquired experimental results with those obtained via simulation, for the same operating conditions, were considered.

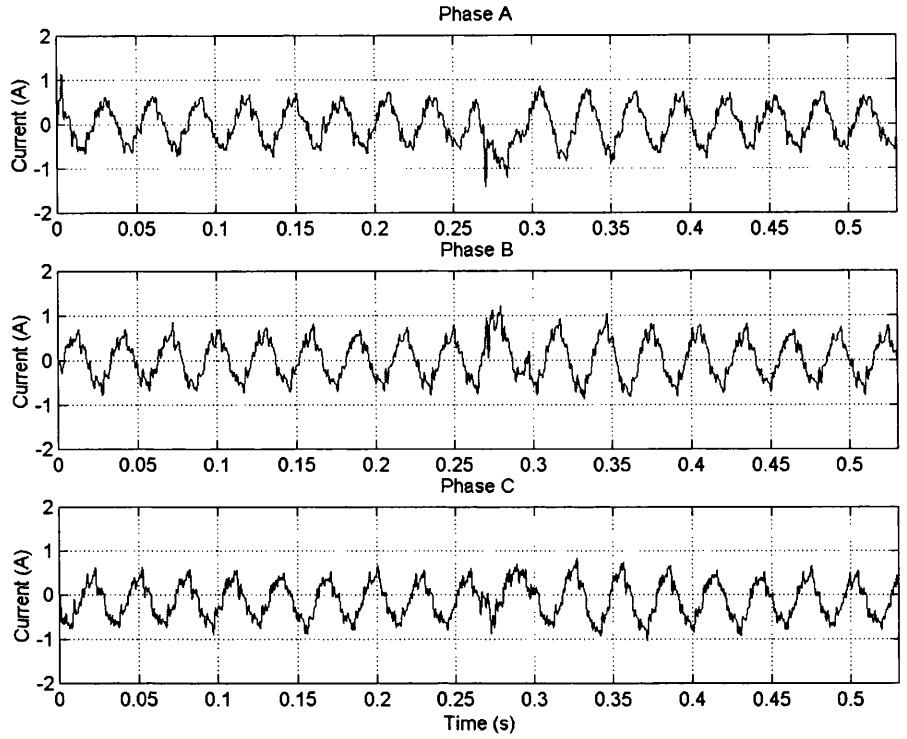

Figure 6-21: The experimental current waveforms for inverter transistor T1 intermittent misfiring fault.

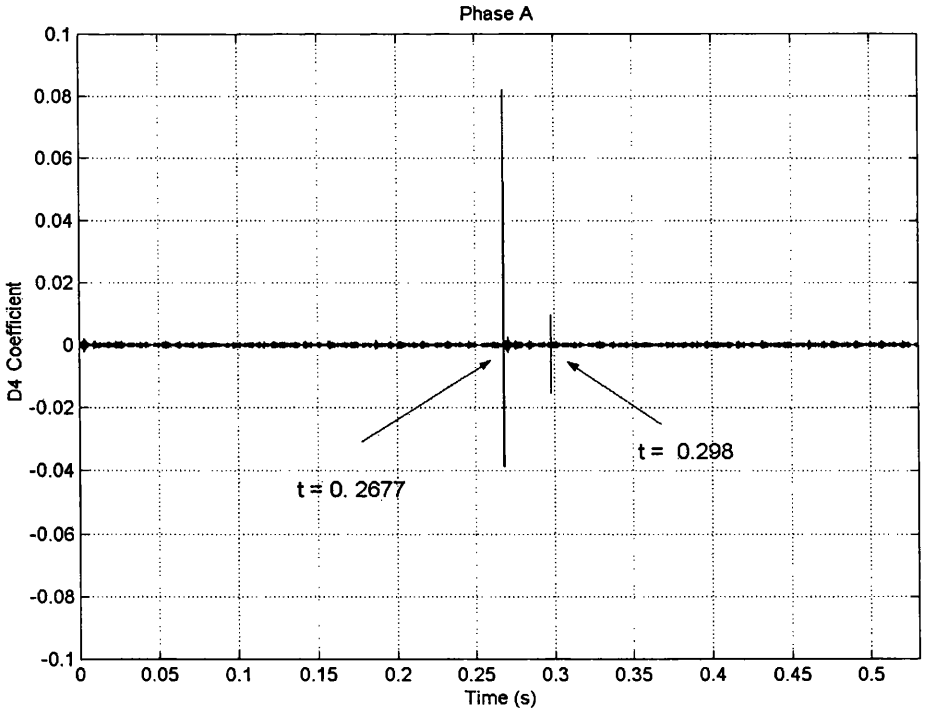

Figure 6-22: The D4 coefficient of phase A for inverter transistor T1 intermittent misfiring fault

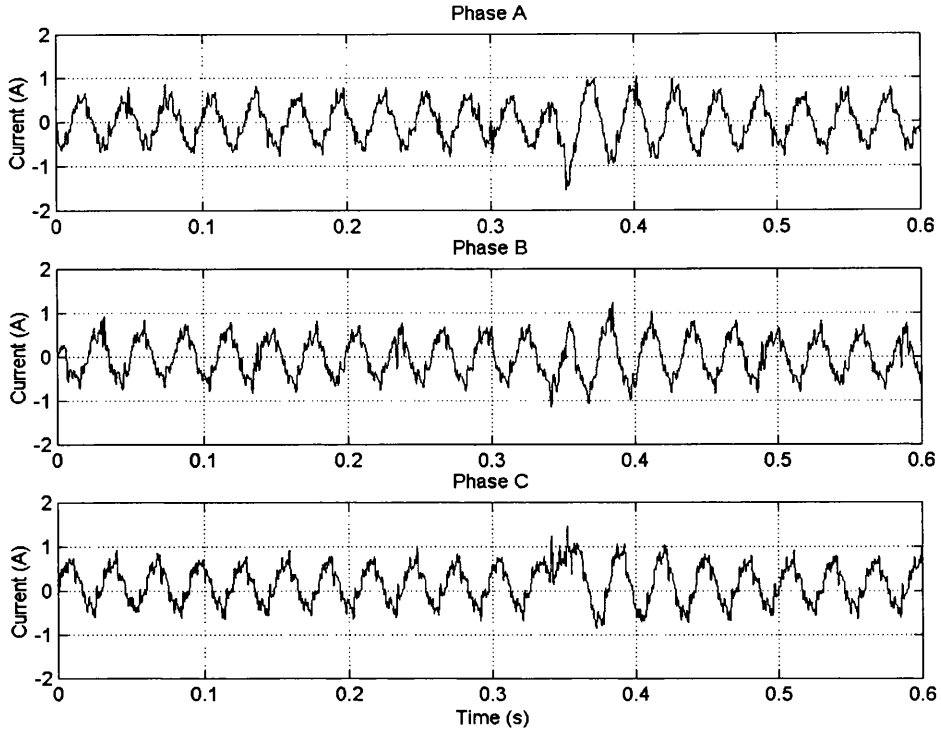

Figure 6-23: The experimental current waveforms for inverter transistor T2 intermittent misfiring fault.

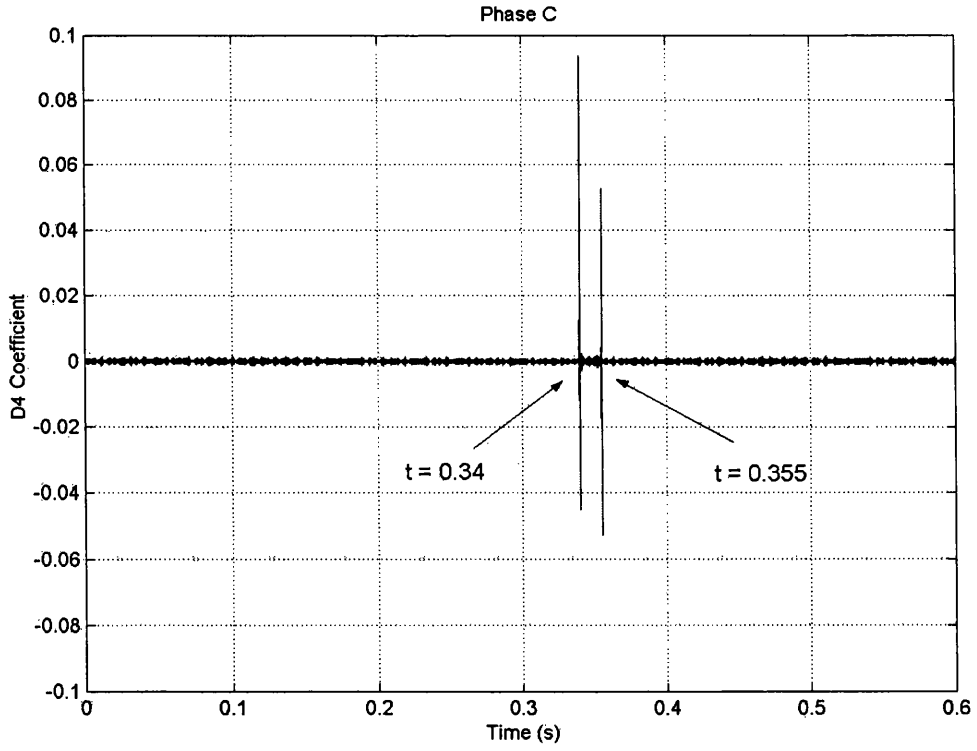

Figure 6-24: The D4 coefficient of phase C for inverter transistor T2 intermittent misfiring fault

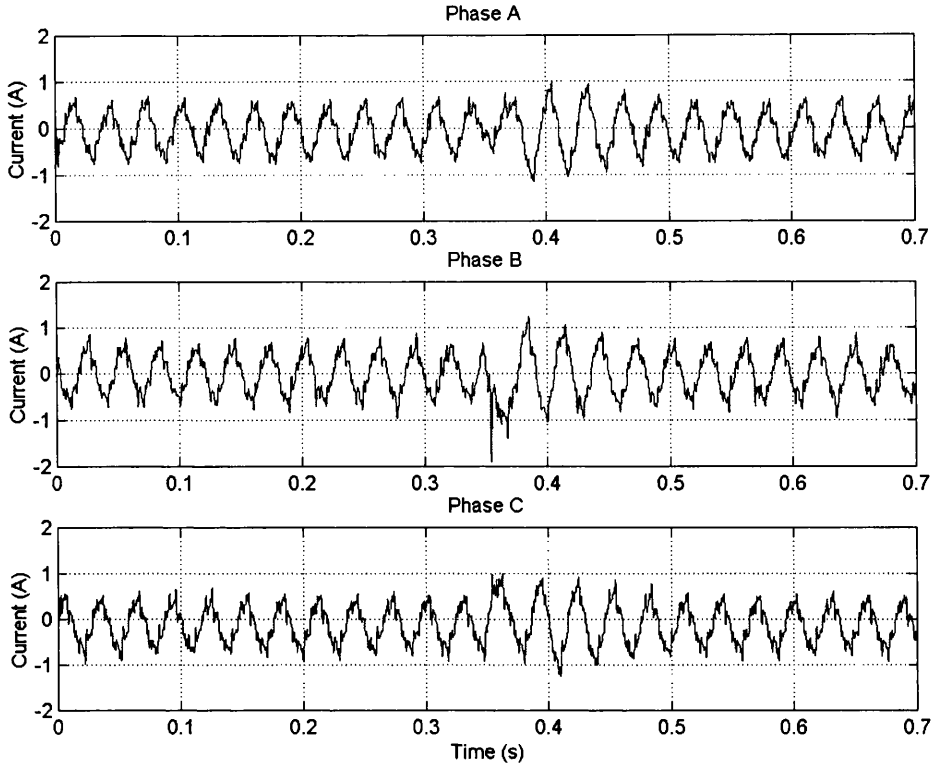

Figure 6-25: The experimental current waveforms for inverter transistor T3 intermittent misfiring fault.

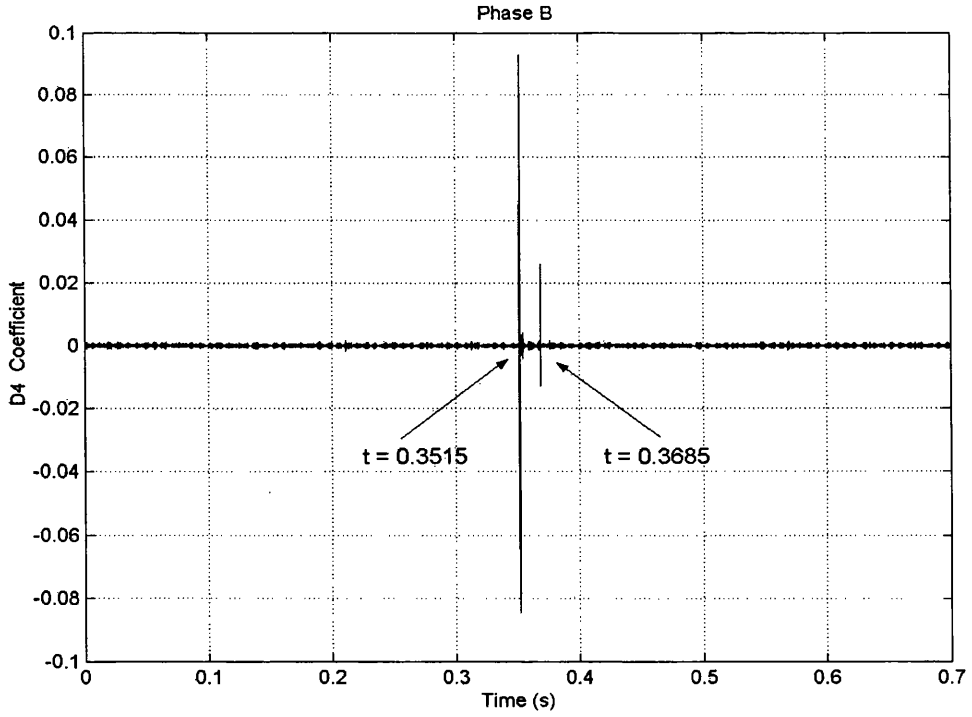

Figure 6-26: The D4 coefficient of phase B for inverter transistor T3 intermittent misfiring fault.

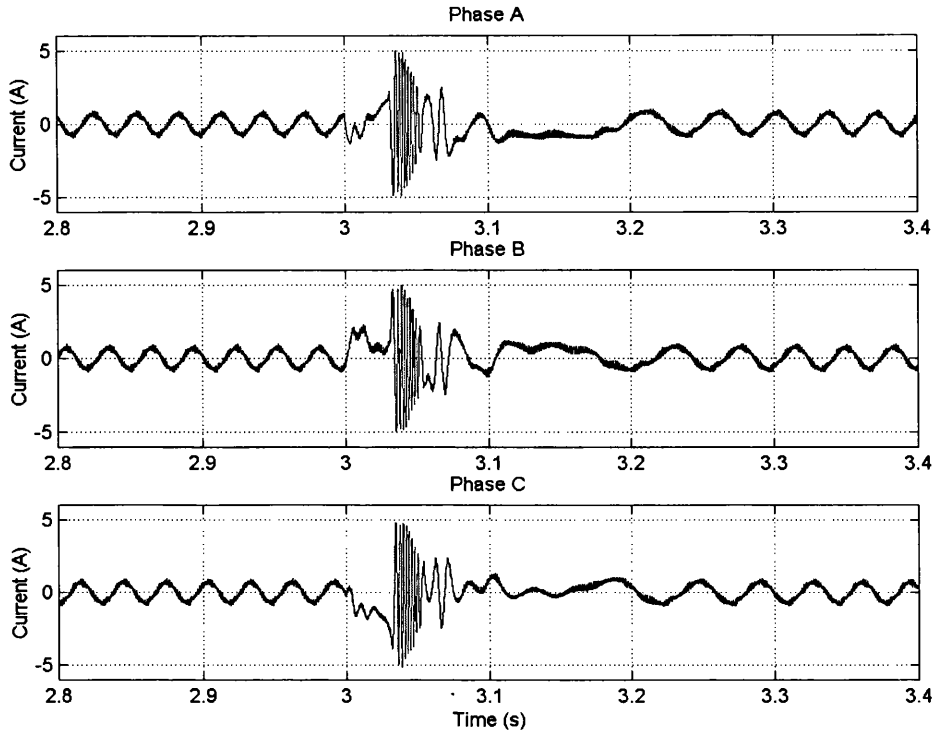

Figure 6-27: The simulated current waveforms for inverter transistor T1 intermittent misfiring fault.

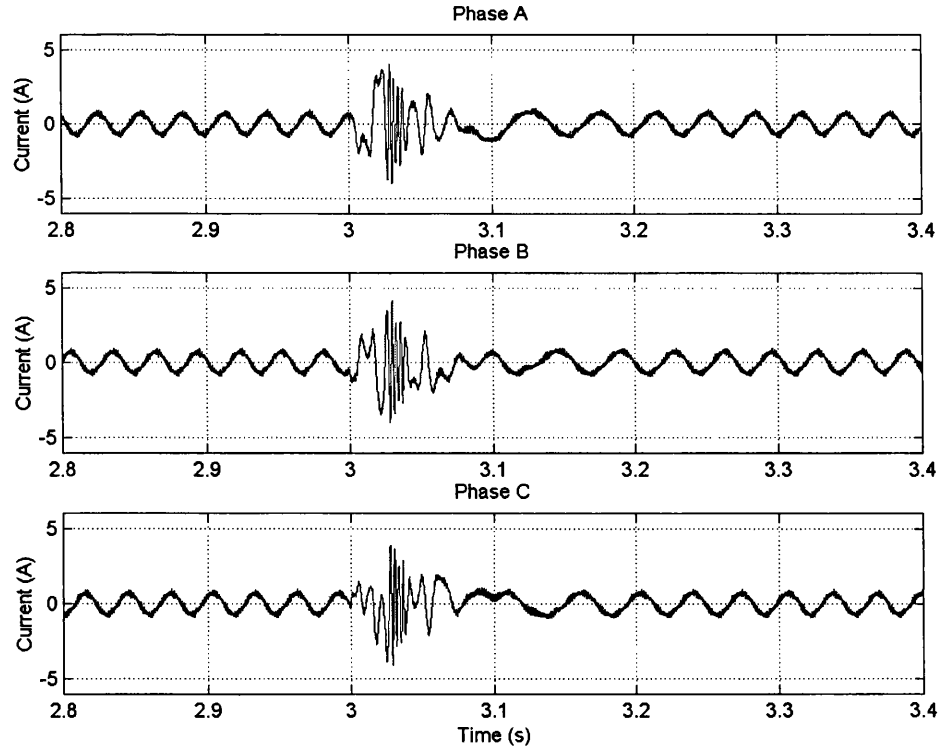

Figure 6-28: The simulated current waveforms for inverter transistor T2 intermittent misfiring fault.

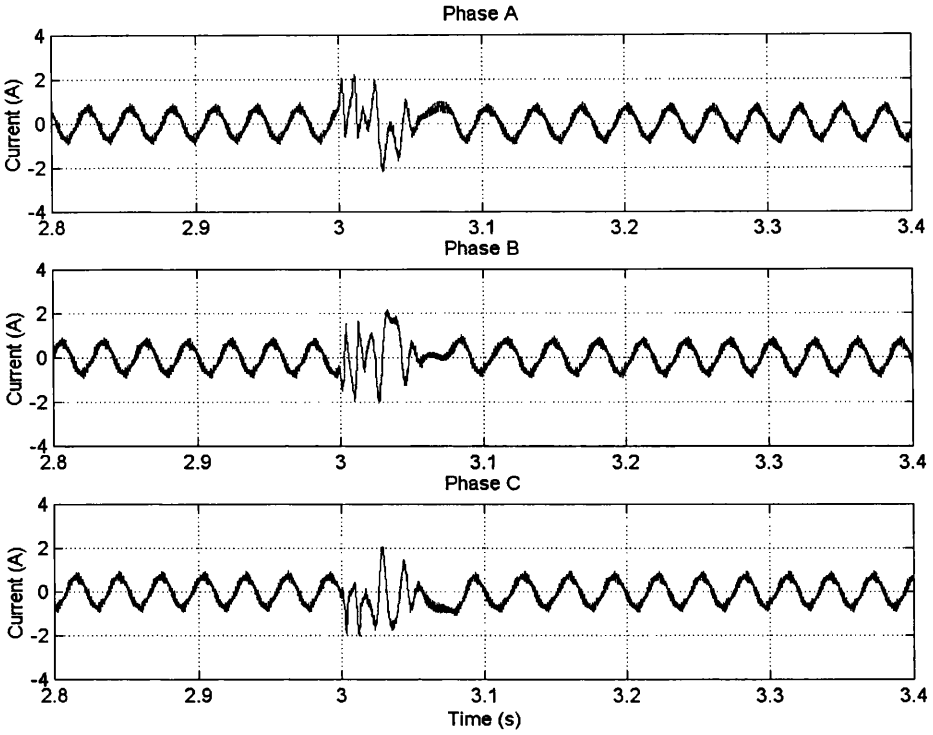

Figure 6-29: The simulated current waveforms for inverter transistor T3 intermittent misfiring fault.

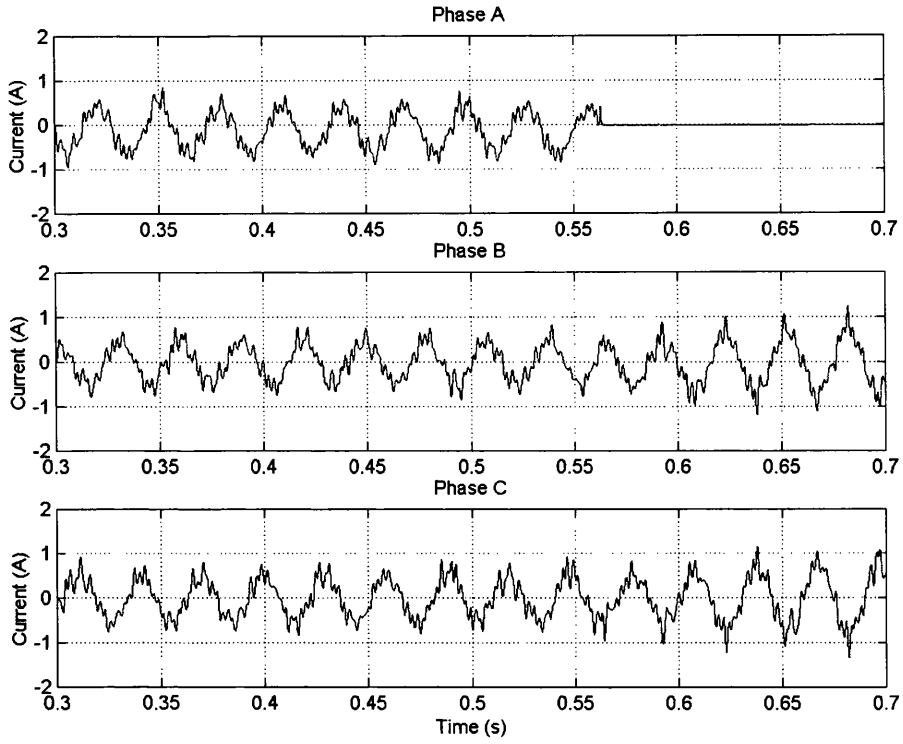

Figure 6-30: The experimental current waveforms for phase A single phasing fault.

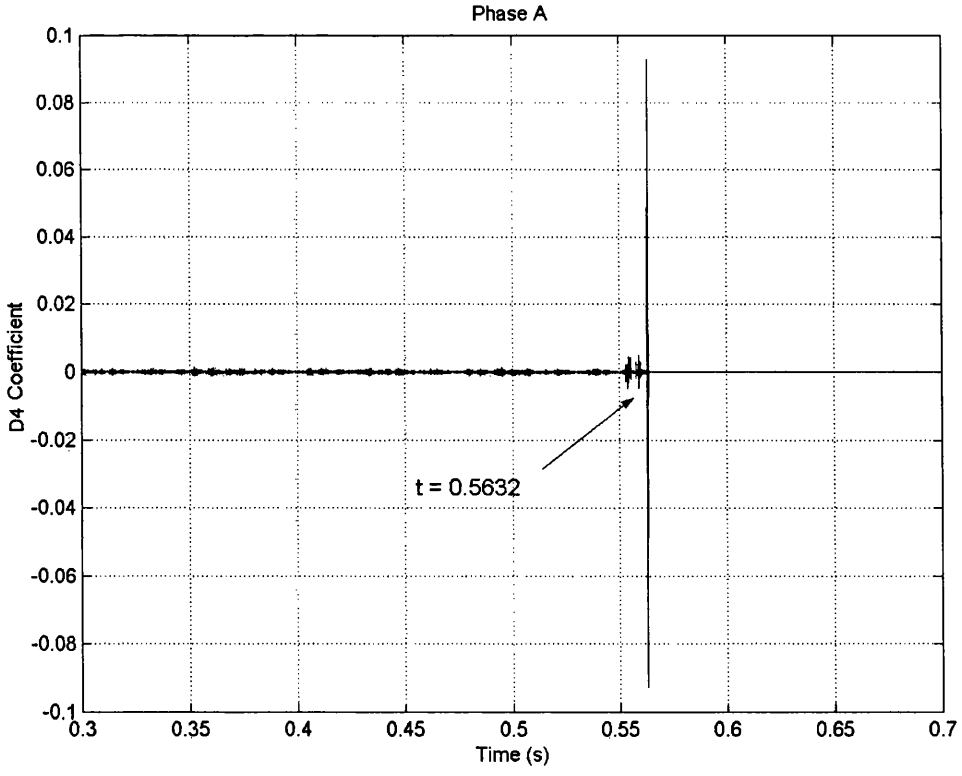

Figure 6-31: The D4 coefficient of phase A single phasing fault.

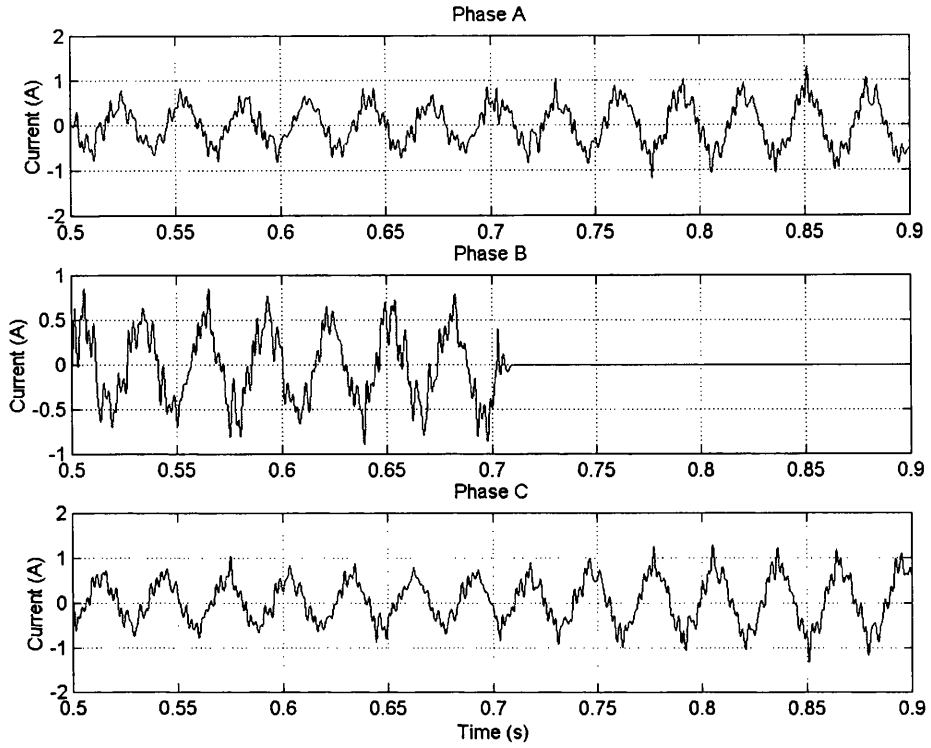

Figure 6-32: The experimental current waveforms for phase B single phasing fault.

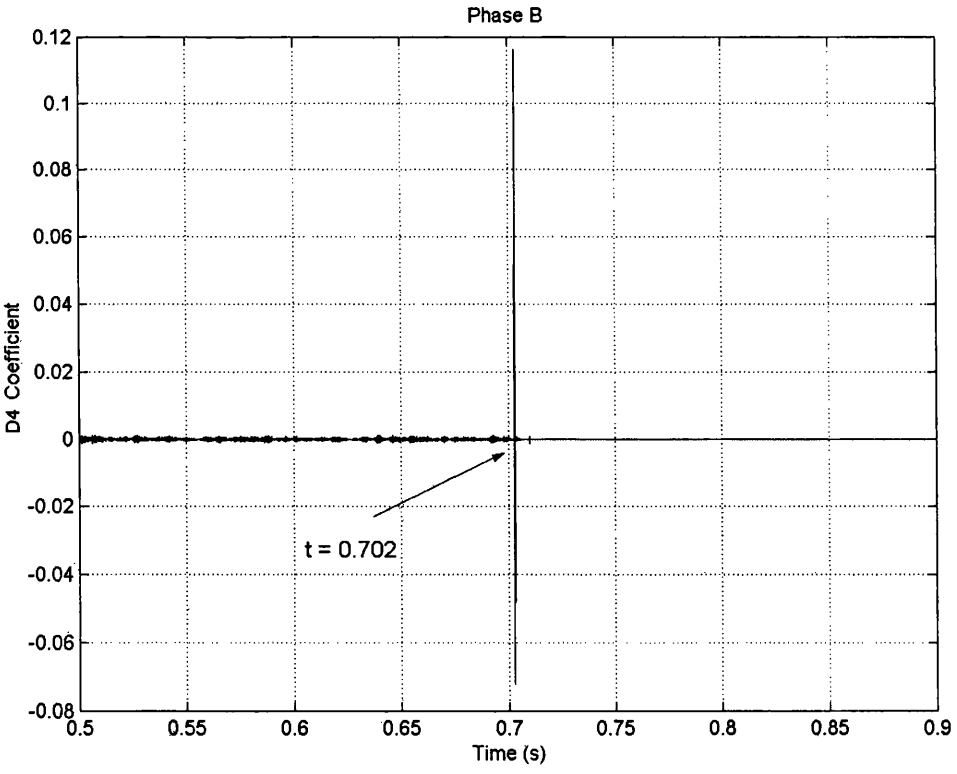

Figure 6-33: The D4 coefficient of phase B single phasing fault.

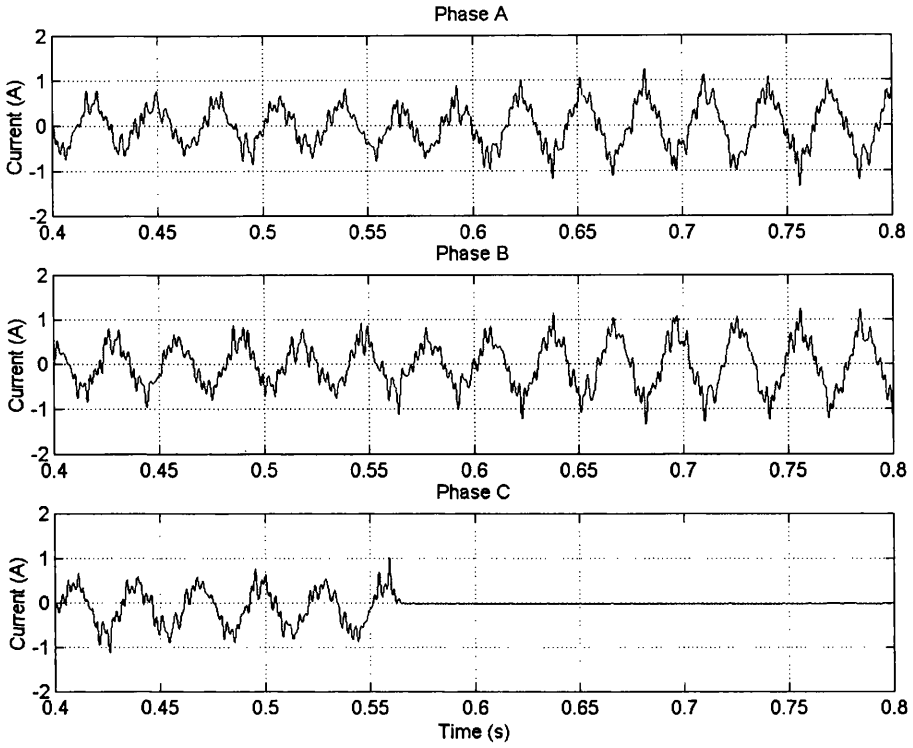

Figure 6-34: The experimental current waveforms for phase C single phasing fault.

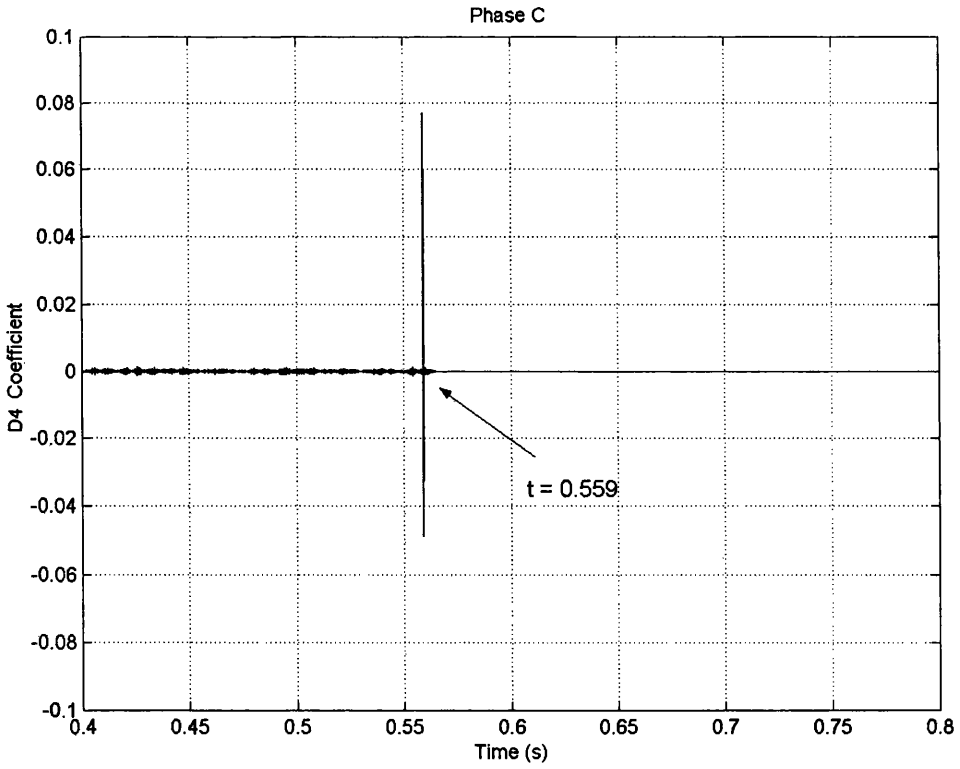

Figure 6-35: The D4 coefficient of phase C single phasing fault.

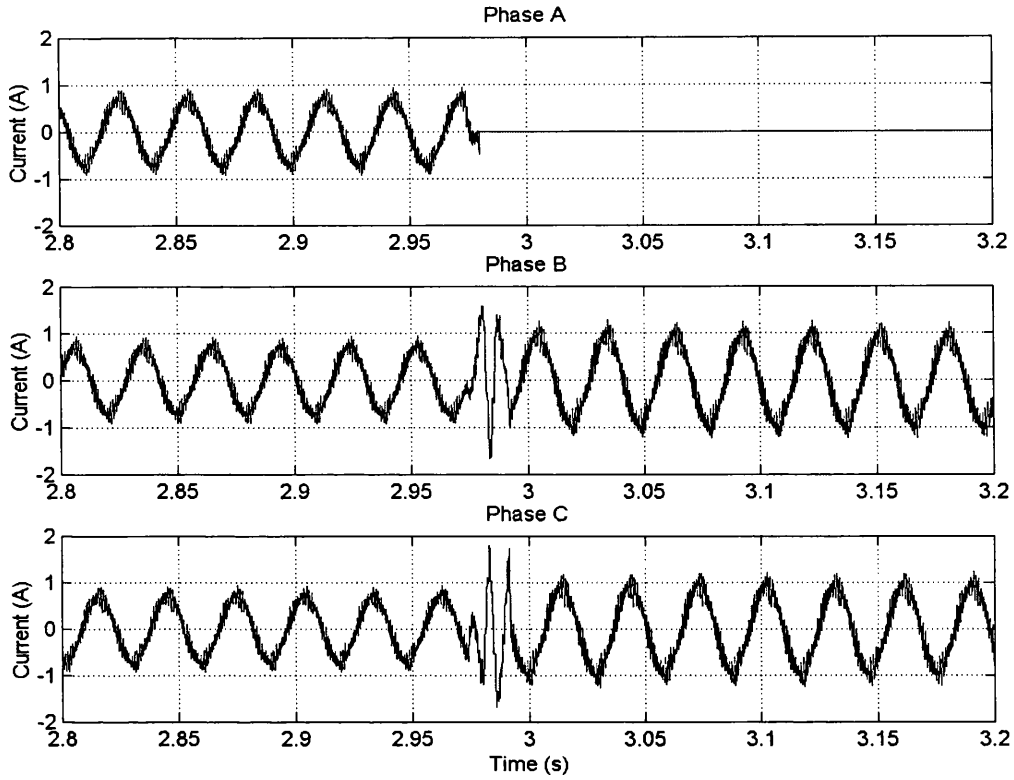

Figure 6-36: The simulated current waveforms for phase A single phasing fault.

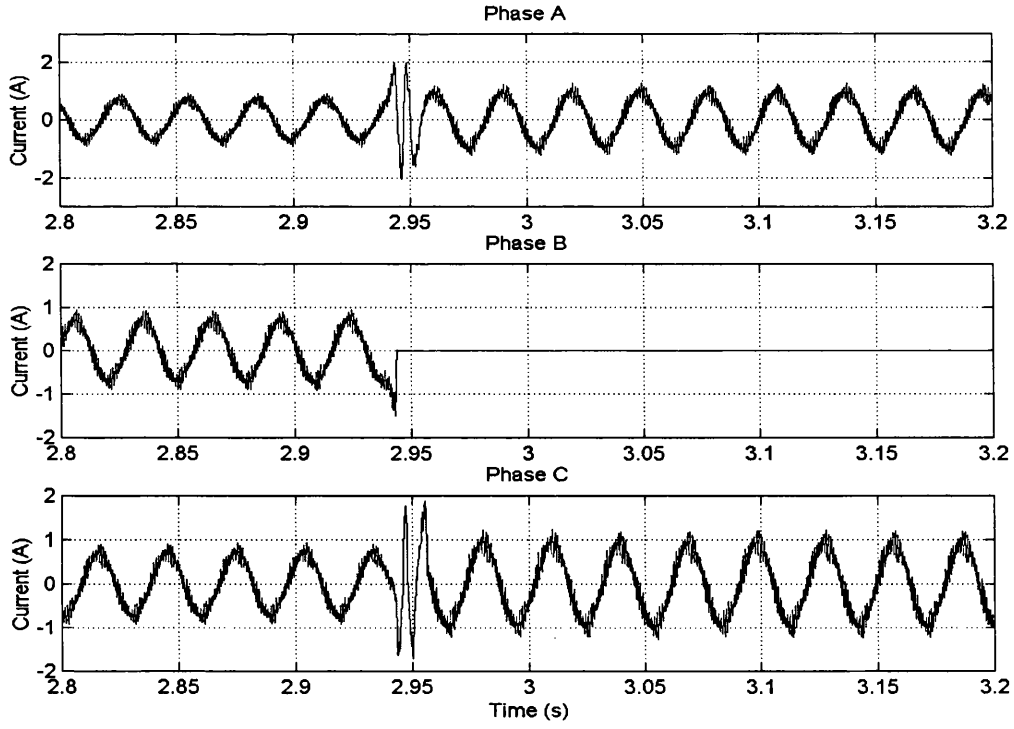

Figure 6-37: The simulated current waveforms for phase B single phasing fault.

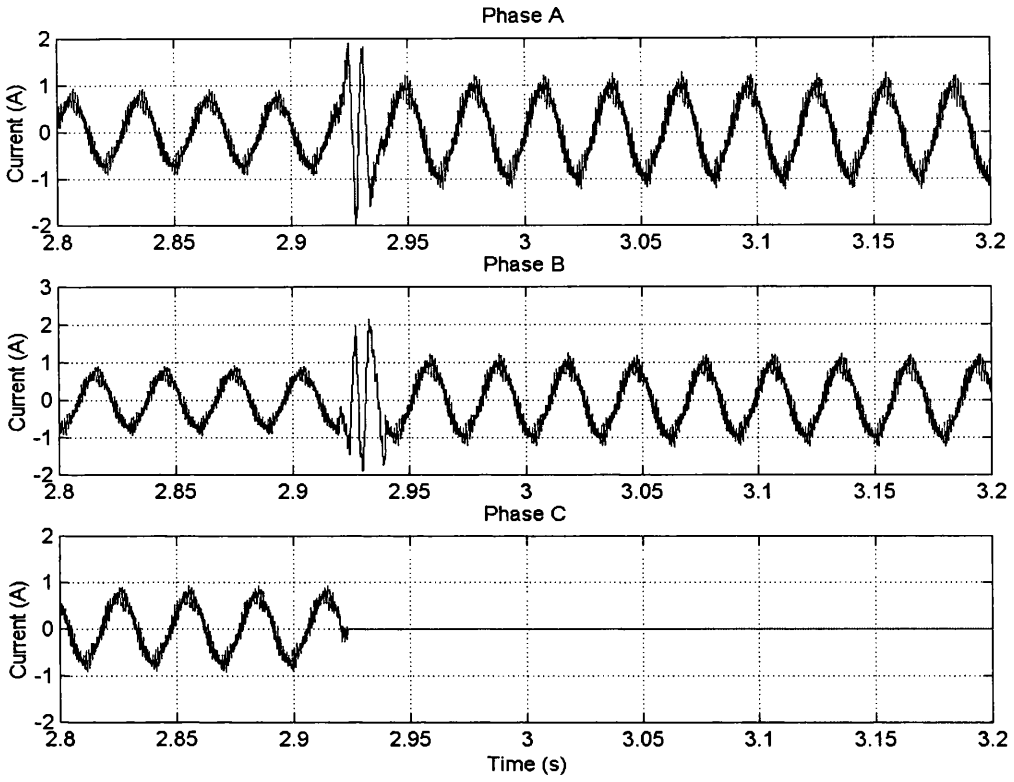

Figure 6-38: The simulated current waveforms for phase C single phasing fault.

Table 6.1: Dc offset reading

Type of fault	1st. Reading			2nd. Reading		
	I_{ADC}	I_{BDC}	I_{CDC}	I_{ADC}	I_{BDC}	I_{CDC}
T1 base drive open-circuit	-0.399	0.2644	0.1776	-.6057	0.4029	0.2776
T2 base drive open-circuit	-.3846	-.2564	0.6999	-.3992	-.3556	0.7226
T3 base drive open-circuit	0.1562	-.369	0.2427	0.3159	-.6283	0.3534
T4 base drive open-circuit	0.4602	-.322	-.1830	0.5892	-.3432	-.2920
T5 base drive open-circuit	0.2369	0.1513	-.4165	0.2072	0.262	-.6025
T6 base drive open-circuit	-.2083	0.4829	-.2924	-0.2903	0.5579	-0.3431
T1 intermittent misfiring	-.5197	0.3271	0.0866	0.0452	0.0189	-.0879
T2 intermittent misfiring	-.1575	-.2735	0.6042	-.0026	-.0186	0.0889
T3 intermittent misfiring	0.1439	-.4632	0.1297	-.0790	-.0063	-.0789

CHAPTER 7

CONCLUSSIONS AND RECOMMENDATIONS

7.1 Conclusions

Safety, reliability, efficiency and performance are some of the major issues and concerns for the motor drive system applications. With factors such as aging systems, high reliability demands and cost competitiveness, the issues of preventive and condition-based maintenance, online-monitoring, system fault detection and diagnosis are of increasing importance. The key issues for the successful motor drive application are a quality of motor, proper choice of drive system, understanding the capabilities of the system and proper maintenance.

However, the use of motor drive in today's industry is extensive and the system can be exposed to different hostile environments, misoperations, or manufacturing defects. Different internal motor faults (e.g., broken rotor bars, bearing damage, inter turn short-circuit) along with external motor faults (e.g., inverter transistor base drive open-circuit, transistor intermittent misfiring, phase-failure, asymmetry of main supply) are expected to happen sooner or later. These types of faults usually refer to the gradual deterioration that can lead to motor drive failure if left undetected. Early fault detection and diagnosis allow preventive and condition-based maintenance to be arranged for the motor drive system during scheduled downtimes and prevent an extended period of downtime caused by extensive system failures, and will also reduce the maintenance costs. Therefore, the objective of this research work is to study, investigate and design the real-time, non-invasive, condition monitoring and fault detection algorithm for a three-phase induction motor drive system. The VSI for the drive system is based on v/f fuzzy control strategy.

It should be stressed that the designed algorithm ought to be sensitive to any type of disturbance occurred in the VSI. For this purpose, comprehensive investigation of state-of-the-art modern condition monitoring and fault diagnosis has been presented in Chapter 2. Moreover, the development of the new algorithm based on discrete wavelet transform and fuzzy logic has been thoroughly discussed in Chapter 5.

The basic theory and general mathematical representation of VSI and PWM switching techniques have been reviewed in Chapter 3. In addition, the VSI faults analysis such as inverter transistor base drive open-circuit fault, intermittent misfiring and single phasing has been described in details.

The normal and faulty VSI operating conditions have been initially assessed through computer modeling and simulation using MATLAB and SIMULINK. The VSI model was based on switching function concept, as successfully presented in Chapter 4. The observations made from simulation results provide a clearer picture in understanding the VSI circuit behaviour, especially under faulty conditions. For example, an open-circuit fault will introduce a dc offset to the stator currents, leading to the healthy transistor of the faulty leg becoming excessively stressed because it now carries the entire phase current. Also, the upper and the lower transistor of other legs carry unequal current stress. Such condition may eventually lead to catastrophic breakdown to the inverter system.

Furthermore, the comprehensive transient study of the drive system, which the induction motor is simulated using the dynamical equations that are formulated in the synchronous reference frame, is also presented in chapter 4. This simulation was found useful for the initial design of the closed loop fuzzy based control system.

The proposed condition monitoring and fault detection algorithm have been extensively tested through experimental works. The assessment of this algorithm was based on its capabilities in detecting and identifying the various VSI faults as presented in Chapter 6. The experimental results revealed that the stator currents contain the important information associated with VSI faults. The proposed algorithm that is the combination of wavelet transform and fuzzy logic proved to be an effective technique in extracting the special VSI fault features in stator currents.

It has also been established that the wavelet transform has the capability to identify the signals, such as VSI faulty current signals that contain short duration, transient features. At low frequency, the wavelet transform has good localisation in frequency but poor localisation in space. At high frequency, the transform has poor localisation in frequency but good localisation in space. The wavelet transform also remove the difficulty of choosing an appropriate width of analysis window, required by other time-frequency transforms, as the width of the wavelet analysis window is incorporated implicitly into the transform.

Fuzzy logic is used to identify typical fault conditions. The fuzzy logic algorithms are systematically designed according to intuition and experiences about the 3-phase VSI behaviour. The advantage of using the fuzzy logic is that it is easy to apply heuristics knowledge and 'rule-of-thumb' experience. The dc offset level of all three stator currents are considered as the variables to the fuzzy system. The results show that the application of fuzzy logic as a VSI identifier is well suited.

7.2 Recommendations for Future Work

The prime targets of the proposed condition monitoring and fault detection algorithm have been successfully fulfilled. The accomplished targets have been demonstrated through series of simulation and experimental studies. To further improve and develop the presently proposed algorithm, a few suggestions are proposed as follows:

a) The proposed condition monitoring and fault detection algorithm is fully built on MATLAB and SIMULINK platform. Therefore, the physical drive system could be easily connected to the proposed algorithm model by using xPC Target (product of Mathworks Inc.). xPC target is a high performance, host targeting prototyping environment that enables SIMULINK model to be connected directly to the system and execute them in real-time on PC-compatible hardware. Furthermore, if the extended real-time tool box (product of Humusoft S.R.C) is used, the designer can access to external analog and digital signals with almost no hardware knowledge needed.

b) As far as power converters for commercial applications of electric drives are concerned, relatively small number of configuration exists. Therefore, a similar circuit topologies should produce similar results for typical faults and hence, it is possible to study a diagnostic system able to operate regardless of different manufacturers and ratings. However, for closed-loop drives, the control itself modifies the behaviour of machine supply variables. So, it is necessary to test the proposed algorithm to other type of controllers to ensure that it can be used as universal VSI condition monitoring and fault detection system.

REFERENCES

[1] Shepherd, W. and Hulley, L. N., "Power electronics and motor control", Cambridge University Press, 1987.

[2] Wildi, T., "Electrical machines, drive and power system", Prentice Hall, 1991.

[3] Debaprasad, K., and Bimal, K. B., "Investigation of fault modes of voltage-fed inverter system for induction motor drive", IEEE Trans. on Industry Applications, Vol.30, No.4, 1994, pp. 1028-1037.

[4] Smith, K. S., Ran, L., and Penman, J., "Real time detection of intermittent misfiring in a voltage-fed PWM inverter induction motor drive", IEEE Trans. on Industrial Electronics, Vol.44, No.4, 1997, pp. 468-476.

[5] Kastha, D., and Bose, B. K., "Fault mode single phase operation of variable frequency induction motor drive and improvement of pulsating torque characteristics", IEEE Trans. on Industrial Electronics, Vol.41, No.4, 1994, pp. 426-433.

[6] Kastha, K., and Majundar, A. K., "An improved starting strategy for voltage source inverter fed three phase induction motor drives under inverter fault conditions", IEEE Trans. on Power Electronics, Vol.15, No.4, 2000, pp. 726-732.

[7] Penman, J., Dey, M. N., Tait, A. J., and Bryan, W. E., "Condition monitoring of electrical drives", IEE Proc. B Electrical Power Application, Vol. 133, No.3, 1986, pp. 142-148.

[8] Ho, S. L., "Condition monitoring of induction motors", Proc. of 5th. International Conference on Electrical Machines and Drives, 1991, pp. 56-60.

[9] Tavner, P. J., Gaydon, G., and Wards, D. M., "Monitoring generators and large motors", IEE Proc. B Electrical Power Application, Vol.133, No.3, 1986, pp. 65-69.

[10] Tavner, P. J., and Penman, J., "Condition monitoring of electrical machines", Research Studies Press Ltd., Lethchworth, 1987.

[11] Cameron, J. R., Thompson, W. T., and Dow, A. B., "Vibration and current monitoring for detecting airgap eccentricity in large induction motors", IEE Proc. B Electrical Power Application, Vol. 133, No. 3, 1986, pp.155-162.

[12] McCully, P. J., and Landy, C. F., "Evaluation of current and vibration signals for squirrel cage induction motor condition monitoring", Proc. of International Conference on Electrical Machines and Drive, No.444, 1997, pp.331-335.

[13] Dalpiaz, G., and Rivola, A., "Condition monitoring and diagnostics in automatic machines: comparison of vibration analysis techniques", Journal of Mechanical Systems and Signal Processing, 1997, pp. 53-73.

[14] Zolghadri, A., "AI algorithm for real time failure detection in Kalman filter", IEEE Trans. on Automatic Control, 1996, pp. 1537-1539.

[15] Filipetti, F., Franceschini, G., and Tassoni, C., "Neural networks approach to electric machine on-line diagnostics", Proc. of 5th. European Conference on Power Electronics and Applications, Vol. 4, 1993, pp. 213-218.

[16] Ammous, A., and Allard, B., "Transient temperature measurements and modelling of IGBT's under short circuit", IEEE Trans. on Power Electronics, Vol.13, No.1, 1998, pp. 12-20.

[17] Ramirez, R. W., "The FFT: fundamental and concept", Prentice-Hall, 1985.

[18] Mendel, J. M., "Tutorial on higher order statistical (spectra) in signal processing and system theory: theoretical results and some applications", Proc. of IEEE, No.79(3), 1991, pp. 278-305.

[19] Nikias, C. L., and Petropulu, A. P., "Higher order spectra analysis", Prentice Hall, 1993.

[20] Howard, I. M., "Higher order spectral techniques for machine vibration condition monitoring", Proc. of Institutional Mechanical Engineers, Vol.211, Pt.G, 1997, pp. 211-219.

[21] Cardoso, A. J. M. and Mendos, A. M. S., "Semi-converter fault diagnosis in dc motor drives, by Park's vector approach", Proc. of 6th. International Conference on Power Electronics and Variable Speed Drives, , 1996, pp. 93-98.

[22] Daubechies, I., "Ten lectures in wavelets", Society Industrial Applied Mathematics, 1992.

[23] Burrus, C. S., Gopinath, R. A., and Guo, H., "Introduction to wavelets and wavelet transform", Prentice Hall, 1998.

[24] Filipetti, F., Franceschini, G., Tassoni, C., and Vas, P., "Recent developments of induction motor drives fault diagnosis using AI techniques", IEEE Trans. on Industrial Electronics, Vol.47, No.5, 2000, pp. 994-1004.

[25] MATLAB -The language of technical computing, ver.6, The Mathhworks Inc., 2000.

[26] SIMULINK – Dynamic system simulation for matlab, ver.3, The Mathhworks Inc., 1999.

[27] Bellini, A., Filippetti, F., Francheschini, G., and Tassoni, C., "Closed loop control impact on the diagnosis of induction motor fault", IEEE – IAS Annual Meeting Rec., 1999, pp. 1913– 921.

[28] Gentile, G., Rotondale, N., and Tursini, M., "Investigation of inverter fed induction motors under fault conditions", Proc. of Power Electronics Specialists Conference, 1992, pp.126-132.

[29] Renfrew, A. C., and Tian, J. X., "Fault diagnosis in power electronic converters", Proc. of Universities Power Engineering Conference, 1993, pp. 565-568.

[30] Craig, E., Macrow, B. C., Atkinson, D. J., and Jack, A.G., "A fault detection procedure for single phase bridge converters", Proc. of 5th. European Conference on Power Electronics and Applications, Vol. 4, 1993, pp. 466-471.

[31] Wiechmann, E. P., Garcia, A. R., Rodriguez, J. R., Amthaver, E. O., and Sanchez, R.W., "Waveform supervision of power phase controlled rectifiers: a real time converter operating surveillance", Proc. of 5th. European Conference on Power Electronics and Applications, Vol. 4, 1993, pp. 461-465.

[32] Aris, I. B., Zhang, L., and Hulley, L. N., "Fault detection of an inverter circuit by digital signal processing and knowledge based approach", Proc. of Universities Power Engineering Conference, 1994, pp. 489-491.

[33] Blaabjerg, F., and Pedersen, J. K., "A new low-cost, fully fault protected PWM_VSI inverter with three phase current information" IEEE Trans. on Power Electronics, Vol.12, No.1, 1997, pp. 187-197.

[34] Retiere, N., Roye, D., and Mannevy, P., "Vector based investigation of induction motor drive under inverter fault operations", Proc. of Power Electronics Specialist Conference, 1997, pp. 1288-1294.

[35] Mendes, A. M. S., Marques Cardoso, A. J., and Saraiva, E. S., "Voltage source inverter fault diagnosis in variable speed ac drives, by Park's vector approach", Proc. of 7th. International Conference on Power Electronics and Variable Speed Drives, 1998, pp. 538-543.

[36] Grimmelius, H. T., Meiler, P. P., Maas, H. L. M. M. Bonnier, B., Grenvink, J. S., and Kuilenberg, R. F. V., "Three state-of-the-art methods for condition monitoring", IEEE Trans. on Industrial Electronics, Vol.46, No.2, 1999, pp. 407-416.

[37] Benbouzid, M. E. H., "A review of induction motors signature analysis as a medium for fault detection", IEEE Trans. on Industrial Electronics, Vol.47, No.5, 2000, pp. 982-993.

[38] Gertler, J., "Survey of model-based failure detection and isolation in complex plants", IEEE Trans. on Control Sys. Mag., Vol.8, 1988, pp. 3-11.

[39] Filipetti, F., Franceschini, G., Tassoni, C., and Vas, P., "Transient model oriented to diagnostics of induction machine with rotor asymmetry", Proc. ICEM, Vol.3, 1994, pp. 62-67.

[40] Krishnaswami, V., and Rizzoni, G., "Model based health monitoring of vehicle steering system using sliding mode observer", Proc. of American Control Conference, 1995, pp. 1652-1656.

[41] Schneider, C., and Filbert, D., "Parameter estimation and residual analysis: a comparison", Proc. of IFAC Fault Detection, Supervision and Safety of Technical Process, 1994, pp. 701-705.

[42] Isermann, R., "Process fault detection based on modelling and estimation methods- a survey", Automatica, Vol.20, 1984, pp. 378-404.

[43] Vas, P., "Condition monitoring, diagnosis and parameter estimation of electrical machines", Oxford Univ. Press, 1993.

[44] Liu X., Q., Zhang, H. Y., Liu, J., and Yang, J., "Fault detection and diagnosis of permanent-magnet dc motor based on parameter estimation and neural network", IEEE Trans. on Industrial Electronics, Vol.47, No.5, 2000, pp. 1021-1030.

[45] Watanabe, K., Sasak, M., and Himmelblan, D. M., "Determination of optimal measuring sites for fault detection of nonlinear system", Journal Syst. Sci., Vol.16, 1985, pp. 1345-1363.

[46] Lee, K. S., Ryu, J. S., and Park, T. G., "An intelligent fault detection and isolation scheme for a class of nonlinear system", Proc. 2nd Asian Control Conference, No.3, 1997, pp. 83-86.

[47] Chan, C. W., Cheung, K. C., Zhang, H. Y., and Wang, Y., "Fault detection of DC motors using nonlinear observer based on recurrent B- spline neurofuzzy network", Proc. 14th IFAC World Congress, Vol.B, 1999, pp. 511-516.

[48] Cho, K. R., Lang, J. H., and Umans, S. D., "Detection of broken rotor bars in industry motor using state and parameter estimation", IEEE Trans. on Industrial Applications, Vol.28, 1992, pp. 702-709.

[49] Ho, S. L., Chan, W. L., and Leung, H. W., "Application of statistical signal processing of condition monitoring of rotor faults in induction motors", Proc. of 6th. International Conference on Electrical Machines and Drives, 1993, pp. 97-102.

[50] Arthur, N and Penman, J., "Supply invariant induction motor condition monitoring", Proc. of 8th. International Conference on Electrical Machines and Drives, 1997, pp. 341-345.

[51] Winterling, M. W., Tuinman, E., and Deleron, W., "Fault analysis of electromechanical traction drives", Proc. of International Conference on Electrical Machines and Drive, No.444, pp.248-252, 1997.

[52] Rajagopalan, V., Debebe,. N. D., and Sankar, T. S., "Expert system for fault diagnosis of VSI fed ac drives", IEEE-AAS Conf. Rec., 1991, pp. 368-373.

[53] Leith, D., Deans, N. D., and Stewart, L. I. D., "Condition monitoring of electrical machines using a real-time expert system", Proc. of ICEM, 1998, pp. 297-302.

[54] Chow, T. S. W. and Law, L. T., "Rotating machines faults identification using back propagation artificial neural network", Proc. of 6th. International Conference on Electrical Machines and Drives, 1993, pp. 412-415.

[55] Knapp, G. M., and Wang, H. P., "Machine fault classification - a neural network approach", International Journal of Production Research, Vol.30, No.4, 1992, pp.811-823.

[56] Altawil, I. A. I., "Non invasive condition monitoring and fault diagnosis of power electronics drives using neural network", PhD Thesis, University of Wales Swansea, 1996.

[57] Li, B., Chow, Y. M., Tipsuwan, Y., and Hung, J. C., "Neural network based motor rolling bearing fault diagnosis", IEEE Trans. on Industrial Electronics, Vol.47, No.5, 2000, pp. 1060-1069.

[58] Nejjari, H., and Benbouzid, M. E. H., "Application of fuzzy logic to induction motors condition monitoring", IEEE Power Engineering Review, 1999, pp. 52-54.

[59] Ritchie, E., Deng, E. X., and Jokinen, T., "Diagnosis of rotor faults in squirrel cage industry motor using fuzzy logic approach", Proc. IEEM, Vol.2, 1994, pp. 348-352.

[60] Filipetti, F., Franceschini, G., Tassoni, C., and Vas, P., "A fuzzy logic approach to on-line induction motor diagnostics based on stator current monitoring", Proc. Symposium Power Technology, 1995, pp. 270-274.

[61] Goode, P. V., and Chow, M., "Using a neural fuzzy system to extract heuristic knowledge of incipient faults in induction-motors. 1. methodology", IEEE Trans. on Industrial Electronics, Vol.42, No.2, 1995, pp.131-138.

[62] Filipetti, F., Franceschini, G., Tassoni, C., and Collamati, L., "NN fuzzy logic synthesis in diagnostic system for electric machines", Proc. Symposium Electrical Machines, 1996, pp. 107-112.

[63] Franceschini, G., Gentile, G., Rotondale, N., Tassoni, C., and Tursini, M., "An approach to knowledge base representation in electric drive fault diagnosis", Proc. ICEM, 1994, pp. 358-362.

[64] Hayes-Roth, F., Waterman, D. A., and Lenat, D. B., "Building expert systems", Addison-Wesley, 1983.

[65] Harvey, R. L., "Neural network principles", Prentice Hall, 1994.

[66] Gallant, S. I., "Neural network learning and expert system", MIT Press, 1993.

[67] Jain, L. C., and Martin, N. M., "Fusion of neural networks, fuzzy sets and genetic algorithms: industrial applications", CRC Press, 1998.

[68] Haykin, S., "Neural network – a comprehensive foundation", Prentice Hall, 1999.

[69] Mendel, J. M. "Fuzzy logic systems for engineering: A tutorial", IEEE Proc., Vol.83, No.3, 1995, pp.345-377.

[70] Pedrycz, W., and Gomide, F., "An introduction to fuzzy sets: analysis and design", MIT Press, 1998.

[71] Nguyen, H. T., and Sugeno, M., "Fuzzy systems: modelling and control", Kluwer Academic Publishers, 1998.

[72] Jang, J. S. R. and Sun, C. T., "Neuro fuzzy modeling and control", IEEE Proc., Vol.83, No.3, 1995, pp.378-403.

[73] Vose, M. D., "The simple genetic algorithm: foundations and theory", MIT Press, 1999.

[74] Coley, D. A., "An introduction to genetic algorithms for scientists and engineers", World Scientific, 1999.

[75] Man, K. F., Tang, K. S., and Kwang, S., "Genetic algorithm: concept and designs", Springer, 1999.

[76] Chambers, L., "Practical handbook of genetic algorithm", CRC Press, 1999.

[77] Burrus, C. S., and Parks, T. W., "DFT/FFT and convolution algorithms: theory and implementation", John Wiley and Sons Inc., 1985.

[78] Chu, E. C. H., and George, A., "Inside the FFT black box: serial and parallel fast Fourier transforming algorithm", CRC Press, 2000.

[79] Rosenblatt, M., and Van Ness, J.W., "Estimation of the bispectrum", Annals of the ISM, 1965, pp. 426-436.

[80] Akaike, H., "Note on higher order spectra", Annals of the ISM, Vol.18, 1966, pp. 123-126.

[81] Brillinger, R., and Rosenblatt, M., "Computation and interpretation of k^{th} order spectra", Spectral Analysis Time Series, John Wiley and Sons Inc., 1967, pp.189-232.

[82] Box, G.E.P., and Jenkins, G.M., "Time-series analysis: forecasting and control", Holden-Day, 1970.

[83] Young, C. K., and Edward, J. P., "Digital bispectral analysis and its applications to nonlinear wave interactions", IEEE Trans. on Plasma Science, Vol. PS-7, No.2, 1979, pp. 120-131.

[84] Fanglin, H., and Songnian, G., "Application of higher order cumulants to structure fault diagnosis", Proc. of 11^{th}. International Conference on Modal Analysis, 1993, pp. 1237-1240.

[85] Nikias, C. L., and Mendel, J .R., "Signal processing with higher order spectra", IEEE Signal Processing magazine, 1993, pp. 10-35.

[86] Chow, T. W. S., and Fei, G., "Three phase induction machines asymmetrical faults identification using bispectrum", IEEE Trans. on Energy Conversion, Vol.10, No.4, 1995, pp. 688-693.

[87] Chow, T. W. S., "Condition monitoring of electrical machines using third-order spectrum analysis", Proc. of Industry Applications Conference, Vol.1, 1996, pp. 679-686.

[88] Arthur, N., Penman, J., McLean, A., and Parsons, A., "Induction machines condition monitoring with higher order spectra part I: fundamentals and fixed frequency operation",

Proc. of the 24th. Annual Conference of IEEE, Industrial Electronics Society, 1998, pp.1889-1894.

[89] Arthur, N., Penman, J., McLean, A., and Parsons, A., "Induction machines condition monitoring with higher order spectra part II: variable frequency operation and automated diagnosis", Proc. of the 24th. Annual Conference of IEEE Industrial Electronics Society, 1998, pp.1894-1900.

[90] Dhanwada, C., and Bartlett, E. B., "Neural-network-based condition monitoring systems", Proc. of the American Power Conference, Vol.58, Ch.287, No.pt 1&2, 1996, pp.303-308.

[91] Heb, T.E, and Hautier, J. P., "Remedial strategies for inverter ac motor system at the occurence of a transistor drive fault", Proc. of EPE Conference, 1991, pp. 4.286 – 4.291.

[92] Bowes S. R., "New sinusoidal pulse width-modulated inverter", IEE Proc., Vol. 122, No. 11, 1975, pp. 1279-1285.

[93] Bowes S. R., and Mount M. J., "Microprocessor control of PWM inverters", IEE Proc., Vol. 128, Pt. B, No. 6, 1981, pp. 293-305.

[94] Bowes S. R., and Clements R. R., "Computer-aided design of PWM inverter systems", IEE Proc., Vol. 129, Pt. B, No. 1, 1982, pp. 1-17.

[95] Bowes S. R., and Midoun A., "Microprocessor implementation of new optimal PWM switching strategies", IEE Proc., Vol. 135, Pt. B, No. 5, 1988, pp. 269-279.

[96] Addoweesh K. E., Shepherd W., and Hulley L. N., "Induction motor speed control using a microprocessor-based PWM inverter", IEEE Trans. on Industrial Electronics, Vol. 36, No. 4, 1989, pp. 516-522.

[97] Boost M. A., and Ziogas P. D., "State-of- the-art carrier PWM techniques: a critical evaluation", IEEE Trans. on Industry Applications, Vol. 24, No. 2, 1988, pp. 271-280.

[98] Murphy, J. M. D., and Turnbull, F. G., "Power electronic control of AC motors", Pergamon Press, 1988.

[99] Mohan, N., Undeland, T. M., and Robbins, W. P., "Power electronics converters, application, and design", John Wiley and Sons Inc., 2nd edition, 1995.

[100] Rashid, M. H., "Power electronics, circuits, devices and applications", Prentice Hall, 2nd Edition, 1993.

[101] Baliga, B.J., "Modern power devices", John Wiley and Sons Inc., 1987.

[102] Lander, C.W., "Power electronics", McGraw Hill Book Company, 1987.

[103] Bird, B. M., and King, K. G., "An introduction to power electronics", John Wiley and Sons Inc., 1983.

[104] Bradley, D. A., "Power electronics", Van Nostrand Reinhold (UK) Co. Ltd., 1987.

[105] Zhenyu, Y., Arefeen, M., and Issa, P., "A review of three PWM techniques", Proc. of the American Control Conference, 1997, pp. 257-261.

[106] Sarma, M. S., "Electric machines steady-state theory and dynamic performance", West Publishing Co., 1986.

[107] Hubert, C. I., "Electric machines theory, operation, applications, adjustment, and control", Macmillan Publishing Co., 1991.

[108] Jamal, W., "Application of modern control techniques in ac speed drive motors", Ph.D. Thesis, University of Wales Swansea, 2001.

[109] Kelkar, S. S., and Fred C. Y. Lee, "A fast time domain digital simulation technique for power converters: application to a buck converter with feedforward compensation", IEEE Trans. on Power Electronics, PE-1, No.1, 1986, pp. 21-31.

[110] Shortt, D. J. and Lee, F. C., "Improved switching converter model using discrete and averaging techniques", IEEE Trans. on Aerospace and Electronic Systems, No.2, 1983, pp. 190 197.

[111] Wang, R. C., Owens, H. A. Jr., and Wilson, T.G., "A fast algorithm for the time domain simulation of switched-mode piecewise linear systems", IEEE Power Electronics Specialists Conf. Rec., 1984, pp. 281-296.

[112] Liu, C.C., Hsieh, J., Conrad H. K.C, Bocek, J. M. and Hsiao, Y.T., "A fast-decoupled method for time-domain simulation of power converters", IEEE Trans. on Power Electronics, Vol.8, No.1, 1993, pp. 37-45.

[113] Middlebrook, R. D., and Slobadan C., "A general unified approach to modelling switching converter power stages", IEEE Power Electronics Specialists Conf. Rec., 1976, pp. 18 - 34.

[114] Polivka, W. M., Chetty, P. R. K., and Middlebrook, R. D., "State space average modeling of converters with parasitics and storage-time modulation", IEEE Power Electronics Specialists Conf. Rec., 1980, pp. 119-142.

[115] Rahim, N. A., and Mamat-Ibrahim, M. R., "Simplified analysis of the dc - dc converter using matlab/simulink", Proc. of IASTED Conference on Modelling, Simulation and Optimization, No.1, 1996, pp. 242 – 222.

[116] Ziogas, P. D., Wiechmann E.P., and Stefanovic, V. R., "A computer aided analysis and design approach for static voltage source inverters" , IEEE Trans. on Industrial Application, Vol. 1A – 21, 1985, pp. 1234 – 1240.

[117] Salazar, L. and Joos, G., "Pspice simulation of three-phase inverters by means of switching functions" , IEEE Trans. on Power Electronics, Vol. 9, No. 1, 1994, pp. 35-42.

[118] Lee, B.K. and Ehsani, M., "A simplified functional simulation model for three-phase voltage-source inverter using switching function concept" , IEEE Trans. on Industrial Electronics, Vol. 48, No. 2, 2001, pp. 309 – 321

[119] Morlet, J., Arens, G., Foorgeou, E., and Giard, D., "Wave propagation and sampling theory – part I: complex signal and scattering in multi layered media", Geophysics, Vol. 47, No. 2, 1982, pp. 203 – 221.

[120] Morlet, J., Arens, G., Foorgeou, E., and Giard, D., "Wave propagation and sampling theory – part II: sampling theory and complex waves", Geophysics, Vol. 47, No. 2, 1982, pp. 222 – 236.

[121] Grosman, A., and Morlet, J., "Decomposition of hardy functions into a square integrable wavelets of constant shape", SIAM Journal of Math. Anal., Vol.15, 1984, pp. 723 – 736.

[122] Daubechies, I., "Orthonormal bases of compactly supported wavelets", Comm. Pure Appl. Math., Vol.41, 1988, pp. 909-996.

[123] Cohen, A., Daubechies, I., and Feauveaux, J., "Biorthogonal bases of compactly supported wavelets", Comm. Pure Appl. Math., Vol.45, 1992, pp. 485-560.

[124] Coifman, R., and Wickerhauser, M., "Entropy-based algorithms for best basis selection", IEEE Trans. on Information Theory, Vol.38, 1992, pp.713-718.

[125] Malvar, H., "Lapped transform for efficient transform subband coding", IEEE Trans on Acoustic, Speech and Signal Process, Vol. 38, 1990, pp. 969 – 978.

[126] Chen, C.M., and Loparo, K. A., "Electric fault detection foe vector-controlled induction motors using the discrete wavelet transform", Proc. of the American Control, 1998, pp. 3297-3301.

[127] Arturi, C.M., Frdrigo, P., Gandelli, A., Leva, S., and Morando, A.P., "Dynamic analysis of electromechanical converters by means of the wavelet transform", Proc. of IEEE Conference on Power electronics and Drive Systems, 1999, pp. 462-465.

[128] Chang, C.S, Feng, T., Khambadkone, A.M, and Kumar, S., "Remote short-circuit current determination in DC railway systems using wavelet transform", IEE Proc. Elect. Power App., Vol.147, No.6, 2000, pp.520-525.

[129] Borras, D., Castilla, M., Moreno, N., and Montana, J.C., "Wavelet and neural structure: a new tool for diagnostic of power system disturbances", IEEE Trans. on Industry Applications, Vol.37, No.1, 2001, pp.184 – 190.

[130] Chang, C.S, Kumar, S., Liu, B., and Khambadkone, A.M., "Real-time detection using wavelet transform and neural network of short-circuit faults within a train in dc transit system", IEE Proc. Elect. Power App., Vol.148, No.3, 2001, pp.251-256.

[131] Zhongming, Y. and Bin, W. "Online rotor bar breakage detection of three phase induction motors by wavelet packet decomposition and artificial neural network", Proc. of Power Electronics Specialists Conference, Vol.4, 2001, pp. 2209 – 2216.

[132] Chan, A.K., and Peng, X., "Fast and robust neural network based wheel bearing fault detection with optimal wavelet features", Proc. of the 2002 International Joint Conference on Neural Networks, Vol.3, 2002, pp. 2076-2080.

[133] Vetterli, M. and Herley, C., "Wavelets and filter banks: theory and design", IEEE Trans. on Signal Processing, Vol.40, No.9, 1992, pp. 2207 – 2232.

[134] Meyer. Y and Roques, S., "Progress in wavelet analysis and applications", Edition Frontieres, 1992.

[135] Kaiser, G., "A friendly guide to wavelet", Birkauser Bostor, 1994,

[136] Hubbard, B., "The world according to wavelets", A.K. Peters, Wellesley, Mass. , 1996.

[137] Williams, J. and Arnaratunga, K., "Introduction to wavelets in engineering", Int. Jounal of Numerical Method Engineering, Vol.37, 1994, pp. 2365 – 2388.

[138] Strang, G. and Nguyen, T., "Wavelets and filter banks", Wellesly-Cambridge press,MA, 1996.

[139] Zadeh, L. A., "Fuzzy sets", Information and Control, Vol. 8, 1965, pp. 338-353.

[140] Zadeh, L. A., "Outline of a new approach to the analysis of complex systems and decision processes", IEEE Trans. Systems, Man and Cybernetics, Vol. SMC-3, No. 1, 1973, pp. 28-44.

[141] Schwartz, D. G., Klir, G. J., Lewis, H. W., and Ezawa, Y., "Applications of fuzzy sets and approximate reasoning", IEEE Proc. Consumer Electronics, Vol. 82, No. 4, 1994, pp. 482-498.

[142] Bonissone, P. P, Badami, V., Chiang, K. H., Khefkar, P. S., Marcelle, K. W., and Schutten, M. J, "Industrial applications of fuzzy logic at General Electric", Proceedings of the IEEE, Engineering App. of Fuzzy Logic, March 1995, pp. 450-465.

[143] Lee, C. C., "Fuzzy logic in control systems: fuzzy logic controller – part 1", IEEE Trans. Systems, Man and Cybernetics, Vol. 20, No. 2, 1990, pp. 404-418.

[144] Dubois, D., and Prade, H., "Fuzzy sets and systems: theory and applications", Academic Press Inc., 1980.

[145] Kruse, R., Gebhardt J., and Klawonn, F., "Foundations of fuzzy systems", John wiley and sons, 1994.

[146] Lee, C. C., "Fuzzy logic in control systems: fuzzy logic controller – part 2", IEEE Trans. Systems, Man and Cybernetics, Vol. 20, No. 2, 1990, pp. 419-435.

[147] Mamdani, E.H. and S. Assilian, "An experiment in linguistic synthesis with a fuzzy logic controller", International Journal of Man-Machine Studies, Vol. 7, No. 1, pp. 1-13, 1975.

[148] Sugeno, M., "Industrial applications of fuzzy control", Elsevier Science Pub. Co., 1985.

[149] Mamdani, E.H., "Advances in the linguistic synthesis of fuzzy controllers," International Journal of Man-Machine Studies,Vol.8,pp. 669-678, 1976.

[150] Mamdani, E.H., "Applications of fuzzy logic to approximate reasoning using linguistic synthesis," IEEE Transactions on Computers, Vol. 26, No. 12, pp. 1182-1191, 1977.

[151] Ying, H., Li, S.K., Shao, S.H. and Ding, Y.S., "Typical Takagi-Sugeno and Mamdani fuzzy systems as universal approximators: necessary conditions and comparison", Proc. of International Conference on Fuzzy Systems, Vol.1, 1998, pp. 824-828.

[152] Langari, R. and Liang, W., "Building Sugeno-type models using fuzzy discretization and orthogonal parameter estimation techniques", IEEE Trans. on Fuzzy Systems, Vol.3, No. 4, 1995, pp.454 - 458.

[153] Bikdash, M., "A highly interpretable form of Sugeno inference systems", IEEE Trans. on Fuzzy Systems, Vol.7, No.6, 1999, pp. 686-696.

[154] Frédéric, R., Phillipe, B., and Thierry A.M., "Failures-tolerance and remedial strategies of a PWM multicell inverter", IEEE Trans. on Power Electronics, Vol.17, No.6, 2002, pp.905-912.

[155] Ohmae, T., Matsuda, T., Kamiyama, K., and Tachikawa, M., "A microprocessor-controlled high-accuracy wide-range speed regulator for motor drives", IEEE Trans. Industrial Electronics, Vol. IE-29, No. 3, 1982, pp. 207-212.

[156] Khanniche, M. S., and Guo, Y. F., "A microcontroller-based real-time speed measurement for motor drive systems", Jounal of Microcomputer Applications, Vol. 18, 1995, pp. 39-53.

[157] Walker, J.S., "Fourier analysis and wavelet analysis", Notices of the AMS, Vol. 44, No. 6, 1997, pp. 658-670.

[158] Ridsdill-Smith, T. A., and Dentith, M. C., "The wavelet transform in aeromagnetic processing", Journal of Geophysics, Vol. 64, No. 4, 1999, pp. 1003-1013.

APPENDIX A

Fuzzy Logic System

In recent years, fuzzy logic (FL) has emerged as one of the most attractive control tools used in several applications in the lack of complete and precise mathematical information. FL is based on human reasoning and an intuitive approach in interpreting problems and finding solutions. It utilises linguistic knowledge to represent a system. FL deals with objects in terms of degree of membership with all possible grades of logic between 0 and 1, and the shades of grey between white and black.

Fuzzy logic is essentially based on the theory of fuzzy sets, which was introduced at first by Lotfi A. Zadeh in 1965 [139]. In 1973 [140], an important breakthrough in fuzzy development was made, which introduced the concept of linguistic variables and fuzzy conditional statements (fuzzy rules). A linguistic variable is defined as a variable whose values are linguistic terms rather than numbers, while the fuzzy conditional statements are expressions of the form IF *A* THEN *B*, where *A* and *B* are fuzzy sets. Since then, the literature on FL has been growing rapidly, which illustrated its useful implication in many industrial applications [141, 142].

Fuzzy Set and Fuzzy Logic

Fuzzy set and fuzzy logic are powerful mathematical tools used to model uncertain system behaviour in the absence of complete and precise information about the system. It will be convenient to summarise the relevant properties of the fuzzy set theory and the basic concepts of FL that are aimed to aid the development of FL in later sections. In what follows, all letters and terms in italic are referred to notation and properties of fuzzy sets, respectively.

A. Definition of Fuzzy Sets and Terminology

A *fuzzy set A* of a universe of discourse U is characterised by a membership function $\mu_A(x)$: $U \rightarrow [0,1]$, where $\mu_A(x)$ specifies the grade or degree to which any element x in U belongs to the fuzzy set A. The general definition of fuzzy set A can be obtained as:

$$A = \left\{ \left(x, \mu_A(x)\right) \mid x \in U,\ \mu_A(x) \in [0,1] \right\} \tag{A.1}$$

Definition (A.1), associates with each element x in U a real number $\mu_A(x)$ in the interval between [0,1], which represents the degree of membership of x in A. Larger values of $\mu_A(x)$ indicate higher degrees of membership and vice versa. Figure A-1 shows a characteristic example of a membership function that maps elements of U to a membership range which is usually in the interval between [0,1].

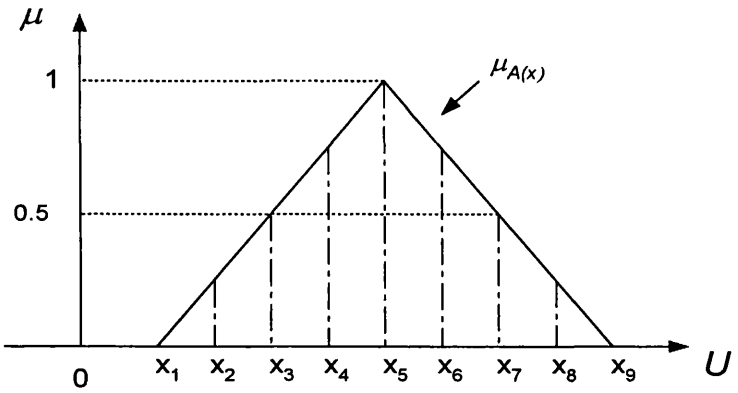

Figure A-1: Membership function of fuzzy set A.

It follows from Figure A-1 that the fuzzy set A can be represented concisely by the summation

$$A = \mu_1 / x_1 + \ldots\ldots + \mu_n / x_n \tag{A.2}$$

or

$$A = \sum_{i=1}^{n} \mu_i / x_i \tag{A.3}$$

in which μ_i, $i = 1,...,n$, is the degree of membership of x_i in fuzzy set A. It should be noted that the + sign in equation (A.2) and (A.3) refers to the set union rather than the arithmetic summation, while the / sign used to connect each element with its membership value and has no connection to the arithmetic division.

The *support* of fuzzy set A is the set of all elements x (x_1, x_2, ...,x_n) in the universe of discourse U, at which $\mu_A(x) > 0$. The *crossover point* in fuzzy set A is an element (or elements) x in U whose degree of membership in A is 0.5 (such as x_3 and x_7 in Figure A-1). However, if the fuzzy set A whose support is just a single element x_1 and $\mu_A(x_1) \in [0,1]$ is called *fuzzy singleton.*

B. Basic Theoretic Operations on Fuzzy Sets

For simplicity of illustration, two fuzzy sets A and B in the universe of discourse U with membership functions μ_A and μ_B, respectively, are considered in which

$$A = \{ (x, \mu_A(x)) \}, \ \mu_A(x) \in [0,1] \quad , x \in U \tag{A.4}$$

$$B = \{ (x, \mu_B(x)) \}, \ \mu_B(x) \in [0,1] \quad , x \in U \tag{A.5}$$

It should be noted that the set operation with A and B are performed based on operations on their membership functions as in the following,

Definition 1: Equality: The fuzzy sets A and B are *equal* denoted by $A = B$ if and only if for every element x in U,

$$\mu_A(x) = \mu_B(x) \quad , x \in U \tag{A.6}$$

Definition 2: Complementation: The fuzzy sets A and $\overline{A}$ are complementary for all element x in U if

$$\mu_{\bar{A}}(x) = 1 - \mu_A(x) \qquad , x \in U \tag{A.7}$$

Definition 3: Intersection: The membership function $\mu_{A \cap B}$ of the intersection operation between the fuzzy sets denoted as $A \cap B$ is defined for every element x in U by

$$\mu_{A \cap B}(x) = \min\{\mu_A(x), \mu_B(x)\} \qquad , x \in U \tag{A.8}$$

Definition 4: Union: The membership function $\mu_{A \cup B}$ of the union operation between the fuzzy sets denoted $A \cup B$ is defined for every element x in U by

$$\mu_{A \cup B}(x) = \max\{\mu_A(x), \mu_B(x)\} \qquad , x \in U \tag{A.9}$$

Definition 5: Algebraic Product : The membership function $\mu_{A \cdot B}$ of the algebraic product operation between the fuzzy sets denoted $A \cdot B$ is defined for every element x in U by

$$\mu_{A \cdot B}(x) = \mu_A(x) * \mu_B(x) \qquad , x \in U \tag{A.10}$$

Definition 6: Cartesian Product : If A and B are fuzzy sets in the universe of discourse U, the Cartesian product (or cross product) denoted $A \times B$ is the set of ordered pairs given as

$$A \times B = \{(a,b) \mid a \in A,\ b \in B\} \tag{A.11}$$

C. Fuzzy Relations and Compositional Operators

A *fuzzy relation* R_f from a fuzzy set A to a fuzzy set B is a fuzzy subset of the Cartesian product $A \times B$, where A and B are subsets of the universes U_1 and U_2, respectively. This leads to the definition of the *fuzzy relation* R_f as

$$R_f = \{((x,y),\mu_R(x,y)) \mid (x,y) \in A \times B, \mu_R(x,y) \in [0,1]\} \qquad \text{(A.12)}$$

where the membership function $\mu_R(x,y)$ gives the degree of membership of the ordered pair (x,y) in the fuzzy relation R_f. In other words, this degree of membership indicates the degree to which x is in relation with y.

If R_f is a relation from fuzzy set A to fuzzy set B and S is a relation from fuzzy set B to fuzzy set C, then the *composition* of R_f and S results in a fuzzy relation denoted by $R_f \circ S$ and defined by

$$R_f \circ S = \left\{\left((x,z), \max_y(\mu_R(x,y) * \mu_S(y,z))\right)\right\} \qquad \text{(A.13)}$$

where * denotes a compositional operators such as *intersection* (*min*), *product*, *bounded product* and *drastic product*. Suitable selection of any of these operators depends highly on the designer, where it is chosen to fit a specific application. In many FLC applications, the *max-min* and the *max-product* compositional operators are the most frequently used due to their ease of implementation [143]. A more detailed discussions on fuzzy relation and compositional rules of inference are presented in [144, 145].

The Principles of Fuzzy Logic System (FLS)

In general, a FLS is a nonlinear mapping of an input data (feature) vector into a scalar output. A FLS maps crisp inputs into crisp outputs. It contains four components: , *fuzzifier, rules, inference engine*, and *defuzzifier*. Figure A-1 shows the basic configuration of a typical FLC.

A. Fuzzification Process

The basic function of the fuzzification stage is to convert the crisp input variable into a fuzzy singleton within a certain universe of discourse. This can be accomplished by mapping the crisp values of the input variable through all the fuzzy sets over the corresponding universe of discourse. The mapped data are further converted into a fuzzy singleton which basically gives the degree of membership for each crisp value in relation with all fuzzy sets within the corresponding universe of discourse. The fuzzification process can be expressed by

$$x = \mathit{fuzzifier}\left(x_0\right) \tag{A.14}$$

where x_0 and x represent the crisp input value from a plant and the pre-defined fuzzy set for the input variable, respectively.

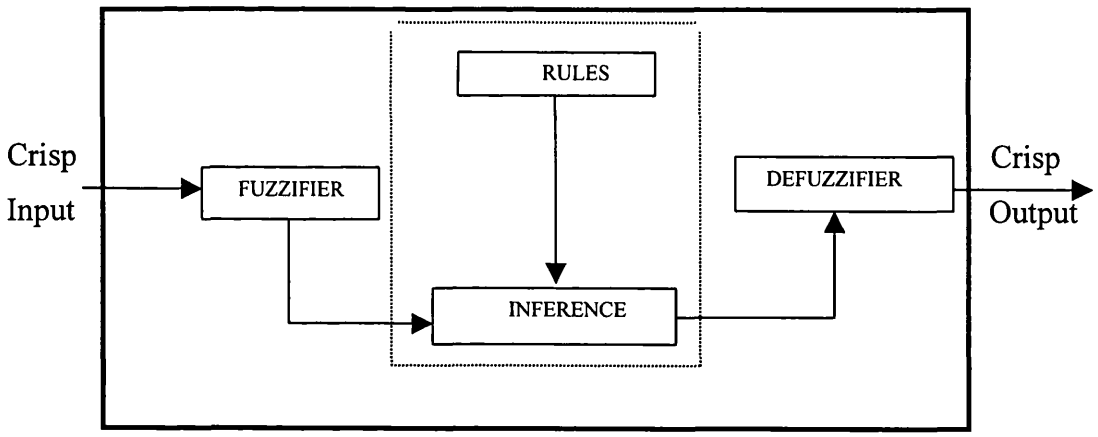

Figure A-2: Block diagram of a typical FLS.

B. Fuzzy Rules

Rules may be provided by experts or can be extracted from numerical data. In either case, engineering rules are expressed as a collection of IF – Then statements, e.g.:

Rule $_i$: IF x is A_i AND y is B_i THEN z is C_i

where x, y and z are linguistic variables representing the plant state variables and the output control variables. A_i, B_i and C_i are fuzzy labels of the linguistic variables x, y, and z in the universes of discourse U, V, and W, respectively. In this rule, the IF part is known as the *antecedent*, while the THEN part is known as the rule *consequent*. Hence, the fuzzy rule is a conditional statement in which the antecedent is a condition and the consequent is a control action for the system under control.

The number of fuzzy rules is determined by computing the product of the number of fuzzy sets in each input linguistic variables, x and y. These rules are then designed to produce as a conclusion l different outputs, where l is the number of fuzzy sets in the output linguistic variable, z. For example, in the case of two-input-single-output fuzzy system, where both input variables have the same number of fuzzy sets 5, then there should be 5*5 = 25 fuzzy rules.

In many cases, large number of rules can be reduced using several methods [143, 146]. One method is achieved by the reduction of the antecedent (linguistic) variables or their fuzzy sets. The other method is to keep track of the rules being computed during real-time or by off-line inferencing of the FLS and trying to eliminate those rules which are either not used at all or used very little.

C. Fuzzy Inference Engine

Fuzzy inference is the process of formulating the mapping from a given input to an output using fuzzy logic. The mapping provides a basis from which decisions can be made. Just as humans use many different types of inferential procedures to help them understand things or to make decisions, there are many different fuzzy logic inferential procedures. Only a very small number of them are actually being used in engineering applications of FL [69]

There are two types of fuzzy inference systems that are normally used, *Mamdani-type* and *Sugeno-type*. These two types vary somewhat in the way output are determined. *Mamdani's* type is the most commonly seen fuzzy methodology. *Mamdani's* method

was among the first control system built using fuzzy set theory. It was proposed in 1975 by Ebrahim Mamdani [147]. *Mamdani's* effort was based on Lotfi Zadeh on fuzzy algorithm for complex systems and decision processes published in 1973 [140]. Meanwhile, the *Sugeno-type* was first introduced in 1985 [148]. It is similar to the *Mamdani* method in many aspects. In fact the first two parts of the fuzzy inference process, fuzzifying the inputs and applying the fuzzy operator, are exactly the same. The main difference is that the output membership functions are only linear or constant for *Sugeno-type* fuzzy inference. Details of these two types can be found in [69, 149-153].

D. Defuzzification Process

This process is needed to maps output sets into crisp output numbers. This can be expressed by

$$y_0 = defuzzifier\,(y) \tag{A.15}$$

where y and y_0 are fuzzy and crisp outputs, respectively. There exist several de-fuzzification methods. Some of the earliest used the *"mean of maxima"*, meaning that the crisp output is taken as the value at which the membership function of the inferred fuzzy set reached its maximum, but if there are many maxima the mean of these is taken. In the present, the *"centroid"* or *"centre of gravity"* method is the most commonly used. It can be computed by defining the contour or aggregate of the inferred control action, which is used to solve the following discrete formula

$$y_0 = \frac{\sum_{k=1}^{N} y_k * \mu_{agg}(y_k)}{\sum_{k=1}^{N} \mu_{agg}(y_k)} \tag{A.16}$$

where y_k represent the subdivided discrete samples into N equal subintervals of the output universe of discourse, while $\mu_{agg}(y_k)$ contain the corresponding aggregated degree of membership for each sample.

E. Fuzzy Linguistic Variables

Linguistic variables are defined as variables whose values are words or sentences in natural or artificial languages. They play an essential role in providing a systematic mean for an approximate characterisation of complex or ill-defined systems. For example, by employing the concept of fuzzy set theory, the stator current *DC offset* can be described approximately. The *DC offset* is a linguistic variable comprising some fuzzy sets such as *NB (Negative Big), NS (Negative Small), ZO (Near Zero), PS (Positive Small),* and *PB (Positive Big)*. In other words, the attribute *DC offset* is a *fuzzy variable*, whose values are *linguistic labels* of fuzzy sets. Each set is defined by an appropriate membership function as shown in Figure A-3, where a normalised universe [+1,-1] is being used. Membership functions having the forms of triangle-shaped and trapezoid-shaped are used here due to their ease of implementation compared to other existing functions.

It should also be noted that the number of fuzzy sets and the correct selection of the membership function have a substantial effect on the performance of the FLS. Moreover, the proper choice of the plant state variables and control variables is essential to characterise the operation of the fuzzy system. And indeed, the essence of the FLS performance depends strongly on the derivation of useful fuzzy control rules.

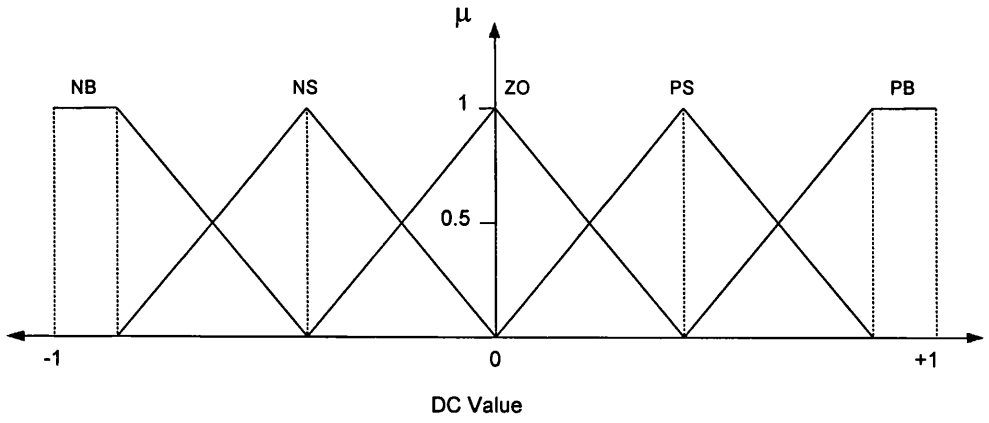

Figure A-3: Example of membership functions for the linguistic variable.

APPENDIX B

Six–Step VSI inverter using 180° mode of operation

In this mode of operations, each IGBT conducts for an interval of 180° in a cycle. This implies that each output terminal of the bridge inverter is connected consecutively for that interval to the positive and negative terminals of the dc supply. Three IGBTs remain on at any instant of time to provide the positive and negative rails for the current. Thus, there are six modes of operation in one cycle and the duration of each mode is 60°. These modes are given below in Table A.1.

Table A.1: Switching patterns of three phase bridge inverter using 180° mode of operation.

IGBTs / Intervals	T_1	T_2	T_3	T_4	T_5	T_6
0° - 60°	on	off	off	off	on	on
60° - 120°	on	on	off	off	off	on
120° - 180°	on	on	on	off	off	off
180° - 240°	off	on	on	on	off	off
240° - 300°	off	off	on	on	on	off
300° - 360°	off	off	off	on	on	on

If this type of inverter is used to feed a balanced star connected load, as shown in Figure 3-2, the phase voltage waveform has six steps per ac cycle and is termed a six-step wave. The equivalent circuits for the six modes of operation in a full cycle are shown in Figure A-1. The equivalent load impedance and load current for all the six modes are defined as follows:

$$Z_{eq} = Z + \frac{Z}{2} = \frac{3}{2}Z \qquad \text{(A.1)}$$

and,

$$i_L = \frac{V_{dc}}{Z_{eq}} = \frac{2}{3}\frac{V_{dc}}{Z} \tag{A.2}$$

Therefore, the computation of the phase and line voltages for a single mode of operation can be defined as follows,

During mode 1 for $0° \leq \omega t < 60°$, the phase voltages are:

$$V_{AN} = V_{CN} = \frac{i_L}{2} * Z = \frac{V_{dc}}{3} \tag{A.3}$$

$$V_{BN} = -i_L * Z = -\frac{2}{3}V_{dc} \tag{A.4}$$

while the line voltages are,

$$V_{AB} = V_{AN} - V_{BN} = \frac{V_{dc}}{3} - \left(-\frac{2}{3}V_{dc}\right) = V_{dc} \tag{A.5}$$

$$V_{BC} = V_{BN} - V_{CN} = -\frac{2}{3}V_{dc} - \frac{V_{dc}}{3} = -V_{dc} \tag{A.6}$$

$$V_{CA} = V_{CN} - V_{AN} = \frac{V_{dc}}{3} - \frac{V_{dc}}{3} = 0 \tag{A.7}$$

If the same procedures applied to the remaining modes of operations, Table A.2 is constructed, in which the six steps phase and line voltages are given.

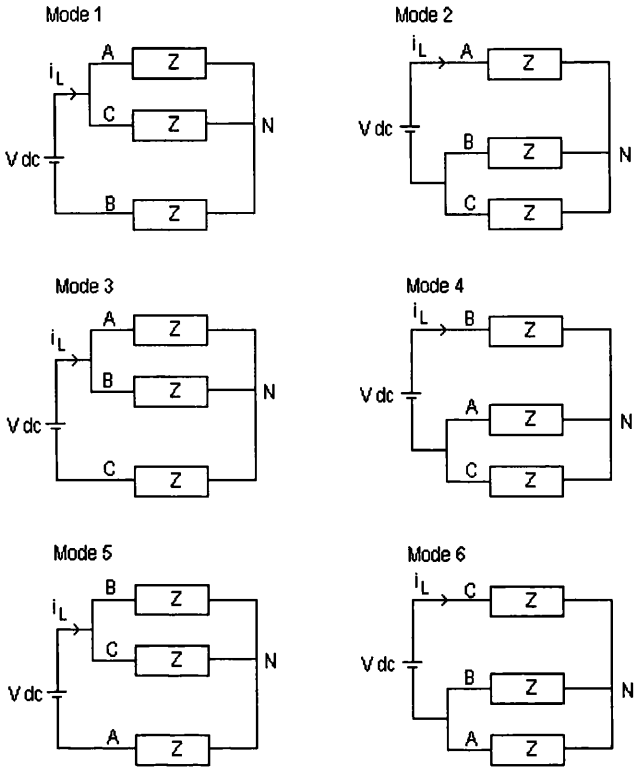

Figure A-1: Equivalent circuits

Table A.2: Six-step phase and line voltages for a balanced wye-connected load.

	Mode 1	*Mode 2*	*Mode 3*	*Mode 4*	*Mode 5*	*Mode 6*
V_{AN}	*1/3* V_{dc}	*2/3* V_{dc}	*1/3* V_{dc}	*-1/3* V_{dc}	*-2/3* V_{dc}	*-1/3* V_{dc}
V_{BN}	*-2/3* V_{dc}	*-1/3* V_{dc}	*1/3* V_{dc}	*2/3* V_{dc}	*1/3* V_{dc}	*-1/3* V_{dc}
V_{CN}	*1/3* V_{dc}	*-1/3* V_{dc}	*-2/3* V_{dc}	*-1/3* V_{dc}	*1/3* V_{dc}	*2/3* V_{dc}
V_{AB}	V_{dc}	V_{dc}	0	$-V_{dc}$	$-V_{dc}$	0
V_{BC}	$-V_{dc}$	0	V_{dc}	V_{dc}	0	$-V_{dc}$
V_{CA}	0	$-V_{dc}$	$-V_{dc}$	0	V_{dc}	V_{dc}

APPENDIX C

(i) Program for compsignal matlab function block.

```
function [y] = compsignal(a)
%This program is to compare two incoming signal.
x1=a(1);
x2=a(2);
if x1 >= x2
   y=1;
else
   y=-1;
end
```

(ii) Program to calculate sf2.

```
function [y] = sf2(a)
x1=a(1);
if x1 >= 0
   y=1;
else
   y=0;
end
```

APPENDIX D

The DWT M-file

```
s= 'data frame';
%
%Perform decomposition at level 3 of s using D4.
[c,l]= wavedec(s,3,'db2');
%extract detail coefficients at level 1,2 and 3 from wavelet
%decomposition structure [c,l].
dc1=wrcoef('d',c,l,'db2',3);
dc2=wrcoef('d',c,l,'db2',2);
dc3=wrcoef('d',c,l,'db2',1);
%plot detail coefficients at level 3, D4.
plot(tout,dc1);grid;ylabel('D4 Coefficient');title('Phase
B');xlabel('Time (s)');
%
function [c,l] = wavedec(x,n,varargin)
%WAVEDEC.
%   WAVEDEC performs a multi-level 1-D wavelet analysis..
%
%   The structure is organized as:
%   C      = [app. coef.(N)|det. coef.(N)|... |det. coef.(1)]
%   L(1)   = length of app. coef.(N)
%   L(i)   = length of det. coef.(N-i+2) for i = 2,...,N+1
%   L(N+2) = length(X).
%
if errargn(mfilename,nargin,[3:4],nargout,[0:2]), error('*'), end
if errargt(mfilename,n,'int'), error('*'), end
if nargin==3
    [LoF_D,HiF_D] = wfilters(varargin{1},'d');
else
    LoF_D = varargin{1};   HiF_D = varargin{2};
end
%
% Initialization.
%
s = size(x); x = x(:)'; % row vector
c = [];      l = [length(x)];
%
for k = 1:n
    [x,d] = dwt(x,LoF_D,HiF_D); % decomposition
    c     = [d c];              % store detail
    l     = [length(d) l];      % store length
end
%
% Last approximation.
c = [x c];
l = [length(x) l];
&
if s(1)>1, c = c'; l = l'; end
%
%
```

```
function x = wrcoef(o,c,l,varargin)
%WRCOEF.
%   WRCOEF reconstructs the coefficients of a 1-D signal,
%   given a wavelet decomposition structure (C and L).
%
%   X = WRCOEF('type',C,L,'wname') and
%   X = WRCOEF('type',C,L,Lo_R,Hi_R) reconstruct coefficients
%   of maximum level N = length(L)-2.
%
%
if errargn(mfilename,nargin,[4:6],nargout,[0:1]), error('*'), end
o = lower(o(1));
rmax = length(l); nmax = rmax-2;
if o=='a', nmin = 0; else , nmin = 1; end
if isstr(varargin{1})
    [LoF_R,HiF_R] = wfilters(varargin{1},'r'); next = 2;
else
    LoF_R = varargin{1};  HiF_R = varargin{2}; next = 3;
end
if nargin>=(3+next) , n = varargin{next}; else, n = nmax; end

if (n<nmin) | (n>nmax) | (n~=fix(n))
    errargt(mfilename,'invalid level value','msg'); error('*');
end

% Get DWT_Mode
dwtATTR = dwtmode('get');

switch o
    case 'a'
        % Extract approximation.
        x = appcoef(c,l,LoF_R,HiF_R,n);
        if n==0, return; end
        F1 = LoF_R;

    case 'd'
        % Extract detail coefficients.
        x = detcoef(c,l,n);
        F1 = HiF_R;

    otherwise
        errargt(mfilename,'invalid argument value','msg'); error('*');
end

imin = rmax-n;
x  = upsaconv('1D',x,F1,l(imin+1),dwtATTR);
for k=2:n , x = upsaconv('1D',x,LoF_R,l(imin+k),dwtATTR); end

function d = detcoef(c,l,n)
%DETCOEF.
%   D = DETCOEF(C,L,N) extracts the detail coefficients
%   at level N from the wavelet decomposition structure [C,L].
%
%   D = DETCOEF(C,L) extracts the detail coefficients
%   at last level n = length(L)-2.
%
if errargn(mfilename,nargin,[2:3],nargout,[0:1]), error('*');end
```

```
rmax = length(l);
nmax = rmax-2;
if nargin==2 , n = nmax; end
if (n < 1) | (n > nmax) | (n ~= fix(n))
    errargt(mfilename,'invalid level value','msg'); error('*');
end
%
% Extract detail coefficients.
k     = rmax-n;
first = sum(l(1:k-1))+1;
last  = first+l(k)-1;
d     = c(first:last);
%
%
function a = appcoef(c,l,varargin)
%APPCOEF.
%   APPCOEF computes the approximation coefficients of a
%   one-dimensional signal.
%
%   A = APPCOEF(C,L,'wname',N) computes the approximation
%   coefficients at level N using the wavelet decomposition
%   structure [C,L].
%
%
if errargn(mfilename,nargin,[3:5],nargout,[0:1]), error('*'), end
rmax = length(l);
nmax = rmax-2;
if isstr(varargin{1})
    [LoF_R,HiF_R] = wfilters(varargin{1},'r'); next = 2;
else
    LoF_R = varargin{1}; HiF_R = varargin{2};  next = 3;
end
if nargin>=(2+next) , n = varargin{next}; else, n = nmax; end

if (n < 0) | (n > nmax) | (n ~= fix(n))
    errargt(mfilename,'invalid level value','msg'); error('*');
end
%
% Initialization.
a = c(1:l(1));
%
% Iterated reconstruction.
imax = rmax+1;
for p = nmax:-1:n+1
    d = detcoef(c,l,p);                % extract detail
    a = idwt(a,d,LoF_R,HiF_R,l(imax-p));
end
%
function [a,d] = dwt(x,varargin)
%DWT .
%   DWT performs a single-level 1-D wavelet decomposition.
%
%
if errargn(mfilename,nargin,[2:7],nargout,[0:2]), error('*'), end

if isstr(varargin{1})
    [LoF_D,HiF_D] = wfilters(varargin{1},'d'); next = 2;
```

```
else
    LoF_D = varargin{1}; HiF_D = varargin{2};  next = 3;
end

% Default: Shift and Extension.
dwtATTR = dwtmode('get');
shift   = dwtATTR.shift1D;
dwtEXTM = dwtATTR.extMode;

% Check arguments for Extension and Shift.
for k = next:2:nargin-1
    switch varargin{k}
      case 'mode'  , dwtEXTM = varargin{k+1};
      case 'shift' , shift   = mod(varargin{k+1},2);
    end
end

% Compute sizes.
lf = length(LoF_D);
lx = length(x);

% Extend, Decompose &  Extract coefficients.
flagPer = isequal(dwtEXTM,'per');
y = wextend('1D',dwtEXTM,x,lf-1);
a = convdown(y,LoF_D,lx,lf,shift,flagPer);
d = convdown(y,HiF_D,lx,lf,shift,flagPer);


%-------------------------------------------------------------------------
-----%
% Internal Function(s)
%-------------------------------------------------------------------------%
function y = convdown(x,f,lx,lf,shift,flagper)
%
y = wconv('1D',x,f);
y = wkeep(y,lx+lf-1);
y = dyaddown(y,shift);
if flagper , y = wkeep(y,ceil(lx/2),1); end
%-------------------------------------------------------------------------%
%
%
function x = idwt(a,d,varargin)
%IDWT Single-level inverse discrete 1-D wavelet transform.
%
%
if errargn(mfilename,nargin,[3:8],nargout,[0:1]), error('*'), end
if isempty(a) & isempty(d) , x = []; return; end

if isstr(varargin{1})
    [LoF_R,HiF_R] = wfilters(varargin{1},'r'); next = 2;
else
    LoF_R = varargin{1}; HiF_R = varargin{2};  next = 3;
end

% Default: Length, Shift and Extension.
lx      = [];
dwtATTR = dwtmode('get');
```

```
% Check arguments for Length, Shift and Extension.
k = next;
while k<=length(varargin)
    if isstr(varargin{k})
        switch varargin{k}
           case 'mode'  , dwtATTR.extMode = varargin{k+1};
           case 'shift' , dwtATTR.shift1D = mod(varargin{k+1},2);
        end
        k = k+2;
    else
        lx = varargin{k}; k = k+1;
    end
end

% Reconstructed Approximation.
x = upsaconv('1D',a,LoF_R,lx,dwtATTR)+ ...   % Approximation.
    upsaconv('1D',d,HiF_R,lx,dwtATTR);       % Detail.
%
%
%
function y = upsaconv(type,x,f,s,dwtATTR,shiFLAG)
%UPSACONV Upsample and convolution.
%
%   Y = UPSACONV('1D',X,F_R) returns the one step dyadic
%   interpolation (upsample and convolution) of vector X
%   using filter F_R.
%
%
%   Y = UPSACONV('2D',X,{F1_R,F2_R},DWTATTR) returns the one step
%   interpolation of matrix X using filters F1_R and F2_R where
%   the upsample and convolution attributes are described by DWTATTR.
%
%   Y = UPSACONV('2D',X,{F1_R,F2_R},S,DWTATTR) combines the
%   other usages.
%
if isempty(x) , y = 0; return; end
%
% Check arguments.
% if errargn(mfilename,nargin,[3:6],nargout,[0:1]), error('*'), end
%
y = x;
if nargin<4 , sizFLAG = 1; else , sizFLAG = isempty(s); end
if nargin<5 , dwtATTR = dwtmode('get'); end
if nargin<6 , shiFLAG = 1; end
dumFLAG = ~isstruct(dwtATTR);
if ~dumFLAG , perFLAG = isequal(dwtATTR.extMode,'per'); else , perFLAG =
0; end
shiFLAG = shiFLAG & ~dumFLAG;

switch type
    case {1,'1','1d','1D'}
        ly = length(y);
        lf = length(f);
        if perFLAG
            I = GetIndices(ly,lf); y = y(I);
            if sizFLAG , s = 2*ly; end
```

```
        elseif sizFLAG
            s = 2*ly-lf+2;
        end
        if shiFLAG , shift = dwtATTR.shift1D; else , shift = 0; end
        y = wconv('1D',dyadup(y,0),f);

    case {2,'2','2d','2D'}
        sy = size(y);
        lf = length(f{1});
        if perFLAG
            I = GetIndices(sy(1),lf); y = y(I,:);
            I = GetIndices(sy(2),lf); y = y(:,I);
            if sizFLAG , s = 2*sy; end
        elseif sizFLAG
            s = 2*sy-lf+2;
        end
        if shiFLAG , shift = dwtATTR.shift2D; else , shift = [0 0]; end
        y = wconv('col',dyadup(y,'row',0),f{1});
        y = wconv('row',dyadup(y,'col',0),f{2});
end
shift = mod(shift,2);
if perFLAG
    y = wkeep(y,s,'c');
    if any(shift) , y = wshift(type,y,shift); end
else
    y = wkeep(y,s,'c',shift);
end


%-------------------------------------------------------------------------
-----%
% Internal Function(s)
%-------------------------------------------------------------------------
-----%
function I = GetIndices(len,lf)

lm  = floor((lf-1)/2);
I   = [1:len , 1:lm];
if lf>2*len
    I  = mod(I,len);
    I(I==0) = len;
end
%-------------------------------------------------------------------------
-----%

function err = errargn(ndfct,nbargin,argin,nbargout,argout)
%ERRARGN Check function arguments number.
%   ERR = ERRARGN('function',NUMARGIN,ARGIN,NUMARGOUT,ARGOUT)
%   is equal to 1 if either the number of input
%   ARGIN or output (ARGOUT) arguments of the specified
%   function do not belong to the vector of allowed values
%   (NUMARGIN and NUMARGOUT, respectively).
%   Otherwise ERR = 0.
%
%
%
```

```
if isempty(find(argin==nbargin)) | isempty(find(argout==nbargout))
    err = errargt(ndfct,'invalid number of arguments','msg');
else
    err = 0;
end
%
function err = errargt(ndfct,var,type)
%ERRARGT Check function arguments type.
%   ERR = ERRARGT(NDFCT,VAR,TYPE)
%   is equal to 1 if any element of input vector or
%   matrix VAR (depending on TYPE choice listed below)
%   is not of type prescribed by input string TYPE.
%   Otherwise ERR = 0.
%
%
[r,c] = size(var);
err = 0;

switch type
    case 'int'
        if (isstr(var) | any(var < 1) | any(var ~= fix(var)))
            err = 1; txt = 'integer(s) > 0 , expected';
        end

    case 'in0'
        if (isstr(var) | any(var < 0) | any(var ~= fix(var)))
            err = 1; txt = 'integer(s) => 0 , expected';
        end

    case 'rel'
        if (isstr(var) | any(var ~= fix(var)))
            err = 1; txt = 'integer(s) expected';
        end

    case 'rep'
        if (isstr(var) | any(var <= 0))
            err = 1; txt = 'real(s) > 0 , expected';
        end

    case 're0'
        if (isstr(var) | any(var < 0))
            err = 1; txt = 'real(s) => 0 , expected';
        end

    case 'str'
        if any(~isstr(var))
            err = 1; txt = 'string expected';
        end

    case 'vec'
        if r ~= 1 & c ~= 1
            err = 1; txt = 'vector expected';
        end

    case 'row'
        if r ~= 1
            err = 1; txt = 'row vector expected';
```

```
        end

    case 'col'
        if c ~= 1
            err = 1; txt = 'column vector expected';
        end

    case 'dat'
        if isempty(var)
            err = 1; txt = 'date expected';
        else
            ss = rem(var,100);
            mn = rem(fix(var/100),100);
            hh = rem(fix(var/10000),100);
            jj = rem(fix(var/1000000),100);
            mm = rem(fix(var/100000000),100);
            aa = fix(var/10000000000);
            if any(...
                    ss < 0 | ss > 59 |...
                    mn < 0 | mn > 59 |...
                    hh < 0 | hh > 24 | (hh == 24 & (ss ~= 0 | mn ~= 0))
|...
                    jj < 1 | jj > 31 | ...
                    mm < 1 | mm > 12 | ...
                    aa < 0 | aa > 9999 ...
                    )
               err = 1; txt = 'date expected';
            end
        end

    case 'mon'
        if (any(var < 1 | var > 12 | var ~= fix(var)))
            err = 1; txt = 'month expected';
        end

    case 'msg'
        err = 1; txt = var;

    otherwise
        err = 1; txt = 'undefined type of variable';
end

if err == 1
    if size(txt,1) == 1
        msg   = [' ' ndfct ' ---> ' txt];
    else
        msg = str2mat([' ' ndfct ' ---> '],txt);
    end
    if type=='msg'
        txttitle = 'ERROR ... ';
    else
        txttitle = 'ARGUMENTS ERROR';
    end
    if ~mextglob('is_on')
        disp(' ')
        disp('****************************************');
        disp(txttitle);
```

```
        disp('---------------------------------------');
        disp(msg);
        disp('***************************************');
        disp(' ')
    else
        errordlg(msg,txttitle,'modal');
    end
end
```